Chemical characterization and aging of ambient aerosols in Australian urban and remote areas with a focus on biomass burning organic aerosols

Andelija Milic

School of Chemistry, Physics and Mechanical Engineering
Science and Engineering Faculty
Queensland University of Technology

SUBMITTED IN FULFILMENT OF THE REQUIREMENT FOR THE DEGREE OF

DOCTOR OF PHILOSOPHY

2017

This page is intentionally left blank

ABSTRACT

Atmospheric aerosols have a significant role in air quality, regulating climate and influencing human health. Aerosols generated during combustion processes such as biomass burning have attracted substantial attention as they are strongly related to a number of environmental and health issues. The biomass burning emissions generated in wild and prescribed fires are globally one of the largest sources of gases and aerosols to the atmosphere. A predominant component of fire emissions is organic aerosol. Most of atmospheric organic aerosols have a secondary origin. Secondary organic aerosol is formed via photochemical atmospheric transformations (aging processes) and it is a subject of significant scientific concern. The aging is coupled to the environment through many mechanisms, including meteorological conditions and atmospheric physicochemistry. The comprehension of the atmospheric physicochemistry associated with secondary organic aerosol formation is still highly unconstrained and therefore continues to be a big scientific challenge. Despite recent considerable progress regarding secondary organic aerosol and aging, there are still considerable gaps in knowledge that need to be addressed. Therefore, it is of utter importance to gain better insight in the atmospheric aging of the organic aerosols including the biomass burning-related organic aerosol.

Australia is a fire-prone land and each year is subject to a number of wild and prescribed fires. Characterisation of biomass burning emissions and aging in Australia, in both urban and remote areas, remains an area of active research. The uncertainties associated with the biomass burning emissions in Australia illustrate the need for more monitoring studies to better represent emission inventories and modelling. There is also a lack of knowledge of differences in biomass burning properties between urban and remote parts of Australia. The main aim of this research is to provide insight into the characterisation and aging of organic biomass burning aerosols in Australian urban and remote areas.

In order to address above-mentioned gaps two field campaigns looking at biomass burning emissions were conducted in Australia. To obtain data for characterization of ambient aerosols, estimation of aerosol aging and influence of biomass burning in urban Australia, a month-long field campaign was performed in Brisbane central district during the prescribed burning season. With the aim to investigate biomass burning emissions in a remote area, the remote station at Gunn Point, Northern Territory was used to monitor the fire emissions over a one month during the intense fire period. This enabled the overall chemical characterisation and source profiles of ambient urban and remote aerosol and more specific, the investigation of biomass burning aerosol properties and aging. A compact Time-of-Flight Aerosol Mass Spectrometer (Aerodyne Research, Inc.) for the real time chemical characterisation of the submicron aerosol was the main instrument used in this research study. To put the biomass burning aerosol characterisation and aging issue into a global context the

comprehensive literature review was done on studies performed to date, making a large database that can be used as a foundation of the performed research on biomass burning emissions around the world with a special focus on China.

The ambient aerosols collected in Brisbane had a typical urban source profile, while remote Gunn Point measurements revealed significant biogenic influence of isoprene-related aerosol. The influence of fires was found in both environments but more prominent during the fire season in northern Australia. The prescribed biomass burnings in Brisbane did not significantly influence the urban ambient aerosol profile. Aerosols in both areas were found to be the subject of significant processing (aging) based on high aging parameter and fraction apportioned to oxygenated organic aerosol. The aging aerosol degree was found to be higher comparing to values for the Northern Hemisphere.

This study illustrates the importance of biomass burning emissions generated in wild and prescribed fires in Australia. Moreover, it suggests that an ambient aerosol including biomass burning fraction is a significant subject to processing and formation of secondary species. Performed studies in urban and remote Australian areas contribute to better understanding of biomass burning aerosol properties and their transformations in the atmosphere, which can further improve Australian and global emission inventories and models.

KEYWORDS

Ambient aerosols, Organic aerosol, Aerosol aging, Oxygenated organic aerosol, Secondary organic aerosol, Ozone, Chemical characterization, Aerosol mass spectrometry, Source apportionment, Biomass burning, Prescribed burnings, Wild burnings, Savannah fires, Australia, Air quality.

STATEMENT OF ORIGINAL AUTHORSHIP

The work contained in this thesis has not been previously submitted to meet requirements for an award at this or any other higher education institution. To the best of my knowledge and belief, the thesis contains no material previously published or written by another person except where due reference is made.

SIGNATURE:

DATE: 03/01/2017

Table of Content

LIST OF RESEARCH PUBLICATIONS

Milic, A., Miljevic, B., Alroe, J., Mallet, M., Canonaco F., Prevot A., and Ristovski, Z.: The ambient aerosol characterization during the prescribed bushfire season in Brisbane 2013, Science of The Total Environment., 560, 225-232, 2016

Mallet, M. D., Desservettaz, M. J., Miljevic, B., **Milic, A.**, Ristovski, Z. D., Alroe, J., Cravigan, L. T., Jayaratne, E. R., Paton-Walsh, C., Griffith, D. W. T., Wilson, S. R., Kettlewell, G., Vanderschoot, M. V., Selleck, P., Reisen, F., Lawson, S. J., Ward, J., Harnwell, J., Cheng, M., Gillett, R. W., Molloy, S. B., Howard, D., Nelson, P. F., Morrison, A. L., Edwards, G. C., Williams, A. G., Chambers, S. D., Werczynski, S., Williams, L. R., Winton, V. H. L., Atkinson, B., Wang, X., and Keywood, M. D.: Biomass burning emissions in north Australia during the early dry season: an overview of the 2014 SAFIRED campaign, Atmos. Chem. Phys. Discuss., doi:10.5194/acp-2016-866, under review, 2016

Milic, A., Mallet, M. D., Cravigan, L. T., Alroe, J., Ristovski, Z. D., Lawson, S. J., Ward, J., Desservettaz, M. J., Paton-Walsh, C., Keywood, M. D., and Miljevic, B.: Fresh and aged aerosols emitted from biomass burning in northern Australia, Atmos. Chem. Phys. Discuss., doi:10.5194/acp-2016-730, under review, 2016

Chen, J., Li, C., Ristovski, Z., Gu, Y., Wang, S., Hao, J., Zhang, H., He, C., Guo, H., Wang, L., Fu, H., Miljevic, B., **Milic, A.**, Morawska, L., Thai, P., Lam, Y. F. N., Pereira, G., Ding, A., and Dumka, U.: A Review of Biomass Burning: Emissions and impacts on air quality, health and climate in China, Science of The Total Environment., 579, 1000-1034 2017

LIST OF FIGURES

LIST OF TABLES

LIST OF ABBREAVIATIONS

PM	Particulate matter
BB	Biomass burning
OA	Organic aerosol
EC	Elemental carbon
BC	Black carbon
OC	Organic carbon
OOA	Oxygenated organic aerosol
POA	Primary organic aerosol
SOA	Secondary organic aerosol
OH	Hydroxyl radical
NMOC	Non-methane organic compound
VOC	Volatile organic compound
AMS	Aerosol mass spectrometer
cToF-AMS	Compact time of flight aerosol mass spectrometer
HR-ToF-AMS	High resolution time of flight aerosol mass spectrometer
SMPS	Scanning mobility particle sizer
ACSM	Aerosol chemical speciation monitor
FTIR	Fourier transform infrared spectroscopy
MAX-DOAS	Multi axis differential optical absorption spectrometer
PTR-MS	Proton transfer reaction-mass spectrometer
CO	Carbon monoxide
CO_2	Carbon dioxide
NO_X	Nitrogen oxides
CH_4	Methane
N_2O	Nitrous oxide
PAHs	Polycyclic aromatic hydrocarbons
GOM	Gaseous oxidized mercury
GEM	Gaseous elemental mercury
BAM	Beta plus particle measurement system
ARADD	Automated regenerating aerosol diffusion dryer

NAIS	Neutral cluster and air ion spectrometer
TGM	Total gaseous mercury
O_3	Ozone
CCN	Cloud condensation nuclei
MCE	Modified combustion efficiency
NR	Non-refractory
CE	Collection efficiency
MS	Mass spectrum
PMF	Positive matrix factorization
ME-2	Multilinear engine
SoFi	Source finder
BBOA	Biomass burning organic aerosol
HOA	Hydrocarbon like organic aerosol
SV-OOA	Semivolatile oxygenated organic aerosol
LV-OOA	Low-volatility oxygenated organic aerosol
COA	Cooking-related organic aerosol
NOA	Nitrogen-enriched organic aerosol
HR	High resolution
UMR	Unit mass resolution
O/C	Organic to carbon ratio
CBD	Central business district
SAFIRED	Savannah fires in the early dry season
ATARS	Australian tropical atmospheric research station
MODIS	Moderate resolution imaging spectroradiometer
VIIRS	Visible infrared imaging radiometer suite

ACKNOWLEDGEMENTS

My big thank you goes to my Principal Supervisor, Prof. Zoran Ristovski, for giving me an opportunity to do a research in such a beautiful and inspiring group. I would like to thank you Zoran for the continuous encouragement and support throughout my PhD. It has been a pleasure having you as a mentor.

My special gratitude goes to my Associate Supervisor, Dr. Branka Miljevic, for all support and motivation. Dear Branka, I could not imagine going through this without you.

I would like to thank my beautiful ILAQH colleagues for all we have been through over these three years. It was a pleasure sharing the office, ideas and fun. My special thanks go to Janka and Farzaneh for precious support and friendship. I would also like to thank you Pierre for being such a good brother.

A special thanks to Dusan for the precious support, love and for keeping me smiled.

At last but not least, I would like to express my deepest gratefulness to my lovely family. I dedicate this thesis to them.

Chapter 1

INTRODUCTION

Chapter 1 introduces the scientific problem that has been a focus of this research. Included are study aims resulted from the research problem and main objectives that have been addressed. The final section provides research progress in the context of published and submitted scientific papers.

1.1 Research problem

Biomass burning (BB) emissions generated in wild and prescribed fires are one of the largest contributors of gaseous and aerosol-phase species to the global atmosphere. The fire emissions are tightly associated with climate, air pollution and adverse public health issues (Luhar et al., 2008; van der Werf et al., 2006). In order to estimate the magnitude of these effects, chemical characterization of aerosols in BB emissions must be known. This is due to the fact that a significant fraction of biomass incomplete combustion is aerosol-phase carbonaceous material, particularly organic aerosol (OA) (Bond et al., 2004; Reid et al., 2005). Fire combustion sources are actually the largest contributors to the primary carbonaceous particles in the atmosphere (Akagi et al., 2013). Due to the number and various structures of existing organic compounds in BB emissions and their complex fate in the atmosphere this research field still has a room for improvement. The composition of organic BB-related aerosols depends on the type of combusted material (e.g. grass, tree, shrub etc.) and burning conditions (flaming/smoldering combustion, fire intensity, surface burned etc.), but also on plume processing (aging) in the atmosphere (meteorological conditions, availability of atmospheric oxidants, etc.). The aging implies gas-to-particle transformations within the atmosphere as well as oxidation of the existing particulate matter. The most significant aging pathway is an atmospheric oxidation of primary gaseous compounds (non-methane organic compounds, NMOCs) emitted from the source to form low-vapour-pressure organic compounds that often condense onto the existing particles and form secondary organic aerosol (SOA). The BB-related aerosol lifetime of approximate 4 days suggests that it is likely to be a subject to the significant atmospheric changes and a source of SOA precursors (DeCarlo et al., 2010; Edwards et al., 2006; Grieshop et al., 2009; Heringa et al., 2011; Jimenez et al., 2009). The aging of the BB-related OA in the ambient atmosphere is often characterised with the increases in the oxygenated organic fraction (OOA) and formation of SOA. There is a confirmed increasing trend of OOA fraction in BB plumes with aging (Cubison et al., 2011; DeCarlo et al., 2008). However, net mass changes in OA (possible SOA formation) are not consistent within BB studies. Some studies have found an enhancement in OA with aging (DeCarlo et al., 2010; Heringa et al., 2011; Lee et al., 2008; Yokelson et al., 2009), while others showed the opposite trend (Akagi et al., 2012; Brito et al., 2014; Capes et al., 2008; Cubison et al., 2011; May et al., 2015). The observed decrease in organic portion can be attributed to evaporation of species due to dilution or fragmentation as competing effects to SOA formation. As SOA presents a great portion of OA in the atmosphere (Jimenez et al., 2009;

Zhang et al., 2007) and affects the health, radiative budget and cloud formation (Hallquist et al., 2009), it is considered as a subject of significant scientific concern. In addition to the quantitative and qualitative estimation of BB aerosol it is therefore important to determine atmospheric aging of BB emissions, especially due to fact that there have not been many studies looking at aging of BB aerosols. In conclusion, the BB-related organics, especially secondary species, are so far not sufficiently characterised and the understanding of the post-emission aging of BB aerosols is still limited.

Areas needing further research in terms of BB emission characterization and aging are the urban and remote areas of Australia (Spracklen et al., 2011). A number of wild and prescribed fires occur every year throughout the Australia. In order to preserve vegetation and mitigate/reduce number and intensity of wild fires, prescribed fire management was developed for all parts of Australia. Globally, the Australian land is a significant source of BB emissions with the most fire-prone area being tropic savannahs in northern Australia (Russell-Smith et al., 2007). The influence of BB emissions on both Australian urban and remote areas needs to be further characterized (Rotstayn et al., 2009). The difference in aging in urban and remote areas has not yet been investigated. In addition, more data are needed to address the lack of information needed for emissions estimation and modelling, as well as to contribute to maintenance of efficient prescribed burning practice. Moreover, there is a lack in comparison studies in BB characterization and aging between Australia and other parts of the world. There is a need for the future research on aging parameters related to OA in the Southern Hemisphere, to confirm the observation of more aged (oxygenated) aerosol portion in the Sothern Hemisphere, compared to the Northern Hemisphere (Crilley et al., 2014).

1.2 Research aims

The aims designed to address the research problem of this project are summarized below:

1. Characterization of ambient aerosols, estimation of aerosol aging and influence of BB on the Australian urban area during a fire season
2. Characterization of ambient aerosols, estimation of aerosol aging and influence of BB in the Australian remote area during a fire season
3. Comparison of BB aerosol properties and aging for urban and remote areas in Australia and comparison of these results with other studies
4. Comparison of BB aerosol properties and aging in the Southern Hemisphere (Australia) and the Northern Hemisphere

1.3 Specific research objectives

The specific objectives designed to fulfill the aims of this research are listed below:

- Characterisation of ambient aerosols during prescribed fire period in the urban Brisbane area
- Estimation of aging of ambient aerosols during prescribed fire period in the urban Brisbane area
- Source apportionment of the OA in the urban Brisbane area
- Estimation of BB influence on the urban atmosphere during prescribed fire period
- Characterisation of ambient aerosols during the intense dry season fire period in the remote area of northern Australia (Gunn Point)
- Estimation of aging of ambient aerosols during the intense early dry season fire period in the remote Gunn Point area
- Source apportionment of the OA in the remote Gunn Point area
- Estimation of BB influence on the remote atmosphere during early dry season fire period
- Comparison of BB aerosol properties and aging in the urban (Brisbane) and the remote (Gunn Point) areas
- Estimation of ambient aerosol aging in Australia in order to enhance our understanding on the degree of aerosol aging in the Southern Hemisphere versus the Northern Hemisphere
- Comparison of BB aerosol properties and aging degree in Australia and other parts of the world including China

1.4 Research progress

The outline of the research progress through individual publications generated from conducted studies during the candidature and their linkage to the listed research aims is summarized in Figure 1.1.

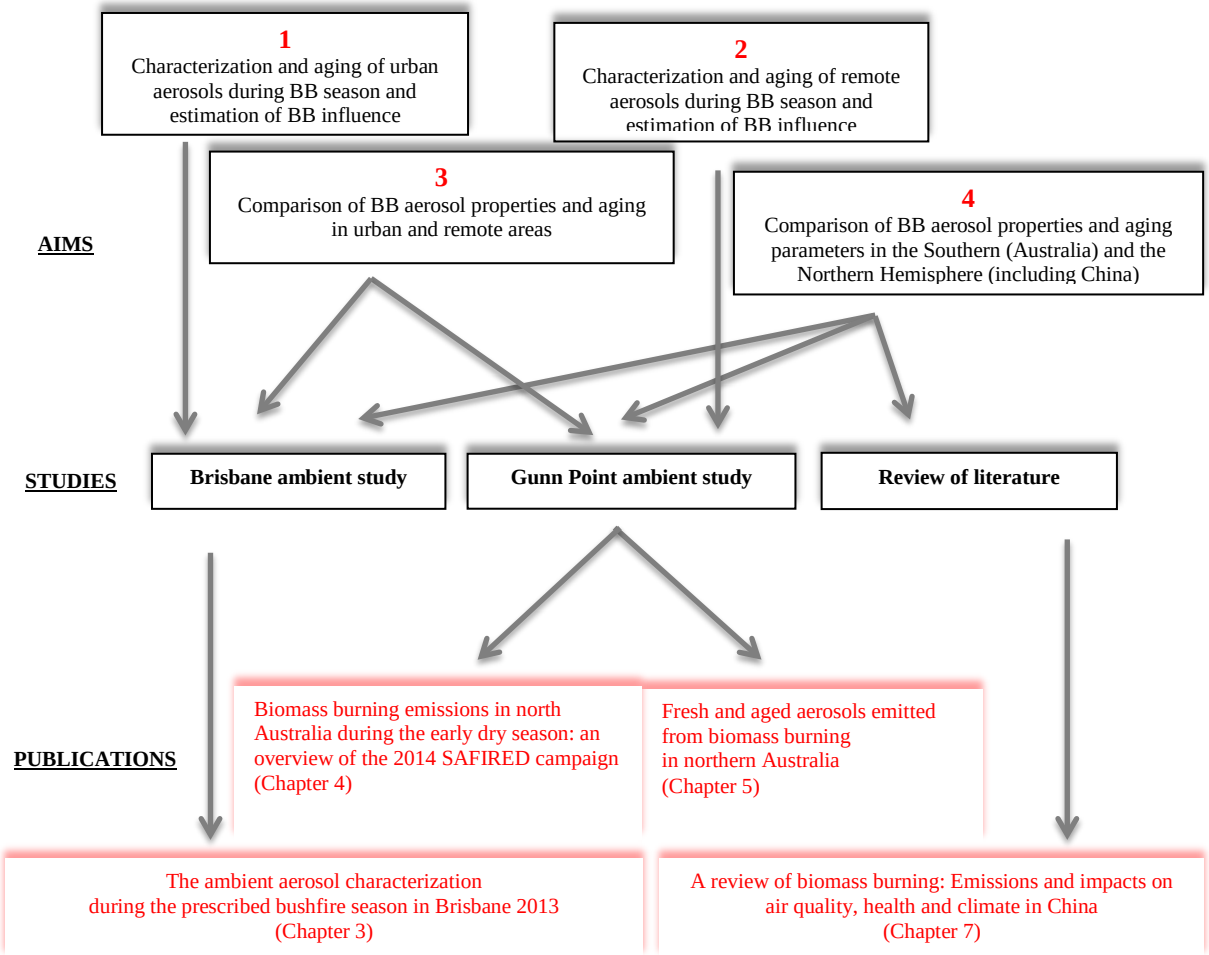

Figure 1.1 Research publications arising from performed studies in order to address the research aims.

In order to address the aims of this research, two field campaigns were conducted: one in the urban Brisbane area during the prescribed fire period and another in the remote region at the north of the Northern Territory (Gunn Point) during the intense early dry fire season. In addition, comprehensive literature research was done on characterisation and aging of BB aerosol in

China to get more detailed insight into global context of BB properties and aging. This would allow comparison between aerosol properties in Australia, China and other parts of the world. The following paragraphs include the brief summary of individual publications in terms of the main findings and linkage to the research aims.

With the aim to investigate urban ambient aerosols influenced by BB, a one month long campaign was conducted in Brisbane Central Business District (CBD) area during the prescribed burning season (August-October, 2013). The study has shown that there was a limited influence of prescribed fires on Brisbane urban area in that specific time period, seen through low contribution of detected BB-related aerosols. The dominance of oxygenated organic species further suggested intense atmospheric photochemistry. Data were analysed and interpreted in the manuscript "The ambient aerosol characterization during the prescribed bushfire season in Brisbane 2013" (Chapter 3), published in the journal "Science of the Total Environment" (Milic et al., 2016b).

The influence of BB emissions in a remote Australian tropical savannah region was investigated with data collected during the Savannah Fires in the Early Dry Season (SAFIRED) campaign. A one month long field research was conducted at remote Gunn Point research station in northern Australia during the early dry intense BB season. The emissions from tropical savannah fires are the most significant regional source of atmospheric gases and aerosols during this period. This comprehensive field study addressed the second aim of this research study, more precisely characterisation of ambient aerosol in remote area during BB period and estimation of the aging of aerosols. The organic source apportionment illustrated significant influence of processed emissions. This study suggests intense photochemistry and likely SOA formation for Australian remote area. Many publications resulted from this campaign, two of which are presented in this thesis, "Biomass burning emissions in north Australia during the early dry season: an overview of the 2014 SAFIRED campaign" (Chapter 4) (Mallet et al., 2016) and "Fresh and aged aerosols emitted from biomass burning in northern Australia" (Chapter 5) (Milic et al., 2016a). Both publications are under review in the journal "Atmospheric Chemistry and Physics" and published as a discussion papers in scientific discussion forum of Atmospheric Chemistry and Physics.

A large literature review was done by the PhD candidate on characterisation and aging of BB-related aerosols, which contributed to the most comprehensive literature review on BB aerosol in China named "A review of biomass burning: Emissions and their impacts on air quality, health and climate in China". The manuscript (presented in Chapter 7) is published in journal "Science of the Total Environment" (Chen et al., 2016). The review paper is a comprehensive database for sources, impact, characterisation and aging of BB aerosol worldwide, with a special focus on China.

Performed field and review studies enable comparison of BB aerosol properties and aging between urban and remote Australian areas and the Southern (Australia) and the Northern (including China) Hemisphere. This will be discussed in the conclusions part (Chapter 6).

1.5 References

Akagi S, Craven J, Taylor J, McMeeking G, Yokelson R, Burling I, et al. Evolution of trace gases and particles emitted by a chaparral fire in California. Atmospheric Chemistry and Physics 2012; 12: 1397-1421.

Akagi S, Yokelson RJ, Burling IR, Meinardi S, Simpson I, Blake D, et al. Measurements of reactive trace gases and variable O 3 formation rates in some South Carolina biomass burning plumes. Atmospheric Chemistry and Physics 2013; 13: 1141-1165.

Bond TC, Streets DG, Yarber KF, Nelson SM, Woo JH, Klimont Z. A technology-based global inventory of black and organic carbon emissions from combustion. Journal of Geophysical Research: Atmospheres (1984–2012) 2004; 109.

Brito J, Rizzo L, Morgan W, Coe H, Johnson B, Haywood J, et al. Ground-based aerosol characterization during the South American Biomass Burning Analysis (SAMBBA) field experiment. Atmospheric Chemistry and Physics 2014; 14: 12069-12083.

Capes G, Johnson B, McFiggans G, Williams P, Haywood J, Coe H. Aging of biomass burning aerosols over West Africa: Aircraft measurements of chemical composition, microphysical properties, and emission ratios. Journal of Geophysical Research: Atmospheres (1984–2012) 2008; 113.

Chen J, Li C, Ristovski Z, Gu Y, Wang S, Hao J, et al. A Review of Biomass Burning: Emissions and their impacts on air quality, health and climate in China. Atmospheric Chemistry and Physics 2017; 579: 1000-1034.

Crilley LR, Ayoko GA, Morawska L. First measurements of source apportionment of organic aerosols in the Southern Hemisphere. Environmental Pollution 2014; 184: 81-88.

Cubison M, Ortega A, Hayes P, Farmer D, Day D, Lechner M, et al. Effects of aging on organic aerosol from open biomass burning smoke in aircraft and laboratory studies. Atmospheric Chemistry and Physics 2011; 11: 12049-12064.

DeCarlo P, Dunlea E, Kimmel J, Aiken A, Sueper D, Crounse J, et al. Fast airborne aerosol size and chemistry measurements above Mexico City and Central Mexico during the MILAGRO campaign. Atmos. Chem. Phys 2008; 8: 4027-4048.

DeCarlo P, Ulbrich I, Crounse J, Foy Bd, Dunlea E, Aiken A, et al. Investigation of the sources and processing of organic aerosol over the Central Mexican Plateau from aircraft measurements during MILAGRO. Atmospheric Chemistry and Physics 2010; 10: 5257-5280.

Edwards D, Emmons L, Gille J, Chu A, Attié JL, Giglio L, et al. Satellite-observed pollution from Southern Hemisphere biomass burning. Journal of Geophysical Research: Atmospheres 2006; 111.

Grieshop A, Logue J, Donahue N, Robinson A. Laboratory investigation of photochemical oxidation of organic aerosol from wood fires 1: measurement and simulation of organic aerosol evolution. Atmospheric Chemistry and Physics 2009; 9: 1263-1277.

Hallquist M, Wenger J, Baltensperger U, Rudich Y, Simpson D, Claeys M, et al. The formation, properties and impact of secondary organic aerosol: current and emerging issues. Atmos. Chem. Phys 2009; 9: 5155-5236.

Heringa M, DeCarlo P, Chirico R, Tritscher T, Dommen J, Weingartner E, et al. Investigations of primary and secondary particulate matter of different wood combustion appliances with a high-resolution time-of-flight aerosol mass spectrometer. Atmos. Chem. Phys 2011; 11: 5945-5957.

Jimenez J, Canagaratna M, Donahue N, Prevot A, Zhang Q, Kroll JH, et al. Evolution of organic aerosols in the atmosphere. Science 2009; 326: 1525-1529.

Lee S, Kim HK, Yan B, Cobb CE, Hennigan C, Nichols S, et al. Diagnosis of aged prescribed burning plumes impacting an urban area. Environmental science & technology 2008; 42: 1438-1444.

Luhar AK, Mitchell RM, Meyer C, Qin Y, Campbell S, Gras JL, et al. Biomass burning emissions over northern Australia constrained by aerosol measurements: II—Model validation, and impacts on air quality and radiative forcing. Atmospheric environment 2008; 42: 1647-1664.

Mallet MD, Desservettaz MJ, Miljevic B, Milic A, Ristovski ZD, Alroe J, et al. Biomass burning emissions in north Australia during the early dry season: an overview of the 2014 SAFIRED campaign, submitted to Atmos. Chem. Phys., 2016

May A, Lee T, McMeeking G, Akagi S, Sullivan A, Urbanski S, et al. Observations and analysis of organic aerosol evolution in some prescribed fire smoke plumes. Atmospheric Chemistry and Physics Discussions 2015; 15: 1953-1988.
Milic A, Mallet MD, Cravigan L, Alroe J, Ristovski ZD, Selleck P, et al. Aging of aerosols emitted from biomass burning in northern Australia. Atmos. Chem. Phys. Discuss., doi:10.5194/acp-2016-730, in review 2016a.
Milic A, Miljevic B, Alroe J, Mallet M, Canonaco F, Prevot A, et al. The ambient aerosol characterization during the prescribed bushfire season in Brisbane 2013. Science of The Total Environment 2016b; 560: 225-232.
Reid J, Koppmann R, Eck T, Eleuterio D. A review of biomass burning emissions part II: intensive physical properties of biomass burning particles. Atmospheric Chemistry and Physics 2005; 5: 799-825.
Rotstayn LD, Keywood MD, Forgan BW, Gabric AJ, Galbally IE, Gras JL, et al. Possible impacts of anthropogenic and natural aerosols on Australian climate: a review. International Journal of Climatology 2009; 29: 461-479.
Russell-Smith J, Yates CP, Whitehead PJ, Smith R, Craig R, Allan GE, et al. Bushfires' down under': patterns and implications of contemporary Australian landscape burning. International Journal of Wildland Fire 2007; 16: 361-377.
Spracklen D, Jimenez J, Carslaw K, Worsnop D, Evans M, Mann G, et al. Aerosol mass spectrometer constraint on the global secondary organic aerosol budget. Atmospheric Chemistry and Physics 2011; 11: 12109-12136.
van der Werf GR, Randerson JT, Giglio L, Collatz GJ, Kasibhatla PS, Arellano Jr A. Interannual variability in global biomass burning emissions from 1997 to 2004. Atmospheric Chemistry and Physics 2006; 6: 3423-3441.
Yokelson RJ, Crounse J, DeCarlo P, Karl T, Urbanski S, Atlas E, et al. Emissions from biomass burning in the Yucatan. Atmospheric Chemistry and Physics 2009; 9: 5785-5812.
Zhang Q, Jimenez J, Canagaratna M, Allan J, Coe H, Ulbrich I, et al. Ubiquity and dominance of oxygenated species in organic aerosols in anthropogenically-influenced Northern Hemisphere midlatitudes. Geophysical Research Letters 2007; 34.

Chapter 2

LITERATURE REVIEW

Chapter 2 introduces the topic of ambient aerosol characterization and aging with a focus on biomass burning aerosol. An insight into overall chemical composition and an impact of biomass burning aerosol is provided, with an accent on Australian BB emissions. An identification of biomass burning aerosol and differentiation of fresh and processed (aged) emissions is discussed by introducing biomass burning and aging markers and source apportionment techniques. Also included is the formation of important secondary BB pollutants, secondary organic aerosol (SOA) and tropospheric ozone. The characterisation and aging of biomass burning emissions in different environments is introduced in the context of the related publications in this field. The final paragraph provides the research gaps resulting from the literature review.

2.1 Biomass burning emissions

An aerosol refers to a suspension of particles or liquid droplets in the air (Hinds, 2012). It includes complex mixtures of inorganic and organic species of different sources and with varying chemical composition and physical properties (size, shape, density, light interaction etc.). These aerosol properties influence aerosol transport and lifetime, which further affect visibility, cloud formation, radiation balance, air pollution and human health (Ziemann and Atkinson, 2012). Aerosols can have either primary or secondary origin. Primary aerosols are emitted into the atmosphere directly from the source while secondary aerosols are formed during atmospheric transformations of primary compounds.

Biomass burning emissions originate from open burning sources including natural fires and prescribed burns (of forests, savannas, grasses, scrubs, agricultural wastes etc.), as well as from domestic and industrial combustion sources. Australia is observed to be one of the significant contributors to biomass burning (BB) emissions, especially from the tropical savannah region (north of Australia). Australian BB contribute approximately 8% of the global BB emissions (Schultz et al., 2008). On average, 550 000 km^2 of Australian tropical savannah burns every year (Russell-Smith et al., 2007). Tropical savannah is strongly affected by BB during the dry season (May to October) when most of the fires take place. Prescribed burns are conducted annually throughout the Australia under controlled conditions, mainly to reduce the extent and intensity of wildfires and to preserve vegetation. Spracklen et al. (2011) indicated that more data are clearly needed to investigate BB in tropics, particularly in the Northern Australia, but also for the entire Southern Hemisphere. In this study, BB emissions were examined in the remote Northern Territory and urban Brisbane area during the BB seasons. Planned burns are conducted in the Northern Territory during the early dry season (May/Jun) with an aim to reduce the frequency of wild fires in the second half of the year, during the late dry season (June/October). The prescribed period in Queensland, including Brisbane land takes place every year between August and November.

The composition of BB emissions varies depending on burning material, burning conditions (flaming vs. smoldering), as well as on complex atmospheric photochemistry that plumes undergo once emitted from their sources (Reid et al., 2005; Weimer et al., 2008). Biomass burning emissions are mainly composed of carbon-dioxide (CO_2), carbon monoxide (CO), nitrogen oxides (NO_X), methane (CH_4), non-methane organic compounds (NMOCs) and aerosol-phase species, primarily carbonaceous compounds. The non-methane organic compounds include non-methane hydrocarbons and oxygenated volatile organic compounds. Fires are the second largest global source of NMOCs, and these species are important precursors in the formation of SOA and ozone (Akagi et al., 2011). Carbonaceous aerosols include organic carbon (OC) and elemental carbon (EC) (Bond et al., 2004; Formenti et al., 2003; Hallquist et al., 2009; Reid et al., 2005; Sandradewi et al., 2008). The estimated distribution of carbonaceous matter in BB particles is ~50-60% OC and ~5-10% BC (Reid et al., 2005). Bond et al., 2004 determined that approximately 70% of OC and 40% of BC global annual emissions are released from open fire sources. It is estimated that Australian BB emissions contribute to almost 9% of global carbon budget emitted in open fires (Schultz et al., 2008). In addition to carbon species, inorganic aerosol is relatively small fraction of BB plumes (Crutzen and Andreae, 1990; Reid et al., 2005).

Carbonaceous aerosols have an important role in radiation-matter interactions, as BC absorbs sunlight, making the atmosphere warmer, while OC cools the atmosphere by scattering the solar radiation (Penner et al., 1998). The carbonaceous particulate material associated with Australian BB sources, especially in the fire-prone Northern Territory savannah zone, likely has considerable influence on radiative heating effect and therefore local (and even possible global) climate (O'Brien and Mitchell, 2003). Carbonaceous BB particles can act as cloud condensation nucleus (CCN) changing clouds generation and properties (Penner et al., 1992), although BB particles are usually weakly hygroscopic (Lawson et al., 2015). Fires can contribute to enrichments in overall concentration of cloud droplets that make whiter clouds, which often have longer lifetime in the atmosphere (Platnick and Twomey, 1994). Moreover, CCN can cool the atmosphere. Fire sources also contribute to various health issues, including cardiovascular and respiratory problems (Pope III and Dockery, 2006). The effects of plume emissions depends on parameters such as concentration and composition of pollutants (Cochrane, 2003).

In order to estimate the impact of listed effects, the chemical characterization of BB aerosols have an important part. This includes determination of characterization and impact of BB aerosols in Australia.

2.2 Ambient chemical characterization

One of the most deployed instruments in aerosol chemical characterization is an aerosol mass spectrometer (AMS). An aerosol mass spectrometry technique has provided a significant contribution to the characterization of atmospheric aerosol chemical profiles. It has been extensively used in BB OA characterization and evolution estimation. Based on different signals in AMS mass spectra BB emissions can be distinguished from aerosols of other origin. AMS mass spectra can also indicate aging degree of BB emissions.

In the following paragraphs details about the AMS operation, application and data analysis are given. This is an introduction of the comprehensive methodology that was used in this research.

2.2.1 Aerosol Mass Spectrometer

The aerosol mass spectrometer (AMS) enables the real-time qualitative and quantitative chemical characterization of the non-refractory (NR) submicron (PM1, 40 nm to ~1 μm for the AMS) aerosol fraction (Canagaratna et al., 2007; Jimenez et al., 2003). Non-refractory fraction refers to a chemical aerosol portion that is volatilized/ionized within the instrument and observed in the AMS spectrum. The submicron NR aerosol fraction is composed of particulate organic compounds and inorganic species (sulfate, ammonia, nitrate and chloride) and not elemental carbon (EC). AMS data allow for the detailed aerosol analysis, including mass spectra and time series of monitored species. Many types of aerosol mass spectrometers have been manufactured including a compact Time-of-Flight (cToF-AMS) (Drewnick et al., 2005), a High Resolution Time-of-Flight (HR-ToF-AMS) (DeCarlo et al., 2006) aerosol mass spectrometer and an Aerosol Chemical Speciation Monitor (ACSM) (Fröhlich et al., 2013). In order to determine the chemical properties of BB aerosol and investigate the aerosol aging, the cToF-AMS has been used in this study. The cToF-AMS provides a size-resolved chemical composition. HR-ToF-AMS has improved mass resolving power comparing to cToF-AMS. ACSM has small resolving power, but it is the most suitable for field studies due to its automated calibrations and operation with minimal maintenance. The most advance technology for size-resolved chemical characterization is a Thermal Desorption Aerosol Gas Chromatograph (TAG) (Williams et al., 2006) coupled with the cToF-AMS (or HR-ToF-AMS) (Williams et al., 2014). Combination of two proven techniques enables the TAG-ToF-AMS to determine size-resolved chemical composition of major inorganic and organic species and simultaneously to provide organic speciation based on specific molecular source-related markers. More details about the cToF-AMS that was used in this research study will be given in the following paragraphs.

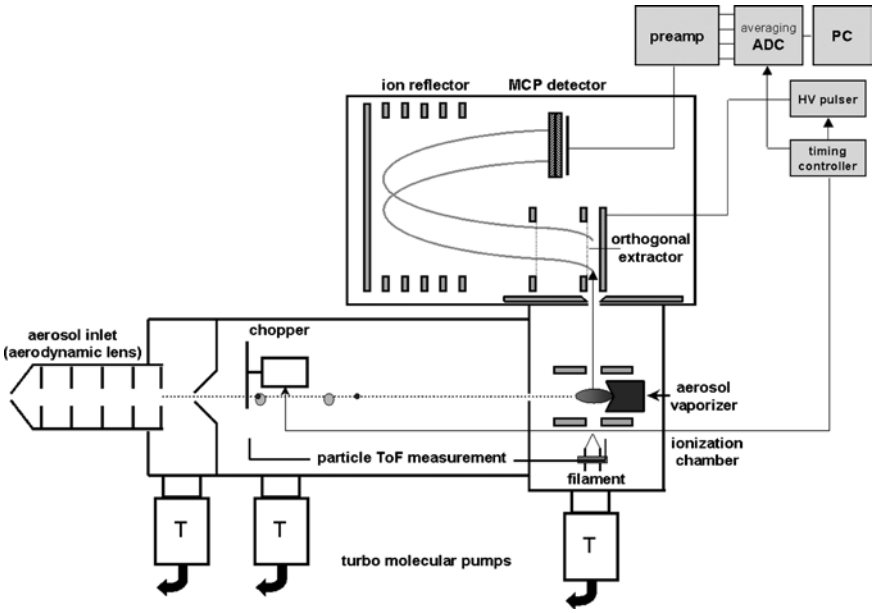

Figure 2.1 Schematic of the Aerodyne compact time-of-flight aerosol mass spectrometer (cToF-AMS) (reused from Drewnick et al. (2007) – Aerosol Science & Technology: A New Time-of-Flight Aerosol Mass Spectrometer (TOF-AMS)-Instrument Description and First Field Deployment. (39):637-658. Copyright 2007. Reston, VA. Reprinted with permission).

The schematic of an Aerodyne (Aerodyne Research, Inc., Billerica) cToF-AMS is illustrated in Fig 2.1. The instrument operates under vacuum pressure provided by a series of turbo-molecular pumps. Air is introduced into an aerodynamic lens through the PM1 inlet. The aerodynamic lens efficiently separates the gaseous and particle-phase species and focuses particles into a narrow beam through the time-of-flight (ToF) chamber onto the heated vaporizer (usually at 600°C). The flash-vaporized NR sample is subsequently ionized by a tungsten filament through the electron impact method. After thermal vaporization and electron impact ionization, ions are deflected in a V shape onto a Multi-Channel-Plate detector. The instrument is equipped with a compact TOFWERK orthogonal acceleration reflectron time-of-flight mass spectrometer. The detector amplifies and converts the ion impact to electrical signals, which are then interpreted by a PC. The ToF measurements provide information about aerodynamic size regarding to particle velocities through ToF mass spectrometer part of the AMS. The AMS does not efficiently detect low-volatility materials such as BC, sodium chloride and crystal oxides. Data obtained from the cToF-AMS are unit mass resolution (UMR) data. The cToF-AMS resolving power is 800 m/Δm. By contrast, the HR-ToF-AMS provides high resolution (HR) data. This instrument provides mass resolving powers of 2000 and 4000 for V-mode and W-mode, respectively. The AMS data are processed in Igor Pro software using the ToF-AMS Analysis Toolkit SQUIRREL (for UMR data) and PIKA (for HR data). It is generally possible to analyze UMR data within the HR PIKA software.

The AMS mass spectrum contains peaks with certain contributions at each m/z, which are directly related to composition and amount of sampled aerosol. Wide spectrum of aerosols can be characterized and distinguished by deploying AMS,

including fresh and processed BB plumes. The AMS mass spectrum has distinctive m/z signals that correspond to different aerosol sources and degree of processing. More details about AMS application will be presented in sections 2.2.2 and 2.2.3.

2.2.2 Biomass burning markers

Aerosol sources can be established based on markers that are source-distinctive. Urban aerosols are mainly products of anthropogenic-related sources (such as industry, traffic, cooking, BBs etc.), while remote areas often have negligible anthropogenic contribution and a higher portion of other important sources such as biogenic, fire and marine.

In order to identify and quantify BB emissions different chemical tracers have been introduced. Levoglucosan-like species (levoglucosan, mannosan, galactosan), are anhydrosaccharides generated in the pyrolysis of cellulose. They are common organic molecular constituents of wood burning emissions (Simoneit et al., 1999). Although atmospheric levoglucosan has been suggested to be semivolatile and non-inert (Hennigan et al., 2010; Hoffmann et al., 2009; May et al., 2012), many studies have used levoglucosan as a distinctive BB chemical signature (Jordan et al., 2006; Simoneit, 2002; Simoneit et al., 1999). Potassium is also used as a BB tracer, but in contrast to source-specific levoglucosan, it can indicate aerosols from more than one origin and therefore is usually used as a qualitative BB marker (Aiken et al., 2010; Zhang et al., 2010). If water soluble potassium is not related to its other important sources such as soil dust and sea salt, it can be an acceptable BB tracer (Andreae, 1983). An important component of fire emissions is acetonitrile, and this gaseous compound is also suggested as a distinctive BB marker (Davis et al., 1990).

Besides "traditional" BB tracers, a mass spectrum of the AMS data contains the characteristic markers for BB aerosols (Aiken et al., 2008; Alfarra et al., 2007; Cubison et al., 2011). Levoglucosan-like species produce prominent signals at m/z 60 (fragment $C_2H_4O_2^+$) and m/z 73 (fragment $C_3H_5O_2^+$). Therefore fragment ions m/z 60 and m/z 73 were defined as levoglucosan-based signals for the evidence of BB emissions (Aiken et al., 2009; Alfarra et al., 2007; Mohr et al., 2012). The parameter f60, the ratio of the integrated organic signal at m/z 60 to the total signal intensity originated from the organic component of mass spectrum, is used as signature of BB plumes (Alfarra et al., 2007). In general, parameter f73 follows the same trend as f60 in smoke plumes. However, f60 is most often used in studies as it gives a more prominent signal in the AMS spectrum. According to Cubison et al. (2011) an f60 value higher than 0.003 indicates detection of BB aerosols. The parameter f60 is the signature of primary BB emissions but during a time it often stays elevated above the background value and decays with time. This f60 decrease is mainly due to mixing with new aerosol mass with not elevated f60 and/or degradation (volatilization) of "levoglucosan-like" species (DeCarlo et al., 2010; Ortega et al., 2013). It is estimated that f60 can be used as a representative BB marker for the time period of up to 1 day (Bougiatioti et al., 2014; Cubison et al., 2011). The AMS-resolved parameter f60, levoglucosan and potassium are used in this study as distinctive BB markers.

2.2.3 Aging markers

An organic aerosol (OA) can have primary or secondary origin, depending on whether it is released directly from a source into the atmosphere, or produced during the atmospheric transformation (aging process). The most common atmospheric oxidizers of organic material are hydroxyl radical (OH) (daytime), ozone (O_3) (daytime and nighttime) and nitrate radical (NO_3) (nighttime) (Jacobson et al., 2000; Lambe et al., 2015; Rollins et al., 2012). The aging process mainly includes variety of gas-to-particle conversions and change in particles within the atmosphere. The gas-to-particle conversion includes nucleation of saturated gaseous components to produce new particles and/or their condensation onto pre-existing particles. A primary organic aerosol (POA) corresponds to the hydrocarbon component of the PM and it is mainly a direct product of combustion. An aged primary organic aerosol (aged POA) is result of atmospheric transformation of fresh particle emissions, while a secondary organic aerosol (SOA) fraction presents the condensation of low-volatility oxygenated organic components that are generated through atmospheric oxidation of NMOCs. Schematic illustration of the atmospheric aging pathways is given in Fig 2.2.

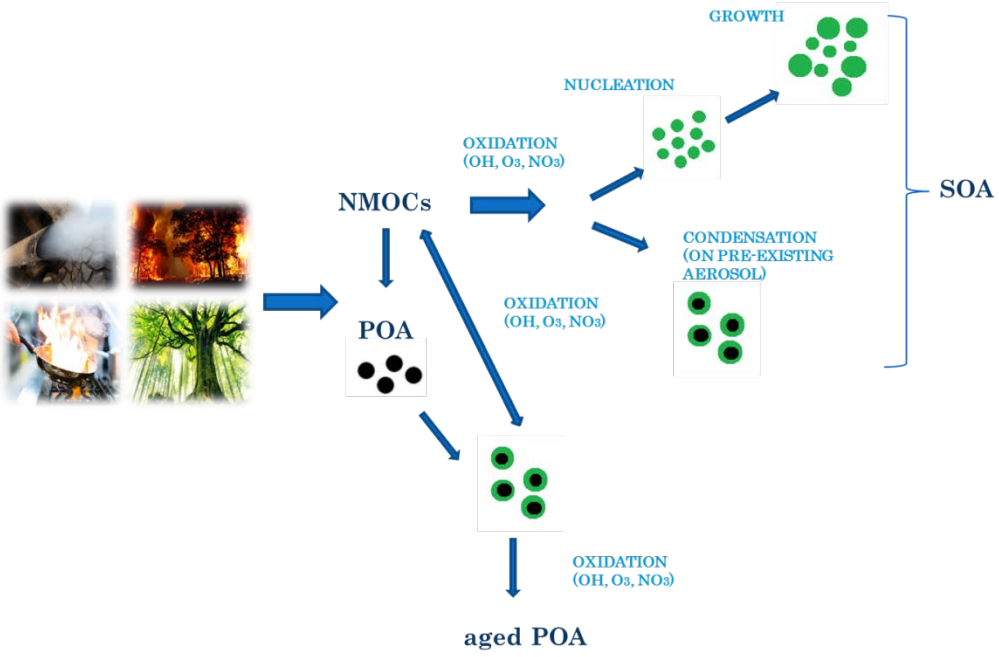

Figure 2.2 Atmospheric aging pathways modified from http://slideplayer.com/slide/4800090/.

In order to estimate OA aging degree and follow aerosol atmospheric transformations, suitable aging parameters have to be applied. During the aging process a hydrocarbon-like organic aerosol (HOA) is transformed to an oxygenated organic aerosol (OOA) (Zhang et al., 2005a; Zhang et al., 2005b). These “fresh” and “aged” OA fractions can be distinguished by different organic signatures in the AMS mass spectrum (Ng et al., 2010). The parameter f44, the ratio of the integrated signal

at m/z 44 and the total signal intensity originated from all organic components of the mass spectrum, measured by the AMS technic, is the marker for OOA fraction (Jimenez et al., 2009; Ortega et al., 2013; Volkamer et al., 2006). Higher values for f44 correspond to more oxygenated organic species. Increased f44 is mainly related to increased concentration of ionized carbon dioxide (CO_2^+) (Aiken et al., 2007; Alfarra et al., 2007; DeCarlo et al., 2010), showing the presence of aged POA and/or SOA in the aerosol (Ortega et al., 2013). The triangle plot suggested by Ng et al. (2010), f44 vs f43 plot (Figure 2.3), can be applied on results in order to establish the aging of OA. An increase in the f44 and a decrease in the f43 is a common pattern for the oxidation process. The ion m/z 43 is observed to be related mainly to $C_2H_3O^+$ (OOA component) and $C_3H_7^+$ (HOA component) (Heringa et al., 2011; Jimenez et al., 2009; Lanz et al., 2007a; Zhang et al., 2007). An atmospheric oxidation promotes reduction of $C_2H_3O^+$ and $C_3H_7^+$ ions which lead to decrease of f43 parameter. In addition, m/z 57 ($C_4H_9^+$) which is valuable marker for a "fresh" aerosol fraction, usually decreases with age of OA mass (Alfarra et al., 2004).

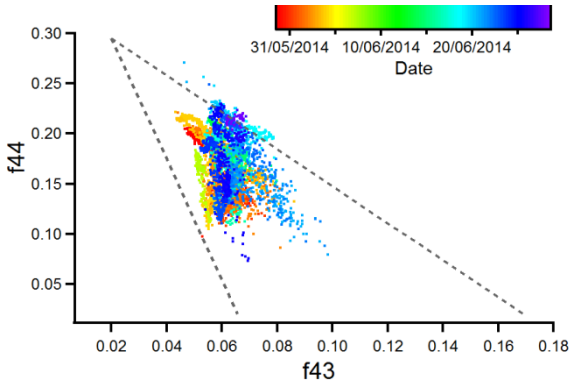

Figure 2.3 f44 versus f43 plot colored by date, for distant fires during SAFIRED campaign (modified from Ng et al. (2010)); The dashed lines represent boundaries for typical ambient aerosol.

Many studies have investigated aging by using HR-ToF-AMS, which allows the determination of atomic ratios e.g. O/C and H/C, as well as an organic mass to organic carbon (OM/OC) ratio (Donahue et al., 2012; Grieshop et al., 2009). The AMS results usually indicate an increase in the O/C ratio (and f44 increase) followed by a decrease in the H/C ratio (f43 decrease), with age of air masses (Chirico et al., 2010; Emanuelsson et al., 2013). The O/C ratio can be predicted from a UMR data using the ambient and improved-ambient equations that illustrate relationship between f44 and O/C, based on experimental data (Aiken et al., 2008; Canagaratna et al., 2015). Secondary inorganic compounds including sulfate (SO_4^{2-}), nitrate (NO_3^-) and ammonia (NH_4^+), can also be robust markers for aging, since their increase with aging is almost certain (Cheng et al., 2014).

2.2.4 Source apportionment of organic aerosol

The source apportionment of OA has an essential part in establishing the efficient control approaches and representative models for the OA and aerosols in general. Considering multiple primary and secondary sources of OA, determination of source profiles is a big challenge. A number of techniques including the principle component analysis (PCA), chemical mass balance (CMB) and positive matrix factorization (PMF) have been applied in order to determine, quantify and extract the relative contributions of various OA sources.

The primary and the secondary OA can be distinguished according to the elemental to organic carbon ratio (EC/OC), which can be determined from filters in an offline sampling (Turpin and Huntzicker, 1991). The primary aerosol sources emit more EC while secondary aerosols contain more OC than EC. The specific source profiles can be also determined based on source-specific molecular tracers sampled onto the filters using CMB and PMF models (Schauer et al., 1996). The AMS real time technique with high time resolution has been widely used in OA source apportionment (Allan et al., 2004; Jimenez et al., 2003). The ambient AMS OA spectrum can distinguish different OA classes. Zhang et al. (2007) performed the first factor analysis of the AMS OA data applying the custom principal component analysis. Two different factors were identified including the hydrocarbon-like organic aerosol (HOA) and oxygenated organic aerosol (OOA) factors (Zhang et al., 2005a; Zhang et al., 2005b). The Positive Matrix Factorization (PMF) evaluation tool (Paatero and Tapper, 1994) has been extensively used in the source apportionment of the AMS OA data (Lanz et al., 2007a; Ulbrich et al., 2009). This multivariate factor model apportions the OA spectrum into different factors that can be related to the specific sources. The positive matrix factorization processes the data depending on how different variables (e.g m/z's) co-vary with time. The word "positive" in the method name indicates that all the values are constrained to be positive. The PMF refer to a statistical method that uses bilinear unmixing model, $X = GF + \mathrm{E}$, where X illustrate a data matrix and G and F are the matrices calculated by the model. In the case of the AMS data, rows in the X (usually organic matrix) are mass concentrations over time while columns are signals at different m/z's. G refers to the time series of the factor and F to the factor profile, while E is a difference between the measured signal and predicted (by the method), in another words the residuals that are not fit by the model. Parameters G and F are fit to the data in order to get the lowest residual matrix (E) and fit parameter (Q) that is defined as:

$$\mathrm{Q} = \sum_{i=1}^{m} \sum_{j=1}^{n} (e_{ij} / \sigma_{ij})^2$$

where *i* refer to a row and *j* to a column of the matrix, *p* is the number of factors and σ_{ij} is the uncertainty for each element, e_{ij}, of the matrix X (Paatero and Tapper, 1994). More details regarding PMF analysis and mathematics behind it can be found elsewhere (Paatero and Tapper, 1994; Ulbrich et al., 2009; Zhang et al., 2007).

After data processing, the solution space is investigated by varying the number of factors (different aerosol components and/or sources), starting conditions (seed runs) and applying rotational parameters (fpeaks and *a* values). Subjective side of the PMF is that user selects the solution that "best" explains the dataset (Ulbrich et al., 2009). It is generally possible to find the solution closest to the "true" solution within these runs, using the supportive analysis of correlation between factors and other compatible data (Canonaco et al., 2013; Ulbrich et al., 2009). Some mathematical metrics can be used to facilitate determination of the best factor solution. The ratio of Q, which refers to the total sum of the squares of the residuals and expected Q, should be 1. If solution gives Q/Q_{exp} ratio lower than 1, the input data errors are likely to be overestimated, while opposite is for Q/Q_{exp} ratio higher than 1, which indicates error underestimation. Therefore, the solution that provides Q/Q_{exp} closest to 1 should be the best solution, the solution with the best fit. The solution is considered to be the best if "mixing of profiles" and "splitting of profiles" are not present. Mixing of profiles refers to a combination of two factor profiles in the one factor, while splitting indicate relocation of m/z's of one factor to two or more.

Chemical Mass Balance is based on completely constrained factor approach. The predetermined factor profiles have to be set before running the software. By contrast, the PMF software does not require any *a priori* information (factor profiles and/or time trends) (Ulbrich et al., 2009). However, application of the PMF using the multilinear engine algorithm (ME-2) technique, introduced by Paatero (1999) and Paatero and Hopke (2009), provides different options to be examined. More precisely, factor profiles and/or time series can be used to different constrained degrees. A graphical user interface, SoFi (Source Finder), uses the ME-2 algorithm appling the pre-set profiles aiming to facilitate extraction of solution that "best" explains the dataset (Canonaco et al., 2013). One of the rotational approaches is *a* value that applies different constraints by choosing certain *a* values which correspond to different deviations from input factor profile and/or time series. For instance, an applied *a* value of 0.1 illustrates that 10 % of the profile/time series is varied by the algorithm during the minimization process (Lanz et al., 2007b). The factor profiles used to constrain the PMF solution can be taken from the database of factor profiles obtained all around the world, from the previous dataset obtained at the same sampling site or taken from your own dataset. If the time of the certain source is known and the source is the most prominent over other sources in that time period, PMF can be run just on data collected in during that time and profile can be obtained. Primary factor profiles that are not subject to significant changes are usually used to constrain the factor solution.

Various factors have been identified by the PMF factor analysis of OA data, with the most common being HOA and OOA (Zhang et al., 2005a; Zhang et al., 2005b). It was suggested by Volkamer et al., 2006 that HOA corresponds to POA, while OOA represents SOA under most conditions. The hydrocarbon-like aerosol provides recognizable AMS signals at m/z 41, 43, 55, 57, which are related to alkyl ion peaks. The hydrocarbon-like profile is mainly related to road traffic sources and often characterized with prominent signals in morning and afternoon traffic peak hours, which are common for urban areas. It correlates with compounds that serve as tracers for primary sources, such as NO_X and CO (Lanz et al., 2007a; Ulbrich et al., 2009). The OOA fraction can be further apportioned to low-volatility oxygenated OA (LV-OOA) and semivolatile

oxygenated OA (SV-OOA) (Jimenez et al., 2009; Lanz et al., 2007a; Ng et al., 2010; Ulbrich et al., 2009). These two OOA factors are characterized by different degrees of oxidation and volatility (Lanz et al., 2007a). As organic material becomes more processed, it often becomes less volatile (Goldstein and Galbally, 2007). The low-volatility oxygenated OA is mainly in aerosol-phase, while SV-OOA fraction often partitions between gas and aerosol phase. It has been established by the majority of studies that LV-OOA is characterized by higher signals at m/z 44 and less intense peaks at m/z 43 compared to SV-OOA (Ulbrich et al., 2009). Contribution of LV-OOA is dominated during midday hours, which illustrates time of intense photochemical activity when low volatility products of NMOCs atmospheric oxidation partition onto the existing aerosol surface.

There are also environment-specific factors such as BB-related OA (BBOA) and cooking-related OA (COA). The BB aerosols measured by the AMS and further investigated with the PMF technique provide the BBOA factor with distinctive levoglucosan-related peaks at m/z 60 and 73. The PMF BBOA factors can identify BB plumes of different degrees of aging through the contribution of m/z 44, 43, 55, 57 and 60 (Bougiatioti et al., 2014; Brito et al., 2014; Capes et al., 2008). The cooking-related aerosols give the PMF factor (COA) that is similar to HOA, with same m/z 41, 43, 55, 57 mass spectrum signals. Both peaks m/z 55 and 57 were attributed to primary combustion-related OA; however, the COA factor has dominant m/z 55 signal over m/z 57 (Allan et al., 2010; Mohr et al., 2012; Sun et al., 2011). Cooking emissions also often give enhanced COA contributions during typical meal times and can be therefore distinguished from other sources including the HOA.

Urban aerosol sources can be distinguished from biogenic, remote sources by different PMF-resolved source apportionment factors. The PMF solution of urban aerosol is mostly comprised of HOA, COA and BBOA factors, while remote areas will likely illustrate biogenic sources and often BBOA. An example of a biogenic factor is isoprene-related OA, which is related to isoprene oxidation products (isoprene epoxydiols, IEPOX) that contribute significantly to the global SOA yields (Budisulistiorini et al., 2013; Hu et al., 2015; Lin et al., 2011; Robinson et al., 2011). The PMF-resolved isoprene-realted factor is characterised by the prominent signals at m/z 82, 53, 43 and 44. A f82 background value of 0.0017 was suggested for the environments strongly influenced by the BB emissions (Hu et al., 2015). Biogenically-emitted isoprene, along with monoterpenes makes up a dominant fraction of the global gas-phase NMOCs. The isoprene-related oxidation products have significant contribution to the SOA formation (Guenther et al., 2012), especially in the tropical regions where isoprene can contribute up to 80 % of the global annual emissions, mostly due to warm conditions (Guenther, 2006). In Australia, isoprene makes up 64-100 % of NMOCs emitted from different eucalyptus species (He et al., 2000), that make up the most of three species in Australia.

2.3 Aging of biomass burning emissions

In the atmosphere, fresh plumes are subject to chemical, physical and mechanical transformations, driven by different physicochemical and meteorological factors (Akagi et al., 2012). A BB aerosol lifetime of 3.8 ± 0.8 days has been suggested (Edwards et al., 2006), which gives enough time for significant atmospheric changes. It was shown that BB emissions contain semivolatile organic compounds that can partition in between particle and gaseous phase (Grieshop et al., 2009; Huffman et al., 2009; Robinson et al., 2007). It has also been observed that, in addition to the gas-phase oxidation in the atmosphere, aqueous phase oxidation can have a partial contribution to the aging of BB aerosol (Zhao et al., 2014).

The characterization and aging of BB aerosols has been investigated in many field and laboratory-based measurements. The field measurements include ground-based sampling, as well as aircraft measurements (Capes et al., 2008; DeCarlo et al., 2010; Yokelson et al., 2009). Tracking BB emissions in a plume provides insight into the real time atmospheric transformation processes (dilution, nucleation, condensation, repartitioning, oxidation, fragmentation etc.), changes in chemical functionality, and SOA and ozone production. There are also many laboratory-based measurements on this subject (Hennigan et al., 2011; Heringa et al., 2011; Ortega et al., 2013).

The chemical evolution of BB emissions can be estimated using different approaches, including previously described fractional analysis through a graphical approach introduced by Cubison et al. (2011), a method suggested by Heald et al. (2010) using elemental ratios and a factor analysis using PMF (Bougiatioti et al., 2014; Brito et al., 2014; Zhang et al., 2015).

The evolution of BB emissions in the ambient atmosphere often results in an enhanced portion of OOA and degradation of BB-related species (Capes et al., 2008; Cubison et al., 2011; DeCarlo et al., 2008). Therefore, most of the studies demonstrated the same trend of f44 increase and f60 decrease with plume aging (Alfarra et al., 2007; May et al., 2015). The graphical approach introduced by Cubison et al. (2011) has been widely applied in characterization and evolution estimation of BB plumes. The fresh BB aerosol can be distinguished from processed fraction by estimating f44 and f60 values from the plot (f44 vs f60) (Fig. 2.4).

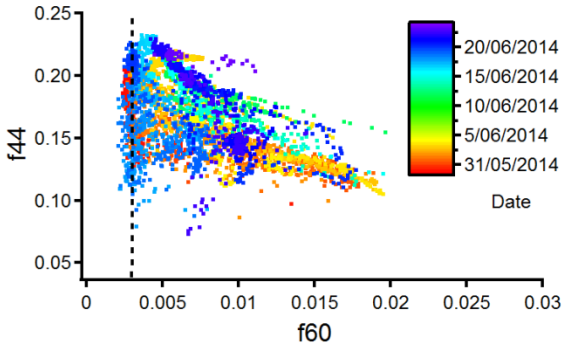

Figure 2.4 f44 versus f60 plot colored by date for distant fires during SAFIRED campaign (modified from Cubison et al. (2011)); vertical black lines refer to the f60 background level of 0.003.

In addition to the fraction analysis approach, a simplified graphical method that utilizes the AMS data to estimate the evolution in total OA composition is the van Krevelen diagram introduced by Heald et al. (2010). Based on a slope of the fitted line within the diagram of bulk elemental ratios, H/C versus O/C, the overall nature of aerosol chemical changes can be assessed. More precisely, the slope that OA data follow indicates functional groups that are adjoined to the OA material and further the changes in the chemical composition of bulk OA in the atmosphere. With the aging processes OA gets enriched in its oxygenated fraction (increase in O/C ratio). Ambient and laboratory data analysed with this approach dominantly followed the slope of -1, which indicates dominate pathways of carboxyl group addition without fragmentation, or simultaneous addition of hydroxyl (-OH) and carbonyl groups (C=O) on different carbon atoms.

A change in the chemical functionality of BB plumes as they move from the source can be also illustrated by different PMF factor profiles. Some studies have reported different PMF factors that correspond to detected BB plumes of different aging degree, like “fresh” and “aged” BBOA factors (Bougiatioti et al., 2014; Brito et al., 2014; Capes et al., 2008). As mentioned earlier, BBOA factors have distinctive m/z 60 and 73. However, fragments related to fresh hydrocarbon-like organic fraction m/z 27, 29, 41, 43, 55, and 57 are prominent in “fresh” BBOA spectrum while on other hand enhanced OOA-related m/z 28 and 44 are signatures of “aged” BBOA mass spectrum. In addition, processed BB aerosol can lose its BB signature during the atmospheric transformations and transit to highly oxygenated aerosol fraction, which corresponds to LV-OOA factor (Jimenez et al., 2009). Contribution of organics at m/z 44 and 43 can also vary due to different burning materials/conditions. More precisely, biomass combustion can contribute to less or more oxygenated species.

2.3.1 Secondary organic aerosol formation

The secondary organic aerosol fraction makes up a significant portion of the total atmospheric aerosol mass. The estimated SOA annual production is 140–910 TgC/yr out of the 1300 TgC/yr emitted volatile organic compounds (VOC) (Goldstein and Galbally, 2007). The SOA is a significant contributor to air pollution, especially during summer when more intensive

photochemical processes are taking place (de Gouw and Jimenez, 2009). Furthermore, these species have considerable effects on the human health (Hallquist et al., 2009; Pope III and Dockery, 2006) and also affect radiation balance and therefore climate by scattering insolation and by acting as a CCN.

Primary BB emissions are the subject of atmospheric chemical aging process that often includes the changes in aerosol chemical composition and condensation and nucleation of species, and therefore they are found to be strongly associated with SOA formation (Cheng et al., 2013; DeCarlo et al., 2010). Recent field and laboratory studies have investigated the evolution of BB plume emissions. There is no observed consistency in the OA production in BB emission with aging. Some studies showed an increase in OA mass with plume age (DeCarlo et al., 2010; Heringa et al., 2011; Lee et al., 2008; Yokelson et al., 2009), while others have found there is no significant change in OA fraction (Akagi et al., 2012; Brito et al., 2014; Capes et al., 2008; Cubison et al., 2011; May et al., 2015). The need for additional OA data in the tropics and the Southern Hemisphere, due to limited information about SOA sources (including biogenic and BB sources), is suggested by Spracklen et al. (2011).

2.3.2 Ozone formation

The aging of BB plumes induce the production of another secondary pollutant, tropospheric ozone (O_3). Major O_3 precursors (NOx, NMOCs and CO) emitted by a fire can promote additional pathways for ozone generation (Jaffe and Wigder, 2012; Parrington et al., 2013; Real et al., 2007). The ozone enhancements in BB emissions are therefore used as a proxy for air mass photochemical activity (Hobbs et al., 2003; Jaffe and Wigder, 2012; Real et al., 2007; Yokelson et al., 2009).

The change of ozone relative to the change of CO ($\Delta O_3/\Delta CO$) has an increased pattern with aging of aerosols (Jaffe et al., 2013; Wigder et al., 2013; Yokelson et al., 2009). According to Mauzerall et al. (1998) and Honrath et al. (2004) $\Delta O_3/\Delta CO$ values for aged BB aerosols range between 0.1 and 0.7, with the average ratio of 0.4 for wildfires in tropical and equatorial areas (Jaffe and Wigder, 2012). The ozone generation from the fires can vary significantly depending on the composition of BB emissions, meteorological conditions, interactions with emissions from other sources and the physicochemistry in the atmosphere.

2.4 Biomass burning characterization and aging around the world with focus on China

In order to put the BB aerosol aging issue into a more wider global context, a comprehensive review on BB-related aerosol emissions and the aging of BB emissions was completed. This resulted in a contribution for a review paper with a special focus on China (Chen et al., 2016), which includes a large database that can be used as a foundation of performed research on BB emissions and the aging of BB emissions around the world. The performed literature review is presented in the following paragraphs (2.4.1 and 2.4.2).

2.4.1 Particulate matter

Particulate matter (PM) is a dominant contributor to the air pollution in China (Fang et al., 2009). In particular, Eastern and Southern China, including Beijing-Tianjin-Hebei (BTH) Province, the Yangtze River Delta (YRD) and the Pearl River Delta (PRD) are subjected to severe PM pollution. Daily average $PM_{2.5}$ concentrations during severe haze periods in 2013 are 159, 91, 69 and 345 μg/m^3 for Beijing, Shanghai, Guangzhou and Xi'an, respectively (Huang et al., 2014). All $PM_{2.5}$ values are significantly higher than 25 μg/m^3,a threshold recommended by the World Health Organization (WHO). Concentrations above this threshold are unhealthy. To address serious PM pollution issue, the Chinese government announced the long-term plan to reduce the $PM_{2.5}$ concentration by 25%, 20%, 15% and 10% comparing to 2012 levels by 2017, in BTH, YRD, PRD and other cities, respectively (*http://www.gov.cn/zwgk/2013-09/12/content_2486773.htm).* For instance, the annual value for $PM_{2.5}$ in Beijing is targeted to 60 μg/m^3, which would be still high comparing to the values recommended by WHO (annual mean of 10 μg/m^3), but a big step in air pollution regulation in China. This is a challenge since heavy pollution is still observed for Beijing, with mean annual PM2.5 of 86 μg/m^3 in 2014 (Zhang et al., 2016a).

Carbonaceous material

In general, carbonaceous matter is the dominant particle-phase fraction detected in BB emissions (Li et al., 2016; Fu et al., 2012, 2014; Bond et al., 2004; Formenti et al., 2003; Hallquist et al., 2009; Reid et al., 2005). In fact BB combustion sources are considered as the largest contributors of primary carbonaceous particles in the atmosphere (Hallquist et al., 2009; Bond et al., 2004; Crutzen et al., 1990). Many studies investigated the dominant sources of $PM_{2.5}$ and carbonaceous species in China, mostly using the offline sampling techniques in urban Beijing region (Zheng et al., 2005; Cheng et al., 2014a; Cheng et al., 2013; Song et al., 2007; Song et al., 2006; Wang et al., 2007; Wang et al., 2009; Yu et al., 2013). Some of these are illustrated in Table 1. For instance, Positive Matrix Factorization (PMF) source apportionment performed on data collected in 2000 over the whole year in Beijing, illustrates that on average, 11% of $PM_{2.5}$ was influenced by BB activities (Song et al., 2006). Using the same source apportionment method, Yu et al. (2013) observe a similar contribution in Beijing in 2010. According to studies summarized in Table 1, the contribution of BB activities can go up to 19%, 25% and 37% in autumn, winter and summer months, respectively. It is observed that BB is one of the main sources that contribute to fine particle and carbonaceous emissions (besides traffic and coal combustion sources) in China (Chan et al., 2008). Moreover, in recent years source apportionment has been performed on the organic aerosol (OA) data collected by Aerosol Mass Spectrometer (AMS) using mostly the PMF technique. The significance of BB emissions (mainly due to burning of crop residues during harvesting periods) in urban and rural areas of China is shown through the high contribution of PMF-resolved BB-related factors. Similar BB OA contribution is found for urban and rural PRD area (24%) and smaller for urban Beijing (12-19%) and Nanjing area (8%) for autumn period (Zhang et al., 2015a; He et al., 2011a; Huang et al., 2011; Xu et al., 2015; Zhang et al., 2010). A significant contribution of BB-related organic aerosol is also found in the winter period (30%) and over the summer months (15%) (Huang et al., 2013; Zhang et al., 2015a). As it can be seen, there is significant seasonality in BB

activities and contribution to PM pollution in China. BB contribution seen through increased $PM_{2.5}$ and its constituents is highly seasonal but present over the whole year. The $PM_{2.5}$ increase in autumn and spring is mainly attributed to BB from crop residues burning. In late September and October harvesting period is taking place and contribution of BB is found to be the highest in this time of a year (Zheng et al., 2005; Duan et al., 2004; Yu et al., 2013; Zhang et al., 2015c). Over summer months, the BB contribution ambient PM is significant from wheat straw burning while winter PM pollution is mainly driven by coal combustion sources that are predominantly used as heating systems, although BB contribution can be significant (Yu et al., 2013; Li et al., 2008). Apart from seasonal differences, the portion of aerosol mass influenced by BB varies depending on the region of China. Huang et al. (2014)(2014) illustrate higher BB contribution in Guangzhou and Xi'an (5-9% of $PM_{2.5}$) compared to Beijing and Shanghai (4-7% of $PM_{2.5}$).

The main component of BB submicron carbonaceous mass is the OA fraction that can go up to 90% (Bond et al., 2004). Global annual emission of OC and BC emitted in open fire events is estimated to be approximately 70% and 40%, respectively (Bond et al., 2004). Studies of both the urban and peri-urban areas of Beijing show that during intense BB pollution episodes, more than the half of OC and EC could be from BB emissions (Yao et al., 2016; Cheng et al., 2013; Cheng et al., 2014b; Duan et al., 2004).

Other important particulate components

Levoglucosan-like species (levoglucosan, mannosan, galactosan) are anhydrosaccharides formed in the pyrolysis of cellulose and common organic molecular constituents of BB emissions (Li et al., 2016b; Simoneit et al., 1999). Many studies worldwide, including in China, have used levoglucosan (dominant anhydrosaccharide emitted) as a distinctive BB chemical signature (Zhang et al., 2010a; Fraser et al., 2003; Jordan et al., 2006; Simoneit, 2002; Simoneit et al., 1999; Song et al., 2007; Wang et al., 2007; Wang et al., 2009a; Zhang et al., 2008c). Levoglucosan concentrations vary considerably depending on season and region (Table 1). For instance, He et al. (2006)(2006) investigated organic tracer compounds including particulate levoglucosan during all seasons in Beijing. Levoglucosan average mass concentrations were observed to be 0.12, 0.08 and 0.03 $\mu g/m^3$ in autumn, winter and summer, respectively. Considerably higher levoglucosan concentrations were observed by Wang et al. (2007)(2007) in autumn (0.1-0.9 $\mu g/m^3$). Moreover, there is a wide range of detected levoglucosan in winter (0.08-3.10 $\mu g/m^3$) and summer (0.03-0.31 $\mu g/m^3$) months. Potassium-rich particles are observed to be a common fraction of plume emissions in China (Li et al., 2007; Li et al., 2010c; Li et al., 2009). BB emissions often have high potassium levels and therefore potassium has been used as a BB tracer (Zhang et al., 2015b; Cheng et al., 2013; Cheng et al., 2014; Duan et al., 2004; He et al., 2011a; Huang et al., 2012a; Wang et al., 2007; Yu et al., 2013; Zhang et al., 2010a). Similar average potassium concentrations can be observed according to studies summarized in Table 1. Potassium average concentrations vary from 2.42 to 2.78 in winter, 1.6 to 4.9 in summer and 1.7 to 2.26 $\mu g/m^3$ in autumn months deepening on the monitored areas. (Yu et al., 2013) (2013) suggest 2.2 $\mu g/m^3$ for the annual potassium value, based on continuous measurements for one year in Beijing. In contrast to source-specific levoglucosan, water-soluble

potassium can indicate particles of more than one origin (Zhang et al., 2010b; Aiken et al., 2010). In the absence of other important sources, such as soil dust, sea salt and meat charbroiling, water soluble potassium can be acceptable BB marker (Schauer et al., 1999; Andreae, 1983). Wang et al. (2007) (2007) show that application of potassium as a reliable smoke tracer is limited in Guangzhou area during the October BB period due to interferences with meat charbroiling and transportation-related potassium emissions. Fireworks are also found to influence enhanced potassium concentration (Zhang et al., 2010; Vecchi et al., 2008). In particular, water soluble potassium has not been considered to be suitable or at least it shouldn't be used as the only BB tracer over winter in Beijing, during periods with significant festival fireworks influence (Yu et al., 2013; Cheng et al., 2014a; Cheng et al., 2013).

Although all results illustrate significant impact of BB sources to PM pollution over China, until recently, it is mostly ignored as a significant contributor in pollution inventories (e.g. Zhang et al., 2009). Zhang and Cao (2015) (2015d) suggest that regulations about BB emissions should be revised and scaled down in both urban and rural areas and for open BB as well as in household consumption. It is estimated by Cheng et al. (2014) (2014b) that $PM_{2.5}$ level could be reduced by 47% in YRD region if open post-harvest BB activities are banned, suggesting significant benefit for the environment and human health.

2.4.2. Atmospheric aging

So far the main approaches used in China to investigate aging of BB emissions are transmission electron microscopy (TEM) coupled with energy-dispersive X-ray (EDX) spectroscopy and aerosol mass spectrometry. More details about studies performed and results obtained related to these approaches are given in the following paragraphs.

TEM coupled with energy-dispersive X-ray spectroscopy (EDX) approach

Changes in morphology, composition and mixing state of individual BB-related particles during the aging were extensively investigated in China using the TEM coupled with EDX spectroscopy. A similar approach has been used in other parts of the world (Semeniuk et al., 2007; Pósfai et al., 2003). Some important features of BB-related particles transformed during the aging are presented here. Soot (EC), organic carbon, potassium nitrate (KNO_3) and potassium sulfate (K_2SO_4) are the dominant species found in BB plumes emitted during the agricultural burning activities (Li et al., 2010), the major source of BB aerosol in China. Potassium species are predominantly composed of KNO_3 and K_2SO_4 that are formed in heterogeneous reactions of nitric and sulfuric acids with potassium chloride (KCl), an important fraction of fresh plume emissions (Li et al., 2015; Engling et al., 2009; Li et al., 2003). It is observed that during the aging of BB smoke, potassium rich particles form inclusions/aggregations with organic matter and that organic species found in these forms are mostly of hydrophobic nature. Potassium rich species in aging studies, observed in China, are also often covered by a layer of organics, which are found to be predominantly water soluble species (Li and Shao, 2010). Organic coatings are associated with SOA formation, more precisely they are formed in the partitioning of low volatility species that are products of VOC oxidation (Yao et al., 2016;

Fu et al., 2012; Li et al., 2010b). Li and Shao (2009) (2009) suggested that organic coatings can be an explanation for the increased cooling effect observed in China during periods of high brown haze and relative humidity. Soot particles in BB emissions can be found in a form of aggregates or inclusions mostly with potassium and sulfur rich compounds and/or organic species (Li et al., 2010b, 2010c; Johnson et al., 2005). Therefore processing of soot aerosol with plume age often alters its inert and hydrophobic structure. Spherical species similar to tar balls, which are suggested to be a fraction of aged plumes (Pósfai et al., 2003), were also found in BB emissions in China (Fu et al., 2012). According to these studies, organics can significantly change the morphology, composition, mixing state, size and hygroscopicity of inorganic and soot particles and can further drive the atmospheric fate of these species (e.g. CCN potential and physicochemical reactivity).

Aerosol mass spectrometry approach

In general, the main aim of monitoring aging of smoke plumes has been directed to organic species as they are mostly non-inert atmospheric fractions with comprehensive structure and therefore complex atmospheric fate. The chemical aging of OA portion in BB plumes has been extensively investigated using the AMS technique (DeCarlo et al., 2010; Capes et al., 2008; Cubison et al., 2011; Yokelson et al., 2009). A graphical approach introduced by Cubison et al. (2011) (Cubison et al., 2011) has been widely applied in characterization and evolution estimation of BB plumes. Fresh BB aerosols can be easily distinguished from aged, highly oxidized species by estimating f_{44} and f_{60} from the plot (f_{44} vs f_{60}). Most of the studies have demonstrated the same trend of f44 increase and f60 decrease with aging (May et al., 2015; Alfarra et al., 2007). This approach has limited use in studies performed in China due to difficulties to separate the BB plume emissions from a number of other pollutants abundant in China (Zhang et al., 2015a; Xu et al., 2015). In the Xu et al. (2015) study that employed the AMS during intense BB periods in China, a decreasing trend of f60 and increasing trend of f44 with aging was observed.

Aging of smoke plumes as they move from the source can also be illustrated by the change in the mass spectrum of different factors extracted by a Positive Matrix Factorization (PMF). A fresh PMF-resolved BBOA factor was extracted during the autumn season in urban and rural areas of Pearl River Delta (PRD) with oxygen to carbon (OC) ratio of 0.32 and 0.27, respectively (Huang et al., 2011; He et al., 2011a). Detected BB aerosol was associated with crop burning emissions. A BBOA profile with the same OC ratio (0.26) was seen in winter for Yangtze River Delta (YRD) region, possibly due to open burning in the farmlands (Huang et al., 2013). Low OC ratio in these studies indicates presence of primary emissions. BBOA profiles with similar OC contribution were extracted in many laboratory and ambient studies (He et al., 2010; Aiken et al., 2009; Chirico et al., 2010; Crippa et al., 2014; DeCarlo et al., 2008; Grieshop et al., 2009). PMF-resolved aged BBOA profile was also extracted in China. During an autumn period in Beijing (Xu et al., 2015) BBOA factor with OC ratio of 0.5 was extracted, similarly to the profile observed in YRD during the same season period (Zhang et al., 2015a). These oxygenated BB profiles are comparable to studies outside of China (DeCarlo et al., 2010; Brito et al., 2014) and can be related to aged plumes probably transported from the surrounding regions. Aged BB aerosol can lose its BB signature during the atmospheric transformations and transit to a highly oxygenated aerosol fraction, which corresponds to the PMF-resolved

low volatility OOA (LVOOA) factor (Jimenez et al., 2009). Zhang et al. (2015) (2015a) observed a decreasing trend of BBOA factors with aging suggesting the fast evolution of smoke organic fraction into OOA-like species.

Aerosol processing has been investigated in Beijing during winter (Sun et al., 2013) and summer (Sun et al., 2012) periods, using an aerosol chemical speciation monitor for chemical composition measurements. The portion of organics was found to be higher in winter time (52%) compared to summer time (40%). This trend was attributed to increased POA fraction (mainly coal emissions but also includes BB and traffic plumes) that contributes to 70% of OC, while SOA contribution was shown to be similar in both seasons. In addition, it is suggested that contrary to the summer period, when photochemical processing is dominant due to increased temperature and solar radiation, winter time is instead characterized by aqueous reactions of primary emissions that are emitted and accumulated over the night, when partitioning of gaseous species due to low temperature and high relative humidity is taking place.

Ozone formation in biomass burning emissions

It has been observed that aging of BB plumes can induce production of tropospheric ozone (Real et al., 2007). Ozone enrichments that have been associated with BB have been observed mainly in Southeast China. The highest ozone concentration over the PRD region was shown to be in the spring season with concentrations up to 138 ppbv (Liu et al., 1999). Increased ozone pollution in this region has frequently been observed by number of studies and attributed to transport of photochemically produced ozone initiated by the BB plumes from fires in the South-East Asia (Indo Burma region) (Deng et al., 2008; Chan et al., 2003; Chan et al., 2000). Increased ozone concentrations related to BB activities (dominantly from post-harvest crop burning) during the summer period has also been observed in YRD (Cheung et al., 2001) and in urban and rural parts of Northern China (Meng et al., 2009; Ding et al., 2007). These authors also suggested a significant impact of transported aged smoke masses that carry photochemically-formed ozone.

As ozone is a secondary pollutant that reflects the photochemical potential of the atmosphere, ozone enhancement in BB emissions has been used as a proxy for air mass photochemical activity (Yokelson et al., 2009; Hobbs et al., 2003; Jaffe et al., 2012; Real et al., 2007). According to studies in China, high photochemical activity illustrated by ozone enrichments can indicate an environment conducive to secondary aerosol formation. The ratio of ozone relative to CO ($\Delta O_3/\Delta CO$) increases with the aging of BB aerosols (Yokelson et al., 2009; Jaffe et al., 2013; Wigder et al., 2013). According to Mauzerall et al. (1998) and Honrath et al. (2004), $\Delta O_3/\Delta CO$ values for aged BB aerosols range between 0.1 and 0.7 (Jaffe et al., 2012). To the best of our knowledge studies like this have not been published so far in China. This again emphasizes the need to perform smoke tracking experiments in China, especially in the highly polluted Eastern part, in order to estimate the potential for SOA formation and the role of ozone in this process in highly polluted areas.

The evolution and processing of smoke emissions and their influence on air quality in China is still poorly understood (Zhang et al., 2015a). It is a challenge to isolate the plume emissions and monitor them in highly polluted environments with a number of different sources. It has been observed that BB emissions which are in the process of aging, can be promptly transformed into the OOA fraction. Therefore, BB emissions can influence the SOA budget in China. Ozone enrichments in BB plumes also suggest intensive photochemistry in the atmosphere across China. It is also important to characterize the mixing of plumes with other regional pollutants in the atmosphere during the aging process (Cubison et al., 2011), as China has many other important pollution sources. According to the reviewed studies, better regulation of BB activities is still needed in order to provide a less polluted environment. Huang et al. (2014) (2014) suggested regulating BB activities in China, especially in Guangzhou and Xi'an where higher non-fossil carbon fractions of SOA (up to 85% of SOA mass) than in Shanghai and Beijing was attributed to enhanced BB contribution.

2.5 Aging in different environments

As mentioned earlier, atmospheric aging is driven by physicochemistry and meteorological conditions of the environment where emissions are emitted and transported. It was recently shown that according to O/C value for PMF-resolved LV-OOA profile, the Southern Hemisphere (Crilley et al., 2014a) has a higher content of OOA than the Northern Hemisphere (He et al., 2011; Huang et al., 2010; Ng et al., 2010; Sun et al., 2011). There are just a few source apportionment OA AMS analyses done for the Southern atmosphere (Crilley et al., 2014a; Crilley et al., 2014b). Results from Brisbane and Gunn Point campaigns that are presented within this thesis can be used as a confirmation of the observed aging parameters.

2.6 Gaps in research

There are high uncertainties in characterization of BB emissions, especially in the organic fraction. This lack of knowledge can contribute to model uncertainties, and incorrect estimation of BB influence onto climate, air pollution and public health. Australia is a globally significant source of BB aerosols; however, there are insufficient observational data of BB emissions characterization and aging in both urban and remote areas. The source apportionment of the urban and remote OA is not sufficiently characterized as well. There is no comparison in OA aging for remote and urban areas in Australia. To confirm the previous observations of the higher degree of aging from the Southern Hemisphere compared to the Northern Hemisphere and to provide more data to be used for climate and air quality model and inventories development, more data collected in unique Australian conditions is needed.

2.7 References

Aiken A, Foy Bd, Wiedinmyer C, DeCarlo P, Ulbrich IM, Wehrli M, et al. Mexico city aerosol analysis during MILAGRO using high resolution aerosol mass spectrometry at the urban supersite (T0)–Part 2: Analysis of the biomass burning contribution and the non-fossil carbon fraction. Atmospheric Chemistry and Physics 2010; 10: 5315-5341.

Aiken A, Salcedo D, Cubison MJ, Huffman J, DeCarlo P, Ulbrich IM, et al. Mexico City aerosol analysis during MILAGRO using high resolution aerosol mass spectrometry at the urban supersite (T0)–Part 1: Fine particle composition and organic source apportionment. Atmospheric Chemistry and Physics 2009; 9: 6633-6653.

Aiken AC, DeCarlo PF, Jimenez JL. Elemental analysis of organic species with electron ionization high-resolution mass spectrometry. Analytical Chemistry 2007; 79: 8350-8358.

Aiken AC, DeCarlo PF, Kroll JH, Worsnop DR, Huffman JA, Docherty KS, et al. O/C and OM/OC ratios of primary, secondary, and ambient organic aerosols with high-resolution time-of-flight aerosol mass spectrometry. Environmental Science & Technology 2008; 42: 4478-4485.

Akagi S, Craven J, Taylor J, McMeeking G, Yokelson R, Burling I, et al. Evolution of trace gases and particles emitted by a chaparral fire in California. Atmospheric Chemistry and Physics 2012; 12: 1397-1421.

Akagi S, Yokelson RJ, Burling IR, Meinardi S, Simpson I, Blake D, et al. Measurements of reactive trace gases and variable O 3 formation rates in some South Carolina biomass burning plumes. Atmospheric Chemistry and Physics 2013; 13: 1141-1165.

Akagi S, Yokelson RJ, Wiedinmyer C, Alvarado M, Reid J, Karl T, et al. Emission factors for open and domestic biomass burning for use in atmospheric models. Atmospheric Chemistry and Physics 2011; 11: 4039-4072.

Alfarra MR, Coe H, Allan JD, Bower KN, Boudries H, Canagaratna MR, et al. Characterization of urban and rural organic particulate in the lower Fraser valley using two aerodyne aerosol mass spectrometers. Atmospheric Environment 2004; 38: 5745-5758.

Alfarra MR, Prevot AS, Szidat S, Sandradewi J, Weimer S, Lanz VA, et al. Identification of the mass spectral signature of organic aerosols from wood burning emissions. Environmental science & technology 2007; 41: 5770-5777.

Allan J, Williams P, Morgan W, Martin C, Flynn M, Lee J, et al. Contributions from transport, solid fuel burning and cooking to primary organic aerosols in two UK cities. Atmospheric Chemistry and Physics 2010; 10: 647-668.

Allan JD, Delia AE, Coe H, Bower KN, Alfarra MR, Jimenez JL, et al. A generalised method for the extraction of chemically resolved mass spectra from Aerodyne aerosol mass spectrometer data. Journal of Aerosol Science 2004; 35: 909-922.

Andreae MO. Soot carbon and excess fine potassium: Long-range transport of combustion-derived aerosols. Science 1983; 220: 1148-1151.

Bond TC, Streets DG, Yarber KF, Nelson SM, Woo JH, Klimont Z. A technology-based global inventory of black and organic carbon emissions from combustion. Journal of Geophysical Research: Atmospheres (1984–2012) 2004; 109.

Bougiatioti A, Stavroulas I, Kostenidou E, Zarmpas P, Theodosi C, Kouvarakis G, et al. Processing of biomass-burning aerosol in the eastern Mediterranean during summertime. Atmospheric Chemistry and Physics 2014; 14: 4793-4807.

Brito J, Rizzo L, Morgan W, Coe H, Johnson B, Haywood J, et al. Ground-based aerosol characterization during the South American Biomass Burning Analysis (SAMBBA) field experiment. Atmospheric Chemistry and Physics 2014; 14: 12069-12083.

Budisulistiorini SH, Canagaratna MR, Croteau PL, Marth WJ, Baumann K, Edgerton ES, et al. Real-time continuous characterization of secondary organic aerosol derived from isoprene epoxydiols in downtown Atlanta, Georgia, using the Aerodyne Aerosol Chemical Speciation Monitor. Environmental science & technology 2013; 47: 5686-5694.

Canagaratna M, Jayne J, Jimenez J, Allan J, Alfarra M, Zhang Q, et al. Chemical and microphysical characterization of ambient aerosols with the aerodyne aerosol mass spectrometer. Mass Spectrometry Reviews 2007; 26: 185-222.

Canagaratna M, Jimenez J, Kroll J, Chen Q, Kessler S, Massoli P, et al. Elemental ratio measurements of organic compounds using aerosol mass spectrometry: characterization, improved calibration, and implications. Atmospheric Chemistry and Physics 2015; 15: 253-272.

Canonaco F, Crippa M, Slowik J, Baltensperger U, Prévôt A. SoFi, an IGOR-based interface for the efficient use of the generalized multilinear engine (ME-2) for the source apportionment: ME-2 application to aerosol mass spectrometer data. Atmospheric Measurement Techniques 2013; 6: 3649-3661.
Capes G, Johnson B, McFiggans G, Williams P, Haywood J, Coe H. Aging of biomass burning aerosols over West Africa: Aircraft measurements of chemical composition, microphysical properties, and emission ratios. Journal of Geophysical Research: Atmospheres (1984–2012) 2008; 113.
Cheng Y, Engling G, He K-b, Duan F-k, Du Z-y, Ma Y-l, et al. The characteristics of Beijing aerosol during two distinct episodes: Impacts of biomass burning and fireworks. Environmental Pollution 2014; 185: 149-157.
Cheng Y, Engling G, He K-B, Duan F-K, Ma Y-L, Du Z-Y, et al. Biomass burning contribution to Beijing aerosol. Atmospheric Chemistry and Physics 2013; 13: 7765-7781.
Chirico R, DeCarlo P, Heringa M, Tritscher T, Richter R, Prévôt A, et al. Impact of aftertreatment devices on primary emissions and secondary organic aerosol formation potential from in-use diesel vehicles: results from smog chamber experiments. Atmospheric Chemistry and Physics 2010; 10: 11545-11563.
Crilley LR, Ayoko GA, Morawska L. First measurements of source apportionment of organic aerosols in the Southern Hemisphere. Environmental Pollution 2014a; 184: 81-88.
Crilley LR, Jayaratne ER, Ayoko GA, Miljevic B, Ristovski Z, Morawska L. Observations on the formation, growth and chemical composition of aerosols in an urban environment. Environmental science & technology 2014b; 48: 6588-6596.
Crutzen PJ, Andreae MO. Biomass burning in the tropics: Impact on atmospheric chemistry and biogeochemical cycles. Science 1990; 250: 1669-1678.
Cubison M, Ortega A, Hayes P, Farmer D, Day D, Lechner M, et al. Effects of aging on organic aerosol from open biomass burning smoke in aircraft and laboratory studies. Atmospheric Chemistry and Physics 2011; 11: 12049-12064.
Davis M, Crowcier C, Richardson Jr J. Importance of biomass burning in the atmospheric budgets of nitrogen-containing gases. Nature 1990; 346.
De Gouw J, Jimenez JL. Organic aerosols in the Earth's atmosphere. Environmental science & technology 2009; 43: 7614-7618.
DeCarlo P, Dunlea E, Kimmel J, Aiken A, Sueper D, Crounse J, et al. Fast airborne aerosol size and chemistry measurements above Mexico City and Central Mexico during the MILAGRO campaign. Atmos. Chem. Phys 2008; 8: 4027-4048.
DeCarlo P, Ulbrich I, Crounse J, Foy Bd, Dunlea E, Aiken A, et al. Investigation of the sources and processing of organic aerosol over the Central Mexican Plateau from aircraft measurements during MILAGRO. Atmospheric Chemistry and Physics 2010; 10: 5257-5280.
DeCarlo PF, Kimmel JR, Trimborn A, Northway MJ, Jayne JT, Aiken AC, et al. Field-deployable, high-resolution, time-of-flight aerosol mass spectrometer. Analytical chemistry 2006; 78: 8281-8289.
Donahue NM, Henry KM, Mentel TF, Kiendler-Scharr A, Spindler C, Bohn B, et al. Aging of biogenic secondary organic aerosol via gas-phase OH radical reactions. Proceedings of the National Academy of Sciences 2012; 109: 13503-13508.
Drewnick F, Hings SS, DeCarlo P, Jayne JT, Gonin M, Fuhrer K, et al. A new time-of-flight aerosol mass spectrometer (TOF-AMS)—Instrument description and first field deployment. Aerosol Science and Technology 2005; 39: 637-658.
Dzepina K, Volkamer RM, Madronich S, Tulet P, Ulbrich IM, Zhang Q, et al. Evaluation of recently-proposed secondary organic aerosol models for a case study in Mexico City. Atmospheric Chemistry and Physics 2009; 9: 5681-5709.
Edwards D, Emmons L, Gille J, Chu A, Attié JL, Giglio L, et al. Satellite-observed pollution from Southern Hemisphere biomass burning. Journal of Geophysical Research: Atmospheres 2006; 111.
Emanuelsson E, Hallquist M, Kristensen K, Glasius M, Bohn B, Fuchs H, et al. Formation of anthropogenic secondary organic aerosol(SOA) and its influence on biogenic SOA properties. Atmospheric Chemistry and Physics 2013; 13: 2837-2855.
Formenti P, Elbert W, Maenhaut W, Haywood J, Osborne S, Andreae M. Inorganic and carbonaceous aerosols during the Southern African Regional Science Initiative (SAFARI 2000) experiment: Chemical characteristics, physical

properties, and emission data for smoke from African biomass burning. Journal of Geophysical Research: Atmospheres (1984–2012) 2003; 108.
Fröhlich R, Cubison M, Slowik J, Bukowiecki N, Prévôt A, Baltensperger U, et al. The ToF-ACSM: a portable aerosol chemical speciation monitor with TOFMS detection. Atmospheric Measurement Techniques 2013; 6: 3225-3241.
Goldstein AH, Galbally IE. Known and unexplored organic constituents in the earth's atmosphere. Environmental Science & Technology 2007; 41: 1514-1521.
Grieshop A, Logue J, Donahue N, Robinson A. Laboratory investigation of photochemical oxidation of organic aerosol from wood fires 1: measurement and simulation of organic aerosol evolution. Atmospheric Chemistry and Physics 2009; 9: 1263-1277.
Guenther A, Jiang X, Heald C, Sakulyanontvittaya T, Duhl T, Emmons L, et al. The Model of Emissions of Gases and Aerosols from Nature version 2.1 (MEGAN2. 1): an extended and updated framework for modeling biogenic emissions. 2012.
Guenther C. Estimates of global terrestrial isoprene emissions using MEGAN (Model of Emissions of Gases and Aerosols from Nature). Atmospheric Chemistry and Physics 2006; 6.
Hallquist M, Wenger J, Baltensperger U, Rudich Y, Simpson D, Claeys M, et al. The formation, properties and impact of secondary organic aerosol: current and emerging issues. Atmos. Chem. Phys 2009; 9: 5155-5236.
He C, Murray F, Lyons T. Monoterpene and isoprene emissions from 15 Eucalyptus species in Australia. Atmospheric Environment 2000; 34: 645-655.
He LY, Huang XF, Xue L, Hu M, Lin Y, Zheng J, et al. Submicron aerosol analysis and organic source apportionment in an urban atmosphere in Pearl River Delta of China using high-resolution aerosol mass spectrometry. Journal of Geophysical Research: Atmospheres (1984–2012) 2011; 116.
Heald C, Kroll J, Jimenez J, Docherty K, DeCarlo P, Aiken A, et al. A simplified description of the evolution of organic aerosol composition in the atmosphere. Geophysical Research Letters 2010; 37.
Hennigan C, Miracolo M, Engelhart G, May A, Presto A, Lee T, et al. Chemical and physical transformations of organic aerosol from the photo-oxidation of open biomass burning emissions in an environmental chamber. Atmospheric Chemistry and Physics 2011; 11: 7669-7686.
Hennigan CJ, Sullivan AP, Collett JL, Robinson AL. Levoglucosan stability in biomass burning particles exposed to hydroxyl radicals. Geophysical Research Letters 2010; 37.
Heringa M, DeCarlo P, Chirico R, Tritscher T, Dommen J, Weingartner E, et al. Investigations of primary and secondary particulate matter of different wood combustion appliances with a high-resolution time-of-flight aerosol mass spectrometer. Atmos. Chem. Phys 2011; 11: 5945-5957.
Hinds WC. Aerosol technology: properties, behavior, and measurement of airborne particles: Wiley-interscience, 2012.
Hobbs PV, Sinha P, Yokelson RJ, Christian TJ, Blake DR, Gao S, et al. Evolution of gases and particles from a savanna fire in South Africa. Journal of Geophysical Research: Atmospheres (1984–2012) 2003; 108.
Hoffmann D, Tilgner A, Iinuma Y, Herrmann H. Atmospheric stability of levoglucosan: a detailed laboratory and modeling study. Environmental science & technology 2009; 44: 694-699.
Honrath R, Owen RC, Val Martin M, Reid J, Lapina K, Fialho P, et al. Regional and hemispheric impacts of anthropogenic and biomass burning emissions on summertime CO and O3 in the North Atlantic lower free troposphere. Journal of Geophysical Research: Atmospheres (1984–2012) 2004; 109.
Hu W, Campuzano-Jost P, Palm B, Day D, Ortega A, Hayes P, et al. Characterization of a real-time tracer for isoprene epoxydiols-derived secondary organic aerosol (IEPOX-SOA) from aerosol mass spectrometer measurements. Atmospheric Chemistry and Physics 2015; 15: 11807-11833.
Huang X-F, He L-Y, Hu M, Canagaratna M, Sun Y, Zhang Q, et al. Highly time-resolved chemical characterization of atmospheric submicron particles during 2008 Beijing Olympic Games using an Aerodyne High-Resolution Aerosol Mass Spectrometer. Atmospheric Chemistry and Physics 2010; 10: 8933-8945.
Huffman J, Docherty K, Mohr C, Cubison M, Ulbrich I, Ziemann P, et al. Chemically-resolved volatility measurements of organic aerosol from different sources. Environmental science & technology 2009; 43: 5351-5357.
Jacobson M, Hansson HC, Noone K, Charlson R. Organic atmospheric aerosols: Review and state of the science. Reviews of Geophysics 2000; 38: 267-294.

Jaffe DA, Wigder N, Downey N, Pfister G, Boynard A, Reid SB. Impact of wildfires on ozone exceptional events in the western US. Environmental science & technology 2013; 47: 11065-11072.
Jaffe DA, Wigder NL. Ozone production from wildfires: A critical review. Atmospheric Environment 2012; 51: 1-10.
Jimenez J, Canagaratna M, Donahue N, Prevot A, Zhang Q, Kroll JH, et al. Evolution of organic aerosols in the atmosphere. Science 2009; 326: 1525-1529.
Jimenez JL, Jayne JT, Shi Q, Kolb CE, Worsnop DR, Yourshaw I, et al. Ambient aerosol sampling using the aerodyne aerosol mass spectrometer. Journal of Geophysical Research: Atmospheres (1984–2012) 2003; 108.
Jordan TB, Seen AJ, Jacobsen GE. Levoglucosan as an atmospheric tracer for woodsmoke. Atmospheric Environment 2006; 40: 5316-5321.
Kleinman LI, Springston SR, Daum PH, Lee Y-N, Nunnermacker L, Senum G, et al. The time evolution of aerosol composition over the Mexico City plateau. Atmospheric Chemistry and Physics 2008; 8: 1559-1575.
Lambe A, Chhabra P, Onasch T, Brune W, Hunter J, Kroll J, et al. Effect of oxidant concentration, exposure time, and seed particles on secondary organic aerosol chemical composition and yield. Atmospheric Chemistry and Physics 2015; 15: 3063-3075.
Lanz V, Alfarra M, Baltensperger U, Buchmann B, Hueglin C, Prévôt A. Source apportionment of submicron organic aerosols at an urban site by factor analytical modelling of aerosol mass spectra. Atmospheric Chemistry and Physics 2007a; 7: 1503-1522.
Lanz VA, Alfarra MR, Baltensperger U, Buchmann B, Hueglin C, Szidat S, et al. Source attribution of submicron organic aerosols during wintertime inversions by advanced factor analysis of aerosol mass spectra. Environmental science & technology 2007b; 42: 214-220.
Lawson S, Keywood M, Galbally I, Gras J, Cainey J, Cope M, et al. Biomass burning emissions of trace gases and particles in marine air at Cape Grim, Tasmania. Atmospheric Chemistry and Physics 2015; 15: 13393-13411.
Lee S, Kim HK, Yan B, Cobb CE, Hennigan C, Nichols S, et al. Diagnosis of aged prescribed burning plumes impacting an urban area. Environmental science & technology 2008; 42: 1438-1444.
Lin Y-H, Zhang Z, Docherty KS, Zhang H, Budisulistiorini SH, Rubitschun CL, et al. Isoprene epoxydiols as precursors to secondary organic aerosol formation: acid-catalyzed reactive uptake studies with authentic compounds. Environmental science & technology 2011; 46: 250-258.
Mauzerall DL, Logan JA, Jacob DJ, Anderson BE, Blake DR, Bradshaw JD, et al. Photochemistry in biomass burning plumes and implications for tropospheric ozone over the tropical South Atlantic. Journal of Geophysical Research: Atmospheres (1984–2012) 1998; 103: 8401-8423.
May A, Lee T, McMeeking G, Akagi S, Sullivan A, Urbanski S, et al. Observations and analysis of organic aerosol evolution in some prescribed fire smoke plumes. Atmospheric Chemistry and Physics Discussions 2015; 15: 1953-1988.
May AA, Saleh R, Hennigan CJ, Donahue NM, Robinson AL. Volatility of organic molecular markers used for source apportionment analysis: measurements and implications for atmospheric lifetime. Environmental science & technology 2012; 46: 12435-12444.
Mohr C, DeCarlo P, Heringa M, Chirico R, Slowik J, Richter R, et al. Identification and quantification of organic aerosol from cooking and other sources in Barcelona using aerosol mass spectrometer data. Atmospheric Chemistry and Physics 2012; 12: 1649-1665.
Ng N, Canagaratna M, Zhang Q, Jimenez J, Tian J, Ulbrich I, et al. Organic aerosol components observed in Northern Hemispheric datasets from Aerosol Mass Spectrometry. Atmospheric Chemistry and Physics 2010; 10: 4625-4641.
O'Brien D, Mitchell R. Atmospheric heating due to carbonaceous aerosol in northern Australia—confidence limits based on TOMS aerosol index and sun-photometer data. Atmospheric Research 2003; 66: 21-41.
Ortega A, Day D, Cubison M, Brune W, Bon D, de Gouw J, et al. Secondary organic aerosol formation and primary organic aerosol oxidation from biomass-burning smoke in a flow reactor during FLAME-3. Atmospheric Chemistry and Physics 2013; 13: 11551-11571.
Paatero P. The multilinear engine—a table-driven, least squares program for solving multilinear problems, including the n-way parallel factor analysis model. Journal of Computational and Graphical Statistics 1999; 8: 854-888.
Paatero P, Hopke PK. Rotational tools for factor analytic models. Journal of Chemometrics 2009; 23: 91-100.

Paatero P, Tapper U. Positive matrix factorization: A non-negative factor model with optimal utilization of error estimates of data values. Environmetrics 1994; 5: 111-126.
Parrington M, Palmer P, Lewis A, Lee J, Rickard A, Carlo PD, et al. Ozone photochemistry in boreal biomass burning plumes. Atmospheric Chemistry and Physics 2013; 13: 7321-7341.
Penner J, Chuang C, Grant K. Climate forcing by carbonaceous and sulfate aerosols, Clim. Dynamm., 14, 839–851. ISI 1998.
Penner JE, Dickinson RE, O'Neill CA. Effects of aerosol from biomass burning on the global radiation budget. Science 1992; 256: 1432-1434.
Pope III CA, Dockery DW. Health effects of fine particulate air pollution: Lines that connect. Journal of the Air & Waste Management Association 2006; 56: 709-742.
Real E, Law K, Weinzierl B, Fiebig M, Petzold A, Wild O, et al. Processes influencing ozone levels in Alaskan forest fire plumes during long-range transport over the North Atlantic. Journal of Geophysical Research: Atmospheres (1984–2012) 2007; 112.
Reid J, Koppmann R, Eck T, Eleuterio D. A review of biomass burning emissions part II: intensive physical properties of biomass burning particles. Atmospheric Chemistry and Physics 2005; 5: 799-825.
Robinson AL, Donahue NM, Shrivastava MK, Weitkamp EA, Sage AM, Grieshop AP, et al. Rethinking organic aerosols: Semivolatile emissions and photochemical aging. Science 2007; 315: 1259-1262.
Robinson N, Hamilton J, Allan J, Langford B, Oram D, Chen Q, et al. Evidence for a significant proportion of Secondary Organic Aerosol from isoprene above a maritime tropical forest. Atmospheric Chemistry and Physics 2011; 11: 1039-1050.
Rollins A, Browne E, Min K-E, Pusede S, Wooldridge P, Gentner D, et al. Evidence for NOx control over nighttime SOA formation. Science 2012; 337: 1210-1212.
Russell-Smith J, Yates CP, Whitehead PJ, Smith R, Craig R, Allan GE, et al. Bushfires' down under': patterns and implications of contemporary Australian landscape burning. International Journal of Wildland Fire 2007; 16: 361-377.
Sandradewi J, Prevot A, Weingartner E, Schmidhauser R, Gysel M, Baltensperger U. A Study of wood burning and traffic aerosols in an Alpine valley using a multi-wavelength aethalometer. Atmospheric Environment 2008; 42: 101-112.
Schauer JJ, Rogge WF, Hildemann LM, Mazurek MA, Cass GR, Simoneit BR. Source apportionment of airborne particulate matter using organic compounds as tracers. Atmospheric Environment 1996; 30: 3837-3855.
Schultz MG, Heil A, Hoelzemann JJ, Spessa A, Thonicke K, Goldammer JG, et al. Global wildland fire emissions from 1960 to 2000. Global Biogeochemical Cycles 2008; 22.
Simoneit BR. Biomass burning—a review of organic tracers for smoke from incomplete combustion. Applied Geochemistry 2002; 17: 129-162.
Simoneit BR, Schauer JJ, Nolte C, Oros DR, Elias VO, Fraser M, et al. Levoglucosan, a tracer for cellulose in biomass burning and atmospheric particles. Atmospheric Environment 1999; 33: 173-182.
Spracklen D, Jimenez J, Carslaw K, Worsnop D, Evans M, Mann G, et al. Aerosol mass spectrometer constraint on the global secondary organic aerosol budget. Atmospheric Chemistry and Physics 2011; 11: 12109-12136.
Sun Y-L, Zhang Q, Schwab J, Demerjian K, Chen W-N, Bae M-S, et al. Characterization of the sources and processes of organic and inorganic aerosols in New York city with a high-resolution time-of-flight aerosol mass apectrometer. Atmospheric Chemistry and Physics 2011; 11: 1581-1602.
Turpin BJ, Huntzicker JJ. Secondary formation of organic aerosol in the Los Angeles Basin: a descriptive analysis of organic and elemental carbon concentrations. Atmospheric Environment. Part A. General Topics 1991; 25: 207-215.
Ulbrich I, Canagaratna M, Zhang Q, Worsnop D, Jimenez J. Interpretation of organic components from Positive Matrix Factorization of aerosol mass spectrometric data. Atmospheric Chemistry and Physics 2009; 9: 2891-2918.
Volkamer R, Jimenez JL, San Martini F, Dzepina K, Zhang Q, Salcedo D, et al. Secondary organic aerosol formation from anthropogenic air pollution: Rapid and higher than expected. Geophysical Research Letters 2006; 33.
Weimer S, Alfarra M, Schreiber D, Mohr M, Prévôt A, Baltensperger U. Organic aerosol mass spectral signatures from wood-burning emissions: Influence of burning conditions and wood type. Journal of Geophysical Research: Atmospheres (1984–2012) 2008; 113.

Wigder N, Jaffe D, Saketa F. Ozone and particulate matter enhancements from regional wildfires observed at Mount Bachelor during 2004–2011. Atmospheric Environment 2013; 75: 24-31.
Yokelson RJ, Crounse J, DeCarlo P, Karl T, Urbanski S, Atlas E, et al. Emissions from biomass burning in the Yucatan. Atmospheric Chemistry and Physics 2009; 9: 5785-5812.
Zhang Q, Alfarra MR, Worsnop DR, Allan JD, Coe H, Canagaratna MR, et al. Deconvolution and quantification of hydrocarbon-like and oxygenated organic aerosols based on aerosol mass spectrometry. Environmental science & technology 2005a; 39: 4938-4952.
Zhang Q, Jimenez J, Canagaratna M, Allan J, Coe H, Ulbrich I, et al. Ubiquity and dominance of oxygenated species in organic aerosols in anthropogenically-influenced Northern Hemisphere midlatitudes. Geophysical Research Letters 2007; 34.
Zhang Q, Worsnop D, Canagaratna M, Jimenez J. Hydrocarbon-like and oxygenated organic aerosols in Pittsburgh: insights into sources and processes of organic aerosols. Atmospheric Chemistry and Physics 2005b; 5: 3289-3311.
Zhang X, Hecobian A, Zheng M, Frank N, Weber R. Biomass burning impact on PM 2.5 over the southeastern US during 2007: integrating chemically speciated FRM filter measurements, MODIS fire counts and PMF analysis. Atmospheric Chemistry and Physics 2010; 10: 6839-6853.
Zhang Y, Tang L, Wang Z, Yu H, Sun Y, Liu D, et al. Insights into characteristics, sources, and evolution of submicron aerosols during harvest seasons in the Yangtze River delta region, China. Atmospheric Chemistry and Physics 2015; 15: 1331-1349.
Zhao R, Mungall EL, Lee AK, Aljawhary D, Abbatt JP. Aqueous-phase photooxidation of levoglucosan–a mechanistic study using Aerosol Time of Flight Chemical Ionization Mass Spectrometry (Aerosol-ToF-CIMS). Atmospheric Chemistry and Physics Discussions 2014; 14: 8819-8850.
Ziemann PJ, Atkinson R. Kinetics, products, and mechanisms of secondary organic aerosol formation. Chemical Society Reviews 2012; 41: 6582-6605.

Chapter 3

THE AMBIENT AEROSOL CHARACTERISATION DURING THE PRESCRIBED BUSHFIRE SEASON IN BRISBANE 2013

A. Milic[1], B. Miljevic[1], J. Alroe[1], M. Mallet[1], F. Canonaco[2], A. S.H. Prevot[2] and Z.D. Ristovski[1]

[1]International Laboratory for Air Quality and Health, Queensland University of Technology, 2 George Street, Brisbane, QLD 4001, Australia
[2]Paul Scherrer Institute, Laboratory of Atmospheric Chemistry, 5232 Villigen PSI, Switzerland

Published in Science of the Total Environment, 560–561 (2016), Pages 225–232.

STATEMENT OF JOINT AUTHORSHIP

The authors listed below have certified that:

1. they meet the criteria for authorship in that they have participated in the conception, execution, or interpretation, of at least that part of the publication in their field of expertise;
2. they take public responsibility for their part of the publication, except for the responsible author who accepts overall responsibility for the publication;
3. there are no other authors of the publication according to these criteria;
4. potential conflicts of interest have been disclosed to (a) granting bodies, (b) the editor or publisher of journals or other publications, and (c) the head of the responsible academic unit, and
5. they agree to the use of the publication in the student's thesis and its publication on the QUT ePrints database consistent with any limitations set by publisher requirements.

In the case of this chapter: Chapter 3

TITLE

The ambient aerosol characterization during the prescribed bushfire season in Brisbane 2013

AUTHORS

Andelija Milic (candidate) run the instrumentation, analysed and interpreted the data and prepared the manuscript;

Branka Miljevic contributed to data analysis and interpretation, and reviewed the manuscript;

Joel Alroe contributed to data interpretation and writing the manuscript;

Marc Mallet installed the instrumentation and contributed to writing the manuscript

Francesco Canonaco provided the software used in the data analysis, contributed to data interpretation and reviewed the manuscript;

Andre Prevot contributed to data interpretation and rewieved the manuscript;

Zoran Ristovski contributed to data interpretation and rewieved the manuscript;

All authors declare that they have no conflict of interest.

Principal Supervisor Confirmation

I have sighted email or other correspondence from all Co-authors confirming their certifying authorship.

Zoran Ristovski		26/09/2016
Name	Signature	Date

The ambient aerosol characterization during the prescribed bushfire season in Brisbane 2013

A. Milic[1], B. Miljevic[1], J. Alroe[1], M. Mallet[1], F. Canonaco[2], A. S.H. Prevot[2] and Z.D. Ristovski[1]
[1]International Laboratory for Air Quality and Health, Queensland University of Technology, 2 George Street, Brisbane, QLD 4001, Australia
[2]Paul Scherrer Institute, Laboratory of Atmospheric Chemistry, 5232 Villigen PSI, Switzerland

Correspondence to: Branka Miljevic (b.miljevic@qut.edu.au)

Abstract. Prescribed burnings are conducted in Queensland each year from August until November aiming to decrease the impact of bushfire hazards and maintain the health of vegetation. This study reports chemical characteristics of the ambient aerosol, with a focus on source apportionment of the organic aerosol fraction (OA), during the prescribed biomass burning (BB) season in Brisbane 2013. All measurements were conducted within the International Laboratory for Air Quality and Health (ILAQH) located in Brisbane's Central Business District. Chemical composition, degree of aging and the influence of BB emission on the air quality of central Brisbane were characterized using a compact Time of Flight Aerosol Mass Spectrometer (cToF-AMS). AMS loadings were dominated by OA (64 %), followed by, sulfate (17 %), ammonium (14 %) and nitrates (5 %). Source apportionment was applied on the AMS OA mass spectra via the multilinear engine solver (ME-2) implementation within the recently developed Source Finder (SoFi) interface. Six factors were extracted including hydrocarbon-like OA (HOA), cooking-related OA (COA), biomass burning OA (BBOA), low-volatility oxygenated OA (LV-OOA), semivolatile oxygenated OA (SV-OOA), and nitrogen-enriched OA (NOA). The aerosol fraction that was attributed to BB factor was 9 %, on average over the sampling period. The high proportion of oxygenated OA (72 %), typically representing aged emissions, could possess a fraction of oxygenated species transformed from BB components on their way to the sampling site.

Keywords. Air quality, Biomass burning, Organic aerosol, Aerosol mass spectrometry, Source apportionment

3.1 Introduction

Biomass burning (BB) aerosol mostly originates from domestic heating sources, natural fires, as well as from prescribed burning. BB aerosol has significant influence on human health, global climate and environment (Luhar et al., 2008; van der Werf et al., 2006). Burning emissions encompass a variety of gaseous and particle-phase species, including primary aerosols released directly from the sources in the atmosphere and secondary aerosols generated through the gas-to-particle conversion processes of primary gaseous compounds. Smoke plumes are considered as one of the largest contributors to the primary carbonaceous particles in the atmosphere, which include organic carbon (OC) and black carbon (BC) (Bond et al., 2004; Hallquist et al., 2009). Moreover, once emitted in the atmosphere, the volatile portion of primary BB aerosol is subject to atmospheric photochemical aging processes and is likely to be a large source of secondary organic aerosol (SOA) precursors

(DeCarlo et al., 2010; Grieshop et al., 2009; Heringa et al., 2011; Jimenez et al., 2009). In order to identify aerosol of BB origin, different chemical markers have been suggested. Anhydrosaccharides, levoglucosan-like species (levoglucosan, mannosan, galactosan), are organic molecules formed during pyrolysis of carbohydrates and common components of BB plumes (Simoneit et al., 1999). Many studies have suggested levoglucosan as a valuable BB chemical signature (Jordan et al., 2006; Simoneit, 2002; Simoneit et al., 1999), although using it as the only indicator has been questioned due to its suggested semivolatile nature and non-inert behaviour in the atmosphere (Hoffmann et al., 2009; May et al., 2012).

Levoglucosan produces a prominent signal at m/z 60 (Org 60) (fragment $C_2H_4O_2^+$) and m/z 73 (fragment $C_3H_5O_2^+$) of the mass spectrum extracted from Aerosol Mass Spectrometer (AMS) data (Aiken et al., 2008; Alfarra et al., 2007; Cubison et al., 2011). The AMS has found an application in real-time mass spectral analysis of quantitative aerosol chemical composition as well as particle size. Originally, the AMS has been designed for investigation of submicron non-refractory (NR) chemical species (species that are flash-vaporized at the AMS heater temperature of approximately 600 °C). A fragmentation table is used to attribute fragments into the major species; organics (Org), nitrates (NO_3^-), sulfates (SO_4^{2-}), ammonium (NH_4^+) and chloride (Cl^-). The fraction of an organic fragment signal, e.g. m/z 60, to total organic mass is useful in characterizing the aerosol and is referred to as *f*60. *f*60 and *f*73 typically represent levoglucosan-based markers in the presence of BB emissions. According to Cubison et al. (2011), a *f*60 value higher than 0.003 indicates substantial BB aerosol contribution. The parameter *f*60 is a signature of primary wood burning emissions. Moreover, Heringa et al. (2011) has suggested that SOA formed through aging processes of BB-related volatile organic compounds also contributes to non-negligible amounts of *f*60. Many studies have demonstrated the same trend of *f*60 decreasing and *f*44, the parameter related to the oxygenated organic aerosol fraction (OOA), increasing with aging (Capes et al., 2008; Cubison et al., 2011; Grieshop et al., 2009; Jolleys et al., 2015; Ng et al., 2010b; Ortega et al., 2013; Zhao et al., 2014). Thus, the ratio of *f*44 and *f*60 indicates the photochemical evolution of BB aerosol over time and fresh BB aerosol can be distinguished from aged, highly oxidized species.

Considering the multiple primary and secondary sources, it is a big challenge to apportion organic aerosol (OA) into its sources. The positive matrix factorization (PMF) technique (Paatero and Tapper, 1994) has been demonstrated to produce meaningful source apportionment results from AMS data (Lanz et al., 2007a; Ulbrich et al., 2009). This local minimum multivariate factor analytical model creates a linear combination of static factor profiles (OA mass spectra) and their contributions over time. The number of factors is highly subjective and needs exploration by the experimentalist. In addition, PMF solutions are known to suffer from rotational ambiguity, i.e. similar solutions with an equal degree of fit may exist (Paatero et al., 2002). This requires an accurate investigation of the solution space, differing the number of factors (different type of aerosol species), applying rotations in the solution space (*a* value) and using different starting conditions (seed runs). Within these runs, it is generally possible to find the solution that "best" explains the data (Canonaco et al., 2013; Ulbrich et al., 2009). In comparison to the chemical mass based method where factors are completely constrained, the PMF algorithm

does not allow any *a priori* information to be applied. The multilinear engine algorithm (ME-2) technique introduced by Paatero (1999) and Paatero and Hopke (2009), however, allows different options to be tested using factor profiles and/or time series applied to different constrained degrees. A graphical user interface, SoFi (Source Finder), outlined in Canonaco et al. (2013) applies the ME-2 algorithm using predetermined profiles aiming to facilitate application of different rotational approaches and to retrieve the solution closest to the "true" solution. One approach to applying constraints involves utilization of the *a* value method first introduced by Lanz et al. (2007b) for AMS data. The *a* value typically ranges from 0 for the completely constrained case, to 1. Different *a* values correspond to different deviations from input factor profile and/or time series, e.g. an applied *a* value of 0.3 means that 30 % of the profile/time series can be varied by the algorithm during the minimization process. Factors that do not show significant variability are considered primary factors including hydrocarbon-like OA (HOA), cooking-related OA (COA) and biomass burning OA (BBOA). Secondary profiles, low-volatility oxygenated OA (LV-OOA) and semivolatile oxygenated OA (SV-OOA), can be highly dependent on features of the environment and thus prone to different degrees of aerosol evolution. Secondary factors, in contrast to primary, are therefore likely not suitable for the constraint method if specific conditions are not known (Canonaco et al., 2015).

Annual prescribed biomass burning in Queensland is conducted from August until November, in order to mitigate wildfire hazards and preserve the vegetation. Prescribed burns are planned based on local conditions including the weather and impact on people and animals. This study reports and interprets an ambient dataset sampled during Brisbane's prescribed bushfire season from a ground-based sampling site, which can be classified as urban background due to its location in the Central Business District (CBD). Collected data were characterized using the cToF-AMS with a focus on OA apportionment, done within the SoFi package, employing the ME-2 engine and using the *a* value constraining approach (Canonaco et al., 2013; Crippa et al., 2014). Source apportionment of the BB aerosol allowed us to assess the contribution of these yearly fires to the aerosol signal in the Brisbane CBD.

The ambient aerosol characterization for the same sampling site has been conducted using the cToF-AMS (Crilley et al., 2014b), but was not performed in continuous measurement during the specific period of the prescribed fires. This work is an important step in characterizing biomass burning aerosol in the Brisbane CBD, a densely populated city area. Furthermore, it will contribute to a wider understanding of BB characteristics in subtropical urban environments, which have not been significantly explored in the Southern Hemisphere.

3.2 Experimental

3.2.1 Sampling site

The ambient measurements took place at the Queensland University of Technology (QUT) campus, located in the Brisbane CBD. All the used instrumentation was located in the International Laboratory for Air Quality and Health (ILAQH)

laboratory (27°28'38.5968”S, 153° 1'40.8828”E). The ambient sampling was conducted during the Queensland prescribed bushfire season, from the 29th of August to the 3rd of October 2013, with a break of two weeks due to instrument malfunction. The bushfire locations were obtained from the Queensland Fire and Rescue Service archive (https://www.fire.qld.gov.au/). A considerable area of Brisbane was affected by bushfire events with 24 fires identified during the measurement period (Fig. 3.1). Most of prescribed fires took place during the first sampling period (from 29th of August to 4th of September) with most of them close to the sampling laboratory (up to 50 km in distance). The second period (from 20th of September to 3th of October) was characterized by a small number of mostly remote burned areas.

Apart from BB plumes, contribution from the traffic sources is significant for this sampling site (around 150 m distance away from a main motorway, the Riverside Expressway), as well as emissions from the industrial part of Brisbane (port and oil refineries). The biogenic species emitted from the City Botanic Gardens and the Brisbane river that surround the monitoring location could also considerably affect the aerosol content (Fig. 3.1) (Crilley et al., 2014b).

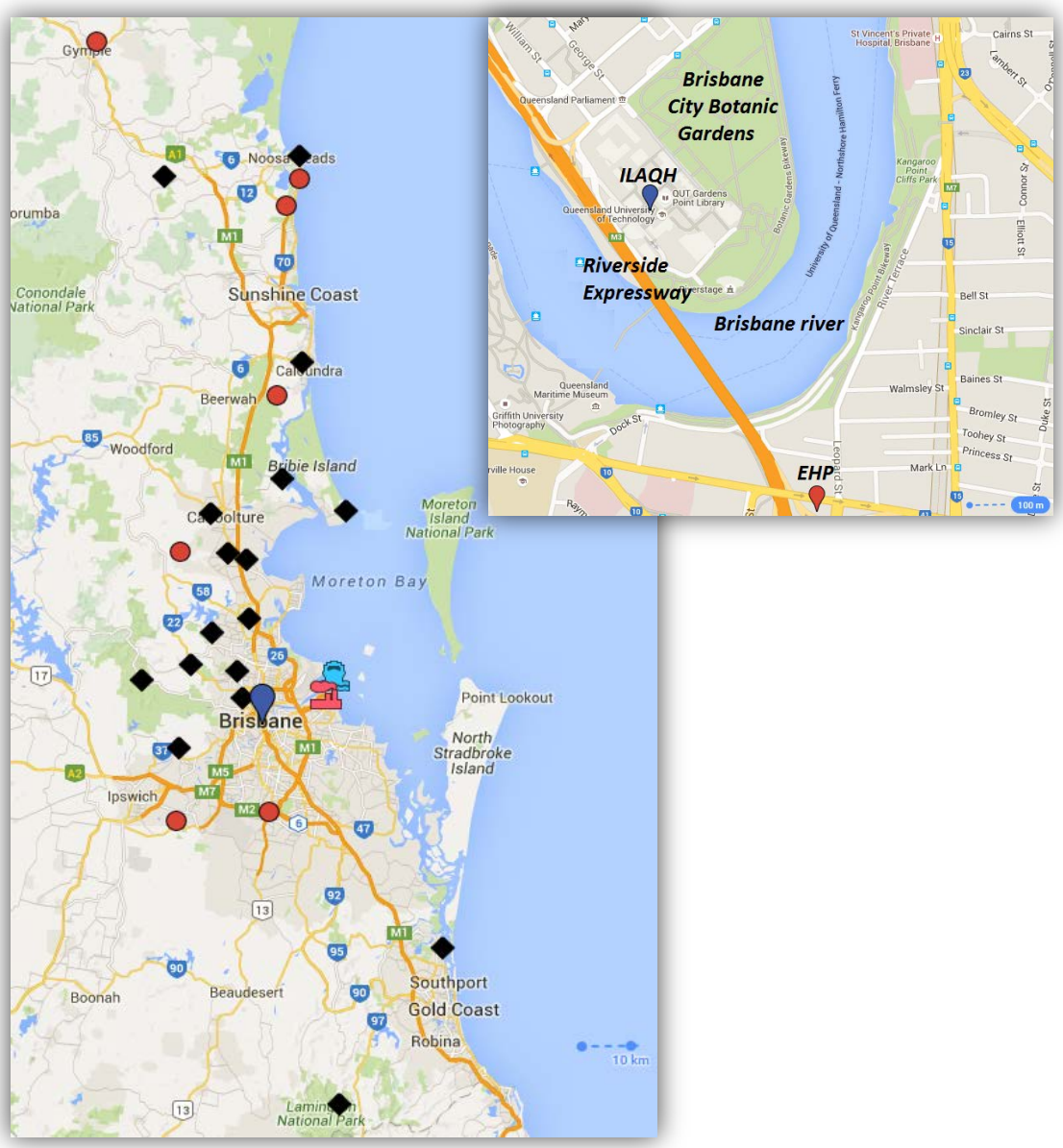

Figure 3.1. Bushfire locations that were identified during the first period (black diamonds) and the second measurement period (red circles) along with labels for the ILAQH sampling site (blue mark), the port of Brisbane and oil refineries. In addition, a local map of the ILAQH sampling site environment (including EHP location) is shown (Google. (n.d.). Google Maps location for Brisbane; Retrieved October 23, 2015).

3.2.2 Instrumentation

An Aerodyne compact Time of Flight Aerosol Mass Spectrometer (cToF-AMS) was deployed to monitor the chemical composition of submicron ambient aerosol. Detailed description of the instrument's operation can be found elsewhere (Canagaratna et al., 2007; Drewnick et al., 2005; Jimenez et al., 2003). Particle number concentration and size distribution were monitored by a Scanning Mobility Particle Sizer (SMPS) consisting of a TSI 3080 Electrostatic Classifier and a TSI 3010 Condensation Particle Counter. The SMPS was measuring in a configured particle size range from 7.6 to 310.6 nm in diameter in 3 minute intervals. Ozone concentrations were measured in 1 minute time resolution using an Ecotech (EC9810) Ozone Monitor. Standard meteorological parameters, including ambient temperature, relative humidity, wind speed and wind direction, were obtained from the Department of Environment and Heritage Protection (EHP) monitoring station located at South Brisbane (27°29'5.4960"S, 153° 1'56.0028"E) (Fig. 3.1). The station also provided supporting ambient air quality data for carbon monoxide (CO) and nitrogen oxides (NO_X). All parameters were recorded over 30-minute intervals.

3.3 Data analysis

The AMS dataset was processed in the Wavemetrics Igor Pro software (Version 6.36) using the standard ToF-AMS Analysis Toolkit named Squirrel (Version 1.55H). A modified fragmentation table (Aiken et al., 2008), was applied to the AMS unit mass resolution data. This fragmentation table was adjusted using information from the background aerosol composition, obtained through filter measurements at the beginning of the measurement period. Collection efficiency (CE) was estimated based on the procedure discussed in Middlebrook et al. (2012) by incorporating ammonium nitrate, organic content and aerosol acidity. The composition dependent collection efficiency was found to be 0.5 for the majority of the samples, so this value was used in all calculations. In order to estimate the degree of oxidation for each factor, oxygen-to-carbon ratio (O/C) was calculated from the f44 value, using the relation suggested by Aiken et al. (2008) (Aiken-ambient O/C values, "O/C_{A-A}"), as well as the "improved-ambient" equation (Improved-ambient O/C values, "O/C_{I-A}"), recently introduced by Canagaratna et al. (2014).

The SoFi toolkit (Version 5.3) was applied to investigate the solution space, and identify and quantify contributions of the main OA sources extracted using the ME-2. The number of possible solutions was investigated without applying any *a priori* information (completely unconstrained PMF run). Subsequently, the HOA, COA and BBOA factor profiles identified in first dataset were used to constrain the solution space for the whole data set. Finally, the *a* value approach was performed by applying a combination of *a* values ranging from 0 to 0.1 for HOA and COA and from 0 to 0.5 for BBOA (in increments of 0.1), as suggested by Crippa et al. (2014). Stronger constraints were examined on HOA and COA profiles compared to BBOA, as the BB-related factor profile can vary more depending on burning material, combustion conditions and environment (Weimer et al., 2008).

3.4 Results and discussion

3.4.1 Meteorological and ambient data

The ambient measurement study was conducted during Brisbane's spring months, with average relative humidity and temperature values of 66 % and 24 °C, respectively (Fig. 3.S1). Daily variation in wind direction showed the characteristic breeze pattern for the Brisbane environment (Fig. 3.S1 and Fig. 3.S4) (Morawska et al., 2002). Land breezes (primarily SSW land breeze - 170-230°) were observed during the night and morning hours, from 12 pm to 11 am, while between midday and midnight winds were mostly blowing from the ocean (NE, E and SE breeze - 40-140°). The daily ocean breeze was characterized by speeds up to 5 m/s higher than the night wind (Fig. 3.S4). Substantially increased particle number concentrations were observed in the weekday morning hours (Fig. 3.S2 and Fig. 3.S3). The morning wind direction was predominately SSW indicating the Riverside Expressway as the main particle source (approximately 150 m S from the measurement site). In addition, morning cleaning activities within the university campus occurred every working day from 5 to 7 am, with cleaning occurring in front of the measurement site around 6 am. Vacuum cleaners and leaf blowers were used. Aerosol emitted during the peak afternoon traffic period was not detected by the SMPS as the wind was typically blowing from the sampling location towards the River Expressway. CO and NO_X measured by the EHP-operated station followed the same daily trend of increased values during morning hours (Fig. 3.S1 and Fig. 3.S4), but demonstrated an increase during the afternoon traffic hour due to the EHP location (Fig. 3.1). Ozone time profiles show a clear characteristic increase during the day (Fig. 3.S2 and Fig. 3.S4). Concentrations fluctuated between a nightly minimum of nearly zero and up to 60 ppb during the ozone peak period, between noon and 3pm, with an average value of 20 ppb.

3.4.2 Aerosol composition (AMS data)

The ambient NR submicron aerosol was mainly composed of OA (63.7 % ± 3.8) with an average concentration of 4.21 μg m^{-3}. Particles also consisted of a substantial amount of sulfate (16.6 % ± 1.0), ammonium (14.1 % ± 1.1), and nitrates (5.3 % ± 0.4) with the respective average concentrations of 1.12 μg m^{-3}, 1.00 μg m^{-3}, 0.42 μg m^{-3} and a negligible average chloride contribution of 0.01 μg m^{-3} (0.2 % ± 0.1) (Fig. 3.2a and Fig. 3.2b).

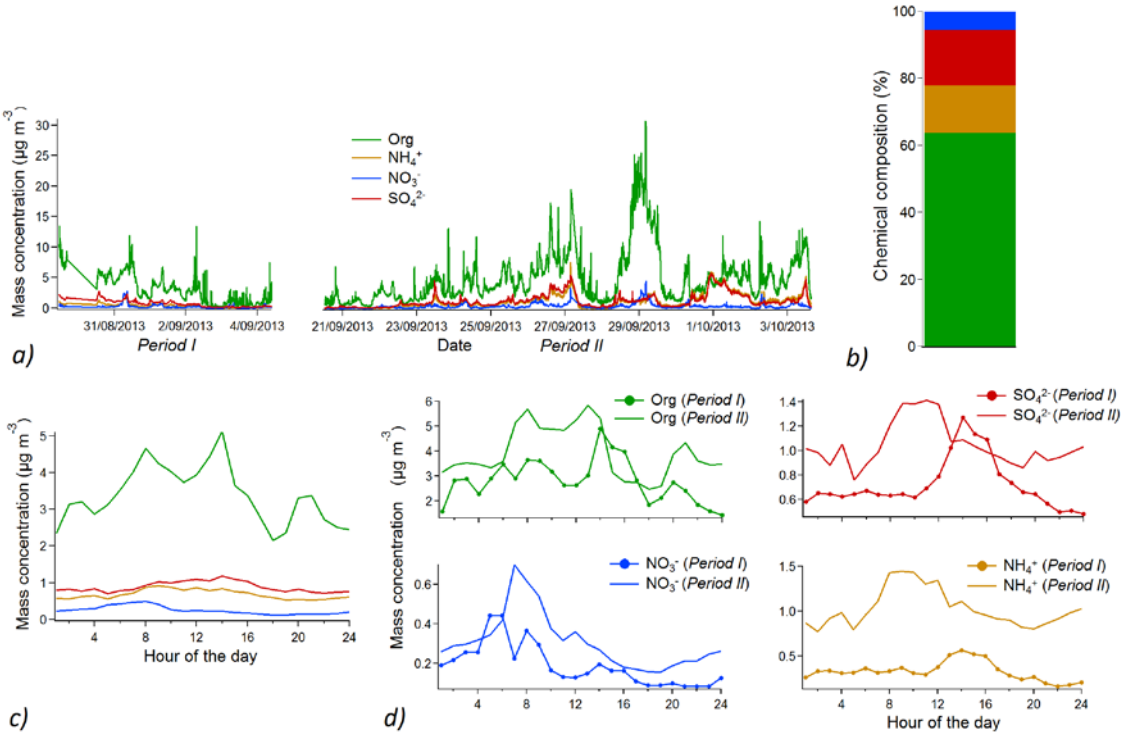

Figure 3.2 Time series (a) and relative contribution (b) of AMS NR species for the whole sampling period, along with their diurnal trends looking at both sampling periods together (c) and separately (d), where Period I and Period II correspond to the first (29/08/13 – 04/09/13) and the second (20/09/13 – 03/10/13) measurement period and the straight line at the beginning of the measurement represents a 6h gap. As chloride concentrations were not significant they were excluded from graphs.

Diurnal trends of NR AMS components for the overall measurement campaign, as well as for the first and the second time period separately, are given in Fig. 3.2c and Fig. 3.2d, respectively. The diurnal pattern of the measured organic mass illustrates its high variation during the sampling period, with morning, afternoon and evening peaks. Diurnal cycles of inorganic NR species demonstrate similar trends in sulfate and ammonium concentrations, while nitrates had a distinctly different trend which suggested different sources of ammonium sulfate and nitrate. Considering the sulfate concentration in the first time interval, the diurnal trend showed a maximum extending from noon till late afternoon. During this period easterly breezes were predominant (Fig. 3.S4), likely carrying sulfates from marine aerosols and industrial and port emissions. The diurnal trend for the second period is not as distinct, compared to the first one. From Fig. 3.2d it can be seen that, during the afternoon hours of period two, sulfates have very similar concentrations as during the afternoon hours of period one, suggesting that ocean breezes and industrial and port emissions contribute to sulfate detection in both periods. However, another source seemed to be more dominant during the morning hours of the second period. During these hours (7

am – 1 pm), land breezes were prevalent (Fig. 3.S4) and we could not relate sulfate masses to any particulate source. Similar diurnal patterns were observed in sulfate and organics for both sampling periods.

f44 vs. f60 plot

The contribution of BB aerosols and their aging degree for both sampling periods are illustrated in the f44 vs. f60 space (Fig. 3.3). According to the proportion of points exceeding the f60 background limit of 0.003 (55% and 35% for the first and the second period respectively), more aerosols with BB origin were detected during the first period. This was expected due to the higher proportion of close fires that occurred in the first sampling period.

Fresh BB aerosols can be distinguished from aged, oxidized species by different f44 values (Fig. 3.3). Ng et al. (2010b) illustrated that aged aerosol has f44 values mostly between 0.1 and 0.25. According to this classification, the majority of the aerosols detected during this campaign were highly processed. It is clear that the second period was characterized by a higher proportion of oxidized species, compared to the first period. 17 % of the sampled aerosol in the second period had f44 above 0.25 indicating a high contribution of aged aerosol. This difference in the proportion of aged aerosol between the periods could be attributed to mostly distant fires in the second period.

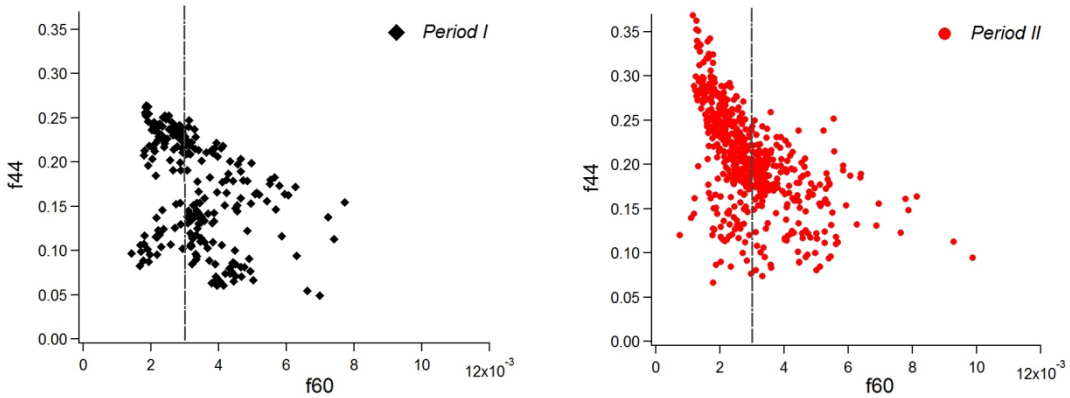

Figure 3.3 f44 vs. f60 space with dots colored by sampling period (data were averaged over the 30-min interval for better illustration; gray line on the graphs illustrates f60 background limit of 0.003).

3.4.3 Source Apportionment

Organic matter was found to be the most abundant NR-PM1 component (64 %) of the total AMS mass that was measured during the campaign. In order to identify and quantify OA sources and estimate the contribution of BB-related source for the Brisbane urban area, the ME-2 apportionment technique using SoFi was applied. There was a gap of two weeks in the sampling due to instrument malfunction. In order to estimate all possible solutions and identify reasonable sources of the sampled aerosol, datasets generated before and after the break were analyzed separately and together. Addressing datasets

separately did not result in factor solutions that were consistent across both datasets. More details can be found in Unconstrained PMF (separate datasets). Further analysis was done by performing PMF on the merged datasets.

Unconstrained PMF run (combined datasets)

An unconstrained PMF run was performed on the whole dataset with the number of factors ranging from 1 to 10 and applying 10 iterations (seeds). More details can be found in Unconstrained PMF (combined datasets). The 6-factor solution was found to best explain the data as a lower number of factors did not give a full explanation of the dataset and seven or more factors resulted in splitting of existing profiles (Fig. 3.S12). The solution with 6 factors included: two primary components, hydrocarbon-like OA (HOA) and cooking-related OA (COA); two OOA factors, low-volatility oxygenated OA (LV-OOA) and semivolatile oxygenated (SV-OOA); biomass burning OA (BBOA); and nitrogen-enriched OA (NOA). In the following paragraphs, the selection of this 6-factor solution will be supported and explained in details. The profile, time series and diurnal pattern of the extracted factors are presented in Fig. 3.S13.

The HOA and COA factors in the 6-factor solution were well separated, compared to solutions with lower number of factors where these primary sources were merged into one profile, with recognizable m/z 41, 43, 55, 57 related to alkyl ion peaks (Fig. 3.S12). Both signals m/z 55 and 57 were attributed to primary OA emitted from combustion sources. The COA factor can be distinguished from HOA when the m/z 55 signal is dominant over m/z 57, as observed here and in many other studies (Allan et al., 2010; Mohr et al., 2012; Sun et al., 2011). The peaks during typical meal times (prominent lunch and dinner-related peaks), present in the COA diurnal profile (Fig. 3.S14b and Fig. 3.S14c), provide further evidence of cooking aerosol contribution, as previously observed (Allan et al., 2010). The diurnal trend of the common factor (HOA+COA) in solutions with less than 6 factors encompassed both the HOA-related morning rush hour peak and the COA-related evening peak (Fig. 3.S14a). On the other hand, the 6-factor solution allowed successful apportionment of these peaks to HOA and COA respectively (Fig. 3.S14b). There was a clear diurnal trend in the COA factor that illustrated meal periods during the day and intensive cooking contribution in the evening hours. The cooking aerosol contribution was more significant during weekend evenings, rather than during weekdays, due to increased restaurant patronage in the Brisbane CBD. The morning traffic peak in the HOA factor disappeared during weekends, when there was less traffic volume (Fig. 3.S14c).

When choosing 6 factors, oxygenated OA was separated into two components, LV-OOA and SV-OOA, that are characterized by different degrees of oxidation and volatility, as illustrated in many other studies (Jimenez et al., 2009; Lanz et al., 2007a; Ng et al., 2010b; Ulbrich et al., 2009). LV-OOA was characterized by a unique factor profile with a prominent m/z 44 signal and strong diurnal trend showing increased levels during midday hours, due to enhanced photochemical activity in the atmosphere. SV-OOA had a less prominent m/z 44 signal and significant m/z 43 contributions compared to LV-OOA, which indicated less oxidized and often more volatile species. Contribution of SV-OOA decreased from midday to the evening hours consistent with the temperature increase and relative humidity decrease. This might be explained by

gas-phase partitioning of the more volatile fraction with temperature increase (Budisulistiorini et al., 2013; Canonaco et al., 2015; Crippa et al., 2014; Lanz et al., 2007a).

The BBOA factor was identified by the prominence of levoglucosan-related ions, m/z 60 and 73. However, there was no observed clear apportionment of its other important m/z's. More precisely, it seemed that m/z 43 and m/z 44, which belong to the BBOA factor, were apportioned to other factor profile. The BBOA diurnal trend is marked by a broad daily peak which indicates the usual time of prescribed burnings.

The last factor, identified in the selected solution, was assumed to be a nitrogen-enriched organic factor (NOA). The main ion signals were m/z 42, 44, 56 and 58. The NOA profile was not marked with ions m/z 30, 46 and 86, which have been related to nitrogen organic species. A similar NOA spectrum was observed and associated with marine sources and/or industrial activities that produce amino compounds (Sun et al., 2011). The observed wind was from the SW (Fig. 3.S15) and did not coincide with the direction of the industrial zone (NE) or the ocean (E, NE, SE). Therefore this uniform trend couldn't be related to a specific source. NOA's distinctive diurnal trend was characterized by a broad peak starting after midnight and continuing until approximately 8am. Increases in the NOA factor were in agreement with increases in relative humidity and decreases in ambient temperature, as previously observed by Carbone et al. (2014). High relative humidity and low temperature could provide a suitable environment for low molecular weight and highly water-soluble amines to stay in particle phase. This was in contrast to the daytime peak observed by Sun et al. (2011), suggesting that photooxidation reactions were not the primary driving force of NOA production for this study. Another possible solution is that semivolatile aminium salts from ocean air masses condensed over the night when high relative humidity and low temperature are taking place. More research is needed to characterize and identify the source(s) of this component.

Performing PMF on the merged datasets resulted in a common factor solution which encompassed the factors that were extracted when PMF was performed on datasets separately. This included SV-OOA profile which was not seen in the separate 6-factor solutions from each period. There was also successful separation of HOA and COA when PMF was applied on the whole dataset, which was not the case for the second set of data alone. The unconstrained 6-factor solution, obtained from the merged dataset, was therefore chosen for further analysis.

Issues with unconstrained PMF run

As stated, the 6-factor solution provided the most representative set of factors, however, there was significant apportionment of the oxidized fraction to the HOA and COA profiles (O/C_{A-A} of 0.25 and 0.26, respectively) (Table 3.S1) compared to the values reported for the same sampling site in the Crilley et al. (2014b) study and primary profiles in other studies (DeCarlo et al., 2010; Jimenez et al., 2009; Ng et al., 2010b). Another issue was an unclear mass spectrum profile of the BBOA component (Fig. 3.S13). In order to improve these extracted profiles, ME-2 was applied using the a priori information.

Factor profiles identified within the analyzed dataset were considered to be more representative of sources of interest than profiles obtained in other studies. In order to improve HOA, COA and BBOA profiles using a priori information, factor profiles generated by running unconstrained PMF separately on the first and second time periods were considered.

Looking at the 5-factor solution for the first dataset, the HOA and COA profiles did not have a significant amount of m/z 44 (O/C_{A-A} of 0.19 and 0.08, respectively) (Table 3.S1). On the other hand, in the second period, HOA and COA were characterized by high O/C values (O/C_{A-A} of 0.30 and 0.21, respectively), similar to values from the combined dataset. The COA diurnal trend was less distinct and the HOA afternoon peak had significant cooking contribution in the evening hours for the second set of data (Fig. 3.S9) compared to the first period where factors were better separated (Fig. 3.S6). The BBOA spectrum identified in the first dataset was characterized with all typical m/z's (Fig. 3.S5), while the BBOA in the second dataset did not have a clear factor profile (Fig. 3.S8). The latter suggested that HOA, COA and BBOA factor profiles revealed in the first dataset could be used as *a priori* information for further analysis.

Constrained *a* value approach

HOA, COA and BBOA, generated for the first data period, were set as constrained factor profiles for the whole dataset. The constrained model was applied on the 6-factor solution, previously chosen for further analysis. The two dimensional *a* value approach was performed for HOA/COA and BBOA, ranging from 0 to 0.1 and from 0 to 0.5 respectively, in increments of 0.1, as suggested by (Crippa et al., 2014). The rest of the factors were not predetermined and were allowed to freely change and thus adapted to minimize the weighted residuals, as in the classical, unconstrained PMF. The selection of the solution was made based on changes in the factors' mass spectra, correlation of factors with compatible external data and diurnal trends of HOA and COA components. Identified profiles for different applied *a* values (model runs) are presented in Fig. 3.4.

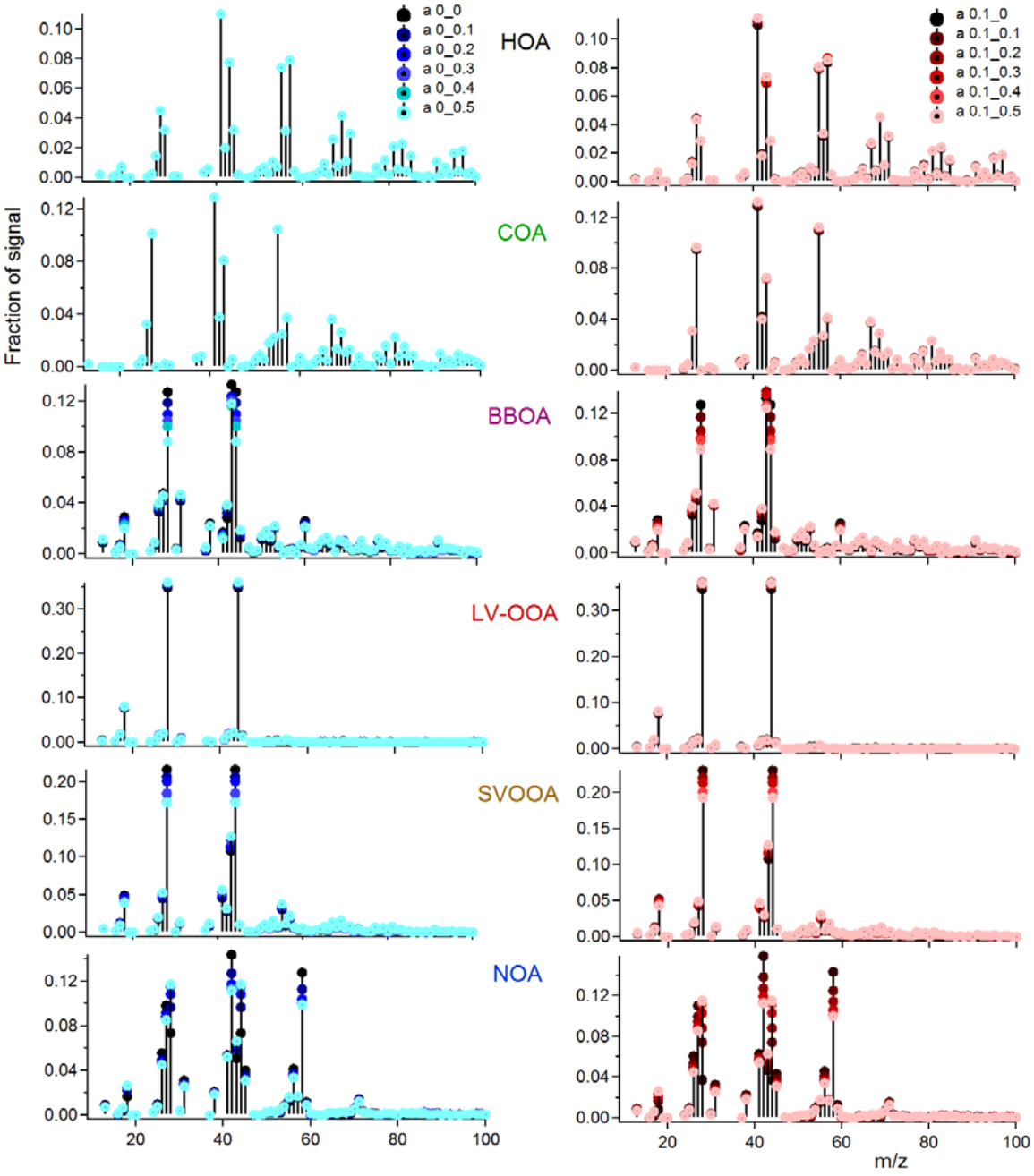

Figure 3.4 Mass spectra of the 6-factor solution profiles for different α value combinations are presented. Each model run is illustrated with a different color. Solutions on the left-hand side comprise factors generated by applying an α value of 0 to HOA and COA, and α values ranging from 0 to 0.5 for BBOA. Solution on the right hand side comprises factors generated when α value of 0.1 was applied on HOA and COA, and α values ranging from 0 to 0.5 for BBOA.

HOA and COA profiles did not vary as more tightly constrained models were applied. The mass spectra of the BBOA constrained profile varied with different *a* values, with the greater change occurring when constraints were more relaxed, as

expected. The unconstrained profiles showed also significant variation, especially the SV-OOA and NOA profiles. These variations were primarily seen in m/z 43 and m/z 44. BBOA and SV-OOA do not possess strong metrics and hence, in particular m/z 43 in the profile of BBOA and SV-OOA is anticorrelated.

The diurnal trend of the HOA factor stayed stable following each model run, while there were minor changes in the COA trend (Fig. 3.S16). General enhancement in the cooking contribution was observed when the BBOA profile was more constrained (α value was increased).

Correlations of retrieved factor time series with corresponding traces were made separately for the first and second period, due to different environmental features between two time periods (Table 3.S2 and Fig. 3.S17). The different locations of the EHP monitoring station and ILAQH sampling site meant that the NO_X and CO data were not representative as external tracers for correlation analysis. However, there were similarities in the diurnal trends of the HOA factor, NO_X and CO, showing a morning peak (Fig. 3.S18).

BBOA and Org 60 had good correlations in both sampling intervals, with R^2 (Pearson) value of 0.9 and 0.4, for the first and the second period respectively. As previously mentioned this discrepancy can probably be attributed to locations of BB events. In the second period, emissions from predominately remote fires may have resulted in more oxidized species and less aerosol with BB features. Previous studies have reported a correlation between two low-volatile secondary species, LV-OOA and SO_4 (Lanz et al., 2007a; Ulbrich et al., 2009). In this study this correlation was stronger in the first period (R^2 of approximately 0.8) compared to the second period (R^2 of approximately 0.4). In the first period, the direct influence of ocean breezes and industrial emissions contributed to detection of secondary sulfate. A similar conclusion cannot be drawn for the second period, when the exact source of sulfate was not known. Moreover, the difference in LV-OOA/sulfate as well as in SV-OOA/nitrate correlations between the periods agrees with observations made by Crippa et al. (2014) that OOA profiles have different correlations with secondary inorganic compounds depending on the sampling environment.

Although increasing the α value from 0 to 0.5 for BBOA profile (in both applied α values for COA/HOA) led in general to the decrease of overall correlations between factors and corresponding markers, there was no considerable difference observed. Moreover, HOA/COA diurnal patterns did not vary significantly. Thus the average of all the considered solutions was taken as the final best solution, considering the spread (Fig. 3.S19). As expected, the values of the spread were lower for constrained profiles than for profiles that were left to freely change. OOA profiles showed the highest variation.

Comparison of the unconstrained and constrained solutions

Application of the constrained α value approach enabled extraction of factor solutions in which the BBOA profile was well apportioned with all typical m/z's, as compared to the unconstrained case (Fig. 3.S20). Unlike the unconstrained solution, the O/C_{A-A} values in the constrained case (Table 3.S) were observed to be comparable to the O/C_{A-A} values for previously

reported profiles (O/C_{A-A} for HOA and COA were 0.18 and 0.12, respectively). This result was made without compromising HOA and COA diurnal trends that still showed good apportionment according to morning HOA and lunch and evening COA peaks (Fig. 3.S20). Negligible changes were observed in the two solutions when looking at the relative contribution of HOA, COA and NOA profiles. The *a* value approach also resulted in negligible decrease in the overall contribution of OOA, however, distribution of LV-OOA and SV-OOA was changed from 56 % and 19 % to 42 % and 31 % for LV-OOA and SV-OOA respectively. More OA was apportioned to the BBOA factor when constraints were applied (from 5 % to 9 %). The aforementioned improvements supported the use of this constrained solution for the final OA source apportionment.

3.4.4 BB aerosol contribution and aging

Source apportionment attributed 9 % of the OA to the BB-related factor. During a study in Brisbane that estimated the effect of ultrafine particles from traffic emissions on children's health, two measurement sites that were 10 km away from each other, measured significantly different BBOA percentage contribution (26 % and 10 %) during the same season (within the prescribed burning period) in different years (2011 and 2012) (Crilley et al., 2014a). Furthermore, another Brisbane study performed measurements at our sampling site (Crilley et al., 2014b), outside of the prescribed burning period, and reported larger BB aerosol contributions (13%) than have been observed in this study. This suggests that the contribution of BB aerosol for the Brisbane urban area varies depending on the year, and more precisely on the frequency, intensity and location of fires and direction of their pathways.

The O/C_{A-A} ratio for BBOA was significantly higher compared to previous results (O/C_{A-A} of 0.25) for the same sampling site (Crilley et al., 2014b), suggesting that this factor includes partially aged BB emissions. Aged BBOA factors with O/C ratios comparable to this study have previously been reported in other BB campaigns (Bougiatioti et al., 2014; Brito et al., 2014). Furthermore, OOA components contributed the highest percentage of OA mass (72 %) from all identified factors. Thus it is possible that BB-related aerosol lost their signature characteristics on their way to the sampling site due to the high oxidation of levoglucosan-like species. The atmospheric processing probably led to oxidation of OA towards LV-OOA with the BB-signature being replaced with an oxidation signature as suggested in Jimenez et al. (2009).

As can be seen from Table 3.S, LV-OOA and SV-OOA factors are characterized with unusually high O/C_{A-A} values (1.44 and 0.67, respectively) compared to reported results for the Northern Hemisphere (0.73 and 0.35 respectively) (Ng et al., 2010b) and for subtropical urban area of Mexico City that is at the same latitude as Brisbane (0.83 and 0.52, respectively) (Aiken et al., 2008). However, similarly high O/C_{A-A} ratios have been already observed in the Brisbane area (Crilley et al., 2014a). This once more suggests high contributions of SOA and confirms the importance of aging processes for central Brisbane air quality.

3.5 Conclusions

The influence of the prescribed bushfire season on air quality was investigated through source apportionment analysis of AMS data. The contribution of BB-related aerosol was 9%, suggesting limited influence of BB events on the central Brisbane area air quality. One explanation may be that BB plumes were not completely apportioned due to mixing with background urban aerosol and intensive aging on their way to the sampling site. In this case processed BB emissions could have contributed to the high proportion of OOA components (72 %). Another possibility is that a limited number of smoke plumes were coming towards the Brisbane CBD.

The high OOA contributions are in line with a prior Brisbane study, further suggesting intense photochemical aging of aerosol in the central Brisbane area. Moreover, the high OOA proportions highlight the importance of SOA for this location.

Application of the recently developed SoFi interface, using the ME-2 algorithm, improved the final solution space when comparing factors generated before and after applying constraints. Both primary (HOA and COA) and secondary (LV-OOA and SV-OOA) factors were revealed by applying the unconstrained PMF method to the separate studied periods, but their profiles would not have been successfully apportioned over the entire period without constraining the primary source profiles.

Acknowledgements. This work was supported by the Australian Research Council Discovery grant (DP120100126). We would like to thank Don Neale for providing valuable ambient data measured by the Department of Environment and Heritage Protection (EHP) monitoring station.

3.6 References

Aiken AC, DeCarlo PF, Kroll JH, Worsnop DR, Huffman JA, Docherty KS, et al. O/C and OM/OC ratios of primary, secondary, and ambient organic aerosols with high-resolution time-of-flight aerosol mass spectrometry. Environmental Science & Technology 2008; 42: 4478-4485.

Alfarra MR, Prevot AS, Szidat S, Sandradewi J, Weimer S, Lanz VA, et al. Identification of the mass spectral signature of organic aerosols from wood burning emissions. Environmental science & technology 2007; 41: 5770-5777.

Allan J, Williams P, Morgan W, Martin C, Flynn M, Lee J, et al. Contributions from transport, solid fuel burning and cooking to primary organic aerosols in two UK cities. Atmospheric Chemistry and Physics 2010; 10: 647-668.

Bond TC, Streets DG, Yarber KF, Nelson SM, Woo JH, Klimont Z. A technology-based global inventory of black and organic carbon emissions from combustion. Journal of Geophysical Research: Atmospheres (1984–2012) 2004; 109.

Bougiatioti A, Stavroulas I, Kostenidou E, Zarmpas P, Theodosi C, Kouvarakis G, et al. Processing of biomass-burning aerosol in the eastern Mediterranean during summertime. Atmospheric Chemistry and Physics 2014; 14: 4793-4807.

Brito J, Rizzo L, Morgan W, Coe H, Johnson B, Haywood J, et al. Ground-based aerosol characterization during the South American Biomass Burning Analysis (SAMBBA) field experiment. Atmospheric Chemistry and Physics 2014; 14: 12069-12083.

Budisulistiorini SH, Canagaratna MR, Croteau PL, Marth WJ, Baumann K, Edgerton ES, et al. Real-time continuous characterization of secondary organic aerosol derived from isoprene epoxydiols in downtown Atlanta, Georgia, using the Aerodyne Aerosol Chemical Speciation Monitor. Environmental science & technology 2013; 47: 5686-5694.

Canagaratna M, Jayne J, Jimenez J, Allan J, Alfarra M, Zhang Q, et al. Chemical and microphysical characterization of ambient aerosols with the aerodyne aerosol mass spectrometer. Mass Spectrometry Reviews 2007; 26: 185-222.

Canagaratna M, Jimenez J, Kroll J, Chen Q, Kessler S, Massoli P, et al. Elemental ratio measurements of organic compounds using aerosol mass spectrometry: characterization, improved calibration, and implications. Atmospheric Chemistry and Physics Discussions 2014; 14: 19791-19835.

Canonaco F, Crippa M, Slowik J, Baltensperger U, Prévôt A. SoFi, an IGOR-based interface for the efficient use of the generalized multilinear engine (ME-2) for the source apportionment: ME-2 application to aerosol mass spectrometer data. Atmospheric Measurement Techniques 2013; 6: 3649-3661.

Canonaco F, Slowik J, Baltensperger U, Prévôt A. Seasonal differences in oxygenated organic aerosol composition: implications for emissions sources and factor analysis. Atmospheric Chemistry and Physics 2015; 15: 6993-7002.

Capes G, Johnson B, McFiggans G, Williams P, Haywood J, Coe H. Aging of biomass burning aerosols over West Africa: Aircraft measurements of chemical composition, microphysical properties, and emission ratios. Journal of Geophysical Research: Atmospheres (1984–2012) 2008; 113.

Carbone S, Aurela M, Saarnio K, Saarikoski S, Timonen H, Frey A, et al. Wintertime Aerosol Chemistry in Sub-Arctic Urban Air. Aerosol Science and Technology 2014; 48: 313-323.

Crilley LR, Ayoko GA, Morawska L. First measurements of source apportionment of organic aerosols in the Southern Hemisphere. Environmental Pollution 2014a; 184: 81-88.

Crilley LR, Jayaratne ER, Ayoko GA, Miljevic B, Ristovski Z, Morawska L. Observations on the formation, growth and chemical composition of aerosols in an urban environment. Environmental science & technology 2014b; 48: 6588-6596.

Crippa M, Canonaco F, Lanz V, Äijälä M, Allan J, Carbone S, et al. Organic aerosol components derived from 25 AMS data sets across Europe using a consistent ME-2 based source apportionment approach. Atmospheric Chemistry and Physics 2014; 14: 6159-6176.

Cubison M, Ortega A, Hayes P, Farmer D, Day D, Lechner M, et al. Effects of aging on organic aerosol from open biomass burning smoke in aircraft and laboratory studies. Atmospheric Chemistry and Physics 2011; 11: 12049-12064.

DeCarlo P, Ulbrich I, Crounse J, Foy Bd, Dunlea E, Aiken A, et al. Investigation of the sources and processing of organic aerosol over the Central Mexican Plateau from aircraft measurements during MILAGRO. Atmospheric Chemistry and Physics 2010; 10: 5257-5280.

Drewnick F, Hings SS, DeCarlo P, Jayne JT, Gonin M, Fuhrer K, et al. A new time-of-flight aerosol mass spectrometer (TOF-AMS)—Instrument description and first field deployment. Aerosol Science and Technology 2005; 39: 637-658.

Grieshop A, Logue J, Donahue N, Robinson A. Laboratory investigation of photochemical oxidation of organic aerosol from wood fires 1: measurement and simulation of organic aerosol evolution. Atmospheric Chemistry and Physics 2009; 9: 1263-1277.

Hallquist M, Wenger J, Baltensperger U, Rudich Y, Simpson D, Claeys M, et al. The formation, properties and impact of secondary organic aerosol: current and emerging issues. Atmos. Chem. Phys 2009; 9: 5155-5236.

Heringa M, DeCarlo P, Chirico R, Tritscher T, Dommen J, Weingartner E, et al. Investigations of primary and secondary particulate matter of different wood combustion appliances with a high-resolution time-of-flight aerosol mass spectrometer. Atmos. Chem. Phys 2011; 11: 5945-5957.

Hoffmann D, Tilgner A, Iinuma Y, Herrmann H. Atmospheric stability of levoglucosan: a detailed laboratory and modeling study. Environmental science & technology 2009; 44: 694-699.

Jimenez J, Canagaratna M, Donahue N, Prevot A, Zhang Q, Kroll JH, et al. Evolution of organic aerosols in the atmosphere. Science 2009; 326: 1525-1529.

Jimenez JL, Jayne JT, Shi Q, Kolb CE, Worsnop DR, Yourshaw I, et al. Ambient aerosol sampling using the aerodyne aerosol mass spectrometer. Journal of Geophysical Research: Atmospheres (1984–2012) 2003; 108.

Jolleys M, Coe H, McFiggans G, Taylor J, O'Shea S, Le Breton M, et al. Properties and evolution of biomass burning organic aerosol from Canadian boreal forest fires. Atmospheric Chemistry and Physics 2015; 15: 3077-3095.

Jordan TB, Seen AJ, Jacobsen GE. Levoglucosan as an atmospheric tracer for woodsmoke. Atmospheric Environment 2006; 40: 5316-5321.

Lanz V, Alfarra M, Baltensperger U, Buchmann B, Hueglin C, Prévôt A. Source apportionment of submicron organic aerosols at an urban site by factor analytical modelling of aerosol mass spectra. Atmospheric Chemistry and Physics 2007a; 7: 1503-1522.

Lanz VA, Alfarra MR, Baltensperger U, Buchmann B, Hueglin C, Szidat S, et al. Source attribution of submicron organic aerosols during wintertime inversions by advanced factor analysis of aerosol mass spectra. Environmental science & technology 2007b; 42: 214-220.

Luhar AK, Mitchell RM, Meyer C, Qin Y, Campbell S, Gras JL, et al. Biomass burning emissions over northern Australia constrained by aerosol measurements: II—Model validation, and impacts on air quality and radiative forcing. Atmospheric environment 2008; 42: 1647-1664.

May AA, Saleh R, Hennigan CJ, Donahue NM, Robinson AL. Volatility of organic molecular markers used for source apportionment analysis: measurements and implications for atmospheric lifetime. Environmental science & technology 2012; 46: 12435-12444.

Middlebrook AM, Bahreini R, Jimenez JL, Canagaratna MR. Evaluation of composition-dependent collection efficiencies for the aerodyne aerosol mass spectrometer using field data. Aerosol Science and Technology 2012; 46: 258-271.

Mohr C, DeCarlo P, Heringa M, Chirico R, Slowik J, Richter R, et al. Identification and quantification of organic aerosol from cooking and other sources in Barcelona using aerosol mass spectrometer data. Atmospheric Chemistry and Physics 2012; 12: 1649-1665.

Morawska L, Jayaratne E, Mengersen K, Jamriska M, Thomas S. Differences in airborne particle and gaseous concentrations in urban air between weekdays and weekends. Atmospheric Environment 2002; 36: 4375-4383.

Ng N, Canagaratna M, Jimenez J, Zhang Q, Ulbrich I, Worsnop D. Real-time methods for estimating organic component mass concentrations from aerosol mass spectrometer data. Environmental science & technology 2010a; 45: 910-916.

Ng N, Canagaratna M, Zhang Q, Jimenez J, Tian J, Ulbrich I, et al. Organic aerosol components observed in Northern Hemispheric datasets from Aerosol Mass Spectrometry. Atmospheric Chemistry and Physics 2010b; 10: 4625-4641.

Ortega A, Day D, Cubison M, Brune W, Bon D, de Gouw J, et al. Secondary organic aerosol formation and primary organic aerosol oxidation from biomass-burning smoke in a flow reactor during FLAME-3. Atmospheric Chemistry and Physics 2013; 13: 11551-11571.

Paatero P. The multilinear engine—a table-driven, least squares program for solving multilinear problems, including the n-way parallel factor analysis model. Journal of Computational and Graphical Statistics 1999; 8: 854-888.
Paatero P, Hopke PK. Rotational tools for factor analytic models. Journal of Chemometrics 2009; 23: 91-100.
Paatero P, Hopke PK, Song X-H, Ramadan Z. Understanding and controlling rotations in factor analytic models. Chemometrics and intelligent laboratory systems 2002; 60: 253-264.
Paatero P, Tapper U. Positive matrix factorization: A non-negative factor model with optimal utilization of error estimates of data values. Environmetrics 1994; 5: 111-126.
Simoneit BR. Biomass burning—a review of organic tracers for smoke from incomplete combustion. Applied Geochemistry 2002; 17: 129-162.
Simoneit BR, Schauer JJ, Nolte C, Oros DR, Elias VO, Fraser M, et al. Levoglucosan, a tracer for cellulose in biomass burning and atmospheric particles. Atmospheric Environment 1999; 33: 173-182.
Sun Y-L, Zhang Q, Schwab J, Demerjian K, Chen W-N, Bae M-S, et al. Characterization of the sources and processes of organic and inorganic aerosols in New York city with a high-resolution time-of-flight aerosol mass apectrometer. Atmospheric Chemistry and Physics 2011; 11: 1581-1602.
Ulbrich I, Canagaratna M, Zhang Q, Worsnop D, Jimenez J. Interpretation of organic components from Positive Matrix Factorization of aerosol mass spectrometric data. Atmospheric Chemistry and Physics 2009; 9: 2891-2918.
van der Werf GR, Randerson JT, Giglio L, Collatz GJ, Kasibhatla PS, Arellano Jr A. Interannual variability in global biomass burning emissions from 1997 to 2004. Atmospheric Chemistry and Physics 2006; 6: 3423-3441.
Weimer S, Alfarra M, Schreiber D, Mohr M, Prévôt A, Baltensperger U. Organic aerosol mass spectral signatures from wood-burning emissions: Influence of burning conditions and wood type. Journal of Geophysical Research: Atmospheres (1984–2012) 2008; 113.
Zhao R, Mungall EL, Lee AK, Aljawhary D, Abbatt JP. Aqueous-phase photooxidation of levoglucosan–a mechanistic study using Aerosol Time of Flight Chemical Ionization Mass Spectrometry (Aerosol-ToF-CIMS). Atmospheric Chemistry and Physics Discussions 2014; 14: 8819-8850.

3.7 Supplementary information

3.7.1 Meteorological and ambient data

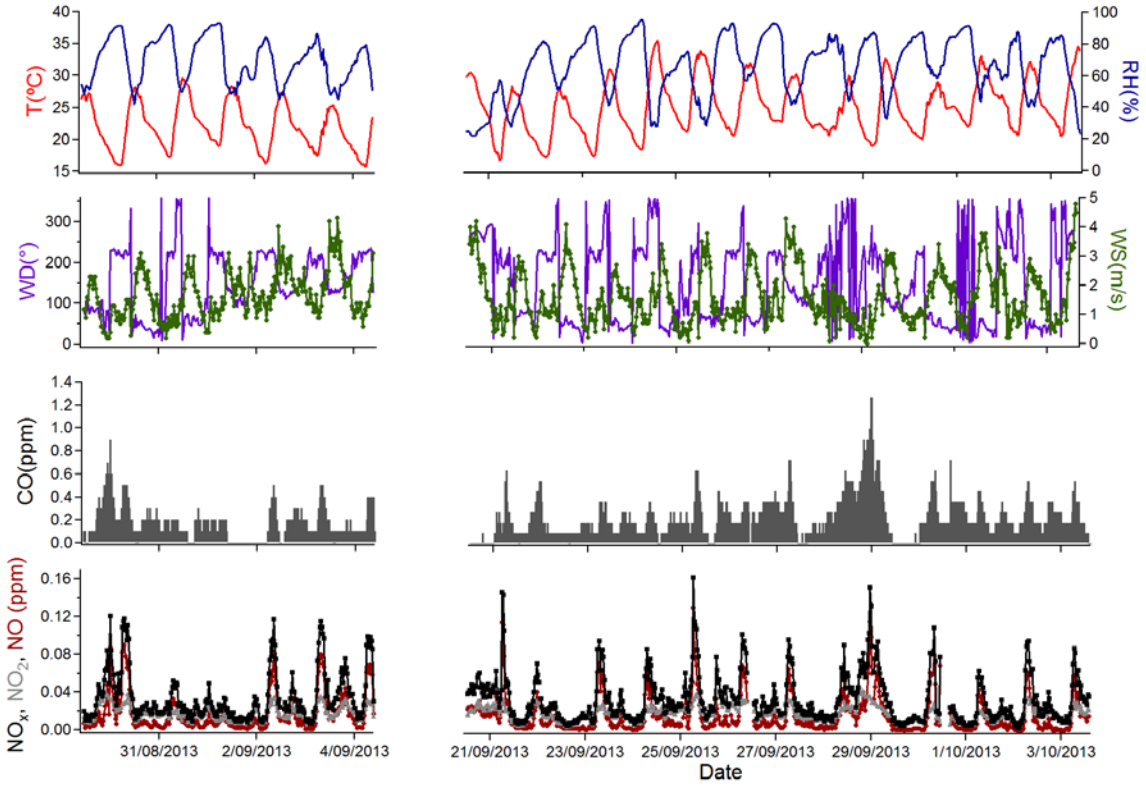

Figure 3.S1 Time trends of meteorological data including temperature (T) and relative humidity (RH), wind direction (WD) and wind speed (WS) and ambient air quality data including carbon monoxide (CO) and nitrogen oxides (NO_X)

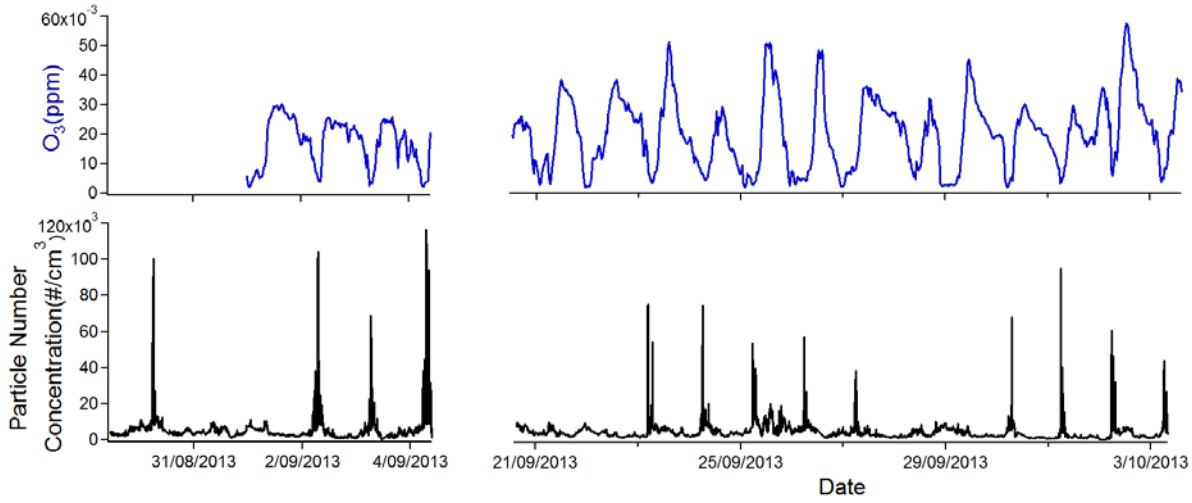

Figure 3.S2 Ozone and particle number concentration

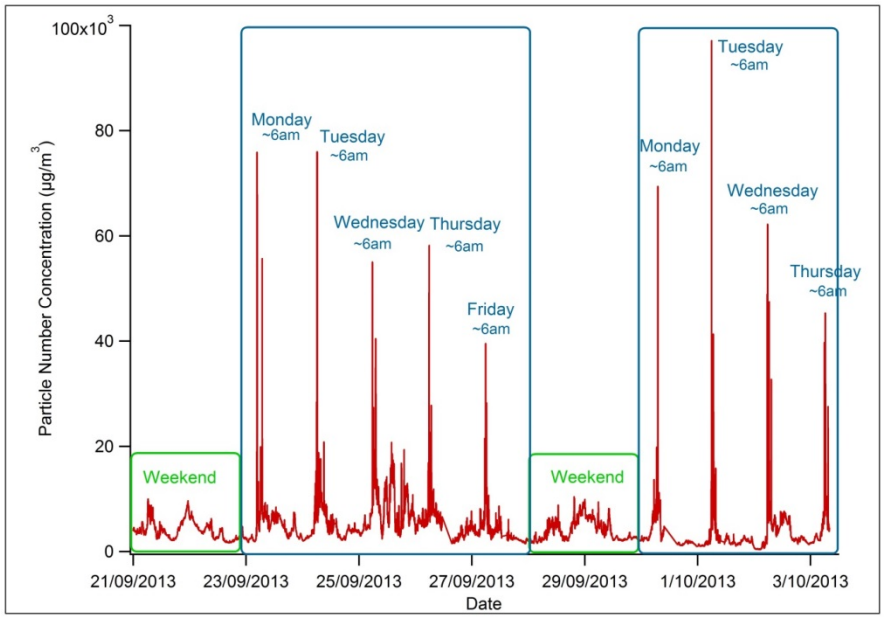

Figure 3.S3 Particle number concentration measured during the ambient sampling as illustration of weekday increases due to campus cleaning activities

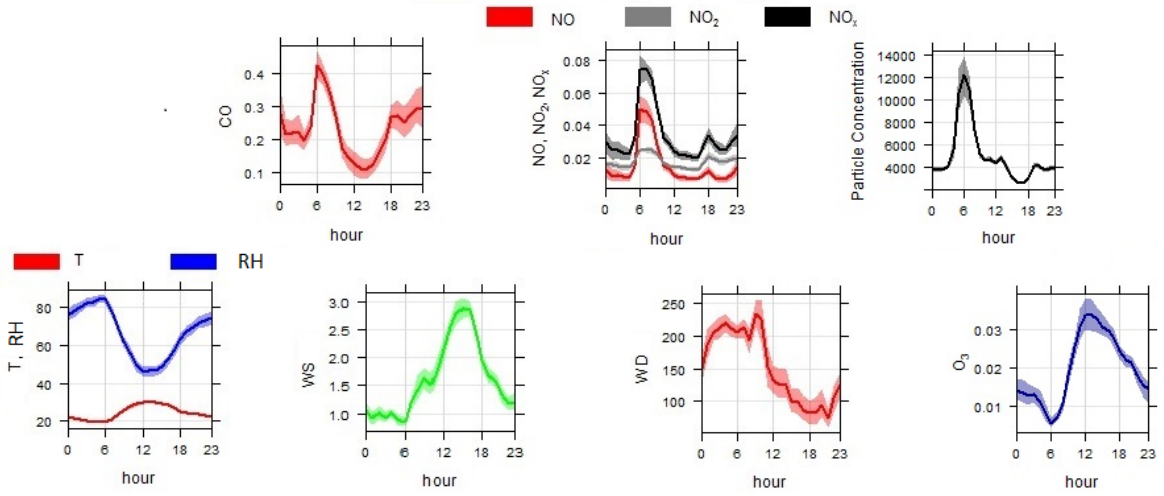

Figure 3.S4 Diurnal trends of ambient air data, meteorological factors and ozone (lines indicate mean values while shaded areas illustrate 95% confidence interval in mean)

3.7.2 Source apportionment

Unconstrained PMF (separate datasets)

An unconstrained PMF run was initially performed on the first and second datasets separately. A number of factors was set, from 1 to 10, with 10 iterations (seeds) applied. The 5-factor solution of ME-2 performed on the first period dataset was chosen as representative, considering the well apportioned peaks in the mass spectra of generated factors (Fig. 3.S5), successful separation of COA and HOA (Fig. 3.S6) and strong correlation of factors with compatible data (LV-OOA/sulfate and BBOA/Org 60) (Fig. 3.S7). Lower factor solutions did not result in HOA and COA profile separation, while solutions with six or more factors split the BBOA profile. The SV-OOA was revealed in the 7-factor solution however, BBOA splitting took place. The HOA diurnal trend resulted in a prominent morning traffic peak, while the cooking contribution was illustrated through clear diurnal peaks during meal times (lunch and evening increases). Strong temporal correlations were observed between both LV-OOA and SO_4 (R^2 of 0.83), and BBOA and Org 60 (R^2 of 0.87). PMF results for the second dataset (Fig. 3.S8) clearly indicate that software was not able to separate HOA and COA with less than 7 factors. The BBOA profile, in all solutions, apart from not enough apportioned 4-factor solution, resulted in factor splitting. As in the case of the first dataset, SV-OOA was extracted when more factors were applied. Although PMF performed on the first dataset resulted in a meaningful 5-factor solution, and both datasets generated similar OA factors, analysis of the two datasets separately did not yield one consistent solution that would cover both periods.

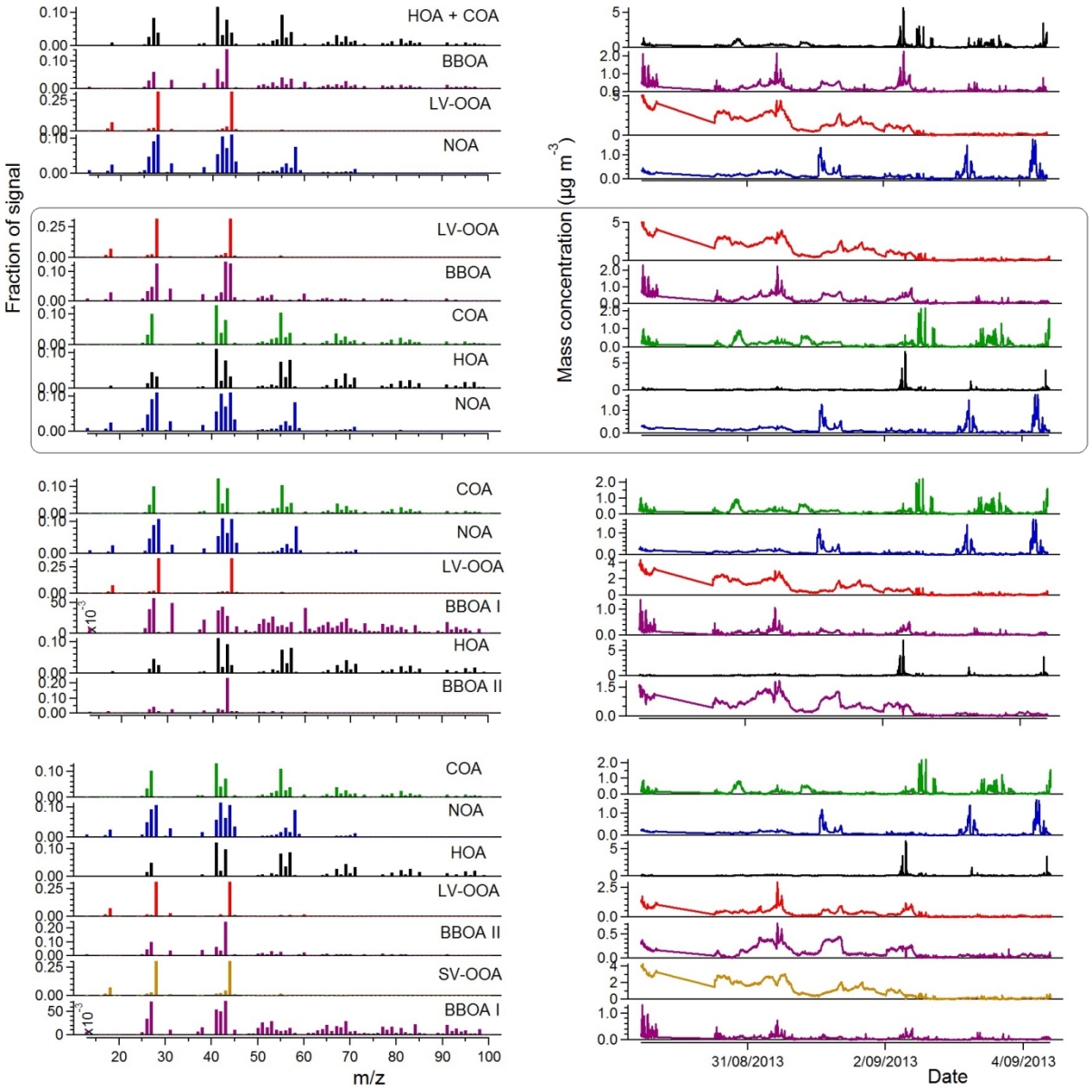

Figure 3.S5 Factor profiles and time series for four, five, six and seven factors after applying PMF on the first dataset (five factor solution is marked)

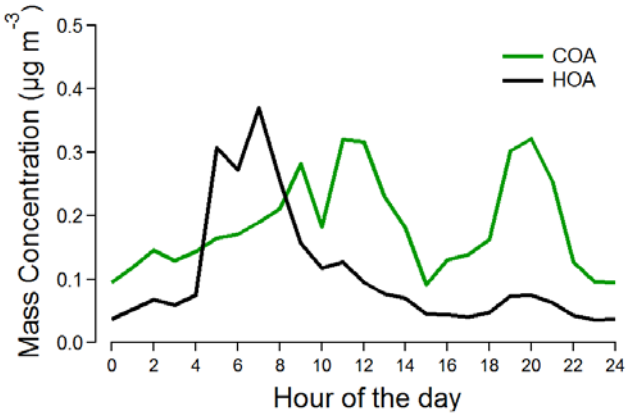

Figure 3.S6 Diurnal trend of HOA and COA for the 5-factor solution (first dataset)

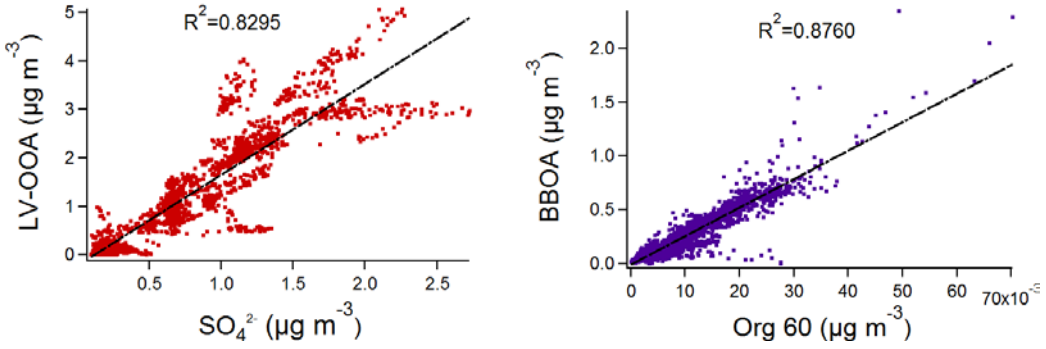

Figure 3.S7 Correlations of LV-OOA with sulfate and BBOA with Org 60 for the 5-factor solution (first dataset)

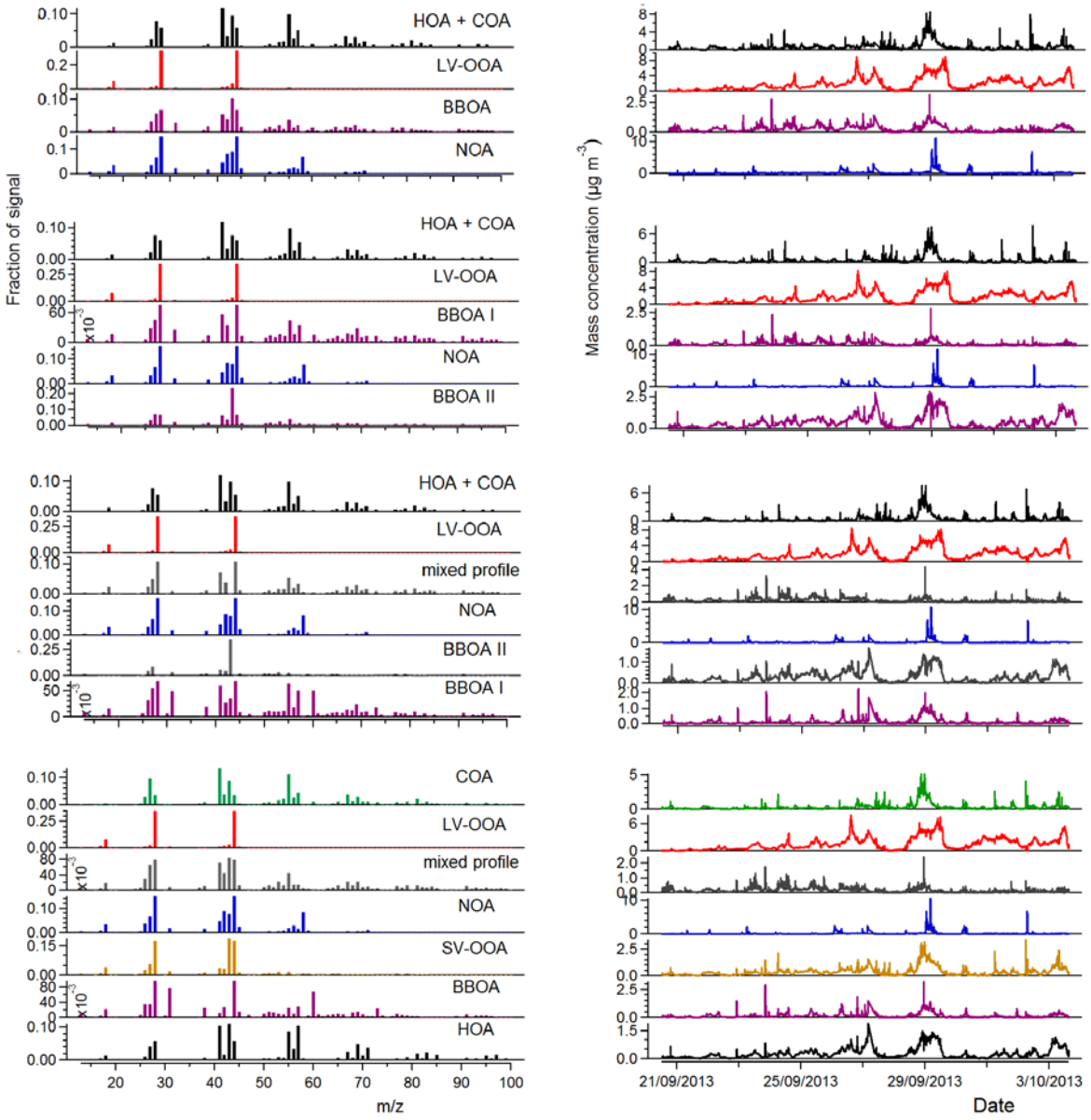

Figure 3.S8 Factor profile and time series for four, five, six and seven factors after applying PMF on the second dataset

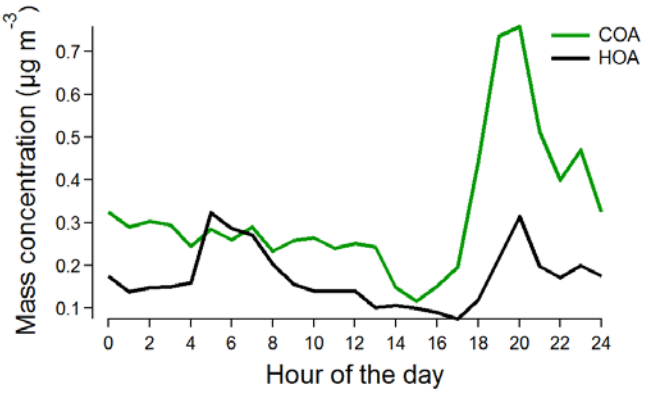

Figure 3.S9 Diurnal trend of HOA and COA for the 7-factor solution where HOA and COA were separated (second dataset)

Unconstrained PMF (combined datasets)

Performing data analysis on the joined dataset produced a wide range of air beam correction factor values even after applying all necessary adjustments within Squirrel. As a result, PMF analysis could not attribute *m/z* 29 and *m/z* 15 to meaningful factors, even when these signals were downweighted or when a high number of factors was generated (10-factor solution) (Fig. 3.S10 and Fig. 3.S11). m/z 29 is often a prominent signal in the BBOA profile factor, however it also contributes considerably to OOA and thus is not a suitably unique signature of any factor (Ng et al., 2010a). Further source apportionment analysis was thus performed without *m/z* 29 and *m/z* 15.

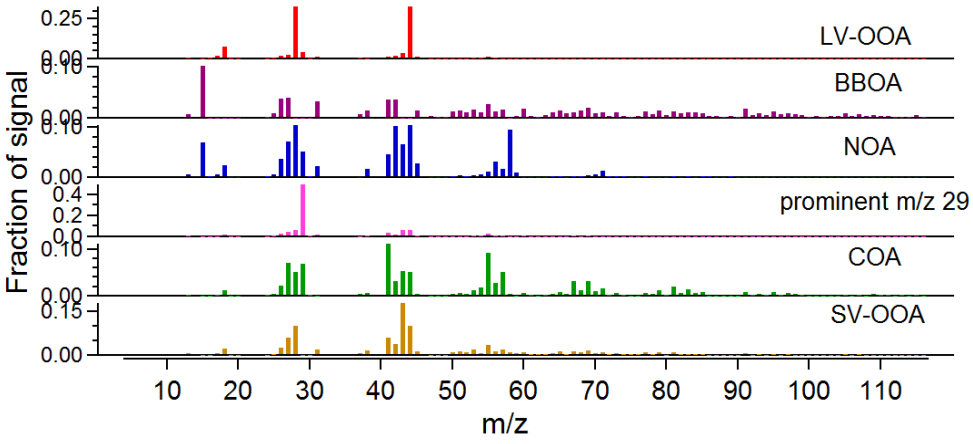

Figure 3.S10 PMF run with all *m/z*'s where the factor with prominent *m/z* 29 was identified

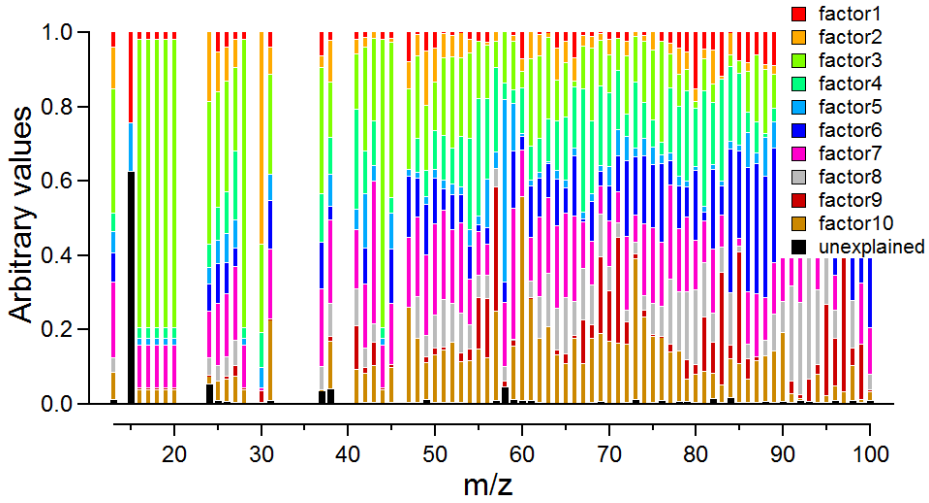

Figure 3.S11 PMF run (10-factor solution) with *m/z* 29 removed, where a significant portion of *m/z* 15 remained unexplained

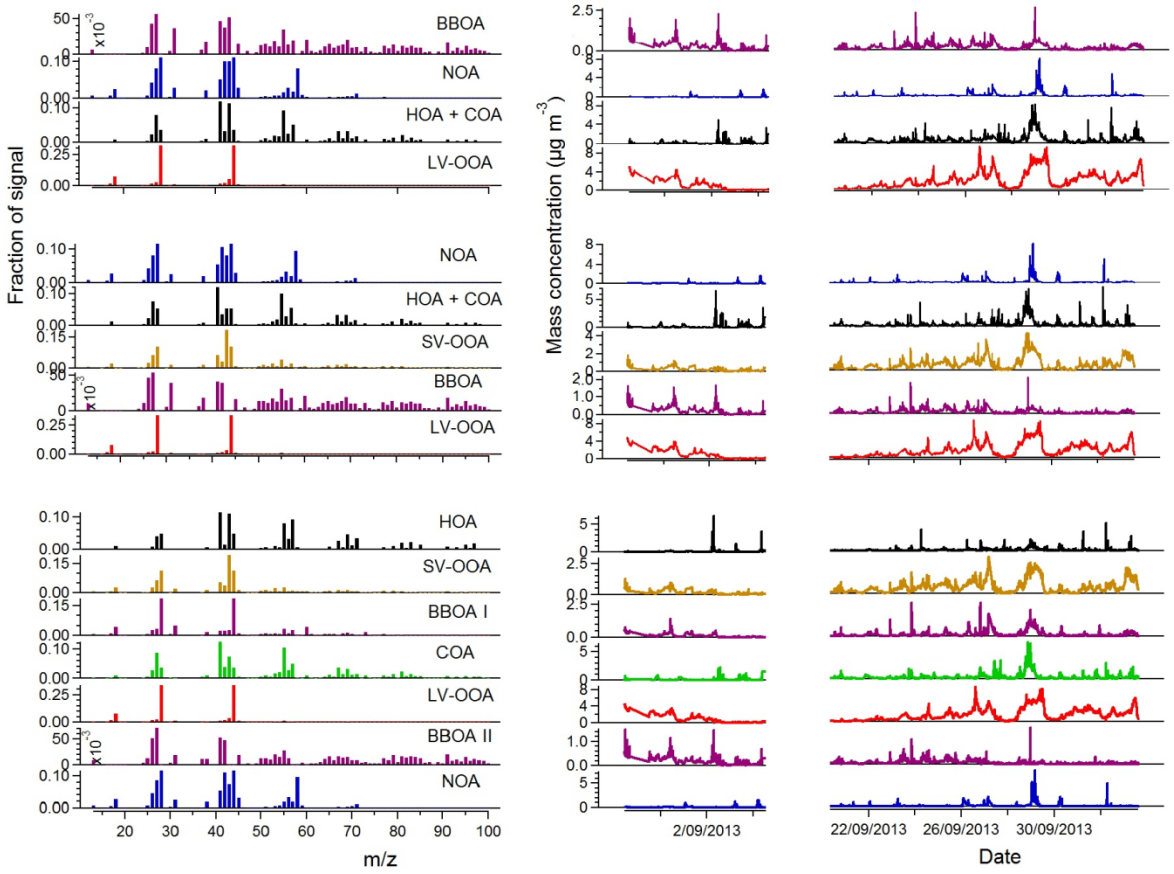

Figure 3.S12 Factor profiles and time series for four and five factors (HOA and COA profiles are merged in one factor) and the 7-factor solution (BBOA was split into two factors)

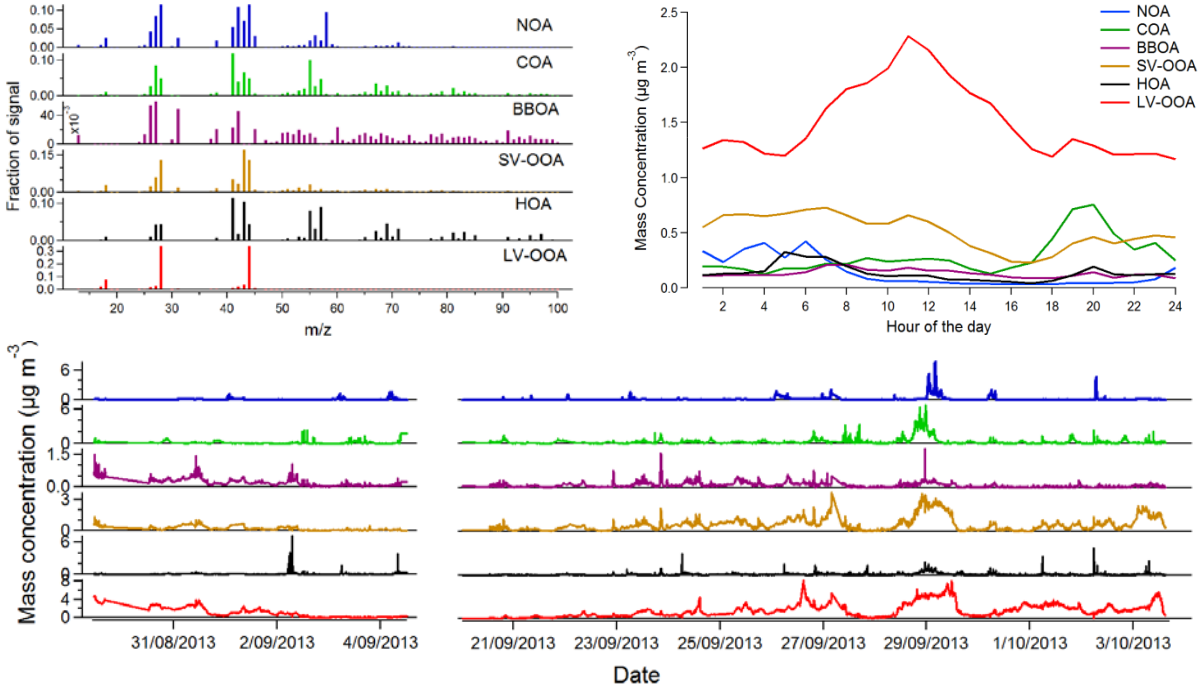

Figure 3.S13 Factor profile, diurnal variation and time series of the unconstrained PMF 6-factor solution

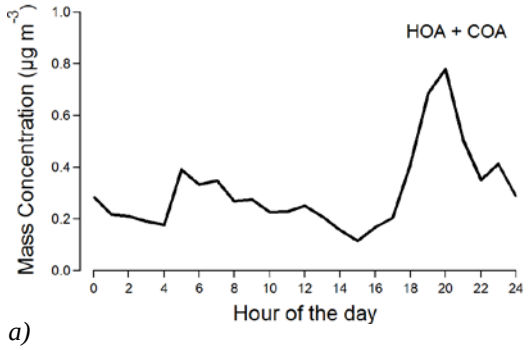

a)

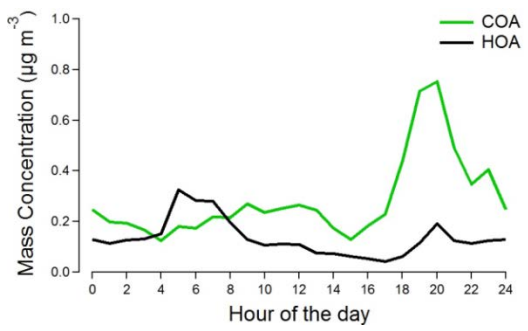

b)

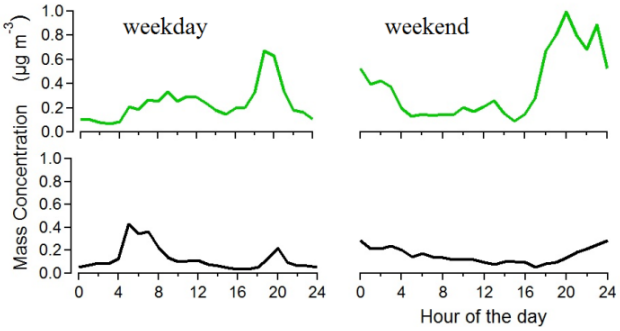

c)

Figure 3.S14 HOA and COA diurnal trend for a) the 5-factor solution where they belong to one combined factor, b) the 6-factor solution where they are separated, and c) the separated factors with the evening cooking peak attributed to COA (which continues and becomes more elevated over the weekend) and the morning traffic peak attributed to HOA (which disappears during weekend)

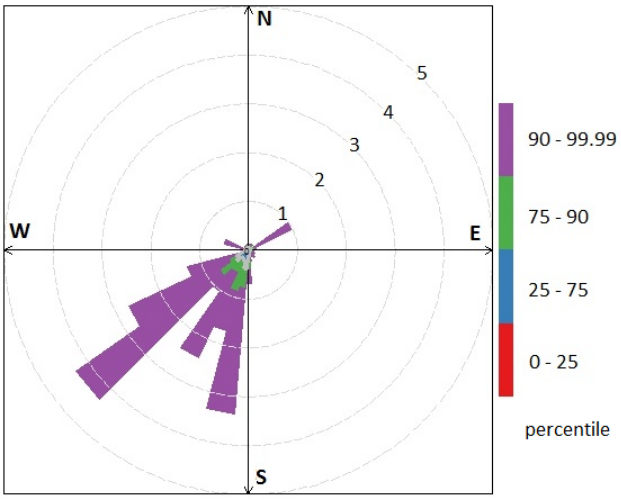

Figure 3.S15 Percentile Rose for NOA factor concentration illustrating uniform wind direction (NOA was taken from the final 6-factor solution) (concentric circles represent concentration (0-5 µg m^{-3}) and colors represent percentile frequency of concentrations in each direction)

Table 3.S1 O/C_{A-A} and O/C_{I-A} values calculated using equations introduced by Aiken et al. (2008) and Canagaratna et al. (2014), respectively, for HOA and COA factors including combined and separate datasets (where I and II illustrate the first and the second period); O/C ratios calculated for this study are elevated compared to other studies, likely due to excluding *m/z* 29 and 15 from the organic matrix.

Factor	COA	HOA	COA_I	HOA_I	COA_II	HOA_II
O/C_{A-A}	0.2659	0.2463	0.0791	0.1925	0.2094	0.3008
O/C_{I-A}	0.2895	0.2673	0.0794	0.2066	0.2257	0.3288

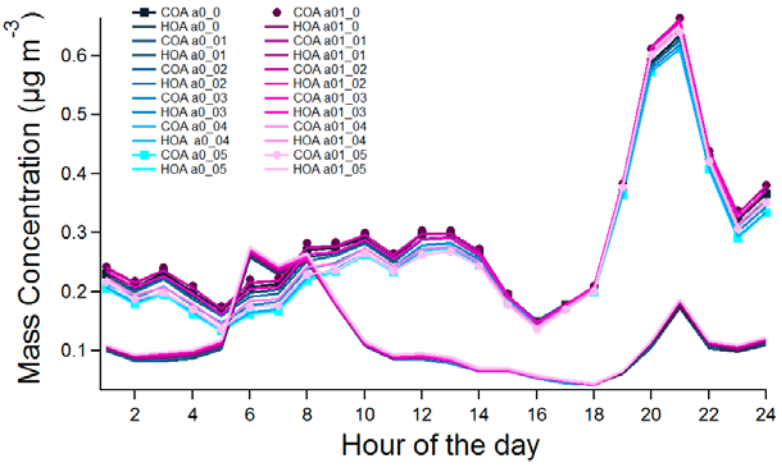

Figure 3.S16 COA and HOA diurnal patterns for different α value combinations

Table 3.S2 Correlations (Pearson - R^2) between factor profiles and corresponding tracers for different α values for the whole dataset and for the first (I) and the second period (II) separately (the first and second numbers after symbol of α values indicate the COA/HOA and BBOA constraint values, respectively)

	BBOA/Org60	*BBOA/Org60 I*	*BBOA/Org60 II*	*LV-OOA/sulfate*	*LV-OOA/sulfate I*	*LV-OOA/sulfate II*	*SV-OOA/nitrate*	*SV-OOA/nitrate I*	*SV-OOA/nitrate II*
a 0_0	**0.3706**	**0.9036**	**0.4186**	**0.4417**	**0.8223**	**0.4242**	**0.6009**	**0.4389**	**0.6188**
a 0_0.1	**0.3547**	**0.8993**	**0.4095**	**0.4454**	**0.8222**	**0.4185**	**0.5824**	**0.4376**	**0.5974**
a 0_0.2	**0.3434**	**0.8946**	**0.4017**	**0.4459**	**0.8219**	**0.4142**	**0.5649**	**0.4016**	**0.5770**
a 0_0.3	**0.3367**	**0.8912**	**0.3975**	**0.4457**	**0.8227**	**0.4035**	**0.5611**	**0.3970**	**0.5720**
a 0_0.4	**0.3365**	**0.8893**	**0.3990**	**0.4439**	**0.8231**	**0.3960**	**0.5634**	**0.4142**	**0.5735**
a 0_0.5	**0.3403**	**0.8891**	**0.4036**	**0.4430**	**0.8225**	**0.3955**	**0.5648**	**0.4245**	**0.5745**
a 0.1_0	**0.3698**	**0.9106**	**0.4256**	**0.4354**	**0.8193**	**0.4297**	**0.6109**	**0.4744**	**0.6260**
a 0.1_0.1	**0.3443**	**0.9074**	**0.4096**	**0.4417**	**0.8190**	**0.4224**	**0.5960**	**0.4618**	**0.6089**
a 0.1_0.2	**0.3309**	**0.9030**	**0.4005**	**0.4407**	**0.8180**	**0.4203**	**0.5778**	**0.4233**	**0.5875**
a 0.1_0.3	**0.3230**	**0.9001**	**0.3954**	**0.4427**	**0.8178**	**0.4169**	**0.5679**	**0.4125**	**0.5758**
a 0.1_0.4	**0.3216**	**0.8987**	**0.3965**	**0.4454**	**0.8190**	**0.4093**	**0.5645**	**0.4210**	**0.5716**
a 0.1_0.5	**0.3233**	**0.8979**	**0.3993**	**0.4448**	**0.8196**	**0.4036**	**0.5632**	**0.4344**	**0.5730**

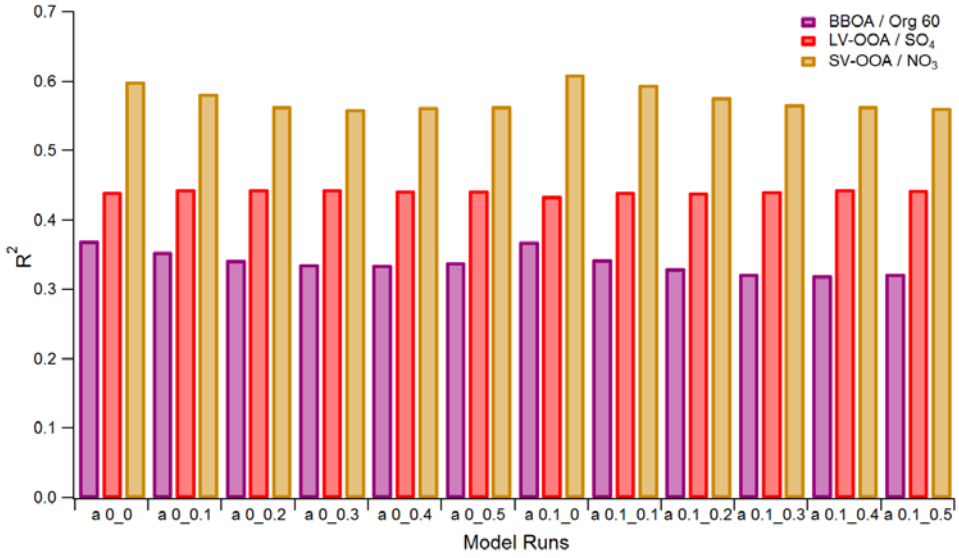

Figure 3.S17 Correlations (R^2) between factor profiles and corresponding tracers for different model runs (first number indicate COA/HOA constraint value and second BBOA constraint value applied) for the whole dataset

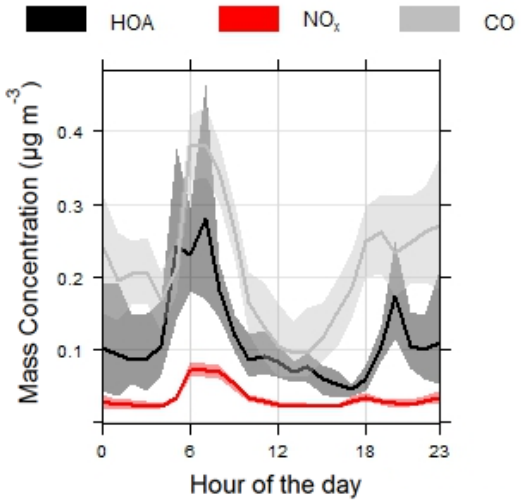

Figure 3.S18 Comparison of diurnal variations of HOA factor, NO_X and CO (HOA was taken from the final, 6-factor solution); lines indicate mean values while shaded areas illustrate the 95% confidence interval in mean

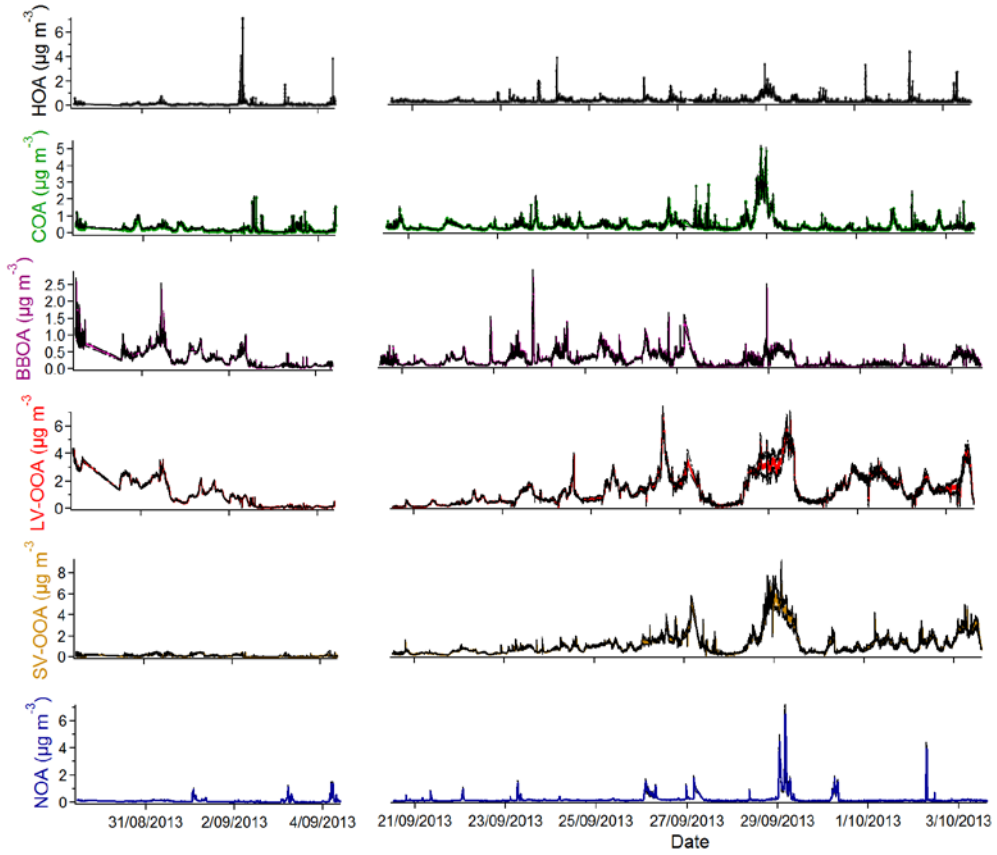

Figure 3.S19 Time series of all retrieved factors in the final solution (averaged profile) with black lines showing the profile spread (max and minimum values of all model runs for certain factor); Calculated mean values and ranges of the spread were 0.1144 ± 0.0174, 0.2785 ± 0.0600, 0.2334 ± 0.0452, 1.1344 ± 0.2282, 0.8255 ± 0.2356 and 0.1183 ± 0.0448 for HOA, COA, BBOA, LV-OOA, SV-OOA and NOA, respectively

Comparison of the unconstrained and constrained solutions

Table 3.S3 $O/C_{A\text{-}A}$ and $O/C_{I\text{-}A}$ values for the final constrained 6-factor solution calculated using equations introduced by Aiken et al. (2008) and Canagaratna et al. (2014), respectively (O/C ratios calculated for this study are elevated compared to other studies, likely due to excluding *m/z* 29 and 15 from the organic matrix).

Factor	COA	HOA	BBOA	NOA	LV-OOA	SV-OOA
$O/C_{A\text{-}A}$	0.0791	0.1887	0.4881	0.4500	1.4393	0.6742
$O/C_{I\text{-}A}$	0.0794	0.2023	0.5402	0.4971	1.6133	0.7501

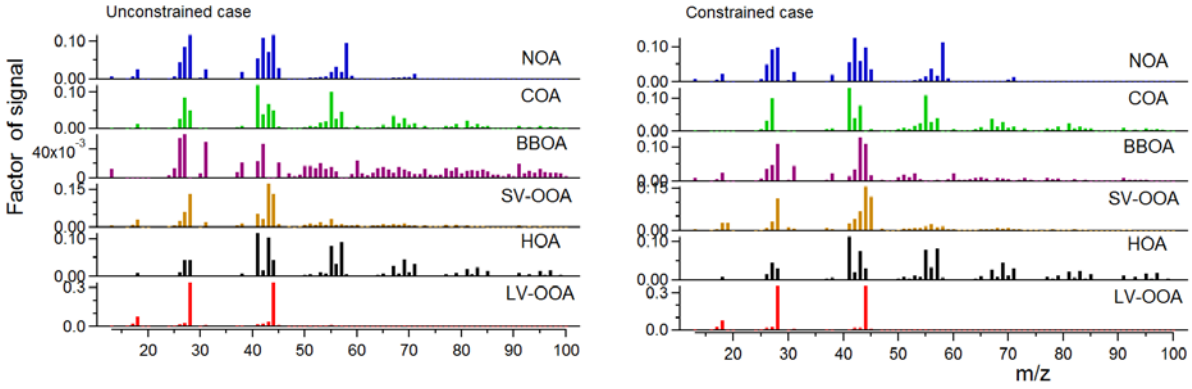
Unconstrained case
Constrained case
Factor of signal
NOA
COA
BBOA
SV-OOA
HOA
LV-OOA
m/z

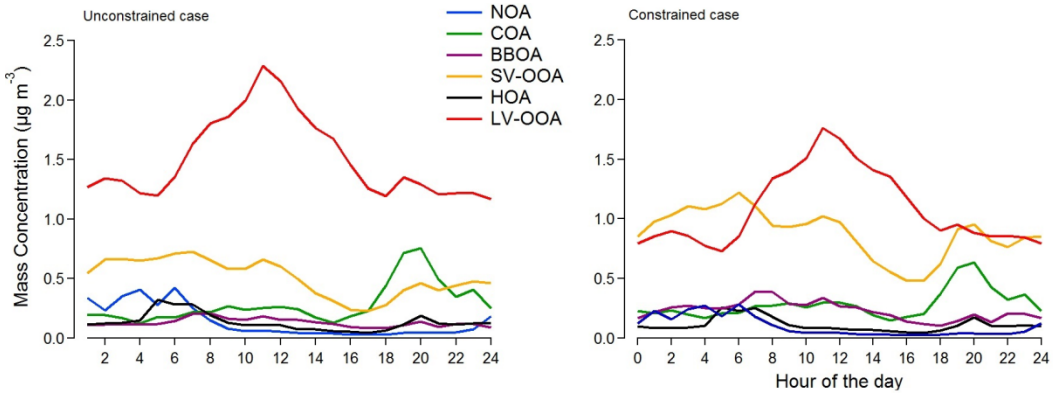
Unconstrained case
Constrained case
Mass Concentration (µg m-3)
NOA
COA
BBOA
SV-OOA
HOA
LV-OOA
Hour of the day

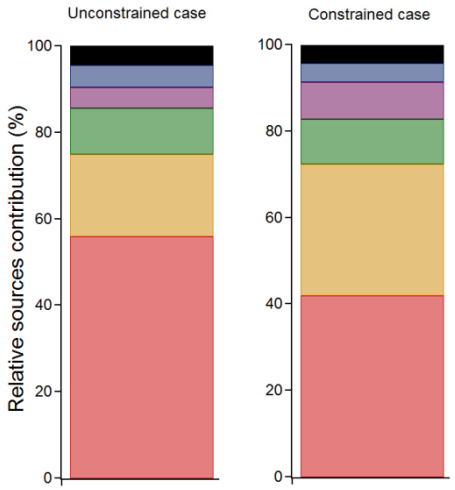
Unconstrained case
Constrained case
Relative sources contribution (%)

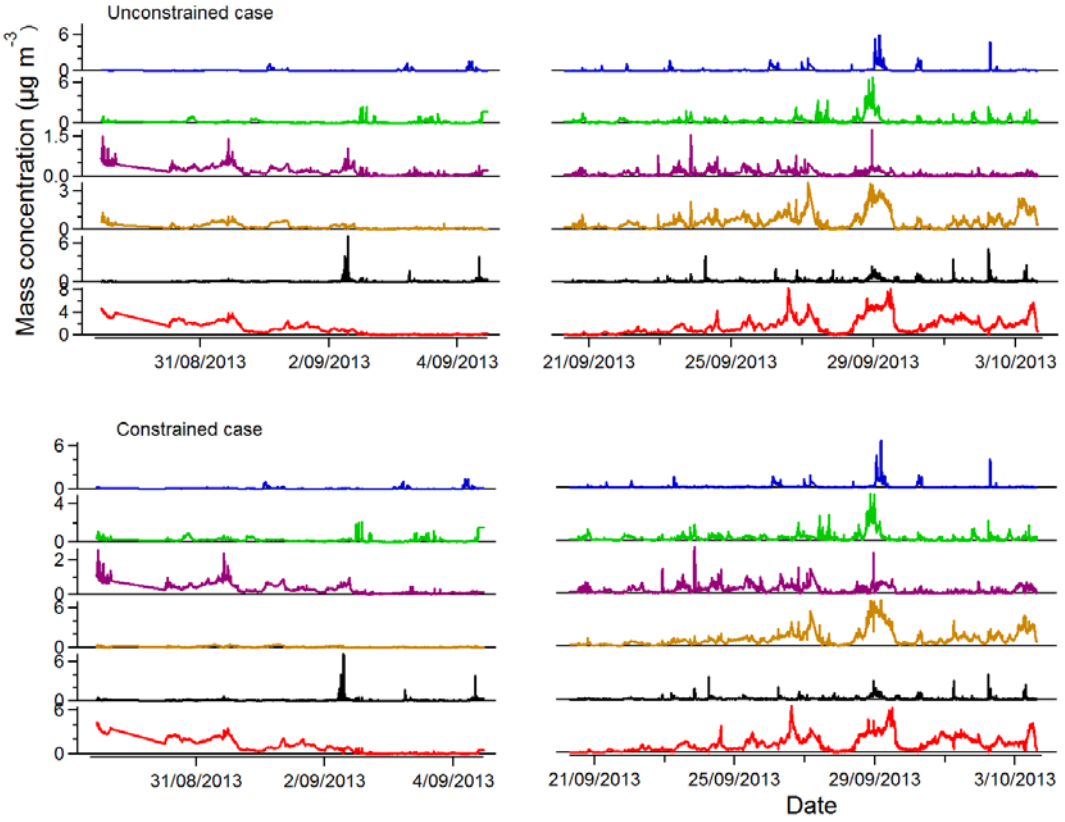

Figure 3.S20 Comparison of factor profiles, diurnal and time trends, and relative contributions for unconstrained and constrained (averaged profile) 6-factor solutions

Chapter 4

BIOMASS BURNING EMISSIONS IN NORTH AUSTRALIA DURING THE EARLY DRY SEASON: AN OVERVIEW OF THE 2014 SAFIRED CAMPAIGN

Marc D. Mallet[1], Maximilien J. Desservettaz[2], Branka Miljevic[1], Andelija Milic[1], Zoran D. Ristovski[1], Joel Alroe[1], Luke T. Cravigan[1], E. Rohan Jayaratne[1], Clare Paton-Walsh[2], David W.T. Griffith[2], Stephen R. Wilson[2], Graham Kettlewell[2], Marcel V. van der Schoot[3], Paul Selleck[3], Fabienne Reisen[3], Sarah J. Lawson[3], Jason Ward[3], James Harnwell[3], Min Cheng[3], Rob W. Gillett[3], Suzie B. Molloy[3], Dean Howard[4], Peter F. Nelson[4], Anthony L. Morrison[4], Grant C. Edwards[4], Alastair G. Williams[5], Scott D. Chambers[5], Sylvester Werczynski[5], Leah R. Williams[6], Victoria H.L. Winton[7n], Brad Atkinson[8], Xianyu Wang[9], Melita D. Keywood[3]

[1] Department of Chemistry, Physics and Mechanical Engineering, Queensland University of Technology, Queensland, Brisbane, 4000, Australia
[2] Centre for Atmospheric Chemistry, University of Wollongong, Wollongong, New South Wales, 2522, Australia
[3]CSIRO Oceans and Atmosphere, Aspendale, Victoria, 3195, Australia
[4] Department of Environmental Sciences, Macquarie University, Sydney, New South Wales, 2109, Australia
[5]Australian Nuclei Science and Technology Organisation, Sydney, New South Wales, 2232, Australia
[6]Aerodyne Research, Inc., Billerica, Massachusetts, 01821, USA
[7]Physics and Astronomy, Curtin University, Perth, Western Australia, 6102, Australia
[8]Bureau of Meteorology, Darwin, Northern Territory, 0810, Australia
[9]National Research Centre for Environmental Toxicology, Brisbane, Queensland, 4108, Australia
[n]Now at the British Antarctic Survey, National Environmental Research Council, Cambridge, 01223, UK

Under review in Atmospheric Chemistry and Physics (doi:10.5194/acp-2016-866)

STATEMENT OF JOINT AUTHORSHIP

The authors listed below have certified that:

1. they meet the criteria for authorship in that they have participated in the conception, execution, or interpretation, of at least that part of the publication in their field of expertise;

2. they take public responsibility for their part of the publication, except for the responsible author who accepts overall responsibility for the publication;

3. there are no other authors of the publication according to these criteria;

4. potential conflicts of interest have been disclosed to (a) granting bodies, (b) the editor or publisher of journals or other publications, and (c) the head of the responsible academic unit, and

5. they agree to the use of the publication in the student's thesis and its publication on the QUT ePrints database consistent with any limitations set by publisher requirements.

In the case of this chapter: Chapter 4

TITLE

Biomass burning emissions in north Australia during the early dry season: an overview of the 2014 SAFIRED campaign

AUTHORS

M.D. Mallet[a,b,c,d,e], M.J. Desservettaz[b,c,d,e], B. Miljevic[b,c,e*], **A. Milic[b,d,e] (candidate)**, Z.D. Ristovski[b,e], J. Alroe[b,e], L.T. Cravigan[b,c,e], E.R. Jayaratne[d,e], C. Paton-Walsh[b,c,e], D.W.T. Griffith[b,e], S.R. Wilson[b,e], G. Kettlewell[b,e], M.V. Vanderschoot[b,e], P. Selleck[b,c,d,e], F. Reisen[b,c,e], S.J. Lawson[b,c,d,e], J. Ward[b,c,d,e], J. Harnwell[b,c,e], M. Cheng[b,c,d,e], R.W. Gillett[b,c,d,e], S.B. Molloy[d,e], D. Howard[b,c,d,e], P.F. Nelson[b,e], A.L Morrison[b,e], G.C. Edwards[b,c,d,e], A.G. Williams[b,c,e], S.D. Chambers[b,c,d,e], S. Werczynski[b,c,e], L.R. Williams[c,e], V.H.L. Winton[b,c,d,e], B. Atkinson[b,c], X. Wang[b,d,e], M.D. Keywood[b,c,d,e*]

[a] Wrote and organised the manuscript

[b] Contributed to the organisation of the campaign

[c] Installed and/or operated instrumentation during the sampling period

[d] Analysed data

[e] Contributed to the manuscript and/or data interpretation

*Corresponding author

All authors declare that they have no conflict of interest.

Principal Supervisor Confirmation

I have sighted email or other correspondence from all Co-authors confirming their certifying authorship.

Zoran Ristovski		26/09/2016
Name	Signature	Date

Biomass burning emissions in north Australia during the early dry season: an overview of the 2014 SAFIRED campaign

Marc D. Mallet[1], Maximilien J. Desservettaz[2], Branka Miljevic[1*], Andelija Milic[1], Zoran D. Ristovski[1], Joel Alroe[1], Luke T. Cravigan[1], E. Rohan Jayaratne[1], Clare Paton-Walsh[2], David W.T. Griffith[2], Stephen R. Wilson[2], Graham Kettlewell[2], Marcel V. van der Schoot[3], Paul Selleck[3], Fabienne Reisen[3], Sarah J. Lawson[3], Jason Ward[3], James Harnwell[3], Min Cheng[3], Rob W. Gillett[3], Suzie B. Molloy[3], Dean Howard[4], Peter F. Nelson[4], Anthony L. Morrison[4], Grant C. Edwards[4], Alastair G. Williams[5], Scott D. Chambers[5], Sylvester Werczynski[5], Leah R. Williams[6], Victoria H.L. Winton[7,n], and Brad Atkinson[8], Xianyu Wang[9], Melita D. Keywood[3*]

[1]Department of Chemistry, Physics and Mechanical Engineering, Queensland University of Technology, Queensland, Brisbane, 4000, Australia
[2]Centre for Atmospheric Chemistry, University of Wollongong, Wollongong, New South Wales, 2522, Australia
[3]CSIRO Oceans and Atmosphere, Aspendale, Victoria, 3195, Australia
[4]Department of Environmental Sciences, Macquarie University, Sydney, New South Wales, 2109, Australia
[5]Australian Nuclei Science and Technology Organisation, Sydney, New South Wales, 2232, Australia
[6]Aerodyne Research, Inc., Billerica, Massachusetts, 01821, USA
[7]Physics and Astronomy, Curtin University, Perth, Western Australia, 6102, Australia
[8]Bureau of Meteorology, Darwin, Northern Territory, 0810, Australia
[9]National Research Centre for Environmental Toxicology, Brisbane, Queensland, 4108, Australia
[n]Now at the British Antarctic Survey, National Environmental Research Council, Cambridge, 01223, UK

Correspondence to: Branka Miljevic (b.miljevic@qut.edu.au) and Melita Keywood (melita.keywood@csiro.au)

Abstract. The SAFIRED (Savannah Fires in the Early Dry Season) campaign took place from 29th of May, 2014 until the 30th June, 2014 at the Australian Tropical Atmospheric Research Station (ATARS) in the Northern Territory, Australia. The purpose of this campaign was to investigate emissions from fires in the early dry season in northern Australia. Measurements were made of biomass burning aerosols, volatile organic compounds, polycyclic aromatic carbons, greenhouse gases, radon, mercury cycle, and trace metals. Aspects of the biomass burning aerosol emissions investigated included; emission factors of various emitted species, physical and chemical aerosol properties, aerosol aging, micronutrient supply to the ocean, nucleation, and aerosol water uptake. Over the course of the month-long campaign, biomass burning signals were prevalent and emissions from several large single burning events were observed at ATARS. Biomass burning emissions dominated the gas and aerosol concentrations in this region. Nine major biomass burning events were identified and associated with intense or close individual smoke plumes. Dry season fires are extremely frequent and widespread across the northern region of Australia, which suggests that the measured aerosol and gaseous emissions at ATARS are likely representative of signals across the entire region of north Australia. Air mass forward trajectories show that these biomass burning emissions are carried northwest over the Timor Sea and could influence the atmosphere over Indonesia and the tropical atmosphere over the Indian Ocean. The outcomes of this campaign will be numerous. This region is an environment with little human impact and provides a unique look into the characteristics of biomass burning aerosol without the influence of other significant

emission sources. Relationships between the aerosol physical and chemical properties, gas concentrations and meteorological data for the entire month will provide fundamental knowledge required to understand the influence of early dry season burning in this tropical region on the atmosphere. In this paper we present characteristics of the biomass burning observed at the sampling site and provide an overview of the more specific outcomes of the SAFIRED campaign.

Keywords. Biomass burning, savannah fires, greenhouse gases, aerosols, mercury

4.1 Introduction

Tropical north Australia is dominated by savannah ecosystems. This region consists of dense native and exotic grasslands and scattered trees and shrubs. Conditions are hot, humid and wet in the summer months of December through March with hot, dry conditions for the rest of the year giving rise to frequent fires between June and November each year. Human settlements are relatively scarce in northern Australia, outside of the territory capital, Darwin (population of 146 000). To the north of the continent are the tropical waters of the Timor Sea, as well as the highly populated Indonesian archipelago. South of the savannah grasslands are the Tanami, Simpson and Great Sandy Deserts, spanning hundreds of thousands of square kilometers. Emissions from fires in the savannah regions of northern Australia are therefore the most significant regional source of greenhouse and other trace gases, as well as atmospheric aerosol. Globally, savannah and grassland fires are the largest source of carbon emissions (Shi et al., 2015; van der Werf et al., 2010) and play a significant role in the earth's radiative budget. It is therefore important to quantify, characterise and fully understand the emissions from savannah fires in northern Australia, taking into account the complexity, variability and diversity of the species emitted.

In Australia approximately 550 000 km^2 of tropical and arid savannahs burn each year (Meyer et al., 2012;Russell-Smith et al., 2007), representing 7% of the continent's land area. In the tropical north of Australia, the fires during the early dry season in May/June consist of naturally occurring and accidental fires, as well as prescribed burns under strategic fire management practice to reduce the frequency and intensity of more extensive fires in the late dry season in October and November (Andersen et al., 2005). These fires in the early dry season burn with a low to moderate intensity and are normally confined to the grass-layer. Events where fires reach the canopy level are rare. These prescribed burns are an important process for the region and are undertaken by local landholders with permits, as well as government supported bodies and volunteers. There has been a recent push to reinstate traditional Aboriginal fire management regimes in this region (Russell-Smith et al., 2013). Other fire management regimes are implemented in similar environments around the world, such as the savannah ecosystems of Africa (Govender et al., 2006) or the chaparral grasses in the United States (Akagi et al., 2012). In general, fire management regimes are considered to benefit regional biodiversity and can lead to the long-term increase in living biomass, resulting in a reduction of greenhouse gas emissions (Russell-Smith et al., 2013). Quantifying the emissions

from dry season fires on regional scales is essential for understanding the impact of these fires on the local and global atmosphere.

The components and concentrations of emissions from savannah fires are dependent upon the vegetation and burning conditions. While CO_2 is the primary product of biomass burning (BB), incomplete combustion also results in the emission of many other trace gases such as CO, CH_4, NOx, N_2O as well as non-methane organic compounds (NMOCs) and aerosol particles composed of elemental carbon, organic carbon and some inorganic material (Crutzen and Andreae, 1990). The state of organics in biomass burning aerosols can vary significantly due to the type of plant material burned, the characteristics of the fires themselves as well as through aging processes in the atmosphere.

The effects of these emissions on radiative forcing are complex. The global average radiative forcing due to biomass burning aerosol-radiation interaction is estimated in the 5th International Panel on Climate Change report as 0.0 W m^{-2} with an uncertainty range of -0.20 to +0.20 Wm^{-2} (Bindoff et al., 2013). It is well known that greenhouse gases have a positive radiative forcing, heating up the atmosphere. Light absorbing carbon in the aerosol phase will also result in a positive radiative forcing (Jacobson, 2001) by absorbing shortwave radiation. Conversely, the presence of aerosol organic and inorganic matter can result in a negative radiative forcing by scattering solar radiation (Penner et al., 1998). In addition, biomass burning has been shown to be a significant source of cloud condensation nuclei (CCN), despite typically being composed of weakly hygroscopic substances (Lawson et al., 2015), due to the high number of particles emitted. This can result in a change in cloud droplet concentrations and volume, thereby influencing cloud formation, albedo and lifetime. The contribution of each species to the overall radiative forcing is also likely to change as smoke plumes age (Liousse et al., 1995). Furthermore, not all biomass burning aerosol will interact with radiation in the same way. For example, fresh BB emissions in the tropics has been observed to be more absorbing than those from boreal forest fires(Wong and Li, 2002). The role of biomass burning emissions is not limited to the Earth's radiative budget. Certain species of emissions (e.g., mercury) can be deposited and sequestered in soil (Gustin et al., 2008), vegetation (Rea et al., 2002) or bodies of water (LaRoche and Breitbarth, 2005).

There is a need for a better scientific understanding of the influence biomass burning has on atmospheric composition and air quality (Kaiser and Keywood, 2015). Furthermore, the tropics are disproportionately under-sampled and the atmospheric and ocean processes in these regions are of both regional and global consequence. The SAFIRED campaign will contribute towards better understanding biomass burning emissions and the atmospheric composition in tropical Australia.

4.2. Description of experiment

4.2.1 Site

The Australian Tropical Atmospheric Research Station (ATARS; 12°14'56.6"S, 131°02'40.8"E) is located on the Gunn Point peninsula in northern Australia (see Fig. 4.1). ATARS is operated by the Australian Bureau of Meteorology and the CSIRO (Commonwealth Scientific and Industrial Research Organization). Standard meteorological measurements (wind velocity, atmospheric pressure, precipitation) run permanently at ATARS and two laboratories are in place for the installation of other instruments. The SAFIRED campaign took place from 29th May 2014 until the 30th June 2014, with personnel and instruments from nine institutes utilizing these laboratories to make comprehensive gaseous and aerosol measurements during this period of the early dry season.

4.2.2 Instruments and measurements

Trace Gases

Greenhouse gases

Continuous measurement of CO_2, CO, CH_4 and N_2O were made using a high precision FTIR trace gas and isotope Spectronus analyser, developed by the Centre for Atmospheric Chemistry at the University of Wollongong. The analyser combines a Fourier Transform Infrared (FTIR) Spectrometer (Bruker IRcube), a pressure and temperature controlled multi-pass cell and an electronically cooled mercury cadmium telluride detector. A detailed description of the instrument and concentration retrieval technique are available in Griffith et al. (2012) and Griffith (1996).

Ozone and other trace gases

A Multi Axis Differential Optical Absorption Spectrometer (MAX-DOAS) was installed on the top of one of the laboratories during the campaign. The technique has been shown to provide vertical profile of nitrogen dioxide, ozone, sulfur dioxide, formaldehyde, glyoxal and aerosol extinction (Sinreich et al., 2005;Honninger et al., 2004). The MAX-DOAS instrument used in this campaign was designed and built at the University of Wollongong. It consists of a vertically rotating prism capturing scattered solar radiation at different angles (1°, 2°, 4°, 8°, 16°, 30° and a reference at 90°) into a fibre optic that carries the radiation to a UV-Visible spectrometer (AvaSpec – ULS3648). Furthermore, a Thermo Scientific model 49i UV Photomeric Ozone analyser was used to measure ozone concentrations.

Non methane organic compounds

Online NMOC measurements were made using a high sensitivity Proton Transfer Reaction-Mass Spectrometer (PTR-MS; Ionicon Analytik) using H_3O^+ as the primary ion. The inlet was 10 m in length and drew air at 5 L min^{-1} from 2 m above the roof (approx 5.5 m above ground level). The PTR-MS ran with inlet and drift tube temperature of 60 ºC, 600 V drift tube,

and 2.2 mbar drift tube pressure, which equates to an energy field of 135 Td. The PTR-MS sequentially scanned masses 15-190, with 1 second dwell time. The PTR-MS operated with the aid of auxiliary equipment which regulates the flow of air in the sample inlet and controls whether the PTR-MS is sampling ambient or zero air or calibration gas (Galbally et al., 2007). During the campaign the PTR-MS was calibrated once per day for the following compounds using certified gas standards from Apel Riemer Environmental Inc, USA and Air Liquide Specialty Gases, USA: acetaldehyde, acetone, acetonitrile, benzene, methacrolein, methanol, methyl ethyl ketone, toluene, 1,3,5-trimethyl benzene, m-xylene, chlorobenzene, alpha pinene, 1,2-dichlorobenzene, 1,3,4 trichlorobenzene, dimethyl sulphide and isoprene. Calibration data were used to construct sensitivity plots, which were used to calculate approximate response factors for other masses not specifically calibrated.

During sampling, carbonyls and dicarbonyls were trapped on S10 Supelco cartridges, containing high-purity silica adsorbent coated with 2,4-dinitrophenylhydrazine (DNPH, where they were converted to the hydrazone derivatives). Samples were refrigerated immediately after sampling until analysis. The derivatives were extracted from the cartridge in 2.5 mL of acetonitrile and analysed by high performance liquid chromatography with diode array detection. The diode array detection enables the absorption spectra of each peak to be determined. The difference in the spectra highlights which peaks in the chromatograms are mono- or dicarbonyl DNPH derivatives and, along with retention times, allows the identification of the dicarbonyls glyoxal and methylglyoxal. Further details can be found in Lawson et al. (2015).

PAHs

PAHs were sampled through a high-volume air sampler (Kimoto Electric Co., LTD.) using a sampling rate typically at ~60 m^{-3} h^{-1}. The sampling rate was calibrated using an orifice plate prior to the sampling campaign and the sampling volume was calculated based on the calibrated sampling rate and sampling duration. A bypass gas meter installed on the sampler was used to monitor any anomalous fluctuation of the sampling rate during the sampling period. Particle-associated and gaseous PAHs were collected on glass fibre filters (Whatman™, 203×254 mm, grade GF/A in sheets) and subsequent polyurethane foam plugs respectively. The glass fibre filters and polyurethane foam, along with the field blank samples, were extracted separately using an Accelerated Solvent Extractor (Thermo Scientific™ Dionex™ ASE™ 350) after being spiked with a solution containing 7 deuterated PAHs (i.e. $^{2}D_{10}$-phenanthrene, $^{2}D_{10}$-fluoranthene, $^{2}D_{12}$-chrysene, $^{2}D_{12}$-benzo[b]fluoranthene, $^{2}D_{12}$-BaP, $^{2}D_{12}$-indeno[1,2,3-cd]pyrene, $^{2}D_{12}$-benzo[g,h,i]perylene) at different levels as internal standards for quantification purposes. Concentrated extracts were cleaned up by neutral alumina and neutral silica. Eluents were carefully evaporated to near dryness and refilled with 250 pg of $^{13}C_{12}$-PCB (polychlorinated biphenyl) 141 (in 25 µL isooctane) employed as the recovery/instrument standard for estimating the recoveries of the spiked internal standards and monitoring the performance of the analytical instrument. Samples were analysed using a Thermo Scientific™ TRACE™ 1310 gas chromatograph coupled to a Thermo Scientific™ double-focusing system™ Magnetic Sector high resolution mass spectrometer. The HRMS was operated in electron impact-multiple ion detection mode and resolution was set to ≥ 10,000 (10% valley definition). An isotopic dilution method was used to quantify 13 PAH analytes including phenanthrene,

anthracene, fluoranthene, pyrene, benzo[a]anthrancene, chrysene, benzo[b]fluoranthene, benzo[k]fluoranthene, benzo[e]pyrene, BaP, indeno[1,2,3-cd]pyrene, dibenzo[a,h]anthracene, benzo[g,h,i]perylene.

Mercury

Total gaseous mercury, gaseous elemental mercury + gaseous oxidised mercury (TGM; GEM + GOM), was sampled from a 10 m mast and measured via gold pre-concentration and cold vapour atomic fluorescence spectroscopy using a Tekran 2537X instrument. Simultaneously, GEM, GOM and PBM were individually measured using a Tekran 2537B connected to a combined Tekran 1130/1135 speciation unit sampling at a 5.4 m height. The sampling train of the 1130/1135 collects first GOM (KCl-coated denuder) then PBM (quartz wool pyrolyser) in series from a 10 L min^{-1} sampling flow, allowing GEM only to flow onwards for detection by subsampling by the 2537B. Due to the small atmospheric concentrations of GOM and PBM, pre-concentration occurred over a 1-hour period with subsequent analysis taking an additional hour. Continuous measurements of GEM at 5-minute resolution were made possible for the 2537B unit by rotating pre-concentration/analysis roles of the two internal gold traps. Both 2537 units sampled at 1 L min^{-1} and were calibrated every 23 hours using an internal mercury permeation source. For more information on the 2537 and 1130/1135 systems see Landis et al. (2002) and Steffen et al. (2008).

GEM fluxes were measured using the methods outlined in Edwards et al. (2005). Air samples were drawn at heights of 5.2 and 8.0 m through 46.4 m of nylon tubing using a PTFE diaphragm pump operating at 10 L min^{-1}. Subsampling from this flow (through a 0.2 µm PTFE filter at 1 L min^{-1} by a Tekran 2537A) and switching between sample intakes, allowed resolution of a GEM gradient every 30 minutes. The transfer velocity was measured using a Campbell Scientific CSAT3 sonic anemometer and LI-COR 7200 closed path infrared gas analyser for CO_2, both located on the same tower as the gradient intakes at 6.6 m and sampling at 20 Hz.

Radon

Radon-222 (radon) is a naturally occurring radioactive noble gas that arises from the alpha-particle decay of radium-226, which is ubiquitous in most soil and rock types. With a half-life of 3.82 days, radon has thus proven to be an excellent indicator of recent (within 2-3 weeks) terrestrial influences on air masses for observations at coastal or island sites (Chambers et al., 2014). Radon is unreactive and poorly soluble, and its only atmospheric sink is radioactive decay. Furthermore, it has a half-life comparable to the lifetimes of short-lived atmospheric pollutants (e.g., NOx, SO_2) and atmospheric residence time of water and aerosols. Radon's unique combination of physical characteristics make it an ideal tracer for (i) regional air mass transport studies, in which it is often used in conjunction with air mass back trajectories for fetch analyses (Williams et al., 2009;Chambers et al., 2014); (ii) investigations of vertical mixing processes within the daytime convective boundary layer (Williams et al., 2011) or nocturnal boundary layer (Chambers et al., 2015); (iii) identifying periods of minimal terrestrial influence on a measured air mass ("baseline" studies; (Chambers et al., 2016)); (iv)

performing regional flux or inventory analyses for trace atmospheric species with similar source distributions (Biraud et al., 2000) and (v) evaluating the performance of transport and mixing schemes in climate and chemical-transport models (Locatelli et al., 2015).

In order to measure Radon concentrations, a 700 L dual-flow-loop two-filter radon detector, designed and built by the Australian Nuclear Science and Technology Organisation (Whittlestone and Zahorowski, 1998;Chambers et al., 2014), was installed at the ATARS in 2011 and has been fully operational since July 2012. The detector provided continuous hourly radon concentrations for the duration of the SAFIRED campaign, sampling air at 40 L min^{-1} from 12 m above ground level through 25 mm high-density polyethylene agricultural pipe. A coarse aerosol filter and dehumidifier were installed "upstream" of the detector, as well as a 400 L delay volume to ensure that thoron (^{220}Rn, half-life 55 s) concentrations in the inlet air stream were reduced to less than 0.5 % of their ambient values. The detector's response time is around 45 minutes, and the lower limit of detection is 40 - 50 mBq m^{-3}. Calibrations are performed on a monthly basis by injecting radon from a PYLON 101.15±4% kBq Ra-226 source (12.745 Bq min^{-1} ^{222}Rn), traceable to NIST standards, and instrumental background is checked every 3 months. In post processing, half-hourly raw counts were integrated to hourly values before calibration to activity concentrations (Bq m^{-3}).

Aerosols

Aerosol Drying System

An Automated Regenerating Aerosol Diffusion Dryer (ARADD) is permanently installed on the roof of the laboratory containing the aerosol instrumentation for this campaign. This was used in front of the aerosol manifold to continuously dry the aerosol sample. The ARADD design, similar to that described by Tuch et al. (2009), continuously conditions the aerosol sample to a relative humidity of below 40% with maximum aerosol transmission efficiency. The ARADD utilizes two diffusion drying columns in parallel, each containing 7 stainless steel mesh tubes of 10 mm internal diameter and approximately 800 mm length, surrounded by a cavity packed with silica gel. The aerosol sampled is directed into one column at a time, while the other column is regenerated by an ultra-dry compressed air system. All flows are controlled by software that directs sample flow and compressed air flow to the appropriate column with a series of valves. The ARADD has a Total Suspended Particulate style intake at the inlet of the aerosol sample path, and a sample manifold at the exit of the system to provide sampling take-offs for the various aerosol instruments connected to the ARADD. Flow through the ARADD is provided by the instruments and pumps connected downstream. The ambient and inlet relative humidity for the entire sampling period were logged and are displayed in Supplementary Fig. 4.S1.

Aerosol Size

Aerosol size distributions were measured with a Scanning Mobility Particle Sizer (SMPS). A TSI 3071 long-column electrostatic classifier with a TSI 3772 Condensation Particle Counter (CPC) measured the size distribution over a range of 14 nm to 670 nm at a scan interval of 5 minutes.

In addition to the aerosol size distributions measured by the SMPS, neutral and charged aerosol particle distributions from 0.8 nm to 42 nm were measured using a Neutral cluster and Air Ion Spectrometer (NAIS)(Manninen et al., 2009;Mirme et al., 2007). In this study, the NAIS was set to operate in a cycle of 4 min including ion and neutral particle sampling periods of 2 and 1 minute, respectively, with the remaining minute being an offset period which is required to neutralize and relax the electrodes. The total sampling air flow was 60 L min^{-1}, the high flow rate being used to minimize ion diffusion losses and maximize the measured ion concentration sensitivity. Ion losses are accounted for during post-processing of the data by the software (Mirme et al., 2007).

Aerosol Composition and Water Uptake

PM_1 and PM_{10} 12-hour filter samples (night and day) were collected on a TAPI 602 Beta plus particle measurement system (BAM). Portions of the PM_1 filters have been analysed for elemental and organic carbon mass loadings using a DRI Model 2001A Thermal-Optical Carbon Analyzer following the IMPROVE-A temperature protocol (Chow et al., 2007b). Additional portions of the PM_1 filters were extracted in 5 ml of 18.2 mΩ de-ionized water and preserved using 1% chloroform. These extracts will be analysed for major water-soluble ions by suppressed ion chromatography and for anhydrous sugars including levoglucosan by high-performance anion-exchange chromatography with pulsed amperometric detection (Iinuma et al., 2009).

Daily aerosol filters were collected using two Ecotech 3000 high-volume volumetric flow controlled aerosol samplers with PM_{10} size selective inlets. One high-volume sampler was used to collect aerosols on acid cleaned Whatman 41 filters to determine the soluble and total fraction of trace metals. Soluble trace metals were extracted from a filter aliquot using ultra-pure water (>18.2 mΩ) leaching experiments. Total trace metal concentrations were determined by digesting a second filter aliquot with concentrated nitric and hydrofluoric acids. Leachates and digested solutions were analysed by high resolution inductively couple plasma mass spectrometry. The second sampler was used to collect a set of aerosol samples on quartz filters for elemental and organic carbon analysis following (Chow et al., 2007a), and major anion and cation analysis.

The volatility and hygroscopicity of 50 nm and 150 nm particles were measured with a custom built Volatility and Hygroscopicity Tandem Differential Mobility Analyser (VH-TDMA). Inlet dried particles were size selected (alternating between 50 and 150 nm) using a TSI 3080 electrostatic classifier. Scans alternated between two different sample pathways.

In the first, after size selection, particles were passed through a thermodenuder set to 120°C. The sample line was then split so that half went to an SMPS comprised of a TSI 3080 classifier and a TSI 3010 CPC (V-TDMA). The rest of the sample was passed through a humidifying system that exposed the particles to a relative humidity of 90% before being brought into another SMPS with a 3080 classifier and 3010 CPC (H-TDMA). Alternatively, the thermodenuder was bypassed in every second scan so that the V-TDMA was used to verify the size selection and the H-TDMA was able to observe the hygroscopic growth of ambient particles. Each scan ran for 3 minutes, giving a full set of data every 12 minutes.

The chemical composition and properties of non-refractory sub-micron particles were investigated with a compact Time-of-Flight Aerosol Mass Spectrometer (cToF-AMS, Aerodyne Research, Inc.) and a Time of Flight Aerosol Chemical Speciation Monitor (ToF-ACSM, Aerodyne Research, Inc.). Both of these instruments operate with the same principle and have many identical components. An aerodynamic lens in the inlet of each instrument focuses the particles into a beam and differential pumping removes most of the gas phase. Particles are flash vaporized at 600°C and ionized by electron impact before passing through a time-of-flight mass spectrometer to a multi-channel plate detector in the cToF-AMS and a dynode detector in the ToF-ACSM. The cToF-AMS has the added benefit of having a particle Time-of-Flight (pToF) mode, which allows the size resolved chemical composition to be measured. Both instruments sampled through a $PM_{2.5}$ inlet and nafion dryer. In addition, the inlet of the cToF-AMS was incorporated into the VH-TDMA system, so that when the VH-TDMA was measuring ambient particles, the cToF-AMS would draw particles through the thermodenuder set at 120°C and vice-versa. This gives additional information about the chemical composition of the volatile component of submicron particles.

The number of particles activated to cloud droplets was measured using a Continuous-Flow Steam Wise Thermal Gradient Cloud Condensation Nuclei Counter (CCNC) from Droplet Measurement Technologies Inc. (DMT, model No. 100). Particles were exposed to a 0.5% supersaturation and activated particles greater than 1µm were counted with an Optical Particle Counter using a 50 mW, 658 nm laser diode.

Back trajectories

Hourly 10-day air mass back trajectories terminating at ATARS were produced using the NOAA HYSPLIT model (Draxler and Rolph, 2003), and catalogued in a data base for use with the SAFIRED campaign data set. Global Data Assimilation System input files with 0.5° resolution were obtained from NOAA ARL FTP site (http://ready.arl.noaa.gov/gdas1.php) to drive the HYSPLIT model.

Satellite detection of fires

Data on the location of fires was collected from the Australian national bushfire monitoring system, Sentinel Hotspots. Hotspot locations are derived from the Moderate Resolution Imaging Spectroradiometer (MODIS) sensors on the Terra and

Aqua satellites and the Visible Infrared Imaging Radiometer Suite (VIIRS) sensor on the Suomi NPP satellite. The Terra, Aqua and Suomi NPP satellites fly over the region around ATARS at approximately 10:30 am, 3 pm and 2:30 pm, respectively. Detection of fires is therefore limited to those that are flaming during these times.

4.3. Overview of Campaign

4.3.1 Fires and air masses

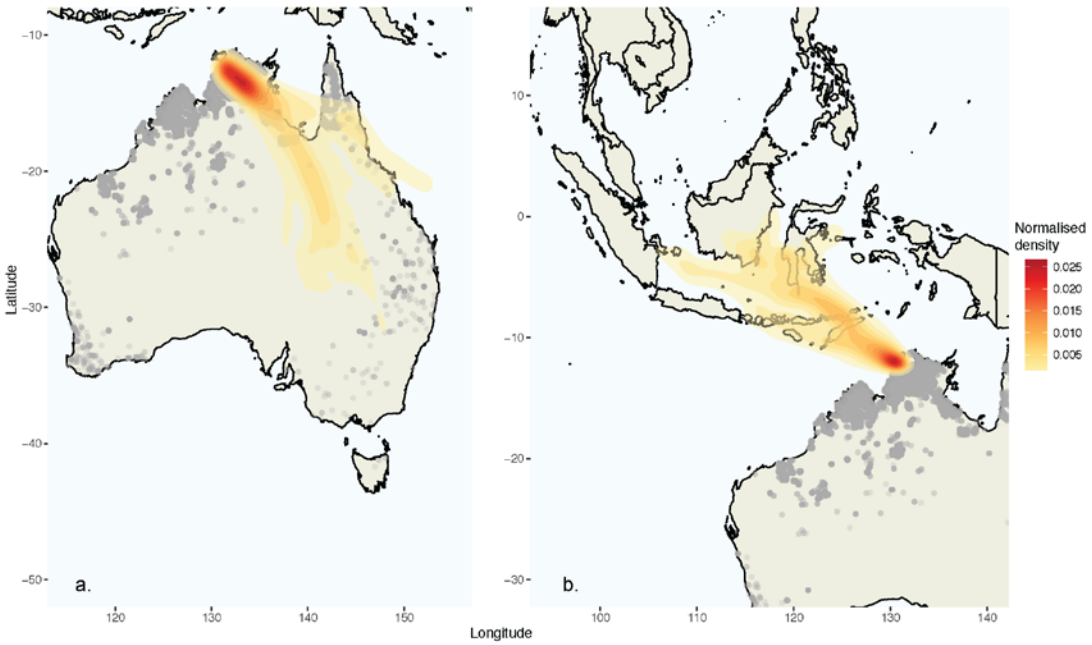

Figure 4.5 The HYSPLIT (a) back and (b) forward trajectories to and from the ATARS site, truncated to five days. The colour scale represents the normalised data. Grey dots are MODIS and VIIRS detected hotspots from the 30th of May 2016 until the 29th of June 2016.

Thousands of fires were observed in during the period of the SAFIRED campaign in Australia by the MODIS and VIIRS sensors on the Terra and Aqua NASA satellites. The vast majority of these occurred in the savannah regions of northern Australia (Fig. 4.1). The number of detected fires on each day within 10 km, 20 km, 50 km, 100 km and 200 km of the sampling location was determined (Fig. 4.2). Several fires within 10km were detected on the 30th of May and the 9th, 10th, 25th and the 26th of June. These correspond with the highest gaseous and aerosol signals. The periods between the 11th and 24th of June had very few detected fires within 50km of the station. Satellite flyby times were in the early afternoon local

time each day and therefore fires not occuring during these times would not be recorded. Airmass back trajectories from the ATARS site show that air masses over the study period were predominately southeasterly (Fig. 4.1 and 4.4c), generally over the regions where fires were frequently detected.

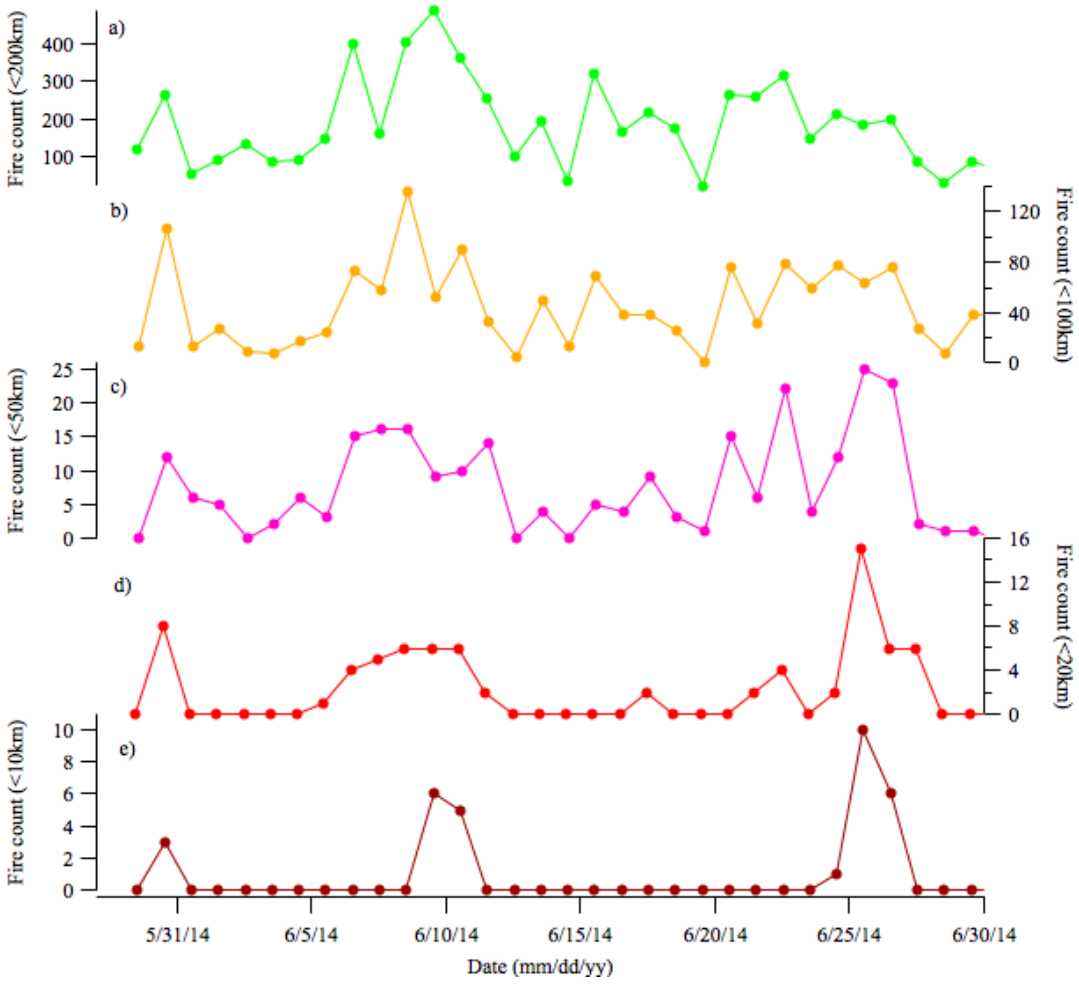

Figure 4.6 The number of hotspots observed each day within (a) 200 km, (b) 100 km, (c) 50 km, (d) 20 km and (e) 10 km of the ATARS, as detected by the MODIS and VIIRS sensors on the Terra and Aqua satellites.

Afternoon radon concentrations provide further information regarding the regional air mass fetch and the degree of contact with the land surface (red line, Fig. 4.3a). Over the campaign period, air masses with the least terrestrial fetch (low radon indicates strongest oceanic signature) were observed on June 4-6 and 20-22, whereas June 8-9, 17-18 and 29-30 represented periods of particularly extensive continental fetch.

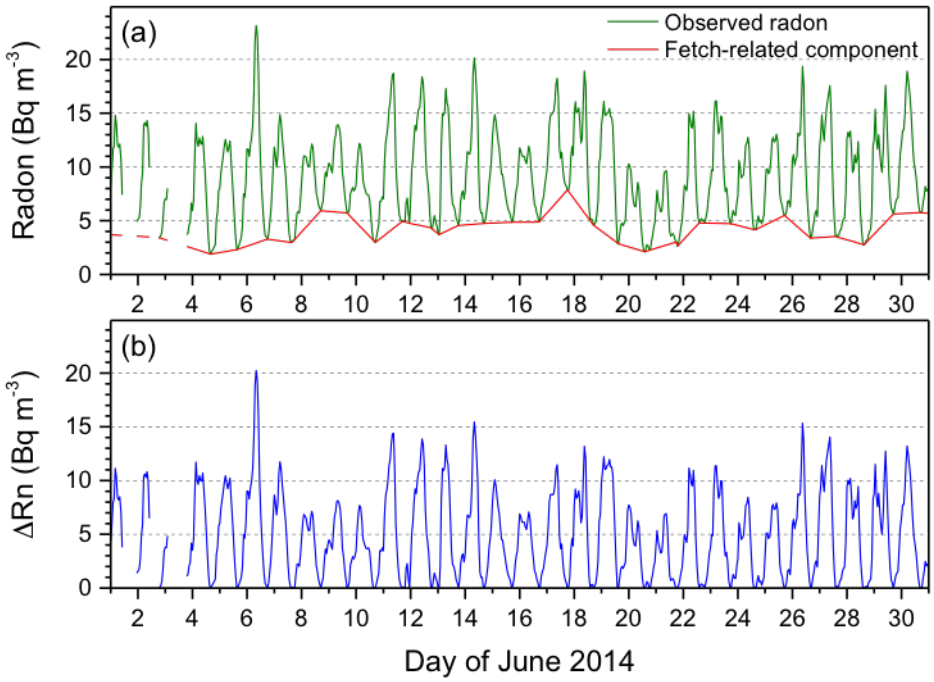

Figure 4.7 Hourly ATARS radon observations for June 2014: (a) observed hourly data, and afternoon-to-afternoon interpolated values (indicative of changes in the regional air mass fetch); and (b) difference in radon concentration between the hourly observations and interpolated afternoon values (indicative of diurnal variability).

A pronounced diurnal variability can clearly be seen in the ΔRn signal (Fig. 4.3b). Mean hourly diurnal composites of radon concentrations, wind speed, wind direction and dew point temperature at the ATARS site during the period of the SAFIRED campaign are shown in Fig. 4.4. Following the technique described in Chambers et al. (2016), these composites have been computed separately for three diurnal mixing categories based on the mean ΔRn over the 12 hour period 2000-0800 h:

Strong mixing: $\Delta Rn_{12} < 5400$ mBq m^{-3}

Moderate mixing: $5400 \leq \Delta Rn_{12} < 6700$ mBq m^{-3}

Weak mixing: $\Delta Rn_{12} \geq 6700$ mBq m^{-3}

The air masses predominantly originated from the southeast as indicated in Fig. 4.1 and Fig. 4.4c. Starting from approximately 10:00 am each morning, however, sea breeze circulations slowly turn the measured wind direction around from southeast to northeast, before reverting back to the dominant wind direction again at around midnight. Wind speeds reached a maximum just before midday and were at their lowest just before midnight (Fig. 4.4b). The "strong mixing" category was associated with generally higher wind speeds, which cause increased mechanical turbulence leading to deeper nocturnal mixing layers (i.e., hinder the development of a shallow nocturnal inversion layer).

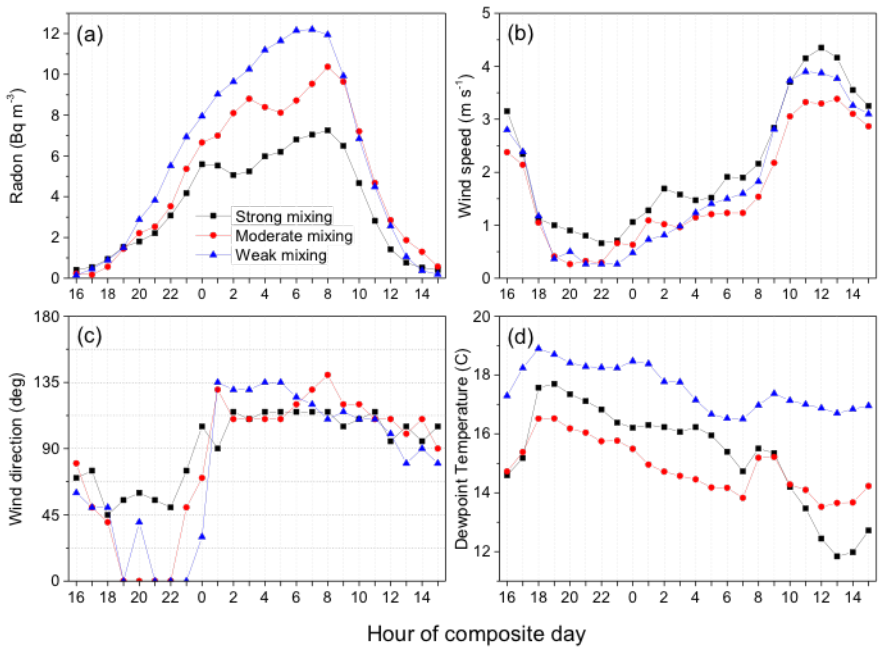

Figure 4.8 Mean hourly diurnal composite (a) radon, (b) wind speed, (c) wind direction, and (d) dew point temperature at ATARS, as a function of radon-based nocturnal mixing categories.

4.3.2 Gas and aerosol measurements

The campaign average, standard deviation, median and Q25/Q75 values for the major gaseous and aerosol species are shown in Table 4.1. The median values for each species are likely to be representative of background concentrations in this region. The average concentrations for most species were higher than the median concentrations, due to the periods of close or intense fires. The extent of the influence of these close fires is demonstrated by the maximum concentrations.

Table 4.1 The campaign average, standard deviation, maximum, median, Q25 and Q75 values for key measured gas and aerosol species. All parts-per notation refer to mole fractions unless otherwise indicated.

Species (unit)	Average	Standard deviation	Maximum	Median	Q25	Q75
CO (ppb)	229	494	18900	130	87	214
CO_2 (ppm)	404.68	11.539	513.578	402.454	394.728	411.299
O_3 (ppbv)	24.616	9.903	99.784	22.771	17.896	29.778
CH_4 (ppb)	1839.88	68.06	3766.81	1820.11	1802.26	1852.97
N_2O (ppb)	326.329	0.449	334.871	326.276	326.121	326.444

GEM (ng m^{-3})	0.992	0.081	1.734	0.986	0.952	1.020
Acetonitrile (ppb)	0.351	0.629	9.775	0.197	0.129	0.337
Organics (ug m^{-3})	11.081	22.385	347.657	4.160	2.335	13.279
SO_4^{2-} (ug m^{-3})	0.514	0.318	2.254	0.411	0.294	0.679
NH_4^+ (ug m^{-3})	0.351	0.676	18.17	0.180	0.096	0.415
NO_3^- (ug m^{-3})	0.187	0.456	10.925	0.042	0.004	0.189
Cl^- (ug m^{-3})	0.166	1.271	53.270	0.029	0.016	0.076
PNC (cm^{-3})	8182	19031	40300	2032	2032	8335
Mode diameter (nm)	104	31	-	102	85	122
Geom. SD	1.71	0.13	-	1.70	1.65	1.75

In order to demonstrate the influence of close fires and the changing inversion layer, the time series of major greenhouse gases (CO, CO_2, CH_4 and N_2O), gaseous elemental mercury, acetonitrile and ozone throughout the campaign are shown in Fig. 4.5. Sub-micron non-refractory aerosol organic, sulfate, ammonium and nitrate mass concentrations, organic mass fraction, PM_1 OC and EC mass concentrations and particle size distributions for the sampling period are shown in Fig. 4.6. Periods of missing data correspond to times when instruments were not operating. Most of these time series display a clear diurnal trend as a result of the varying inversion layer height. Other enhancements in concentrations can be clearly seen and correspond to periods of frequent close fires (Fig. 4.2). Over the entire sampling period from the 29th of May 2014 until the 28th of June 2014, four biomass burning related periods (BBP) and a "coastal" period (CP) have been distinguished. The dates for these periods are shown in Table 4.2. These periods are also displayed in Fig. 4.5 and Fig. 4.6.

Table 4.2 The start and end dates for the four identified Biomass Burning Periods (BBP1, BBP2, BBP3 and BBP4) and the Coastal Period (CP).

Period	Start date (mm/dd/yy hh:mm)	End date (mm/dd/yy hh:mm)
BBP1	05/30/14 00:00	05/31/14 23:59
BBP2	06/06/14 00:00	06/12/14 23:59
BBP3	06/14/14 00:00	06/17/14 23:59

CP	06/19/14 12:00	06/22/14 23:59
BBP3	06/23/14 00:00	06/28/14 23:59

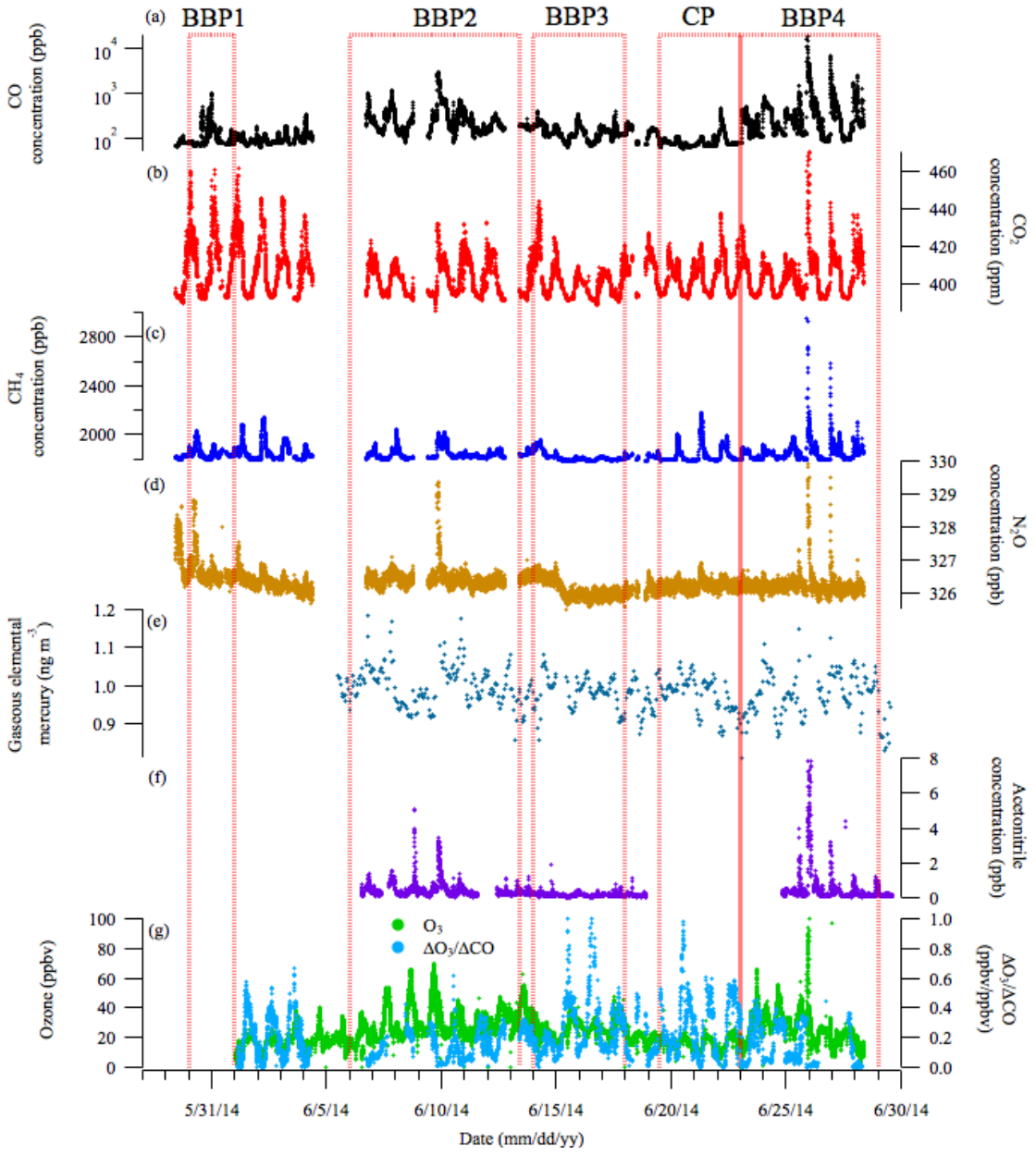

Figure 4.5 The time series of the major measured gaseous species during the SAFIRED campaign: (a) carbon monoxide, (b) carbon dioxide, (c) methane, (d) nitrogen dioxide, (e) gaseous elemental mercury, (f) acetonitrile and (g) ozone and $\Delta O_3/\Delta CO$. The biomass burning and coastal periods are indicated by the red dotted lines. All parts-per notation refer to mole fractions unless otherwise indicated. .

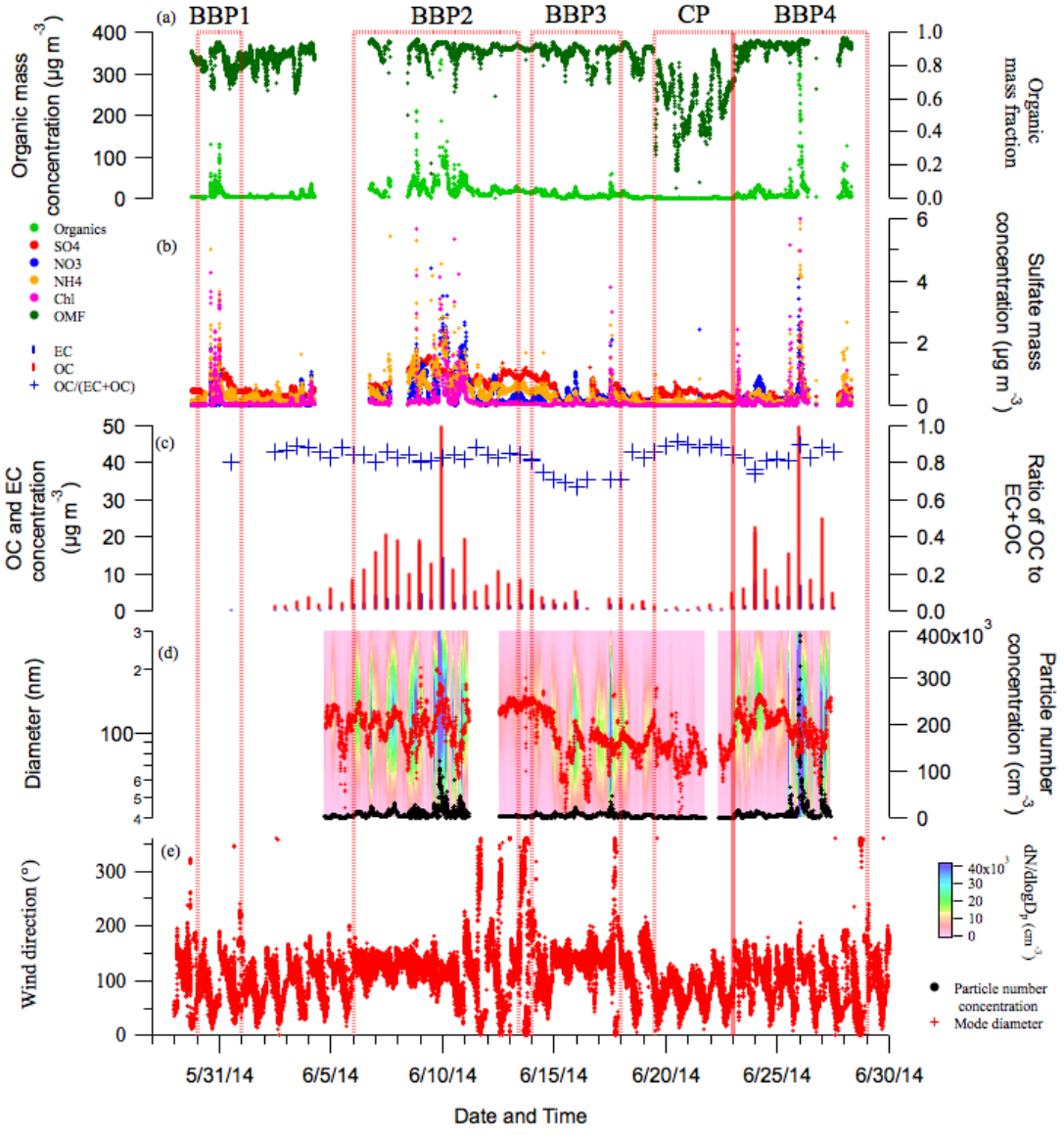

Figure 4.6 The times series of the major aerosol properties during the SAFIRED campaign: (a) the non-refractory PM_1 organic mass concentration (left) and organic mass fraction (right), b) the inorganic non-refractory PM_1 mass concentrations, (c) the 12-hour filter OC and EC PM_1 mass concentrations (left) and the ratio of OC to OC+EC (right), (d) the particle size distributions and particle size mode (left) and the total particle number concentration (right) and (e) the wind direction at ATARS.

Over the campaign organics dominated the non-refectory sub-micron aerosol mass contributing, on average 90% (median; 86%) of the total mass. Sulphate, nitrates, ammonium and chloride species contributed the rest of this mass, with the largest contributions from sulphate and ammonium. Sulphate contributions were very significant during the coastal period, contributing up to 32% of the total mass. Although chlorides contributed the least to the total mass, on average, during clear biomass burning events where sharp increases in CO and organics were observed, chlorides made up the largest component

of inorganic aerosol. The maximum chloride concentration during the campaign reached 53 μg m^{-3}. High soil and vegetation chloride contents have been observed in savannah and coastal environments (Lobert et al., 1999;Andreae et al., 1996). The strong elevations of chloride signals observed, particularly during burning events BBP1, BBP2 and BBP4 are likely a result of emission of these chloride ions. Outside of the "burning events" where very sharp increases in concentrations were observed, chloride concentrations were very low. This either suggests that these chloride species are short-lived, or only present in fires very close to the coast and therefore the ATARS site.

Particle size distributions were unimodal for the majority of the sampling period with a mode of approximately 100 nm on average (see Fig. 4.6d and Fig. 4.7). The SMPS was not operational during BBP1. Although the shape of the BBP4 size distribution was similar to the campaign average, concentrations were much higher and a result of close fires. BBP2 had a slightly larger size distribution centered on 110 nm. The size distribution during BBP3 was slightly smaller than the campaign average and BBP2 and BBP4, with a mode centered on ~95 nm. The contrast between these size distributions could be a result of atmospheric aging and dilution in which organic mass condenses onto or evaporates from the particle. Variations in fuel load or burning conditions could also contribute to this difference. The size and concentration of particles during the Coastal Period (CP) were much smaller than the rest of the campaign. There were two periods during CP where a bimodal size distribution was observed; one from approximately 3 pm until midnight on the 19th of June and the other between 2 pm and 6 pm on the 20th of June. As mentioned earlier, air masses during this time had a stronger oceanic influence, with back trajectories in this period originating along the east coast of Australia and passing over very little land before arriving at the station. The size distributions for both of these periods had a mode at approximately 20 nm and another at approximately 85 nm. Submicron sulfates made up to 32% of the total submicron non-refractory mass concentrations, as reported by the cToF-AMS from the period of midday on the 19th of June until midnight on the 22nd of June, whereas the average sulfate contribution for the rest of the campaign was approximately 8%. The low radon fetch, small particle concentrations, bimodal size distributions and significant contributions of sulfate during this period suggest very little biomass burning signal and a more marine-like aerosol. No particle nucleation events were observed over the entire sampling period (See Supplementary Fig. 4.S2). This is likely due to the elevated particle concentrations acting as a condensation sink.

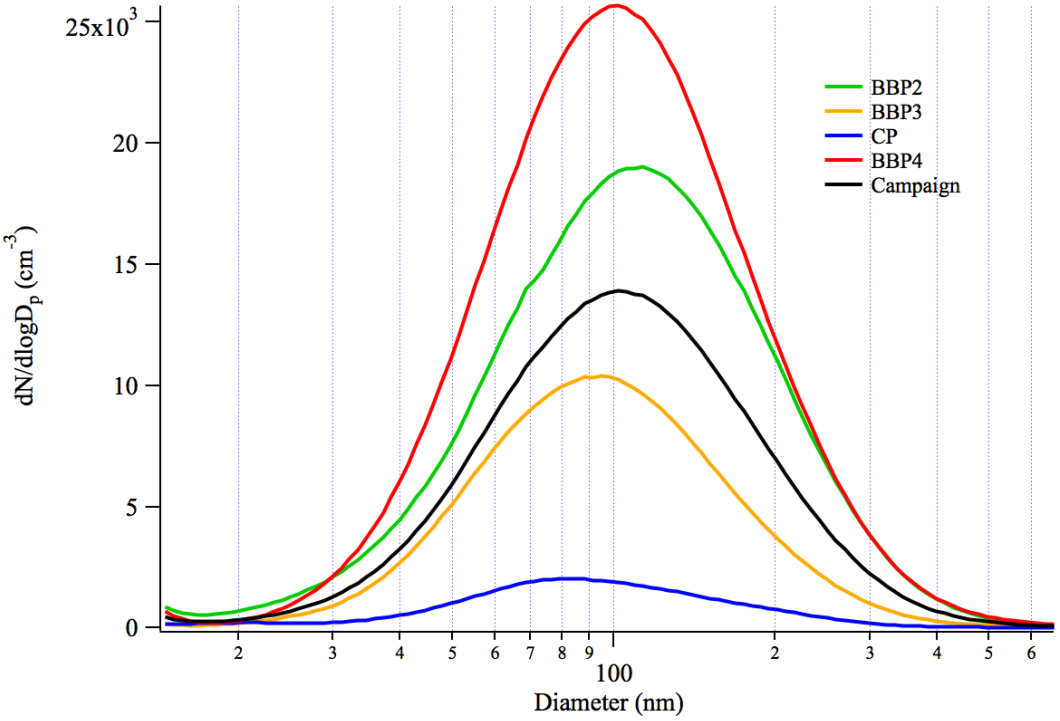

Figure 4.7 The average size distribution during BBP2, BBP3, BBP4, CP and the campaign average. The SMPS was not operational during BBP1.

BBP1, BBP2 and BBP4 correspond to the periods when fires were burning within 10 km of ATARS. Large enhancements of biomass burning related emissions were observed during these three periods. There were distinct enhancements of all measured gaseous and aerosol species during these periods. Differences between the maximum and background concentrations were very prominent for CO (note the logarithmic scale in Fig. 4.5a), CH_4, N_2O, acetonitrile (an established marker for biomass burning) and organic, nitrate and chloride non-refractory sub-micron aerosol species. Similar enhancements of CH_4 were also observed outside of these BB periods suggesting another source of methane in this region. Only slight enhancements of GEM concentrations above background were observed during BBP2 and BBP4. Similar to much of the rest of the campaign sampling period, the non-refractory submicron aerosol was dominated by organics, with contributions typically varying between 70% and 95% of the mass. Relative to background concentrations, there were also large enhancements of nitrate and chloride species during these periods. While there were also enhancements of sulfate and ammonium species during these periods, similar enhancements were observed outside of these periods, again indicating a non-fire source of these species. The ratio of O_3 to CO concentrations above background (taken as 10 ppbv and 66 ppbv, respectively) gives an indication of the photochemical age of a smoke plume. $\Delta O_3/\Delta CO$ were lowest during BBP2 and BBP4 (and not measured during BBP1) relative to the rest of the campaign, indicating that the biomass burning signals during these periods had not undergone extensive photochemical aging and are therefore characteristic of fresh smoke.

Elevated signals during BBP1 were likely a result of a series of close fires within 5 km ENE of ATARS. The VIIRS and MODIS sensors on the SUMO NPP, Terra and Aqua satellites observes smaller fires at approximately 2 pm on the 30th of May. Winds were northeasterly during these two events. It is therefore likely that these signals were continuation or evolution of those fires. Burned vegetation was also visually observed the next morning at these locations. The large burst event later on the evening of the 31st of May is unlikely to be associated with these fires as the wind direction during this event was from the SSW and SSE. Large clusters of fires were observed at approximately 100 km and 150 km SE of the station by the Terra and Aqua satellites. The signals observed during this event could be a result of the plumes from this fire, although the possibility of a fire ignited after the satellite flyovers, or a combination of these cannot be eliminated.

Large signal enhancements on the 8th of June during BBP2 are likely a result of a cluster of fires approximately 100 km south east of the station. The MODIS sensors on the Terra and Aqua satellites observed the small cluster of fires along the back-trajectory at 11:14 am and 1:56 pm. The source of BB emissions for the large event on the 9th of June during this period is unclear. Several fires approximately 5 km from the station along the back-trajectory were detected by the MODIS sensor on Aqua and the VIIRS sensor on SUOMI NPP at approximately 2:30 pm on the 9th of June. There were also numerous fires detected between 100 km and 200 km southeast along this trajectory. The signals associated with this event could therefore be a result of the closer fires that started to blaze later in the evening, the distant fires or a combination of both.

Only one fire within 20km of ATARS was observed during BBP3 on the 17th of June. Numerous fires were observed further than 20km from the station and is possible that the signals during this period were more aged. While photochemical aging and coagulation typically lead to larger particles, particle size distributions were smaller during this period and the ratio of OC to OC+EC was 70%, 10% lower than the ratio during the rest of the campaign. Whether these observations were a result of burn conditions or aging processes (i.e. evaporation of organic compounds from the aerosol phase) is unclear, although the highest $\Delta O_3/\Delta CO$ values during the campaign were observed during BBP3, which indicates photochemical aging was more extensive during this period.

One close fire was also observed during CP, however wind directions during this period were typically north-easterly and concentrations were therefore much lower. 5-day HYSPLIT trajectories also show that air mass during the CP originated along the east coast of Australia before travelling towards the sampling station with very little terrestrial influence.

4.3.3 Close proximity fires

With numerous fires occurring across the region and the limitations of once-per-day satellite fly-overs and stationary measurements, it can be difficult to identify the exact source of these elevated signals. For a portion of BBP4, however, fires were burning within several kilometers of ATARS and several plumes were easily observed from the station. The signals from these plumes are shown in Fig. 4.8. The observed enhancements between 12:30 pm and 3:00 pm on the 25th June

during BBP4 were a result of grass fires burning approximately 1 km south-east from the station. During this event, the wind direction (Fig. 4.8k) was highly variable, changing between 140° and 80° True Bearing (TB) multiple times. As a result, the sampling changed from measuring the air mass with and without the plume from this fire, which led to sharp increases and decreases in biomass burning-related signals (Fig. 4.8a through 4.8j). Visually, the fire area and extent of the plume was larger at 4:00pm than earlier, however the wind direction changed to north-easterly which directed the plume away from the station. From 4:00 pm until 10:00 pm, the wind direction was stable at approximately 50° TB. At 10:00 pm, the wind direction rapidly changed to directly south and the largest enhancements for the whole campaign were observed until approximately 2:00 am on the 26th of June. It is very likely that these signals were a result of a continuation and evolution of these fires as the night progressed. Portions of a ~0.25 km^2 grassland field within 500 m directly south of ATARS were observed to be burned upon arrival at the station on the morning of the 26th of June and we speculate that the burning of this field contributed to the large enhancements in measured biomass burning emissions. The emissions during this portion of BBP4 are likely to be the most representative of fresh biomass burning smoke during the SAFIRED campaign.

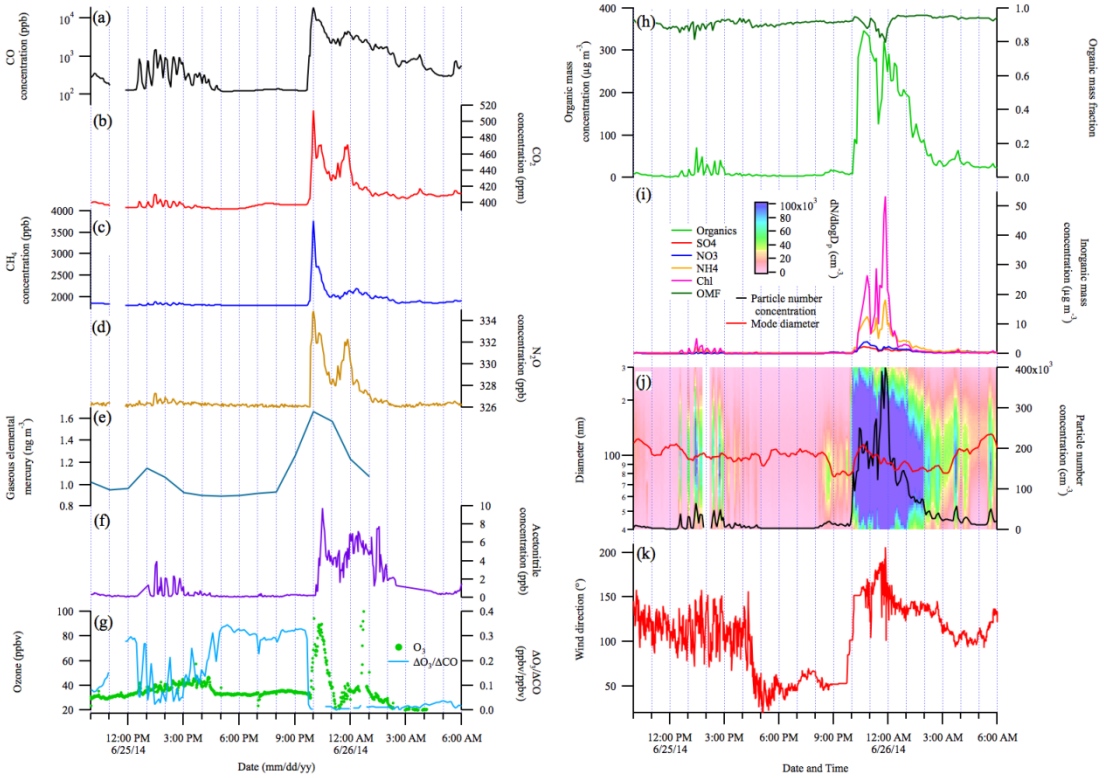

Figure 4.9 The major gas and aerosol concentrations measured during two biomass burning events within 1 km of ATARS during BBP4. (a) through (g) and (h) through (k) are as per Figures 4.5 and 4.6, respectively. All parts-per notation or mole fractions unless otherwise indicated.

4.4. Outcomes of SAFIRED

The overall aim of this study was to investigate the characteristics of BB emissions in the tropical savannah region of northern Australia during the early dry season. For many gaseous and aerosol species, elevated signals were observed for much of the month-long sampling period due to the high frequency of fires. The more specific outcomes of SAFIRED are outlined below.

4.4.1 Emission factors

Australian fires are responsible for 6% of global CO_2 biomass burning emissions, most of which is due to savannah fires (Shi et al., 2015). Carbon sequestering during regrowth periods is considered to balance carbon emissions in tropical Australia (Haverd et al., 2013). Greenhouse gases emitted from savannah fires that are not sequestered, such as methane (CH_4) and nitrous oxide (N_2O), have been shown to contribute 2-4% of the annual accountable greenhouse gas emissions from Australia (Meyer et al., 2012). Seasonal emission factors for the major greenhouse gases are important for national greenhouse gas inventories and in understanding the impact of savannah fires. Furthermore, emission factors of CO_2 and CO can be used to infer mechanisms behind the emissions of other species, such as the connection between particulate matter and burning conditions.

The gaseous and aerosol data for the sample period were investigated to identify BB events and determine the emission factors of CO_2, CO, CH_4, N_2O, as well as Aitken and Accumulation mode aerosols and submicron particle species (organics, sulfates, nitrates, ammonium and chlorides) for several individual BB events. These emission factors were mostly found to be dependent on the combustion conditions (using the modified combustion efficiency as a proxy) of the fires. These results will be the first set of emission factors for aerosol particles from savannah fires in Australia. Furthermore, the variability in emission factors for different fires calls for a separation of single-value emission factors that are usually reported for savannah fires into grass and shrub components. A full discussion of these results are presented in Desservettaz et al. (2016, submitted).

4.4.2 Non-methane organic compounds (NMOCs)

Biomass burning is the second largest source of NMOCs globally with a recent global estimate of at least 400 Tg $year^{-1}$, second only to biogenic sources (Akagi et al., 2011). Biomass burning produces a complex mix of NMOCs, which may be saturated or unsaturated, aliphatic or aromatic, and contain substitutions of oxygen, sulfur, nitrogen, halogens and other atoms. NMOC emission rates are strongly tied to the efficiency of combustion, with smoldering fires emitting NMOC at higher rates than flaming fires (Andreae and Merlet, 2001). Biomass burning derived NMOCs fuel the production of tropospheric ozone in diluted, aged biomass burning plumes, with higher ozone enhancements observed when biomass

burning plumes interact with NOx-rich urban plumes (Jaffe and Wigder, 2012;Wigder et al., 2013;Akagi et al., 2013). Oxidation of NMOCs results in lower volatility products that partition to the aerosol phase and contribute significantly to secondary organic aerosol (Hallquist et al., 2009). Biomass burning produces significant amounts of semi-volatile NMOC which can be difficult to quantify and identify with current measurement techniques. However recent studies have shown that including semi volatile NMOC chemistry in models improves the agreement between the modeled and observed organic aerosol (Alvarado et al., 2015; Konovalov et al., 2015) and ozone (Alvarado et al., 2015). High quality NMOC emission factors are crucial for models to assess the impact of biomass burning plumes on air quality and climate.

4.4.3 PAHs

Polycyclic aromatic hydrocarbons (PAHs) are a group of chemicals that are formed and emitted during combustion processes. Globally, major sources include residential/commercial biomass burning, open-field biomass burning and vehicular emissions (Shen et al., 2013). In Oceania in 2007, 31% of PAH emissions were estimated to be attributed to deforestation and wildfires (Shen et al., 2013). With control strategies targeting and reducing vehicular emission of PAHs over the last few decades, the relative contribution of other emission sources, such as savannah fires, has increased (Friedman et al., 2013;Kallenborn et al., 2012;Wang et al., 2016). Although most of these emissions are in the gas-phase (Jenkins et al., 1996;Atkins et al., 2010), the particle-phase PAHs, such as benzo[a]pyrene (BaP), may have high genotoxicity (IARC., 2015). However, field-based studies on emissions of PAHs from open-field biomass burning, including savannah fires remain limited in Australia (Freeman and Cattell, 1990).

Emission factors of PAHs from biomass burning related to savannah fires in northern Australia will be estimated form the data collected during this campaign. This estimation will be based on the (background subtracted) concentrations of PAHs and CO_2 (and CO) during the events where biomass burning contributes most to these concentrations measured at the sampling site. The concentrations of 13 major PAHs (gaseous plus particle-associated phase) varied from ~ 1 to over 15 ng m^{-3} within different BB events. In the gas phase, 3- and 4-ring compounds typically contributed ~ 90% to the sum concentrations whereas the particle-associated PAHs were dominated by 5- and 6-ring compounds (> 80%). Measured PAH concentrations were significantly higher (paired *t*-test, $P < <0.05$) during BBP2 and BBP4 periods. For these periods, concentrations of BaP exceeded the monitoring investigation level for atmospheric BaP in Australia (National-Environment-Protection-Council-Service-Corporation, 2011). A full discussion of these results can be found in (Wang et al., 2016, under review).

4.4.4 Mercury

The atmosphere is the dominant transport pathway for mercury globally, with emissions to the atmosphere from both natural and anthropogenic origins (Driscoll et al., 2013). Whilst our understanding of the natural cycling of mercury has improved

markedly over the past decades (Pirrone et al., 2010), large uncertainties still exist; specifically, global emission estimates to the atmosphere from biomass burning currently range between 300 and 600 Mg $year^{-1}$ (Driscoll et al., 2013). In the atmosphere, mercury exists as one of three operationally-defined species: gaseous elemental mercury (GEM), gaseous oxidized mercury (GOM) and particulate-bound mercury (PBM), each with differing abundances, solubility and depositional characteristics and with in-air conversion between all three species possible (Lin and Pehkonen, 1999). Mercury can be scavenged from the atmosphere through both wet and dry depositional processes, and the monsoonal climate of northern Australia results in varying significance of each of these processes through the year (Packham et al., 2009). Upon deposition, mercury may be stored in plant tissue via stomatal or cuticular uptake (Rea et al., 2002) or sequestered within soils (Gustin et al., 2008). Release from both of these pools is achieved from burning events that may volatilise or thermally desorb mercury from biomass and soil, respectively (Melendez-Perez et al., 2014). Subsequently this mercury pool is redistributed through the atmospheric pathway to ecosystems that may methylate mercury, thereby enhancing its bioavailability to the local food chain.

SAFIRED represents the first measurements of atmospheric mercury undertaken in the tropical region of the Australian continent. The mean observed GEM concentration over the study period was 0.99 ± 0.09 ng m^{-3}, similar to the average over that month (0.96 ng m^{-3}) for 5 other Southern Hemisphere sites and slightly lower than the average (1.15 ng m^{-3}) for 5 tropical sites (Sprovieri et al., 2016). Mean GOM and PBM concentrations were 11 ± 5 pg m^{-3} and 6 ± 3 pg m^{-3} respectively, representing 0.6 – 3.4% of total observed atmospheric mercury.

Atmospheric mercury measurements were available only during the final four identified burn events. During these events, spikes in GEM concentrations were observed, though there were no significant increases in GOM or PBM. Emission ratios calculated during the campaign were two orders of magnitude higher than those reported by Andreae and Merlet (2001), though those were from scrub, rather than grass, BB events (Desservettaz et al., 2016). Future outcomes from the SAFIRED campaign will focus on the use of micrometeorological techniques and the passive tracer radon to quantify delivery of atmospheric mercury to tropical savannah ecosystems. ATARS also now serves as an additional site measuring continuous GEM as part of the Global Mercury Observation System (GMOS), one of only two tropical observing sites in the Eastern Hemisphere and the third such site located in Australia.

4.4.5 Aging of aerosols

Atmospheric chemistry and radiative forcing will depend on how gaseous and aerosol emissions from fires age as they move and interact with each other and existing species in the atmosphere. Biomass burning aerosols can be involved in condensation and coagulation (Radhi et al., 2012), undergo water uptake (Mochida and Kawamura, 2004) form cloud droplets (Novakov and Corrigan, 1996), and be exposed to photochemical aging processes, including those involving the gaseous components of fire emissions (Keywood et al., 2011;Keywood et al., 2015). With a reported lifetime of 3.8 ± 0.8

days (Edwards et al., 2006), biomass burning aerosols are able to travel intercontinental distances (Rosen et al., 2000) and are therefore present in the atmosphere long enough for substantial changes due to aging. Furthermore, tropical convection is likely to affect the aging of BB emissions in the region around ATARS, due to the immediate proximity to the warm waters in the Timor Sea (Allen et al., 2008). This introduces further uncertainty to the effect of BB emissions on radiation flux.

Primary organic aerosol directly emitted from biomass burning can interact with NMOCs to change composition and mass, resulting in secondary organic aerosol (Hallquist et al., 2009). Photochemical oxidation of NMOCs occurs during the daytime by either hydroxyl radicals or ozone. Ozone is also typically produced in the aging processes of tropical biomass burning plumes when NMOCs can oxidise to produce peroxy radicals that react with NO. Photochemical reactions also may lead to an overall increase in total aerosol mass through the condensation of NMOCs onto existing particles (Reid et al., 1998;Yokelson et al., 2009;Akagi et al., 2012;DeCarlo et al., 2008). Some studies have shown the opposite, i.e., photo-oxidation can also lead to the evaporation of some primary organic constituents, resulting in an overall mass reduction (Hennigan et al., 2011;Akagi et al., 2012). With thousands of organic compounds in the atmosphere, each with different volatilities and potential reaction mechanisms, our understanding of secondary organic aerosol production is limited (Goldstein and Galbally, 2007;Keywood et al., 2011). Furthermore, secondary organic aerosol can also form through aqueous phase reactions where water-soluble organics dissolve into water on existing particles (Lim et al., 2010).

Further analysis into the aerosol chemical composition will elucidate the aging of early dry season biomass burning emissions. Fractional analysis (e.g., f44 and f60, the fraction of m/z 44 and m/z 60 to all organic masses, indicated oxygenation and BB sources, respectively) and factor analysis using positive matrix factorization (PMF) of cToF-AMS data has been investigated over the entire sampling period. Outside of the periods of significant influence from BB events, three PMF-resolved organic aerosol factors were identified. A BB organic aerosol factor was found to comprise 24% of the submicron non-refractory organic mass, with an oxygenated organic aerosol factor and a biogenic isoprene-related secondary organic aerosol factor comprising 47% and 29%, respectively. These results indicate the significant influence of fresh and aged BB on aerosol composition in the early dry season. The emission of precursors from fires is likely responsible for some of the SOA formation. A full discussion of these results can be found in Milic et al. (2016). Future analysis will investigate the gas and particle-phase composition for individual BB events.

4.4.6 Water uptake of aerosols

The water uptake by aerosols is determined by their size and composition, as well as the atmospheric humidity (McFiggans et al., 2006). The hygroscopic properties of all of the different components of an aerosol particle contribute to its total hygroscopicity (Chen et al., 1973;Stokes and Robinson, 1966). The presence of different water-soluble and water-insoluble organics and inorganics will therefore strongly influence water uptake. Furthermore, chamber studies that have investigated emissions from biomass fuels, both separately and in combination, have shown that the hygroscopic response can vary

significantly depending on fuel type (Carrico et al., 2010). Understanding the water uptake of atmospheric aerosols is further complicated when considering other aging processes as described previously. Nonetheless, it is important to characterise the water uptake, as this will, in turn, influence other atmospheric chemistry processes, radiation scattering and absorption as well as cloud processing.

Biomass burning aerosols can act as cloud condensation nuclei if they are large enough for water to easily condense onto their surface, or if the particles have a large affinity for water due to their composition (Novakov and Corrigan, 1996). Ultimately, this means that BB emissions can lead to a higher number of cloud droplets. This is important in reflecting solar radiation and cooling the earth's surface. Cloud albedo is more susceptible to changes when cloud condensation nuclei concentrations are relatively low (Twomey, 1991), such as in marine environments like the Timor Sea off the coast of northern Australia.

The water uptake of aerosols has been further investigated to identify the possible influence of early dry season BB in this region on cloud formation. The concentrations of cloud condensation nuclei at a constant supersaturation of 0.5% were typically of the order of 2000 cm^{-3} and reached well over 10000 cm^{-3} during intense BB events. Variations in the ratio of aerosol particles activating cloud droplets showed a distinct diurnal trend, with an activation ratio of 40% ± 20% during the night and 60% ± 20% during the day. The particle size distribution and the hygroscopicity of the particles were found to significantly influence this activation ratio. A full discussion of these results can be found in Mallet et al. (2016, submitted). Future analysis will elucidate the contribution of different biomass burning aerosol components on the hygroscopicity.

4.4.7 Trace metal deposition

The deposition and dissolution of aerosols containing trace metals into the ocean may provide important micronutrients required for marine primary production. Conversely, the deposition of soluble iron can trigger toxic algal blooms, such as Trichodesmium, in nutrient-poor tropical and subtropical waters (LaRoche and Breitbarth, 2005). Trichodesmium blooms require large quantities of soluble iron, of which aerosols are a source (Boyd and Ellwood, 2010;Rubin et al., 2011). To date, most studies have assumed that mineral dust aerosols represent the primary source of soluble iron in the atmosphere (Baker and Croot, 2010); however fire emissions and oil combustion are other likely sources (Ito, 2011;Schroth et al., 2009;Sedwick et al., 2007). A few studies have shown that iron contained in biomass burning emissions is significantly more soluble than mineral dust (Guieu et al., 2005;Luo et al., 2008;Schroth et al., 2009) but, to date, no data exists for Australian fires.

The aim of the trace metal aerosol component of SAFIRED is to quantify, for the first time, the fractional solubility of aerosol iron, and other trace metals, derived from Australian dry season BB. The fractional iron solubility is an important variable determining iron availability for biological uptake. On a global scale, the large variability in the observed fractional iron solubility results, in part, from a mixture of different aerosol sources. Estimates of fractional iron solubility from fire

combustion (1 - 60 %) are thought to be greater than those originating from mineral dust (1 - 2%) (Chuang et al., 2005;Guieu et al., 2005;Sedwick et al., 2007), and may vary in relationship to biomass and fire characteristics as well as that of the underlying terrain (Paris et al., 2010;Ito, 2011). Iron associated with BB may provide information with respect to BB inputs of iron to the ocean (Giglio et al., 2013;e.g. Meyer et al., 2008). The ATARS provides an ideal location to further investigate BB derived fractional iron solubility at the source. The results from this study can be found in Winton et al. (2016) and show that soluble iron concentrations from BB sources are significantly higher than those observed in Southern Ocean baseline air masses from the Cape Grim Baseline Air Pollution Station, Tasmania, Australia (Winton et al., 2015). Aerosol iron at SAFIRED was a mixture of fresh BB, mineral dust, sea spray and industrial pollution sources. The fractional iron solubility (2 - 12%) was relatively high throughout the campaign and the variability was related to the mixing and enhancement of mineral dust iron solubility with BB species.

4.5. Looking forward

While the specific outcomes of the SAFIRED campaign are reviewed above, the general importance of this study can be discussed in a greater context. This is the first large-scale collaborative project undertaken in this region and draws on the resources and expertise of most of Australia's research institutes focused on atmosphere chemistry and composition. Large scale, multidisciplinary measurement campaigns in the tropics, such as SAFIRED, are needed to make distinctions between different types of fires in different regions to reduce uncertainties in global climate models (Keywood et al., 2013). This need has been recognized with the formation of global collaborative initiatives promoting interdisciplinary collaboration in biomass burning research (Kaiser and Keywood, 2015). As the world moves towards a warmer climate, biomass burning is likely to increase in frequency and intensity, and these emissions will become an increasingly important source of trace gases and aerosols to the atmosphere. SAFIRED lays the foundation for future measurements at ATARS that could make measurements throughout the whole dry season and on a more long-term scale. Future work in this region should focus on 1) the detailed characterisation of individual fires and their emissions, 2) biomass burning emissions throughout the late dry season and 3) the vertical and horizontal transport of biomass burning emissions in this region.

Data availability. All data are available upon request from the corresponding authors (Branka Miljevic, b.miljevic@qut.edu.au; Melita D. Keywood; melita.keywood@csiro.au).

Author Contributions

M.D. Mallet[a,b,c,d,e], M.J. Desservettaz[b,c,d,e], B. Miljevic[b,c,e*], A. Milic[b,d,e], Z.D. Ristovski[b,e], J. Alroe[b,c,e], L.T. Cravigan[b,c,e], E.R. Jayaratne[d,e], C. Paton-Walsh[b,c,e], D.W.T. Griffith[b,d,e], S.R. Wilson[b,d,e], G. Kettlewell[b,e], M.V. van der Schoot[b,e], P. Selleck[b,c,d,e], F. Reisen[b,c,e], S.J. Lawson[b,c,d,e], J. Ward[b,c,d,e], J. Harnwell[b,c,e], M. Cheng[b,c,d,e], R.W. Gillett[b,c,d,e], S.B. Molloy[d,e], D.

Howard[b,c,d,e], P.F. Nelson[b,e], A.L Morrison[b,e], G.C. Edwards[b,c,e], A.G. Williams[b,c,e], S.D. Chambers[b,c,d,e], S. Werczynski[b,c,e], L.R. Williams[c,d,e], V.H.L. Winton[b,c,d,e], and B. Atkinson[b,c], X. Wang[b,d,e], M.D. Keywood[b,c,d,e,f*]

a: Wrote and organised the manuscript

b: Contributed to the organisation of the campaign

c: Installed and/or operated instrumentation during the sampling period

d: Analysed data

e: Contributed to the manuscript and/or data interpretation

f: Designed and led the campaign.

*: Corresponding author

Competing interests

The authors declare that they have no conflict of interest.

Acknowledgements. The majority of the campaign was internally funded. The input of QUT was supported by the Australian Research Council Discovery (Grant DP120100126). The work on aerosol iron solubility was supported by Curtin University (RES-SE-DAP_AW-47679-1), the University of Tasmania (B0019024) and the Australian Research Council (Grant FT130100037).

4.6. References

Aiken AC, de Foy B, Wiedinmyer C, DeCarlo PF, Ulbrich IM, Wehrli MN, et al. Mexico city aerosol analysis during MILAGRO using high resolution aerosol mass spectrometry at the urban supersite (T0) - Part 2: Analysis of the biomass burning contribution and the non-fossil carbon fraction. Atmospheric Chemistry and Physics 2010; 10: 5315-5341.

Akagi S, Yokelson RJ, Burling IR, Meinardi S, Simpson I, Blake DR, et al. Measurements of reactive trace gases and variable O_3 formation rates in some South Carolina biomass burning plumes. Atmospheric Chemistry and Physics 2013; 13: 1141-1165.

Akagi S, Yokelson RJ, Wiedinmyer C, Alvarado M, Reid J, Karl T, et al. Emission factors for open and domestic biomass burning for use in atmospheric models. Atmospheric Chemistry and Physics 2011; 11: 4039-4072.

Akagi SK, Craven JS, Taylor JW, McMeeking GR, Yokelson RJ, Burling IR, et al. Evolution of trace gases and particles emitted by a chaparral fire in California. Atmospheric Chemistry and Physics 2012; 12: 1397-1421.

Allen G, Vaughan G, Bower K, Williams P, Crosier J, Flynn M, et al. Aerosol and trace-gas measurements in the Darwin area during the wet season. Journal of Geophysical Research: Atmospheres (1984–2012) 2008; 113.

Andersen AN, Cook GD, Corbett LK, Douglas MM, Eager RW, Russell-Smith J, et al. Fire frequency and biodiversity conservation in Australian tropical savannas: implications from the Kapalga fire experiment. Austral Ecology 2005; 30: 155-167.

Andreae MO, Merlet P. Emission of trace gases and aerosols from biomass burning. Global biogeochemical cycles 2001; 15: 955-966.

Atkins A, Bignal KL, Zhou JL, Cazier F. Profiles of polycyclic aromatic hydrocarbons and polychlorinated biphenyls from the combustion of biomass pellets. Chemosphere 2010; 78: 1385-1392.

Baker A, Croot P. Atmospheric and marine controls on aerosol iron solubility in seawater. Marine Chemistry 2010; 120: 4-13.

Bindoff NL, Stott PA, AchutaRao KM, Allen MR, Gillett N, Gutzler D, et al. Detection and Attribution of Climate Change: from Global to Regional. In: Stocker TF, Qin D, Plattner G-K, Tignor M, Allen SK, Boschung J, et al., editors. Climate Change 2013: The Physical Science Basis. Contribution of Working Group I to the Fifth Assessment Report of the Intergovernmental Panel on Climate Change. Cambridge University Press, Cambridge, United Kingdom and New York, NY, USA, 2013, pp. 867–952.

Biraud S, Ciais P, Ramonet M, Simmonds P, Kazan V, Monfray P, et al. European greenhouse gas emissions estimated from continuous atmospheric measurements and radon 222 at Mace Head, Ireland. Journal of Geophysical Research: Atmospheres (1984–2012) 2000; 105: 1351-1366.

Boyd P, Ellwood M. The biogeochemical cycle of iron in the ocean. Nature Geoscience 2010; 3: 675-682.

Carrico C, Petters M, Kreidenweis S, Sullivan A, McMeeking G, Levin E, et al. Water uptake and chemical composition of fresh aerosols generated in open burning of biomass. Atmospheric Chemistry and Physics 2010; 10: 5165-5178.

Chambers S, Williams A, Crawford J, Griffiths A. On the use of radon for quantifying the effects of atmospheric stability on urban emissions. Atmospheric Chemistry and Physics 2015; 15: 1175-1190.

Chambers SD, Hong S-B, Williams AG, Crawford J, Griffiths AD, Park S-J. Characterising terrestrial influences on Antarctic air masses using Radon-222 measurements at King George Island. Atmospheric Chemistry and Physics 2014; 14: 9903-9916.

Chambers SD, Williams AG, Conen F, Griffiths AD, Reimann S, Steinbacher M, et al. Towards a Universal “Baseline” Characterisation of Air Masses for High-and Low-Altitude Observing Stations Using Radon-222. Aerosol Air Qual. Res 2016; 16: 885-899.

Chen H, Sangster J, Teng T, Lenzi F. A general method of predicting the water activity of ternary aqueous solutions from binary data. The Canadian Journal of Chemical Engineering 1973; 51: 234-241.

Chow JC, Watson JG, Chen LWA, Chang MCO, Robinson NF, Trimble D, et al. The IMPROVE-A temperature protocol for thermal/optical carbon analysis: maintaining consistency with a long-term database. Journal of the Air & Waste Management Association 2007a; 57: 1014-1023.

Chow JC, Watson JG, Chen LWA, Chang MO, Robinson NF, Trimble D, et al. The IMPROVE-A temperature protocol for thermal/optical carbon analysis: maintaining consistency with a long-term database. Journal of the Air & Waste Management Association 2007b; 57: 1014-1023.

Chuang PY, Duvall RM, Shafer MM, Schauer JJ. The origin of water soluble particulate iron in the Asian atmospheric outflow. Geophys. Res. Lett. 2005; 32: L07813.

Crutzen PJ, Andreae MO. Biomass burning in the tropics: Impact on atmospheric chemistry and biogeochemical cycles. Science 1990; 250: 1669-1678.

DeCarlo PF, Dunlea EJ, Kimmel JR, Aiken AC, Sueper D, Crounse J, et al. Fast airborne aerosol size and chemistry measurements above Mexico City and Central Mexico during the MILAGRO campaign. Atmos. Chem. Phys 2008; 8: 4027-4048.

Desservettaz MJ, Paton-Walsh C, Griffith DWT, Kettlewell G, Keywood MD, van der Schoot MV, et al. Emission factors of trace gases and particles from tropical savanna fires in Australia, submitted to J. Geophys. Res, 2016

Draxler RR, Rolph G. HYSPLIT (HYbrid Single-Particle Lagrangian Integrated Trajectory) model access via NOAA ARL READY website (http://www. arl. noaa. gov/ready/hysplit4. html). NOAA Air Resources Laboratory, Silver Spring. Md, 2003.

Driscoll CT, Mason RP, Chan HM, Jacob DJ, Pirrone N. Mercury as a global pollutant: sources, pathways, and effects. Environmental science & technology 2013; 47: 4967-4983.

Edwards D, Emmons L, Gille J, Chu A, Attié JL, Giglio L, et al. Satellite-observed pollution from Southern Hemisphere biomass burning. Journal of Geophysical Research: Atmospheres (1984–2012) 2006; 111.

Edwards GC, Rasmussen PE, Schroeder WH, Wallace DM, Halfpenny-Mitchell L, Dias GM, et al. Development and evaluation of a sampling system to determine gaseous Mercury fluxes using an aerodynamic micrometeorological gradient method. Journal of Geophysical Research: Atmospheres 2005; 110.

Freeman DJ, Cattell FCR. Woodburning as a source of atmospheric polycyclic aromatic hydrocarbons. Environmental Science and Technology 1990; 24: 1581-1585.

Friedman CL, Zhang Y, Selin NE. Climate change and emissions impacts on atmospheric PAH transport to the Arctic. Environmental science & technology 2013; 48: 429-437.

Giglio L, Randerson JT, Werf GR. Analysis of daily, monthly, and annual burned area using the fourth-generation global fire emissions database (GFED4). Journal of Geophysical Research: Biogeosciences 2013; 118: 317-328.

Goldstein AH, Galbally IE. Known and unexplored organic constituents in the earth's atmosphere. Environmental Science & Technology 2007; 41: 1514-1521.

Govender N, Trollope WS, Van Wilgen BW. The effect of fire season, fire frequency, rainfall and management on fire intensity in savanna vegetation in South Africa. Journal of Applied Ecology 2006; 43: 748-758.

Griffith DWT. Synthetic calibration and quantitative analysis of gas-phase FT-IR spectra. Applied Spectroscopy 1996; 50: 59-70.

Griffith DWT, Deutscher NM, Caldow C, Kettlewell G, Riggenbach M, Hammer S. A Fourier transform infrared trace gas and isotope analyser for atmospheric applications. Atmospheric Measurement Techniques 2012; 5: 2481-2498.

Guieu C, Bonnet S, Wagener T, Loÿe-Pilot MD. Biomass burning as a source of dissolved iron to the open ocean? Geophysical Research Letters 2005; 32.

Gustin MS, Lindberg SE, Weisberg PJ. An update on the natural sources and sinks of atmospheric mercury. Applied Geochemistry 2008; 23: 482-493.

Hallquist M, Wenger JC, Baltensperger U, Rudich Y, Simpson D, Claeys M, et al. The formation, properties and impact of secondary organic aerosol: current and emerging issues. Atmospheric Chemistry and Physics 2009; 9: 5155-5236.

Haverd V, Raupach M, Briggs P, Canadell J, Isaac P, Pickett-Heaps C, et al. Multiple observation types reduce uncertainty in Australia's terrestrial carbon and water cycles. Biogeosciences 2013; 10: 2011-2040.

Hennigan CJ, Miracolo MA, Engelhart GJ, May AA, Presto AA, Lee T, et al. Chemical and physical transformations of organic aerosol from the photo-oxidation of open biomass burning emissions in an environmental chamber. Atmospheric Chemistry and Physics 2011; 11: 7669-7686.

Honninger G, von Friedeburg C, Platt U. Multi axis differential optical absorption spectroscopy (MAX-DOAS). Atmospheric Chemistry and Physics 2004; 4: 231-254.

IARC. Agents Classified by the IARC Monographs. World Health Organization. http://monographs.iarc.fr/ENG/Classification/. The International Agency for Research on Cancer., 2015.

Iinuma Y, Engling G, Puxbaum H, Herrmann H. A highly resolved anion-exchange chromatographic method for determination of saccharidic tracers for biomass combustion and primary bio-particles in atmospheric aerosol. Atmospheric Environment 2009; 43: 1367-1371.

Ito A. Mega fire emissions in Siberia: potential supply of bioavailable iron from forests to the ocean. Biogeosciences 2011; 8: 1679-1697.

Jacobson MZ. Strong radiative heating due to the mixing state of black carbon in atmospheric aerosols. Nature 2001; 409: 695-697.

Jaffe DA, Wigder NL. Ozone production from wildfires: A critical review. Atmospheric Environment 2012; 51: 1-10.

Jenkins BM, Jones AD, Turn SQ, Williams RB. Emission Factors for Polycyclic Aromatic Hydrocarbons from Biomass Burning. Environmental Science & Technology 1996; 30: 2462-2469.

Kaiser JW, Keywood M. Preface for Atmos. Env. Special issue on IBBI. Atmospheric Environment 2015; 121: 1-3.

Kallenborn R, Halsall C, Dellong M, Carlsson P. The influence of climate change on the global distribution and fate processes of anthropogenic persistent organic pollutants. Journal of Environmental Monitoring 2012; 14: 2854-2869.

Keywood M, Cope M, Meyer CM, Iinuma Y, Emmerson K. When smoke comes to town: The impact of biomass burning smoke on air quality. Atmospheric Environment 2015; 121: 13-21.

Keywood M, Guyes H, Selleck P, Gillett R. Quantification of secondary organic aerosol in an Australian urban location. Environmental Chemistry 2011; 8: 115-126.

Keywood M, Kanakidou M, Stohl A, Dentener F, Grassi G, Meyer CP, et al. Fire in the air: Biomass burning impacts in a changing climate. Critical Reviews in Environmental Science and Technology 2013; 43: 40-83.

Landis MS, Stevens RK, Schaedlich F, Prestbo EM. Development and characterization of an annular denuder methodology for the measurement of divalent inorganic reactive gaseous mercury in ambient air. Environmental science & technology 2002; 36: 3000-3009.

LaRoche J, Breitbarth E. Importance of the diazotrophs as a source of new nitrogen in the ocean. Journal of Sea Research 2005; 53: 67-91.

Lawson SJ, Keywood MD, Galbally IE, Gras JL, Cainey JM, Cope ME, et al. Biomass burning emissions of trace gases and particles in marine air at Cape Grim, Tasmania. Atmospheric Chemistry and Physics 2015; 15: 13393-13411.

Lim Y, Tan Y, Perri M, Seitzinger S, Turpin B. Aqueous chemistry and its role in secondary organic aerosol (SOA) formation. Atmospheric Chemistry and Physics 2010; 10: 10521-10539.

Lin C-J, Pehkonen SO. The chemistry of atmospheric mercury: a review. Atmospheric Environment 1999; 33: 2067-2079.

Liousse C, Devaux C, Dulac F, Cachier H. Aging of savanna biomass burning aerosols: Consequences on their optical properties. Journal of Atmospheric Chemistry 1995; 22: 1-17.

Locatelli R, Bousquet P, Hourdin F, Saunois M, Cozic A, Couvreux F, et al. Atmospheric transport and chemistry of trace gases in LMDz5B: evaluation and implications for inverse modelling. Geoscientific Model Development 2015; 8: 129-150.

Luo C, Mahowald N, Bond T, Chuang P, Artaxo P, Siefert R, et al. Combustion iron distribution and deposition. Global Biogeochemical Cycles 2008; 22.

Mallet MD, Cravigan LT, Milic A, Alroe J, Ward J, Keywood MD, et al. Composition, size and cloud condentation nuclei activity of biomass burning aerosol from north Australian savannah fires, submitted to Atmos. Chem. Phys., 2016

Manninen HE, Petaja T, Asmi E, Riipinen I, Nieminen T, Mikkila J, et al. Long-term field measurements of charged and neutral clusters using Neutral cluster and Air Ion Spectrometer (NAIS). Boreal Environ. Res 2009; 14: 591-605.

McFiggans G, Artaxo P, Baltensperger U, Coe H, Facchini MC, Feingold G, et al. The effect of physical and chemical aerosol properties on warm cloud droplet activation. Atmospheric Chemistry and Physics 2006; 6: 2593-2649.

Melendez-Perez JJ, Fostier AH, Carvalho JA, Windmöller CC, Santos JC, Carpi A. Soil and biomass mercury emissions during a prescribed fire in the Amazonian rain forest. Atmospheric Environment 2014; 96: 415-422.

Meyer C, Cook G, Reisen F, Smith T, Tattaris M, Russell-Smith J, et al. Direct measurements of the seasonality of emission factors from savanna fires in northern Australia. Journal of Geophysical Research: Atmospheres (1984–2012) 2012; 117.

Meyer CP, Luhar AK, Mitchell RM. Biomass burning emissions over northern Australia constrained by aerosol measurements: I—Modelling the distribution of hourly emissions. Atmospheric Environment 2008; 42: 1629-1646.

Milic A, Mallet MD, Cravigan LT, Alroe J, Ristovski ZD, Selleck P, et al. Aging of aerosols emitted from biomass burning in northern Australia, Atmos. Chem. Phys. Discuss., doi:10.5194/acp-2016-730, under review, 2016

Mirme A, Tamm E, Mordas G, Vana M, Uin J, Mirme S, et al. A wide-range multi-channel Air Ion Spectrometer. Boreal Environmental Research 2007; 12: 247-264.

Mochida M, Kawamura K. Hygroscopic properties of levoglucosan and related organic compounds characteristic to biomass burning aerosol particles. Journal of Geophysical Research: Atmospheres (1984–2012) 2004; 109.

National-Environment-Protection-Council-Service-Corporation. National Environment Protection (Air Toxics) Measure, 2011.

Novakov T, Corrigan C. Cloud condensation nucleus activity of the organic component of biomass smoke particles. Geophysical Research Letters 1996; 23: 2141-2144.

Packham D, Tapper N, Griepsma D, Friedli H, Hellings J, Harris S. Release of Mercury from Biomatter after Burning: A Preliminary Investigation of Biomatter and Soils. Air Quality and Climate Change 2009: 24-27.

Paris R, Desboeufs K, Formenti P, Nava S, Chou C. Chemical characterisation of iron in dust and biomass burning aerosols during AMMA-SOP0/DABEX: implication for iron solubility. Atmospheric Chemistry and Physics 2010; 10: 4273-4282.

Penner J, Chuang C, Grant K. Climate forcing by carbonaceous and sulfate aerosols. Climate Dynamics 1998; 14: 839-851.

Penner JE, Dickinson RE, O'Neill CA. Effects of aerosol from biomass burning on the global radiation budget. Science 1992; 256: 1432-1434.

Pirrone N, Cinnirella S, Feng X, Finkelman RB, Friedli HR, Leaner J, et al. Global mercury emissions to the atmosphere from anthropogenic and natural sources. Atmospheric Chemistry and Physics 2010; 10: 5951-5964.

Radhi M, Box MA, Box GP, Mitchell RM. Biomass-burning aerosol over northern Australia. Australian Meteorological and Oceanographic Journal 2012; 62: 25.

Rea AW, Lindberg SE, Scherbatskoy T, Keeler GJ. Mercury accumulation in foliage over time in two northern mixed-hardwood forests. Water, Air, and Soil Pollution 2002; 133(1-4): 49-67.

Reid JS, Hobbs PV, Ferek RJ, Blake DR, Martins JV, Dunlap MR, et al. Physical, chemical, and optical properties of regional hazes dominated by smoke in Brazil. Journal of Geophysical Research: Atmospheres (1984–2012) 1998; 103: 32059-32080.

Rosen J, Young S, Laby J, Kjome N, Gras J. Springtime aerosol layers in the free troposphere over Australia: Mildura Aerosol Tropospheric Experiment (MATE 98). Journal of Geophysical Research: Atmospheres (1984–2012) 2000; 105: 17833-17842.

Rubin M, Berman-Frank I, Shaked Y. Dust-and mineral-iron utilization by the marine dinitrogen-fixer Trichodesmium. Nature Geoscience 2011; 4: 529-534.

Russell-Smith J, Cook GD, Cooke PM, Edwards AC, Lendrum M, Meyer C, et al. Managing fire regimes in north Australian savannas: applying Aboriginal approaches to contemporary global problems. Frontiers in Ecology and the Environment 2013; 11: e55-e63.

Russell-Smith J, Yates CP, Whitehead PJ, Smith R, Craig R, Allan GE, et al. Bushfires' down under': patterns and implications of contemporary Australian landscape burning. International Journal of Wildland Fire 2007; 16: 361-377.

Schroth AW, Crusius J, Sholkovitz ER, Bostick BC. Iron solubility driven by speciation in dust sources to the ocean. Nature Geoscience 2009; 2: 337-340.

Sedwick PN, Sholkovitz ER, Church TM. Impact of anthropogenic combustion emissions on the fractional solubility of aerosol iron: Evidence from the Sargasso Sea. Geochemistry, Geophysics, Geosystems 2007; 8.

Shen H, Huang Y, Wang R, Zhu D, Li W, Shen G, et al. Global Atmospheric Emissions of Polycyclic Aromatic Hydrocarbons from 1960 to 2008 and Future Predictions. Environmental Science & Technology 2013; 47: 6415-6424.

Shi Y, Matsunaga T, Saito M, Yamaguchi Y, Chen X. Comparison of global inventories of CO_2 emissions from biomass burning during 2002–2011 derived from multiple satellite products. Environmental Pollution 2015; 206: 479-487.

Sinreich R, Friess U, Wagner T, Platt U. Multi axis differential optical absorption spectroscopy (MAX-DOAS) of gas and aerosol distributions. Faraday Discussions 2005; 130: 153-164.

Sprovieri F, Pirrone N, Bencardino M, D'Amore F, Carbone F, Cinnirella S, et al. Atmospheric Mercury Concentrations observed at ground-based monitoring sites globally distributed in the framework of the GMOS network. Atmos. Chem. Phys. Discuss. 2016; 2016: 1-32.

Steffen A, Douglas T, Amyot M, Ariya P, Aspmo K, Berg T, et al. A synthesis of atmospheric mercury depletion event chemistry in the atmosphere and snow. Atmospheric Chemistry and Physics 2008; 8: 1445-1482.

Stokes R, Robinson R. Interactions in aqueous nonelectrolyte solutions. I. Solute-solvent equilibria. The Journal of Physical Chemistry 1966; 70: 2126-2131.

Tuch TM, Haudek A, Müller T, Nowak A, Wex H, Wiedensohler A. Design and performance of an automatic regenerating adsorption aerosol dryer for continuous operation at monitoring sites. Atmospheric Measurement Techniques 2009; 2: 417-422.

Twomey S. Aerosols, clouds and radiation. Atmospheric Environment. Part A. General Topics 1991; 25: 2435-2442.

van der Werf GR, Randerson JT, Giglio L, Collatz G, Mu M, Kasibhatla PS, et al. Global fire emissions and the contribution of deforestation, savanna, forest, agricultural, and peat fires (1997–2009). Atmospheric Chemistry and Physics 2010; 10: 11707-11735.

Wang X, P.K. T, Mallet MD, Desservettaz MJ, Hawker DW, Keywood MK, et al. Emissions of selected semivolatile organic chemicals from forest and savannah fires. Environmental Science & Technology 2016, under review.

Wang X, Thai PK, Li Y, Li Q, Wainwright D, Hawker DW, et al. Changes in atmospheric concentrations of polycyclic aromatic hydrocarbons and polychlorinated biphenyls between the 1990s and 2010s in an Australian city and the role of bushfires as a source. Environmental Pollution 2016; 213: 223-231.

Whittlestone S, Zahorowski W. Baseline radon detectors for shipboard use: Development and deployment in the First Aerosol Characterization Experiment (ACE 1). Journal of Geophysical Research: Atmospheres 1998; 103: 16743-16751.

Wigder N, Jaffe D, Saketa F. Ozone and particulate matter enhancements from regional wildfires observed at Mount Bachelor during 2004–2011. Atmospheric Environment 2013; 75: 24-31.

Williams AG, Chambers S, Zahorowski W, Crawford J, Matsumoto K, Uematsu M. Estimating the Asian radon flux density and its latitudinal gradient in winter using ground-based radon observations at Sado Island. Tellus B 2009; 61: 732-746.

Williams AG, Zahorowski W, Chambers S, Griffiths A, Hacker JM, Element A, et al. The vertical distribution of radon in clear and cloudy daytime terrestrial boundary layers. Journal of the Atmospheric Sciences 2011; 68: 155-174.

Winton V, Bowie A, Edwards R, Keywood M, Townsend A, van der Merwe P, et al. Fractional iron solubility of atmospheric iron inputs to the Southern Ocean. Marine Chemistry 2015; 177: 20-32.

Winton V, Edwards R, Bowie A, Keywood M, Williams A, Chambers S, et al. Dry season aerosol iron solubility in tropical northern Australia, in review in Atmos. Chem. Phys., 2016.

Wong J, Li Z. Retrieval of optical depth for heavy smoke aerosol plumes: uncertainties and sensitivities to the optical properties. Journal of the Atmospheric Sciences 2002; 59: 250-261.

Yokelson RJ, Crounse JD, DeCarlo PF, Karl T, Urbanski S, Atlas E, et al. Emissions from biomass burning in the Yucatan. Atmospheric Chemistry and Physics 2009; 9: 5785-5812.

4.8. Supplementary information

Figure 4.S1 shows the ambient relative humidity and the aerosol sample relative humidity after drying by the Automated Regenerating Aerosol Diffusion Dryer (ARADD). The ARADD was effective in keeping the sample relative humidity below 40% for the entire sampling period. The two periods with RH > 40% correspond to power outages at ATARS.

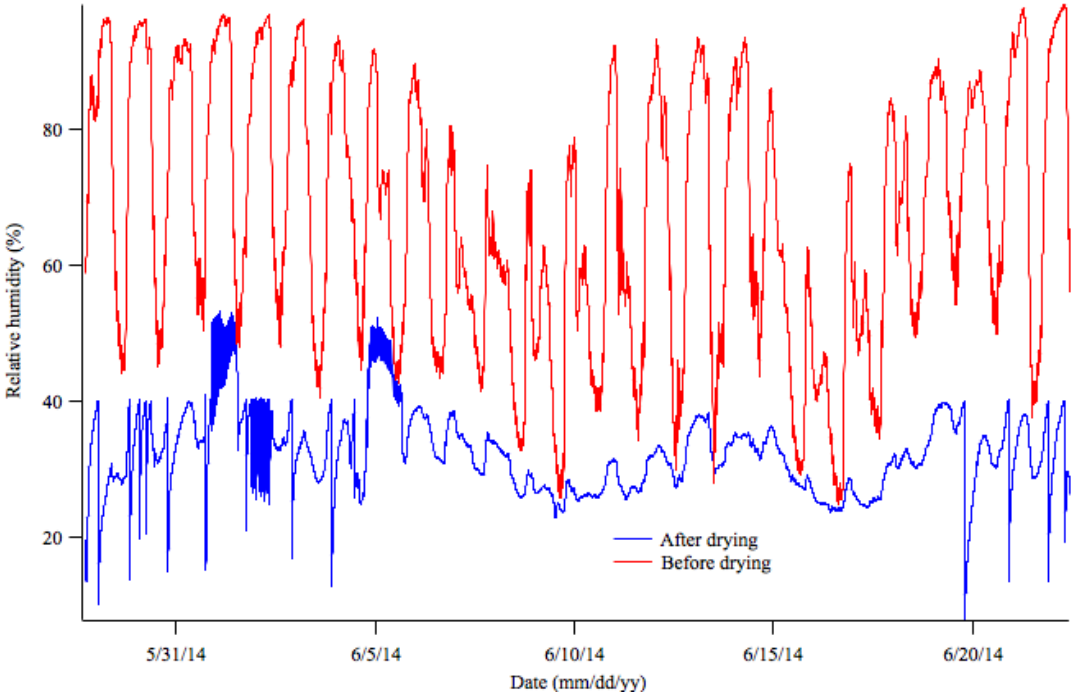

Figure 4.S1 The ambient and sample relative humidity for the campaign.

Figure 4.S2 shows the spectrogram of particle sizes between 1 and 40 nm. There was a distinct lack of new particle formation over the entire month, likely attributed to high particle mass loadings acting as a condensation sink.

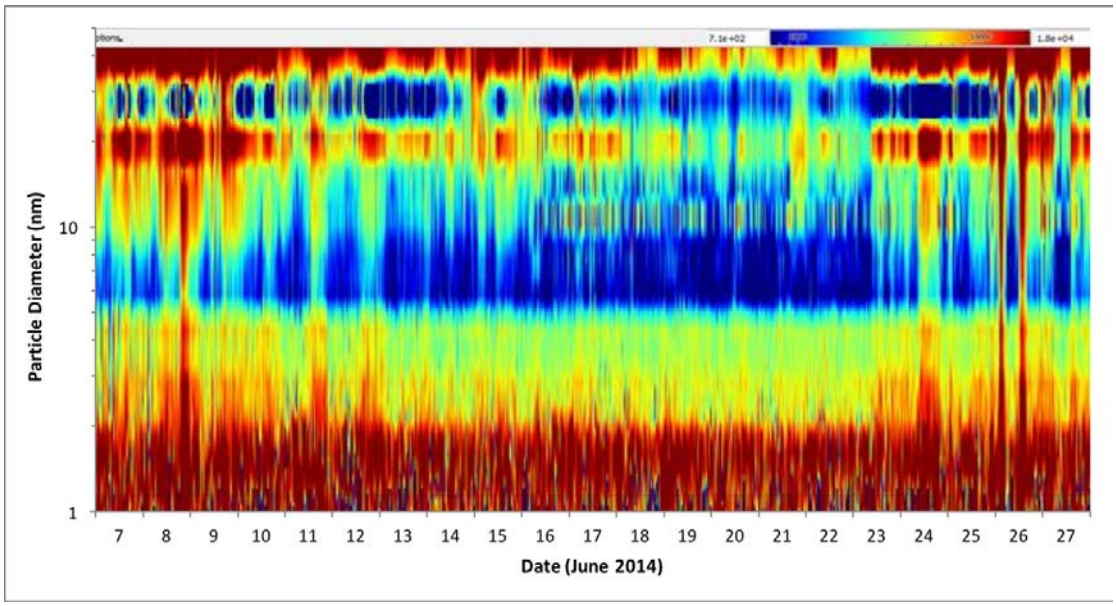

Figure 4.S2 The particle size distributions measured from 1nm up to 40 nm, demonstrating no nucleation events.

Chapter 5

FRESH AND AGED AEROSOLS EMITTED FROM BIOMASS BURNING IN NORTHERN AUSTRALIA

Andelija Milic[1], Marc D. Mallet[1], Luke T. Cravigan[1], Joel Alroe[1], Zoran D. Ristovski[1], Paul Selleck[2], Sarah J. Lawson[2], Jason Ward[2], Maximilien J. Desservettaz[3], Clare Paton-Walsh[3], Leah R. Williams[4], Melita D. Keywood[2], Branka Miljevic[1]

[1]International Laboratory for Air Quality and Health, Queensland University of Technology, Brisbane, Queensland, 4000, Australia
[2]CSIRO Oceans and Atmosphere, Aspendale, Victoria, 3195, Australia
[3]Centre for Atmospheric Chemistry, University of Wollongong, Wollongong, New South Wales, 2522, Australia
[4]Aerodyne Research, Inc., Billerica, Massachusetts, 01821, USA

Under review in Atmospheric Chemistry and Physics (2016), doi:10.5194/acp-2016-730

STATEMENT OF JOINT AUTHORSHIP

The authors listed below have certified that:

1. they meet the criteria for authorship in that they have participated in the conception, execution, or interpretation, of at least that part of the publication in their field of expertise;
2. they take public responsibility for their part of the publication, except for the responsible author who accepts overall responsibility for the publication;
3. there are no other authors of the publication according to these criteria;
4. potential conflicts of interest have been disclosed to (a) granting bodies, (b) the editor or publisher of journals or other publications, and (c) the head of the responsible academic unit, and
5. they agree to the use of the publication in the student's thesis and its publication on the QUT ePrints database consistent with any limitations set by publisher requirements.

In the case of this chapter: Chapter 5

TITLE

Fresh and aged aerosols emitted from biomass burning in northern Australia

AUTHORS

Andelija Milic (candidate) analysed and interpreted the data and prepared the manuscript;

Marc D. Mallet operated the cToF-AMS and contributed to data analysis, interpretation and writing;

Luke T. Cravigan set up the SMPS and contributed to data interpretation;

Joel Alroe assisted in organizing the QUT instrumentation, data interpretation and writing the manuscript;

Zoran D. Ristovski contributed to campaign organization and data interpretation and supervised the work of Andelija Milic;

Paul Selleck operated the BAM, analysed the data and contributed to data interpretation;

Sarah J. Lawson operated the PTR-MS and analysed the data;

Jason Ward operated the Ozone analyser and analysed the data;

Maximilien J. Desservettaz operated the FTIR and SMPS and analysed the data;

Clare Paton-Walsh contributed to campaign organization and running the campaign;

Leah R. Williams contributed to setting up the cToF-AMS, preliminary data analysis and data interpretation;

Melita D. Keywood organized and led the campaign;

Branka Miljevic installed the cToF-AMS, contributed to data analysis, interpretation and writing and supervised the work of Andelija Milic;

All authors declare that they have no conflict of interest.

Principal Supervisor Confirmation

I have sighted email or other correspondence from all Co-authors confirming their certifying authorship.

Zoran Ristovski		26/09/2016
Name	Signature	Date

Fresh and aged aerosols emitted from biomass burning in northern Australia

Andelija Milic[1], Marc D. Mallet[1], Luke T. Cravigan[1], Joel Alroe[1], Zoran D. Ristovski[1], Paul Selleck[2], Sarah J. Lawson[2], Jason Ward[2], Maximilien J. Desservettaz[3], Clare Paton-Walsh[3], Leah R. Williams[4], Melita D. Keywood[2], Branka Miljevic[1]

[1]International Laboratory for Air Quality and Health, Queensland University of Technology, Brisbane, Queensland, 4000, Australia
[2]CSIRO Oceans and Atmosphere, Aspendale, Victoria, 3195, Australia
[3]Centre for Atmospheric Chemistry, University of Wollongong, Wollongong, New South Wales, 2522, Australia
[4]Aerodyne Research, Inc., Billerica, Massachusetts, 01821, USA

Correspondence to: Branka Miljevic (b.miljevic@qut.edu.au)

Abstract. There is a lack of knowledge of how biomass burning aerosols in the tropics age, including those in the fire-prone Northern Territory in Australia. This paper reports chemical characterization of fresh and aged aerosols monitored during the one month long SAFIRED (Savannah Fires in the Early Dry Season) field study, with an emphasis on chemical signature and aging of organic aerosols. The campaign took place in June 2014 during the early dry season when the surface measurement site, the Australian Tropical Atmospheric Research Station (ATARS), located in the Northern Territory, was heavily influenced by thousands of wild and prescribed bushfires. ATARS was equipped with a wide suite of instrumentation for gaseous and aerosol characterization. A compact time-of-flight aerosol mass spectrometer was deployed to monitor aerosol chemical composition. Approximately 90 % of submicron non-refractory mass was composed of organic material. Ozone enhancement in biomass burning plumes indicated increased air mass photochemistry and increased organic aerosol with the aging parameter (f44) suggested secondary organic aerosol formation. Diversity of biomass burning emissions was illustrated through variability in chemical signature (e.g. wide range in f44, from 0.06 to 0.18) for five intense fire events. The background particulate loading was characterized using Positive Matrix Factorization (PMF). A PMF-resolved BBOA (biomass burning organic aerosol) factor comprised 24 % of the submicron non-refractory organic aerosol mass, confirming the significance of fire sources. A dominant PMF factor, OOA (oxygenated organic aerosol), made up 47 % of sampled aerosol fraction, illustrating the importance of aerosol aging in the Northern Territory. Biogenic isoprene-derived organic aerosol factor was the third significant fraction of the background aerosol (28 %).

Keywords. Biomass burning, savannah fires, organic aerosol, aerosol aging

5.1 Introduction

Tropical regions are some of the most fire-prone areas in the world (Crutzen and Andreae, 1990). As one of them, Northern Australia is observed to be a significant contributor to the global biomass burning (BB) budget (Russell-Smith et al., 2007). Fire emissions are made up of a variety of gaseous and particle-phase species, with the particle-phase consisting primarily of carbonaceous particles, including organic carbon (OC) and elemental carbon (EC) (Bond et al., 2004;Hallquist et al., 2009;Formenti et al., 2003;Crutzen and Andreae, 1990). Open fires are the largest contributors to carbonaceous emissions; approximately 70 % and 40 % of the global annual emissions of OC and EC are formed in open fire events, respectively (Bond et al., 2004). Annually, 60-75 % of Australia's carbon emissions are attributed to BB emissions in tropical savannahs (Hurst et al., 1994). Organic carbon and EC affect the Earth's radiation balance by scattering and absorbing solar radiation, respectively (Penner et al., 1998;Haywood and Boucher, 2000). O'Brien and Mitchell (2003) suggested that atmospheric heating caused by UV absorbing carbonaceous aerosol, related to BB events in the Northern Territory during a dry season, can be significant and will likely have an influence on local (and possibly even global) climate. Carbonaceous species can also serve as condensation nuclei in cloud formation processes (Roberts et al., 2002). It is therefore important to build a comprehensive knowledge of BB emissions as they play a key role in the climate.

The characterization, processing and estimation of impact of BB emissions is a complex and challenging issue due to a wide range of burning material and combustion conditions (flaming/smouldering), as well as complex atmospheric physics and chemistry that BB plumes undergo once emitted (Reid et al., 2005;Weimer et al., 2008). Besides the characterization of fresh BB emissions, it is important to address their evolution in the atmosphere since aging of the BB emissions will alter their properties and thus how they interact with the climate system. Fresh BB emissions are those released directly from BB sources, while processed emissions refer to fresh particle or gaseous species transformed in the atmosphere through photochemical processing (aging). Organic aerosols (OA) can be differentiated as directly emitted primary organic aerosols (POA), aged primary organic aerosols (aged POA) and secondary organic aerosols (SOA) that form via condensation of lower volatility photo-oxidation products. A large fraction of BB-related POA is observed to be semivolatile (Grieshop et al., 2009) and can therefore change upon dilution with background air by evaporation of its content into the gas phase and be exposed to further transformations in the atmosphere.

Processing of BB emissions in the ambient atmosphere and in laboratory experiments is characterized by increases in the oxygenated fraction of OA (OOA) and degradation of species that are indicators of BB origin (Cubison et al., 2011;DeCarlo et al., 2008;Capes et al., 2008). However, there is no agreement on whether the aging of BB emissions leads to additional OA production. Some recent field and laboratory studies investigating the evolution of BB plumes have shown that OA mass increases with aging (DeCarlo et al., 2008;Yokelson et al., 2009;Heringa et al., 2011), while others have found no significant change or a decrease in OA with atmospheric processing (Akagi et al., 2012;Brito et al., 2014;Cubison et al., 2011;Capes et al., 2008). In addition to SOA formation, BB plumes promote the production of another important secondary pollutant,

tropospheric ozone (Real et al., 2007). An excess of nitrogen oxides (NO_X), non-methane organic compounds (NMOCs) and carbon monoxide (CO) in the atmosphere from fire emissions promote additional pathways for ozone production (Parrington et al., 2013). Ozone enhancement in BB emissions has been extensively used as a proxy for air mass photochemical activity (Hobbs et al., 2003;Jaffe and Wigder, 2012;Yokelson et al., 2009;Akagi et al., 2012).

An extensive area of the Northern Territory of Australia is burned each year during the dry season (May-October) and the region is strongly affected by BB emissions. Considering that this area is a globally significant source of BB aerosol emissions (Mitchell et al., 2013), and that there have been a limited number of studies on aerosol characterization and aging, there is a need for more research. Information about the composition and degree of aging of OA that makes up the majority of emitted species generated in these fires will facilitate the estimate of the influence of BB in the Northern Territory. This will also contribute to a better understanding of fire emissions in tropical regions. In order to address these issues, the one month long SAFIRED (Savannah Fires in the Early Dry Season) field study was conducted at the Australian Tropical Atmospheric Research Station (ATARS) during a frequent burning period (late May/June 2014). This publication presents insights into fresh and aged aerosols emitted during the SAFIRED, while a detailed description of the campaign can be found in Mallet et al. (2016) (Chapter 4).

5.2 Measurement site and period

The Australian Tropical Atmospheric Research Station (ATARS) is situated on the Gunn Point peninsula in the Northern Territory (12°14'56.6" S, 131°02'40.8" E). The northern Australian tropical land mass is mostly covered by savannah biomes including scattered eucalypt trees, shrubs and grasses (Lacey et al., 1982). The sampling site can be described as rural background due to its remote location, with the closest populated centre, the city of Darwin, approximately 80 km south west of the ATARS. During the measurement period, the dominant sources of gaseous and aerosol species were wild and prescribed fires. Apart from planned burns, anthropogenic inputs to this region can be considered negligible (Bowman et al., 2007) and observations have highlighted the importance of biogenic sources for this area (Allen et al., 2008). The sampling site can also be impacted by marine aerosols (Bouya et al., 2010); however, fires are the major source of aerosols during the dry season.

The SAFIRED campaign was conducted from the 29th of May until the 30th of June, 2014 at the beginning of the dry season. The early dry period is characterized by natural fires as well as prescribed burns conducted to reduce the extent, intensity and frequency of wildfires in the late dry season (October-November). Thousands of fires in the Northern Territory during the campaign were detected by MODIS and VIIRS satellite sensors (Mallet et al., 2016) (Chapter 4). Fire emissions sources ranged from approximately two to up to hundreds of kilometres distant from the sampling station.

The early dry season was characterized by dry weather conditions (average relative humidity of 67 ± 23 %) and warm days with an average daily and nightly temperatures of 27 ± 5 °C (up to 34 °C) and 19 ± 4 °C (with a minimum of 10 °C), respectively. There were no days of rainfall. Wind direction was predominantly southeast, suggesting that the sampled air masses had mainly passed over land affected by fire emissions. However, on some days (e.g. between 3rd and 6th of June) in the afternoon hours northeast wind direction was dominant, directing the air masses from land to pass over the ocean before being detected at ATARS. Moreover, an oceanic influence was observed between 19th and 22nd of June (Mallet et al., 2016) (Chapter 4).

5.2.1 Instrumentation and method

Ground level characterization was performed using a wide range of instrumentation for gas- and particle-phase measurements. Detailed description of all instruments used in SAFIRED is given in Mallet et al. (2016) (Chapter 4). The focus of this study was on the aerosol chemical composition and aging using the instrumentation listed in the following paragraphs.

Compact Time-of-Flight Aerosol Mass Spectrometer (cToF-AMS)

A compact time-of-flight aerosol mass spectrometer (cToF-AMS or AMS, Aerodyne Research, Inc.) was deployed to monitor the chemical composition of non-refractory submicron (PM_1) aerosol. Monitored species were submicron particulate organic and inorganic compounds (sulfate, ammonium, nitrates and chlorides). Details about instrument operation during this campaign can be found in Mallet et al. (2016) (Chapter 4).

Unit mass resolution (UMR) and high resolution (HR) AMS data analysis was performed in Wavemetrics Igor Pro software (version 6.36) using the standard AMS Analysis Toolkits, Squirrel (Version 1.56D) and PIKA (Version 1.16), respectively. Data collection with a filter at the instrument inlet was used to correct for contributions from air in the fragmentation table (Aiken et al., 2008). Measured time-resolved gas-phase CO_2 concentrations were applied instead of the fragmentation table default value. The AMS collection efficiency was determined using the calculations provided within the PIKA Toolkit. The composition dependent collection efficiency panel enables an estimate of the collection efficiency based on ammonium nitrate, organic content, aerosol acidity and relative humidity (Middlebrook et al., 2012). The time-resolved collection efficiency (with an average value of 0.61) was applied to the entire dataset. High OA loadings during the campaign caused interferences in the detection of sulfate in the UMR analysis. Significant improvement was made in distinguishing sulfate fragments from organic fragments at the same m/z by performing HR peak fits in PIKA (Sect. 5.6.1 in supplementary information). Therefore, HR peak fitting data (PIKA) were chosen for further analysis.

AMS fragments analysis

Organic aerosols measured by the AMS encompassed aerosols that were processed in the atmosphere for different periods of time and included both POA and SOA. As such, a tool was needed to distinguish BB aerosol from other sources and fresh

from processed BB aerosol. An extensively employed fragments analysis using the AMS-extracted parameters f43 (ions $C_3H_7^+$ and $C_2H_3O^+$), f44 (CO_2^+) and f60 ($C_2H_4O_2^+$) was applied here. The ratio of an integrated organic signal, e.g. m/z 43, to total organic signal is referred to as f43. Parameters f43 and f44 were used to estimate the level of OA processing, as they illustrate OA fractions of different aging degree. While f43 is mainly associated with hydrocarbon-like and semivolatile OA fractions (fragments $C_3H_7^+$ and $C_2H_3O^+$, respectively) (Jimenez et al., 2009;Lanz et al., 2007;Zhang et al., 2007;Heringa et al., 2011), f44 is assigned to highly oxygenated OA species (fragment CO_2^+) (Aiken et al., 2007;DeCarlo et al., 2010;Alfarra et al., 2007). The AMS parameter f60 and accompanying f73 ($C_3H_5O_2^+$) are widely used as BB emission signatures as they are directly related to levoglucosan-like species, which are a substantial fraction of organics emitted in pyrolysis of cellulose (Alfarra et al., 2007;Simoneit et al., 1999). The f60 can be applied as a valuable BB marker for time periods of up to one day (Cubison et al., 2011;Bougiatioti et al., 2014). Ambient aerosols characterized by an f60 value higher than 0.003 are considered to be influenced by BB emissions (Cubison et al., 2011). A graphical approach of comparing f44 vs. f60 introduced by Cubison et al. (2011) was used in this study to estimate the degree of aging of BB emissions.

Positive Matrix Factorization (PMF)

Positive Matrix Factorization (PMF) analysis (Paatero and Tapper, 1994) using the PMF evaluation tool (Ulbrich et al., 2009) was used in source apportionment of the AMS OA data. PMF splits the OA spectrum into different factors that can be related to specific sources. (Paatero, 1999;Paatero and Hopke, 2009). Various factors have been identified by PMF analysis of AMS OA data, with the most common being hydrocarbon-like OA (HOA) and oxygenated OA, that can sometimes be further apportioned to low-volatility oxygenated OA (LV-OOA) and semivolatile oxygenated OA (SV-OOA) (Ulbrich et al., 2009;Lanz et al., 2007;Ng et al., 2010;Jimenez et al., 2009). Other factors include environment specific factors such as biomass burning OA (BBOA) and cooking-related OA (COA). The solution space in this study was investigated by varying the number of factors and starting conditions (seeds, 0 to 50 in increments of 1) and applying rotational parameters (fpeaks, -1 to 1 in increments of 0.1).

Beta plus particle measurement system (BAM)

PM_1 mass was measured and collected onto pre baked (600 °C) quartz 47 mm filters (Pall Tissuquatz p/n 7202) using a Beta plus particle measurement system (BAM, Teledyne API Model 602), every 12 hours. All of the species measured on BAM filters were blank corrected. Particles collected on filters were further analysed for anhydrous sugars, including levoglucosan, by high performance anion exchange chromatography with pulsed amperometric detection and for water soluble ions including potassium (K^+), nitrates (NO_3^-), sulfates (SO_4^{2-}), ammonium (NH_4^+) and chlorides (Cl^-) by ion suppressed chromatography. Levoglucosan and non-sea salt K^+ were used as metrics for BB emissions. BAM PM_1 filters were analysed by a Thermal-Optical Carbon Analyser (DRI Model 2001A) using the IMPROVE-A temperature protocol (Chow et al., 2007) to determine contributions of EC and OC. Water soluble inorganic ions and OC were also used for comparison with AMS-resolved species.

Fourier Transform Infrared Spectrometer (FTIR)

The Spectronus trace gas and isotope Fourier Transform Infrared Spectrometer (FTIR) analyser, built by the Centre of Atmospheric Chemistry at the University of Wollongong, was deployed to monitor gaseous species including carbon monoxide (CO) and carbon dioxide (CO_2) (Griffith et al., 2012;Griffith, 1996). Details about the instrument operation can be found elsewhere (Desservettaz et al., 2016). In order to include dilution effects, OA and ozone data are presented relative to CO. CO is an important BB product that can remain in the atmosphere for a relatively long time period (one to two months depending on the environment) without observed decay or interactions with oxidative agents (Wang and Prinn, 1999;DeCarlo et al., 2010;Edwards et al., 2006). CO has therefore been employed as a long-lived, conservative tracer in many studies (DeCarlo et al., 2010;Kleinman et al., 2008;Brito et al., 2014;Yokelson et al., 2009;Akagi et al., 2012). Gas-phase CO_2 data, as previously mentioned, were applied in the AMS fragmentation table adjustment. CO and CO_2 were also used in modified combustion efficiency (MCE) calculations, with details presented in Desservettaz et al. (2016). MCE refers to the ratio of ΔCO_2 (measured value relative to background value) to the sum of ΔCO_2 and ΔCO (Ward and Radke, 1993). The MCE parameter was used to distinguish smouldering (usually lower than 0.9) from flaming (usually higher than 0.9) fires. The MCE value can also indicate the burning material.

Scanning Mobility Particle Sizer (SMPS)

Aerosol size and number concentration were monitored by a Scanning Mobility Particle Sizer (SMPS, a TSI 3071 long-column electrostatic classifier coupled to a TSI 3772 Condensation Particle Counter). The SMPS measured the particle size distribution from 14 nm up to 670 nm every 5 minutes. Changes in the size distribution due to aging were investigated.

Proton Transfer Reaction-Mass Spectrometer (PTR-MS)

A high sensitivity Proton Transfer Reaction-Mass Spectrometer (PTR-MS, Ionicon Analytik) with a quadrupole mass spectrometer and an H_3O^+ ion source was employed to measure non-methane organic compounds (NMOCs) that include non-methane hydrocarbons and oxygenated volatile organic compounds. These species are important in the formation of SOA and ozone. Isoprene and monoterpenes make up a dominant fraction of global gas-phase NMOCs, contributing significantly to the production of SOA (Guenther et al., 2012). Tropical regions can contribute up to 80 % of global annual isoprene emissions due to warm weather conditions (Guenther, 2006). He et al. (2000) investigated NMOCs emitted from eucalyptus trees, which make up 95 % of all tree species in Australia. Isoprene accounts for 64-100 % of NMOCs emitted from different eucalyptus species. The isoprene/furan fraction (signal at m/z 69) of measured NMOCs is used here in the analysis of isoprene-derived OA. Other studies suggest that the contribution of isoprene to m/z 69 prevails in non-BB periods while the furan contribution is more significant in BB plumes (Warneke et al., 2011). In order to distinguish furan and isoprene contribution over the sampling period, a gas chromatography-mass spectrometry method was used.

Ozone analyser

Ozone concentration was monitored by an Ultraviolet Photometric Ozone analyser (Model 49i, Thermo Scientific). Ozone enhancement in BB emissions has been used as a proxy for air mass photochemical activity.

Fire data

Information about the location and duration of fires was obtained from the Sentinel Hotspots system. Hotspots data used for this campaign were derived from the MODIS (Moderate Resolution Imaging Spectroradiometer) sensor (Terra and Aqua satellites) and VIIRS (Visible Infrared Imaging Radiometer Suite) sensor (Suomi NPP satellites). Only the hotspots with confidence level higher than 50 % were considered in the analysis. Hotspots are detected by satellite once a day which limited the fire analysis to events that occurred between approximately 11 am and 3 pm. During the SAFIRED campaign thousands of fires were detected in the Northern Territory. Distance-resolved fire frequencies are presented in Mallet et al. (2016) (Chapter 4). Moreover intense fires characterized by plumes detected without considerable influence from other fire sources, were extracted from the whole dataset (Desservettaz et al., 2016). Five events that were categorised as single, intense fires are analysed here. Air mass backtrajectories were computed using the NOAA/ARL HYSPLIT (Hybrid Single-Particle Lagrangian Integrated Trajectory) model.

5.3. Results and Discussion

5.3.1 Aerosol chemical characterization

PM_1 ambient aerosols sampled during the SAFIRED campaign were dominated by an organic fraction. Organic carbon made up 72 % and EC 15 % of the measured PM_1 on the BAM filters (Fig. 5.1a). Data from the AMS (Fig. 5.1b and 5.1c), indicate that organics made up approximately 90 % of submicron non-refractory mass with an average concentration of 11.1 µg m^{-3} and concentrations of up to 350 µg m^{-3} during intense and nearby BB events. The organic mass (OM) sampled by the BAM was converted from OC using the conversion factor of 1.4, which was determined in PIKA. This value is within the span of OM/OC conversion factors for the biomass burning aerosol suggested by Reid et al. (2005). The BAM OM and mass concentration of organics sampled by the AMS are in good agreement (R value of 0.94), with slightly higher concentrations measured by the BAM (Fig. 5.S2c) probably due to the lower collection efficiency of the AMS above 700 nm. Organic mass has been observed to be the dominant fraction of PM_1 ambient aerosols during the early dry season in the Northern Territory (Carr et al., 2005). The organic fraction was also dominant in other studies strongly impacted by BB emissions (Brito et al., 2014;Capes et al., 2008). In this study, the remaining submicron non-refractory mass was made up of inorganics including sulfates (4.2 %), ammonium (2.8 %), nitrates (1.5 %) and chlorides (1.3 %), with average concentrations of 0.51 ± 0.32 µg m^{-3}, 0.35 ± 0.68 µg m^{-3}, 0.19 ± 0.45 µg m^{-3} and 0.17 ± 1.28 µg m^{-3}, respectively.

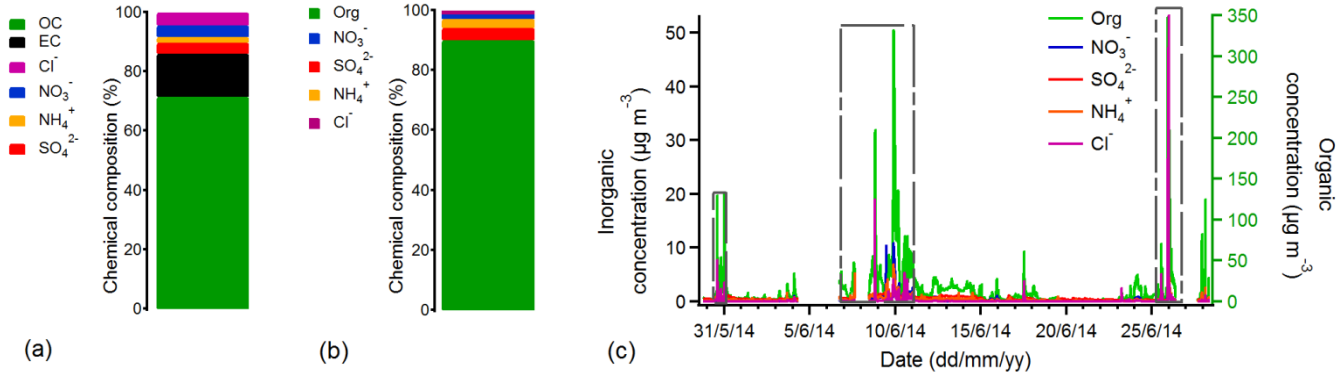

Figure 5.10 Contributions of (a) EC, OC and inorganics collected on filters and the contribution of (b) AMS organic and inorganics in non-refractory submicron aerosol fraction as well as (c) their time series. Close BB periods are marked in the AMS time series with grey dashed boxes. The distant BB periods cover all days of the measurement other than days included in close BB periods. Gaps in the AMS time series indicate gaps in the sampling.

The sampling site was constantly impacted by fire emissions with periods of heavy BBs characterized by high aerosol and gas phase concentrations, for instance CO reaching up to ~10^4 ppb and organics up to 350 µg m^{-3} (Fig. 5.2). The most intense BB episodes were on the 30th of May, between the 7th and 11th of June, and on the 25th and 26th of June (Fig. 5.1c) (Mallet et al., 2016) (Chapter 4). During intense fire periods, organics, CO and particle number concentration showed correlated increases (Fig. 5.2). Moreover, looking at Sentinel Hot spots during these periods, hot spots were detected within 20 km from the ATARS. Based on this, the dataset was separated into periods of "close BB" (corresponding to high organics, CO and particle number concentration signals and close events (< 20 km)) and "distant BB" (corresponding to less intense organics, CO and particle number concentration signals and distant events (> 20 km)). It is important to emphasize that all periods during the measurement that have not been included in close BB periods have been assigned to distant BB periods, as ATARS was constantly influenced by BBs. The selection does not mean that emissions from distant fires were not present during the close BB periods but that the influence of fires near the measurement station during these periods was dominant. Nine intense BB events were identified from close BB periods as single source emissions (Desservettaz et al., 2016). Five of the nine events (Fig. 5.2) were analysed here (Sect. "Biomass burning events"), due to the instrument not sampling during the remaining events. Most of the events occurred in the afternoon/night time (Table 5.1).

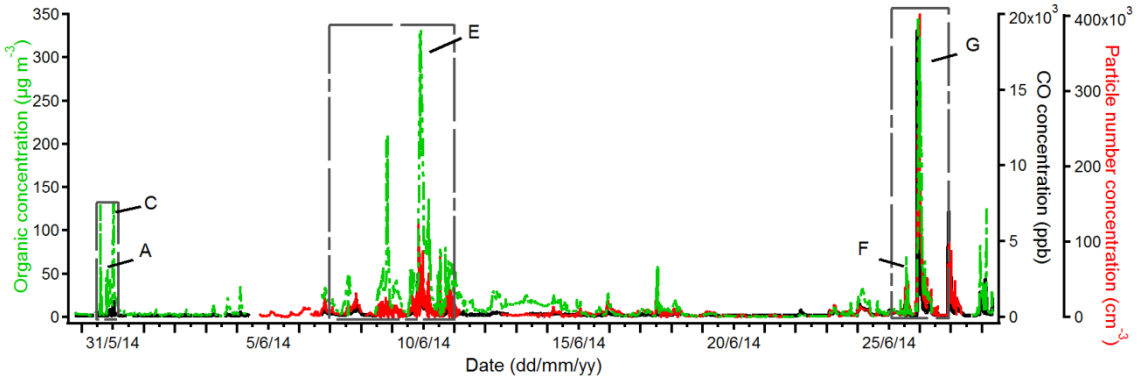

Figure 5.11 Time series for AMS organics, CO and particle number concentration during the SAFIRED campaign. Close BB periods are marked with grey dashed boxes and selected BB events are labelled. The distant BB periods cover all days of the measurement other than days included in close BB periods. Gaps in the time series indicate gaps in the sampling (no data for the instrument).

Table 5.1 Selected BB event values for f44, f60, organic concentration, CO, MCE, mode diameter and $\Delta O_3/\Delta CO$ ratios, along with the measurement start and end time. ND refers to no data.

	Date (start/end)	f44±SD (range)	mean f60±SD (range)	mean Org±SD* (range)	mean CO±SD* (range)	MCE	$\Delta O_3/\Delta CO$	Mode diameter (nm)
A	30/05/14 18:34-30/05/14 19:25	0.087±0.08 (0.079-0.105)	0.016±0.002 (0.010-0.018)	22.6±12.5 (4.6-45.2)	185.9±95.5 (90.2-370.1)	0.97± 0.06	ND	ND
C	30/05/14 23:41-31/05/14/ 00:59	0.066±0.005 (0.060-0.079)	0.027±0.002 (0.021-0.028)	75.5±40.0 (13.7-131.2)	627.1±345.4 (185.8-1181.6)	0.98± 0.11	ND	ND
E	09/06/14 19:45-10/06/14 00:32	0.078±0.013 (0.062-0.093)	0.032±0.002 (0.030-0.035)	175.9±105.0 (87.3-331.8)	1558.5±965.5 (671.6-3382.5)	0.91± 0.05	0.024	146
F	25/06/14 12:28-25/06/14 16:59	0.134±0.031 (0.073-0.178)	0.009±0.002 (0.007-0.014)	13.2±14.5 (2.4-70.8)	479.0±348.8 (139.5-1642.7	0.93± 0.04	0.134	98
G	25/06/14 21:40-26/06/14 03:59	0.062±0.017 (0.045-0.098)	0.046±0.004 (0.035-0.052)	144.6±104.7 (25.8-347.7)	2744.6±2299.8 (592.8-11275.7)	0.90± 0.06	0.011	88

*unit is µg m^{-3}

Coupled with elevated organic concentrations, AMS-measured inorganics also increased during close BB periods (Fig. 5.1c). A high AMS signals for all monitored species corresponded to close BB periods. During SAFIRED, high correlation was observed between organics and ammonium species (R of 0.92), with better agreement during the close BB (R of 0.92) than in the distant BB periods (R of 0.73) (Table 5.S1), suggesting that these ammonium species originated from fire emissions. Moreover, plume emissions included high chloride concentrations (up to approximately 50 µg m^{-3} during close BB periods). Increased chloride concentration during the close BB periods was also indicated by the BAM data (Fig. 5.S3a). This is not surprising since the dominant fine particle inorganic fraction emitted in flaming savannah fires has been shown to be composed of KCl (potassium chloride) and NH_4Cl (ammonium chloride) compounds and/or their mixtures (Liu et al., 2000). There was a better correlation between organics and chlorides for close BB periods (R of 0.67), than for distant BB periods

(R of 0.47). This can be explained by the depletion of chloride with transport and aging of BB plumes (Li et al., 2003;Li et al., 2010;Liu et al., 2000). Correlations for nitrate and sulfate with organics show similar patterns in this work regardless of the BB emissions influence (R of 0.72 and 0.77 for nitrate and R of 0.49 and 0.48 for sulfate for close and distant periods, respectively). AMS inorganic species were compared to soluble ions concentrations measured on the filter samples collected using the BAM. There was a strong correlation between all compared species (R values of 0.85, 0.68 and 0.81 for sulfates, ammonium and nitrate, respectively) except in the case of chloride (R of 0.18) (Fig. 5.S2). Mg^{2+}/Na^{+} ratio values for the filters collected during the high oceanic influence (between 3rd and 6th and 19th and 22nd of June) were close to the sea salt Mg^{2+}/Na^{+} ratio of 0.12 (Fig. 5.S3b). At the same time low terrestrial fetch (low radon concentration) was observed (Mallet et al., 2016) (Chapter 4). Moreover, the chlorides collected on filters were prominent during the period of oceanic influence (Fig. 5.S3a). This suggests that a significant portion of chlorides detected on the BAM filters was of a sea salt origin, which is refractory and therefore not well measured by the AMS, thereby explaining the poor chloride correlation.

5.3.2 Biomass burning aerosols and aging

In general, BB-related particulate matter can be easily distinguished from other aerosol sources by chemical composition. Levoglucosan is a common molecular tracer of plume emissions (Simoneit et al., 1999) and has been extensively used as a BB chemical signature (Jordan et al., 2006;Simoneit, 2002). Moreover, the AMS organic signal intensity (fragment $C_2H_4O_2^{+}$) (Org 60) is directly correlated to the concentration of levoglucosan-like species (Alfarra et al., 2007;Simoneit et al., 1999) and can therefore be applied as a valuable BB marker. Fire sources also contribute to high potassium levels (Li et al., 2003). Figure 5.3 illustrates the time series of Org 60 obtained from the AMS and levoglucosan and soluble non-sea salt potassium sampled by the BAM. Prominent signals of these BB tracers were present during the observed close BB periods, which confirm that the fire source of the detected aerosols is BB.

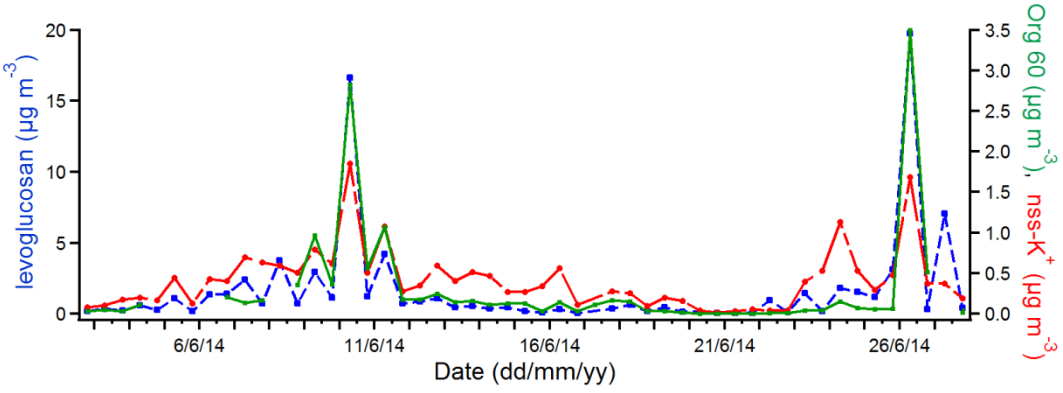

Figure 5.12 Time series of BB tracers: levoglucosan, soluble non-sea salt potassium (nss-K^{+}) (both 12h resolution) and AMS Org 60 (averaged to BAM 12h).

In order to discriminate BB aerosol from other sources and estimate the degree of BB aerosol aging (processing), a graphical method introduced by Cubison et al. (2011) has been applied here (Fig. 5.4). The majority of data points (94 % of the dataset) had f60 values above the background limit of 0.003, indicated with a vertical dashed lines in Fig. 5.4. Thus, the detected OA during SAFIRED can be attributed mostly to BB aerosol.

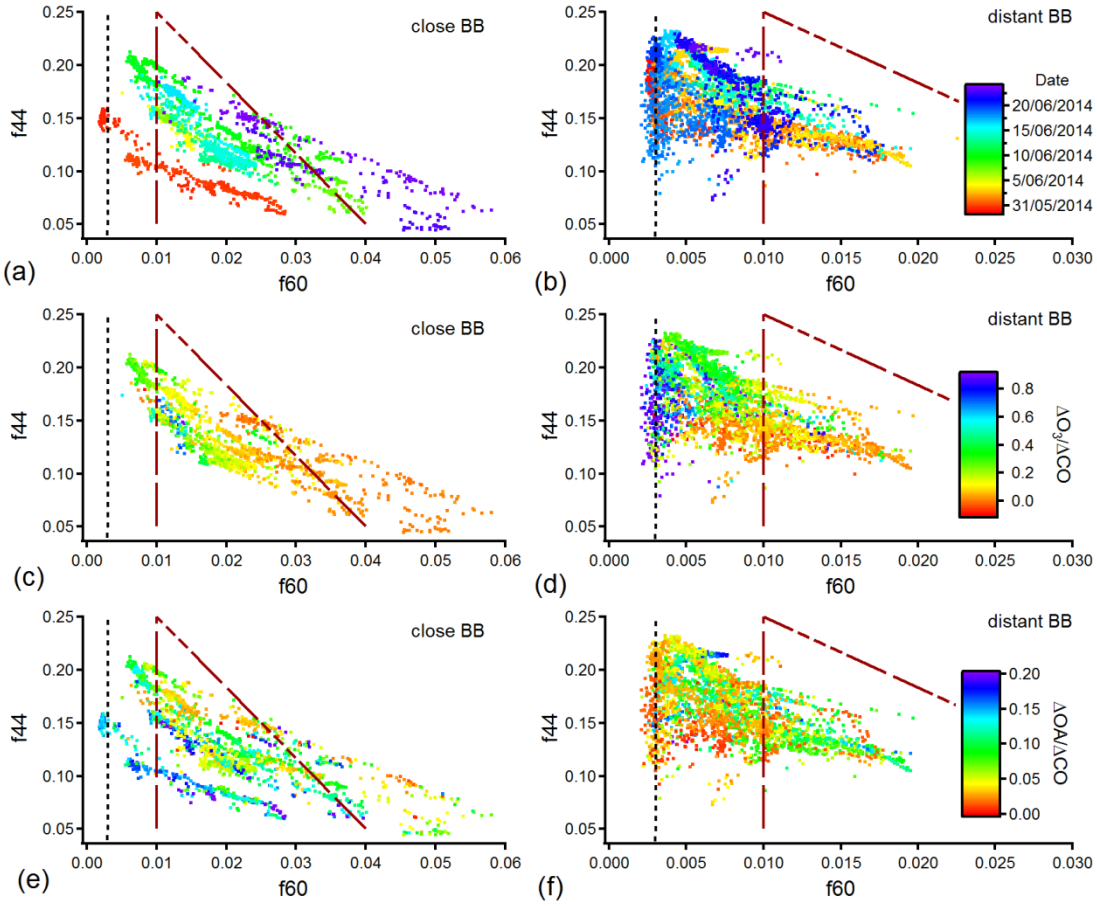

Figure 5.13 f44 vs. f60 coloured by date for (a) close and (b) distant BB periods, by $\Delta O_3/\Delta CO$ ratio for (c) close and (d) distant BB periods, and by ΔOA/ΔCO ratio for (e) close and (f) distant BB periods (vertical black lines refer to the f60 background level of 0.003). Red dashed lines refer to the ambient BBOA-related data introduced by (Cubison et al., 2011). Note: ozone data from 29th of May until the 1st of June were not available.

Chemical aging of BB-related OA typically leads to f60 depletion and increased f44 (Grieshop et al., 2009;Cubison et al., 2011;Ortega et al., 2013;Ng et al., 2010;Zhao et al., 2014;Capes et al., 2008;Jolleys et al., 2015). In general, this trend was observed in this study for distant fires, with the data trending towards the top left corner of the diagram (Fig. 5.4b). Apart from aerosol processing, changes in f44 and f60 can be attributed to burning conditions and/or materials. The variability observed in f44 vs. f60 for close BB events (Fig. 5.4a) can reflect BB plumes generated during different burning conditions but also different atmospheric processing of BB masses. On average distant BB plumes were characterized by lower fire

tracer f60 compared to the close BB emissions. Furthermore, distant fire plumes indicated a higher portion of oxygenated compounds (i.e., higher f44 values), relative to close plumes. The maximum f44 value ranged between 0.20 and 0.23 in this study, which agrees well with previously observed f44 values for oxidized BB emissions in ambient measurements (Cubison et al., 2011). The f44 parameter increased to values characteristic of LV-OOA in the distant BB and yet f60 values were substantially above the background value of 0.003. This confirms that levoglucosan-like species carried by the BB plume did not degrade to background levels even as oxidized species were formed. Thus, f60 is a reasonable marker of distant BB in this study.

All data fall into the f44 vs. f43 triangular plot range for ambient data, introduced by Ng et al. (2010) (Fig. 5.S4). Ng et al. (2010) observed that typical ambient OA data slopes from the bottom right to the top left of the f44 vs. f43 plot, and that this trend can be attributed to photochemical processing of ambient air masses. A similar pattern was observed in this study for distant periods (Fig. 5.S4b). A wide range in f44 can be attributed to different processed (aged) BB-related OA, but different burning material and/or conditions cannot be excluded. The observed evolution trend in f44 vs f43 for distant fires can be also influenced by mixing between the plumes. In contrast the f43 values for close BB (Fig. 5.S4a) are located in a narrow f43 range from 0.05 to 0.08 and do not change considerably with increasing f44. This can be a result of insignificant atmospheric processing in case of close fires. The wide range in f44 can be attributed to difference in burning conditions for close BB. One more factor that can influence f44 vs f60 trend for both close and distant fire is dilution effect.

Ozone formation

The emissions from BB sources promote ozone production in the troposphere by increasing the concentrations of key ozone-forming precursors (NMOCs, NO_X and CO). Air mass photochemical activity can be estimated through the observation of changes in ozone concentration with aging, particularly the change in the $\Delta O_3/\Delta CO$ ratio, where ΔCO and ΔO_3 refer to enhancements above background concentrations. ΔCO accounts for dilution, as it is a relatively long lived atmospheric species. The minimum CO value of 80 ppb measured during June at the ATARS site was used as the background concentration level. Similarly a minimum ozone concentration of 10 ppb was considered to be the background level in these calculations. On average, the $\Delta O_3/\Delta CO$ ratio increases with f44 and decreases with f60, indicating increased photochemical processing of OA in plumes with atmospheric aging and ozone production (Fig. 5.4c and Fig. 5.4d).

$\Delta O_3/\Delta CO$ values vary between -0.1 and 0.9 which is within the observed range in other studies (Jaffe and Wigder, 2012). A negative ratio may indicate fresh BB emissions where ozone was removed by atmospheric reaction with nitric oxide (NO) emitted in high amounts from fire sources, as suggested by Yokelson et al. (2003). Close fire emissions were characterized by significantly lower ozone enrichments (average $\Delta O_3/\Delta CO$ of 0.15) compared to plumes detected from the distant BB emissions (average $\Delta O_3/\Delta CO$ of 0.31) which represent higher photochemical activity within more processed air masses. These values agree with observed $\Delta O_3/\Delta CO$ ratio values for plumes aged for less than 1-2 days (average $\Delta O_3/\Delta CO$ of 0.14) and for 2-5 days (average $\Delta O_3/\Delta CO$ of 0.35) in tropical/subtropical regions (Jaffe and Wigder, 2012). The $\Delta O_3/\Delta CO$ enrichments for close BB period indicate that aging of close emissions cannot be excluded. These significant ozone

enrichments in BB plumes illustrate high NO_X and NMOC loadings emitted from fire sources and photochemically active air masses.

Secondary organic aerosol (SOA) formation

Since increased photochemical activity was identified in BB air masses, the change in ΔOA/ΔCO ratio was investigated in order to determine whether additional OA was produced in the BB plumes (Fig. 5.4e and Fig. 5.4f). The lowest OA concentration observed during the campaign of 0.09 μg m^{-3} was taken as a background value in these calculations. Figures show no particular trend in ΔOA/ΔCO ratio with f44. The ΔOA/ΔCO ratio also remains quite constant despite increases in f44 (Fig. 5.S5). In addition, diurnal patterns of the f44, $\Delta O_3/\Delta CO$ and ΔOA/ΔCO ratios were investigated, for close and distant BB periods separately (Fig. 5.5a and Fig. 5.5b, respectively). The parameter f44 was used to indicate the level of oxygenation that can be caused by the photochemical changes and $\Delta O_3/\Delta CO$ as a parameter of photochemical activity. It must be noted that simply examining ΔOA/ΔCO vs time of day is a simplified approach which does not fully take into account the total photochemical history of the air mass. There was an increase in ΔOA/ΔCO ratio with an increase in f44 and $\Delta O_3/\Delta CO$ in the late morning and early afternoon for close and for distant BB periods. This is likely due to condensation of organics onto pre-existing particles. The decrease in the ΔOA/ΔCO ratio later in the afternoon could indicate OA loss due to fragmentation and subsequent evaporation from the particulate phase. As suggested by Kroll et al. (2009), OA loss can reflect dominance of the fragmentation pathways in the formation of more oxidized OA. Therefore it is suggested that increased photochemical activity of BB-influenced air masses, illustrated by increase in $\Delta O_3/\Delta CO$ and likely due to oxygenation of OA (f44 increase), was accompanied by an increase in ΔOA/ΔCO ratio, indicating SOA formation. Moreover, the decrease in ΔOA/ΔCO ratio later in the day can be a result of fragmentation and subsequent evaporation.

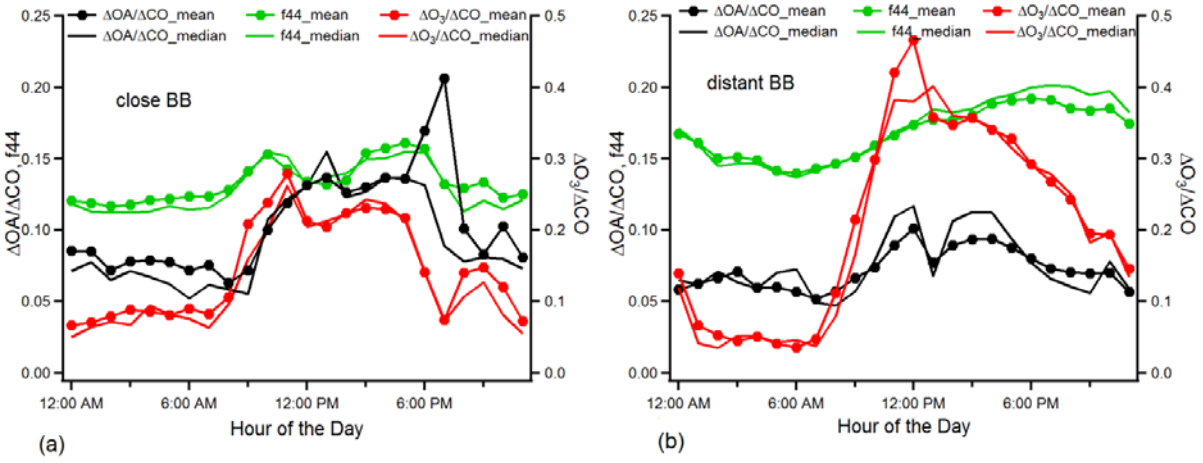

Figure 5.14 Diurnal trend of f44 (mean and median), $\Delta O_3/\Delta CO$ ratio (mean and median) and ΔOA/ΔCO ratio (mean, median)for close (a) and distant (b) BB periods.

f44-resolved size distribution

Atmospheric aging of plume particles increases particle diameter due to gas to particle transfer of organic and inorganic gaseous species (Martins et al., 1998). In order to estimate whether the aging of BB masses during SAFIRED influenced particle size, average SMPS size distributions and AMS size distributions for organics, both categorised based on different f44 ranges, were examined (Fig. 5.6). It is important to emphasise that SMPS uses electrical mobility diameter, while AMS uses vacuum aerodynamic diameter. The close and distant BB periods were analysed separately. The f44 values were classified into four groups that represent different aging stages ($0.05<f44<0.1$, $0.1<f44<0.15$, $0.15<f44<0.2$, $0.2<f44<0.25$). The first f44 bin ($0.05<f44<0.1$) was not considered in case of the distant BB periods, as only a few data points were in this range (Fig. 5.4). The same was done for the highest f44 bin ($0.2<f44<0.25$) for close BB periods. According to SMPS data, the average particle mode varied between 101 – 113 nm and 104 – 106 nm for close and distant BB periods, respectively. The average mode for organics showed larger sizes and varied between 259 – 293 nm and 293 – 305 nm for close and distant BB periods, respectively. Increased f44 was accompanied by a reduction in SMPS particle size for close plumes, going from 113 nm ($0.05<f44<0.1$) to 101 nm ($0.1<f44<0.15$). The same trend was observed for the organic aerosols. Considering both AMS and SMPS data for distant fires, there was no considerable change in diameter with aging from less aged BB plumes to more aged BB air masses. The particle modes show only slight differences between different f44 bins. This is not consistent with the observed increase in OA for distant fires. Changes in size distribution will be discussed further in the Sect. “Biomass burning events”, where results related to specific BB events are presented.

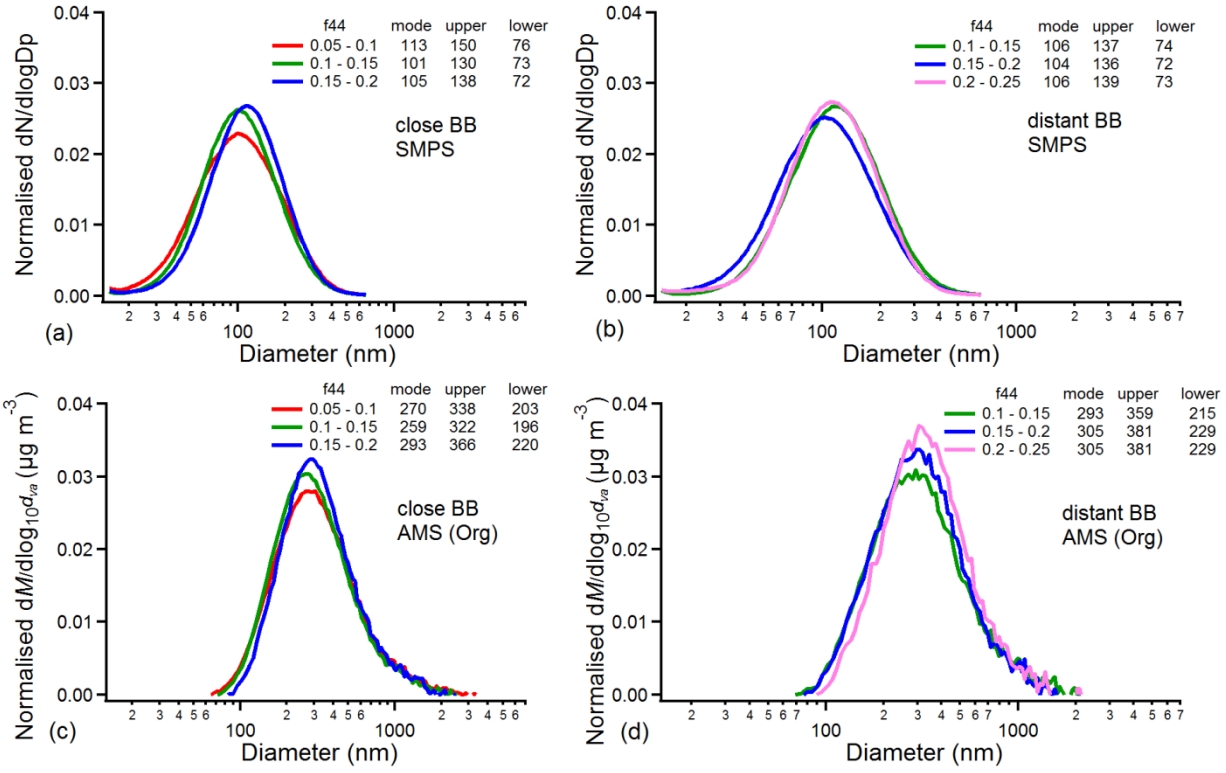

Figure 5.15 SMPS size distributions (dN/dlogDp, normalised to total particle number concentration, versus diameter) binned by the AMS f44 for close (a) and distant (b) BB periods and AMS size distributions ($dM/dlog_{10}d_{va}$, normalised to total organic concentration, versus diameter) binned by the AMS f44 for close (c) and distant (d) BB periods.

Biomass burning events

Five single source BB events were analysed here (Fig. 5.2). These episodes were within previously defined close BB periods. Mass spectra for selected signatures and their time of detection are given in Fig. 5.S6. The spectral signature is similar for these events, with prominent BB-related signals at m/z 60, 73, 29 and 39. However, a significant variation in m/z fragments, especially in m/z 44, can be observed. More detail about these BB events is given in Table 5.1 and discussed in the following paragraphs. Different factors were considered including f44, time of day, $\Delta O_3/\Delta CO$, f60, f60/f73, organic concentration and MCE.

On 30th of May at around 2pm three hot spots (two having confidence level of approximately 50% and one of 70%) were detected within 2km on the NE from the ATARS (Fig. 5.S7a-Fig.5.S7d). These hot spots likely illustrated two fire events. On the same day and time, 11km on the SE from the sampling site, cluster of events was observed, including 4 hot spots with the confidence level between 94% and 100% and one of 78% confidence level. As all of them were spotted at the same time and within 1km distance, it is most likely that the one big fire has occured. No other close events were observed over this

time period. Cluster of hot spots was detected on the SE approximately 50km from the ATARS and big clusters at 100km and 150km, as well as on the SE. Moreover, 200km on E along the backtrajectories cluster of hot spots was observed.

Two single source events, A and C, were identified and analysed here (Fig. 5.2). The event A illustrated the increased signals in the afternoon hours, when wind was coming from the NE. Therefore, the event A is likely result of the hot spots detected within 2km from the ATARS (Fig. 5.S7a and Fig. 5.S7b). According to backtrajectories air masses during these time period were passing over the land affected by these fires and they were transported from the fire events to ATARS within approximately 10 min. The average organic concentration was found to be 23 μg m^{-3}, with the concentrations going up to 45 μg m^{-3}. High average MCE value of 0.97 likely suggests flaming fire as emission source and/or grass as a burning material (Desservettaz et al., 2016). The signal named as a C event was detected over the night (Table 5.1). At that time wind direction was abruptly changed from the NE to SE. Therefore, the signal can be likely associated to cluster of fires 11 km on the SE (Fig. 5.S7c and Fig. 5.S7d). According to the backtrajectories air masses reached the ATARS within 20 min from the fire cluster. Comparing to the event A, the average organic concentration for the event C was more than threefold with the maximum value of approximately 130 μg m^{-3}. As MCE was found to be similar (0.98) to event A value, most likely higher signals illustrate larger fire. The number of hot spots detected on the same time with high confidence level confirms this. Higher fire intensity can also be a reason for the higher f60 values for the event C (0.027) compared to event A (0.016) (Table 5.1).

On 25th of June three hotspot clusters were observed close to ATARS (2km on E, 5km on NE and 10km on SE) (Fig. 5.S7e-Fig. 5.S7h). The cluster of hot spots observed 10 km from the sampling site had one of the highest hot spot's power (energy released by the fire) observed close to the ATARS (within 20 km) during the campaign (120 MW/km^2). Besides the close fires two big clusters around 60 km and 120 km on the SE from ATARS were detected on the same day. On the 25th of June, two single-source events were observed and labelled as events F and G. Event F was related to a close fire (two hot spots of 60 and 100% confidence level, within 2 km on E) whose emissions were clearly visible from ATARS (Fig. 5.S7e and Fig. 5.S7f). The detected plumes included a considerable portion of oxygenated OA (average f44 value of 0.13, up to 0.18) that could be caused by high daytime photochemical activity (aged air masses). The BB event F began at noon and ended at approximately 5 pm, i.e., it occurred during the period of highest photochemical activity. The relatively high $\Delta O_3/\Delta CO$ ratio (0.13) was elevated relative to the other close BB events, which suggests additional photochemical activity in the plume. This value falls into the range for fire emissions aged less than 1-2 days in tropical/subtropical regions (Jaffe and Wigder, 2012). However, the f44 value was highly variable during the event F, ranging from 0.07 to 0.18. Other parameters including f60 and organics varied as well. On that time, the wind direction significantly varied between 140° and 80° and likely influenced changes in detected air mass. One of the explanations can be detection of fresh plume and aged masses coming from the distant fires with the change in wind. The low correlation between f60 and f73 might also be an indicator for detection of different BB air masses (Fig. 5.S8). Relatively low organic mass loading and f60 values may be due to highly

variable wind direction and/or area rather than combustion conditions (MCE of 0.93), as higher organics are expected for this MCE value. In contrast, event G resulted in the highest organic mass loading measured at ATARS (PM_1 concentration of ~350 µg m^{-3}). Moreover, the highest chloride concentration observed over the campaign was at the time of G event. The source of emissions was probably within 10 km on SE of the sampling site (Fig. 5.S7g and Fig. 5.S7h) and the fire magnitude was illustrated by a large burned area observed the following morning (Mallet et al., 2016) (Chapter 4) and high power of fire observed (30 MW/km^2). Backtrajectories analysis indicated that less than half an hour was needed for the air mass to reach the ATARS. High fire intensity was accompanied with smouldering burning conditions (MCE of 0.90) that resulted in high organic loadings and high levoglucosan concentrations (high f60) (Table 5.1). A low OOA fraction, f44, $\Delta O_3/\Delta CO$ value (0.01) indicated that the plume was likely not aged, which is to be expected due to the proximity and time of the event (started at 10 pm and finished at 4 am).

Intense signals, including high organic concentrations, were also detected on the 9th of June (Fig. 5.S7i and Fig. 5.S7j). On that day cluster of hot spots (all with the confidence level higher than 70%) was detected 5 km from ATARS. Number of distant hot spots was detected between 100 km and 200 km, on the SE from the ATARS. Mallet et al. (2016) (Chapter 4) suggested that possible sources of this event E might be close fires, distant fires or a combination of both. According to backtrajectories less than 10 min was enough for air masses to cross the distance between 5 km cluster and the research station. Values for f44 (0.08) and $\Delta O_3/\Delta CO$ (0.02) suggested detection of fresh emissions. Moreover, the high f60 value of 0.032 supported this, as distant fires are not likely to be characterized with such a high portion of levoglucosan-like species. However, the possibility of contribution from distant BB plumes cannot be excluded, especially when considering the particle size distribution during event E. The particle size distribution had a mode of 146 nm, while events F and G showed smaller size distributions with modes of 98 and 88 nm, respectively (Table 5.1). However, different burning material and conditions could also contribute to the larger size distribution mode during event E.

In general, diversity of biomass burning plumes was illustrated through high variability in chemical signature (e.g. large range of f44, from 0.06 to 0.18) for five intense fire events. Events were characterised with different f60/f73 ratios (varying between 1.2 and 2.5), but there was no trend in the relationship of f60/f73 ratio and burning material/conditions (MCE values) (Fig. 5.S8).

5.3.3 Positive Matrix Factorization (PMF)

Initially PMF was performed to assist with analysis of the aging observations rather than to apportion sources since the main source (BB) is already known. This approach was intended to estimate whether the ratios of the different factors, e.g., fresh BBOA, aged BBOA or OOA, exhibited relationships with the age of separate BB plumes. The diversity of the plumes (including close fire plumes with spectra presented in Fig. 5.S6), however, made PMF analysis difficult. The thousands of fires that occurred during the SAFIRED campaign contributed to a wide range of OA composition that reflect different

burning materials, conditions, mixed fresh and aged emissions and processing in the atmosphere. The ratio of m/z 43 and 44 differed between plumes (Fig. 5.S11) and since the AMS mass spectra were dominated by these masses, the PMF analysis returned factors that corresponded to individual plumes, even when distant fires were separately examined. In addition, high residuals during BB events could not be reduced even with an unreasonably large number of factors (Fig. 5.S9). The PMF diagnostic plots can be found in Sect. 5.6.3.

Instead PMF analysis was applied on "background" data in order to determine the contribution of BB emissions and SOA to regional ambient PM_1 outside of the time periods dominated by BB events. The background time periods were determined by examining the plot of f44 vs. f43 (Fig. 5.S11). Cut-offs of 0.15 for m/z 43 and 0.4 for f44 were chosen to remove the influence of periods dominated by BB events which show up as individual lines in f43 vs. f44 space.

PMF performed on the background OA showed significantly smaller residuals (Fig. 5.S12) and resulted in three factors, including a biomass burning OA factor (BBOA), oxygenated OA (OOA) and a factor that represented isoprene-derived OA (Fig. 5.7). A two-factor solution did not extract the biogenic isoprene-derived OA factor while a four-factor solution resulted in splitting of profiles (Fig. 5.S13). The biomass burning factor, with distinct m/z 60 and 73 signals, contributed to 24 % of the background aerosol. BBOA was also characterized by fragments related to fresh hydrocarbon-like organics, e.g., m/z 27, 29, 41, 43, 55, and 57, and by prominent OOA-related m/z 28 and 44 signals. The large f44 value (an average f44 of 0.09) (Fig. 5.S4) may indicate either the presence of processed BB aerosol and/or fresh emissions that contain oxygenated OA species possibly due to the burning conditions (Heringa et al., 2012;Weimer et al., 2008). A good correlation was observed between the BBOA factor and Org 60 and CO signals (Fig. 5.7d and Fig. 5.7e). An OOA profile with prominent m/z 28 and 44, similar to LV-OOA profiles observed in previous studies, was extracted. Its diurnal trend is marked by a broad daily peak which correlates with the maximum temperature and reflects intense daytime photochemical activity. The OOA dominance (contribution of 47 %) and high degree of oxygenation (an average f44 of 0.23) (Fig. 5.S4) illustrate the significance of OOA for this area. The third PMF factor can be related to background biogenic SOA, and is discussed in more detail in the next Section (Isoprene-derived OA).

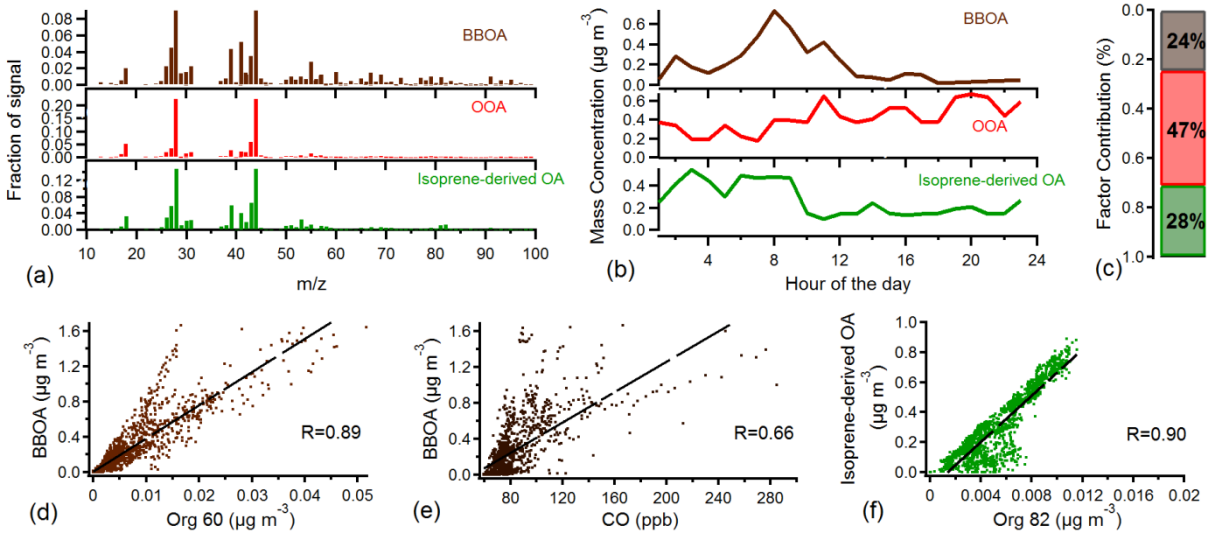

Figure 5.16 (a) Mass spectra, (b) diurnal trends, (c) contribution and (d), (e), (f) correlations for the PMF 3-factor solution for background periods including BBOA, OOA and isoprene-derived OA factors.

Isoprene-derived OA

Isoprene epoxydiols (IEPOX) are important gas-phase precursors for IEPOX-SOA and are products of isoprene oxidation, mostly in low-NO_X environments (Paulot et al., 2009). Recent studies have showed that PMF performed on AMS OA data can be used to determine total IEPOX contribution to SOA (Robinson et al., 2011;Lin et al., 2011;Budisulistiorini et al., 2013;Hu et al., 2015;Xu et al., 2016). A similar distinct PMF-resolved factor has been extracted in this study. In order to consider other possible pathways in isoprene-derived OA formation (Schwantes et al., 2015), the PMF factor has been named as isoprene-derived OA (Xu et al., 2016;Pye et al.)The isoprene-derived OA mass spectrum can be clearly distinguished from BBOA and OOA by an enhanced m/z 82 signal (Fig. 5.9a). In the HR analysis of this dataset, $C_5H_6O^+$ is the most dominant peak that contributes to m/z 82 (Fig. 5.S13) and has been confirmed to be a reliable tracer for isoprene-derived OA (Hu et al., 2015). There was a strong correlation observed between the isoprene- derived OA factor and Org 82 ($C_5H_6O^+$) (R of 0.90) (Fig. 5.7f). The isoprene- derived OA factor profile was also characterized with enhanced peaks at m/z 53, 43 and 44. An AMS spectrum with the same prominent peaks was reported by Allen et al. (2008) for the Darwin region in the Northern Territory. This was observed during the monsoon-break period during the wet season in February, when fires were not common, and clean air of biogenic origin was suggested as a source. Moreover, our spectrum is similar to isoprene-related OA spectra reported previously (Robinson et al., 2011;Lin et al., 2011;Budisulistiorini et al., 2013). The average isoprene concentration measured during the campaign was 0.49 ± 0.78 ppb. However, it should be emphasised that monoterpene-derived OA can also influence the background level of $C_5H_6O^+$ (Hu et al., 2015). The average monoterpenes concentration for this study was found to be 0.22 ± 0.41 ppb.

The main path for isoprene-derived OA formation is proposed to be acid-catalysed IEPOX uptake (Lin et al., 2011;Lambe et al., 2015). According to calculations for the composition depended collection efficiency, 22% of the aerosol were acidic. In order to estimate whether the acidity of the particles had an influence on isoprene- derived OA generation in ATARS, the correlation between sulfate (taken as proxy of aerosol acidity) and the isoprene-derived OA factor was examined. The correlation between the factor and sulfate can be considered as weak (R of 0.3) (Fig. 5.S18). However, two periods can be clearly distinguished from the graph: the period before 5th of June and the period after 15th of June. While there is no correlation between sulfate and the isoprene-derived OA factor for the first period, when plotting only data collected from 15th of June, correlation is found to be slightly higher than the correlation for all background data (R of 0.4).

The isoprene/furan concentrations at m/z 69 (PTR-MS) were treated as an isoprene contribution due to the dominance of isoprene signal compared to furan, according to the samples analysed by gas chromatography-mass spectrometry (Fig. 5.S17). The furan contribution was more significant in BB plumes during the close BB period, as suggested previously (Warneke et al., 2011). As expected, the isoprene/furan gas-phase concentration measured by the PTR-MS increased from noon till the late afternoon (Fig. 5.S16). According to diurnal patterns of PMF isoprene- derived OA, there is no considerable change in isoprene- derived OA concentration from noon throughout the day. The isoprene- derived OA fraction is expected to increase during daytime hours in accordance with enhancements in isoprene and gas-phase IEPOX (Hu et al., 2015). However, the isoprene- derived OA factor was prominent during night and morning hours. Significant isoprene- derived OA factor enhancement during the night time might be due to partitioning of lower volatility species onto the particles when the temperature drops and relative humidity increases as suggested by Budisulistiorini et al. (2013), due to transport of distant air masses, or lower boundary layer height. During the night, the boundary level lowers which increases the concentration of gaseous compounds and can induce partitioning of gases onto the particles. Therefore, the lower night-time boundary layer might create conditions for low volatility isoprene-derived OA partitioning and an increase in isoprene-derived OA.

A plot of f44 (CO_2^+) vs. f82 ($C_5H_6O^+$) (Org CO_2^+/Org and Org $C_5H_6O^+$/Org from HR data analysis, respectively) (Fig. 5.8) introduced by Hu et al. (2015) can be used to distinguish IEPOX-SOA from SOA originating from other sources, including isoprene- derived SOA that are generated from species other than IEPOX. This plot also indicates the degree of aging of the IEPOX-SOA. The general pattern of f44 increase with f82 decrease is observed. With aging, OA becomes more oxidized and the $C_5H_6O^+$ signature decreases. This can be due to oxidation processes or mixing with more aged aerosol masses.

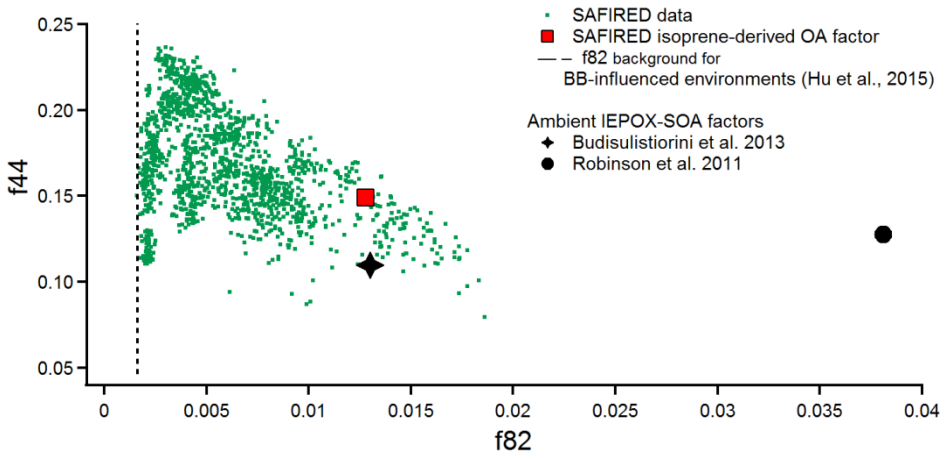

Figure 5.17 f44 (CO_2^+) vs. f82 ($C_5H_6O^+$) for the SAFIRED data; The isoprene-derived OA factor from SAFIRED and two other ambient campaigns (Budisulistiorini et al., 2013;Robinson et al., 2011) are marked. Vertical black dashed line indicates proposed background f82 value in environments strongly influenced by BB (Hu et al., 2015).

A background value for f82 ($C_5H_6O^+$) in environments strongly influenced by BB was suggested to be 0.0017 and is indicated by the vertical dashed black line (Hu et al., 2015). Looking at our data plotted in f44 vs. f82 a similar observation can be made. All data points are positioned above 0.0016 of f82 with an average value of 0.0061 ± 0.0036. The isoprene-derived OA factor average values for this campaign and two other ambient studies are marked in the plot. The f82 value for isoprene-derived OA factor observed here is similar to the reported f82 value for an urban site (Budisulistiorini et al., 2013), but lower compared to the factor observed for Borneo forest (Robinson et al., 2011). The lower value for SAFIRED compared to Borneo forest, considering that biogenic influence is significant for both environments, can be attributed to the high influence of BB emissions.

As the most abundant NMOC, isoprene is a significant contributor to the global SOA budget (Guenther et al., 2012;Hallquist et al., 2009;Paulot et al., 2009). isoprene-derived OA during the SAFIRED campaign accounted for 28 % of the total background OA which is similar to previous observations where the isoprene-derived OA fraction contribution varied from 6-36 %, depending on the environment (Hu et al., 2015). This confirms the importance of isoprene-derived SOA for the Northern Territory environment even in times of high BB influence.

5.4. Conclusions

A one month long campaign called SAFIRED was conducted in northern Australia during a period of significant burning (early dry season). There was a significant influence of BB plumes on the atmospheric chemical profile at the time of campaign, reflected by high concentrations of gaseous and particle species including CO and PM_1 organics, reaching maxima of ~10^4 ppb and 350 µg m^{-3} respectively during heavy BB episodes. Emitted aerosols were predominantly organic

species (90 %) with a wide range of levels of oxidation. There was a clear overall increase of the highly oxygenated OA fraction and degradation of BB-related signatures with OA processing. This was shown by an overall trend of f44 increase and f60 decrease for distant fires. Plume emissions formed over the month period were photochemically active resulting in the production of tropospheric ozone. Close fire emissions were characterized by lower ozone enrichments (average $\Delta O_3/\Delta CO$ of 0.15) than plumes detected from the distant BB sources (average $\Delta O_3/\Delta CO$ of 0.31) which illustrate higher photochemical activity with more processed air masses. This emphasizes air mass ability for photochemical processing and production of SOA. An increase in the $\Delta OA/\Delta CO$ ratio with increase of f44 also suggests SOA formation. According to results, the OA oxidation level did not significantly influence particle size distribution. Diversity in BB emissions was illustrated through investigation of five selected events. The chemical signature varied for different fire events (e.g. wide range in f44, from 0.06 to 0.18).

PMF was employed to estimate BB influence on and SOA portion of background regional aerosol. A significant portion of oxygenated OA, identified through high f44 (majority of data points between 0.1 and 0.25), and a significant portion of aged BBOA (47 and 24 %, respectively) were observed. The latter suggests considerable processing of aerosol in the atmosphere for this area. The remaining OA was attributed to isoprene-derived OA factor (28 %), identified here for the first time in Australia. The OA mass spectrum with isoprene-derived OA characteristics previously reported in the wet season and now observed with prominent BB influence during the dry period, suggests the importance of biogenic isoprene sources for the Northern Territory area at all times of the year.

Observed photochemical activity of air masses and enhancement of OA with aging illustrate the importance of aging and SOA formation in the Northern Territory during the dry early season. SOA is recognized as a significant contributor to climate, environment and adverse human health effects. This study is an important step in addressing suggested further research related to tropical biomass burns and biogenic-related SOA in Australia (Rotstayn et al., 2009). As SOA yields are considerably underestimated and its formation is still not sufficiently understood, this study can facilitate understanding of SOA formation for Northern Territory savannah areas and also for the tropics in general. Additional measurements during late dry season (September-October) are needed as more intense and frequent fires occur during this period (Andersen et al., 2005;Williams et al., 1998). Moreover, the late dry season is suggested to have more aged emissions (Ristovski et al., 2010;Wardoyo et al., 2007). Therefore it is important to characterize SOA formation, and yield during this period.

Data availability. The underlying research data can be accessed upon request to the corresponding author (Branka Miljevic; b.miljevic@qut.edu.au).

Author contributions. Andelija Milic analysed and interpreted the data and prepared the manuscript. Marc Mallet operated the cToF-AMS and contributed to data analysis, interpretation and writing. Branka Miljevic installed the cToF-AMS, contributed to data analysis, interpretation and writing and supervised the work of Andelija Milic. Luke Cravigan set up the

SMPS and contributed to data interpretation. Joel Alroe assisted in organizing the QUT instrumentation, data interpretation and writing the manuscript. Zoran Ristovski contributed to campaign organization and data interpretation and supervised the work of Andelija Milic. Leah Williams contributed to setting up the cToF-AMS, preliminary data analysis and data interpretation. Melita Keywood organized and led the campaign. Paul Selleck operated the BAM, analysed the data and contributed to data interpretation. Sarah Lawson operated the PTR-MS and analysed the data. James Ward operated the Ozone analyser and analysed the data. Maximilian Desservettaz operated the FTIR and SMPS and analysed the data. Clare Paton-Walsh contributed to campaign organization and running the campaign. All authors declare that they have no conflict of interest.

Acknowledgements. The authors thank Manjula Canagaratna for valuable discussions about interpreting the PMF analysis. The authors thank Min Cheng for providing the gas chromatography-mass spectrometry data. This work was supported by the Australian Research Council Discovery grant (DP120100126).

5.5 References

Aiken, A. C., DeCarlo, P. F., and Jimenez, J. L.: Elemental analysis of organic species with electron ionization high-resolution mass spectrometry, Analytical Chemistry, 79, 8350-8358, 2007.
Aiken, A. C., DeCarlo, P. F., Kroll, J. H., Worsnop, D. R., Huffman, J. A., Docherty, K. S., Ulbrich, I. M., Mohr, C., Kimmel, J. R., Sueper, D., Sun, Y., Zhang, Q., Trimborn, A., Northway, M. J., Ziemann, P. J., Canagaratna, M., Onasch, T., Alfarra, M. R., Prevot, A. S., Dommen, J., Duplissy, J., Metzger, A., Baltensperger, U., and Jimenez, J.: O/C and OM/OC ratios of primary, secondary, and ambient organic aerosols with high-resolution time-of-flight aerosol mass spectrometry, Environmental Science & Technology, 42, 4478-4485, 2008.
Akagi, S., Craven, J., Taylor, J., McMeeking, G., Yokelson, R., Burling, I., Urbanski, S., Wold, C., Seinfeld, J., Coe, H., Alvarado, M., and Weise, D.: Evolution of trace gases and particles emitted by a chaparral fire in California, Atmospheric Chemistry and Physics, 12, 1397-1421, 2012.
Alfarra, M. R., Prevot, A. S., Szidat, S., Sandradewi, J., Weimer, S., Lanz, V. A., Schreiber, D., Mohr, M., and Baltensperger, U.: Identification of the mass spectral signature of organic aerosols from wood burning emissions, Environmental science & technology, 41, 5770-5777, 2007.
Allen, G., Vaughan, G., Bower, K., Williams, P., Crosier, J., Flynn, M., Connolly, P., Hamilton, J., Lee, J., Saxton, J., Watson, N., Gallagher, M., Coe, H., Allan, J., Choularton, T., and Lewis, A.: Aerosol and trace-gas measurements in the Darwin area during the wet season, Journal of Geophysical Research: Atmospheres (1984–2012), 113, 2008.
Andersen, A. N., Cook, G. D., Corbett, L. K., Douglas, M. M., Eager, R. W., Russell-Smith, J., Setterfield, S. A., Williams, R. J., and Woinarski, J. C.: Fire frequency and biodiversity conservation in Australian tropical savannas: implications from the Kapalga fire experiment, Austral Ecology, 30, 155-167, 2005.
Bond, T. C., Streets, D. G., Yarber, K. F., Nelson, S. M., Woo, J. H., and Klimont, Z.: A technology-based global inventory of black and organic carbon emissions from combustion, Journal of Geophysical Research: Atmospheres (1984–2012), 109, 2004.
Bougiatioti, A., Stavroulas, I., Kostenidou, E., Zarmpas, P., Theodosi, C., Kouvarakis, G., Canonaco, F., Prévôt, A., Nenes, A., Pandis, S., and Mihalopoulos, N.: Processing of biomass-burning aerosol in the eastern Mediterranean during summertime, Atmospheric Chemistry and Physics, 14, 4793-4807, 2014.
Bouya, Z., Box, G. P., and Box, M. A.: Seasonal variability of aerosol optical properties in Darwin, Australia, Journal of Atmospheric and Solar-Terrestrial Physics, 72, 726-739, 2010.

Bowman, D. M., Dingle, J. K., Johnston, F. H., Parry, D., and Foley, M.: Seasonal patterns in biomass smoke pollution and the mid 20th-century transition from Aboriginal to European fire management in northern Australia, Global Ecology and Biogeography, 16, 246-256, 2007.
Brito, J., Rizzo, L., Morgan, W., Coe, H., Johnson, B., Haywood, J., Longo, K., Freitas, S., Andreae, M., and Artaxo, P.: Ground-based aerosol characterization during the South American Biomass Burning Analysis (SAMBBA) field experiment, Atmospheric Chemistry and Physics, 14, 12069-12083, 2014.
Budisulistiorini, S. H., Canagaratna, M. R., Croteau, P. L., Marth, W. J., Baumann, K., Edgerton, E. S., Shaw, S. L., Knipping, E. M., Worsnop, D. R., and Jayne, J. T.: Real-time continuous characterization of secondary organic aerosol derived from isoprene epoxydiols in downtown Atlanta, Georgia, using the Aerodyne Aerosol Chemical Speciation Monitor, Environmental science & technology, 47, 5686-5694, 2013.
Capes, G., Johnson, B., McFiggans, G., Williams, P., Haywood, J., and Coe, H.: Aging of biomass burning aerosols over West Africa: Aircraft measurements of chemical composition, microphysical properties, and emission ratios, Journal of Geophysical Research: Atmospheres (1984–2012), 113, 2008.
Carr, S. B., Gras, J., Hackett, M., and Keywood, M.: Aerosol Characteristics in the Northern Territory of Australia During the Dry Season With an Emphasis on Biomass Burning, DTIC Document, 2005.
Chow, J. C., Watson, J. G., Chen, L.-W. A., Chang, M. O., Robinson, N. F., Trimble, D., and Kohl, S.: The IMPROVE_A temperature protocol for thermal/optical carbon analysis: maintaining consistency with a long-term database, Journal of the Air & Waste Management Association, 57, 1014-1023, 2007.
Crutzen, P. J., and Andreae, M. O.: Biomass burning in the tropics: Impact on atmospheric chemistry and biogeochemical cycles, Science, 250, 1669-1678, 1990.
Cubison, M., Ortega, A., Hayes, P., Farmer, D., Day, D., Lechner, M., Brune, W., Apel, E., Diskin, G., and Fisher, J.: Effects of aging on organic aerosol from open biomass burning smoke in aircraft and laboratory studies, Atmospheric Chemistry and Physics, 11, 12049-12064, 2011.
DeCarlo, P., Dunlea, E., Kimmel, J., Aiken, A., Sueper, D., Crounse, J., Wennberg, P., Emmons, L., Shinozuka, Y., and Clarke, A.: Fast airborne aerosol size and chemistry measurements above Mexico City and Central Mexico during the MILAGRO campaign, Atmos. Chem. Phys, 8, 4027-4048, 2008.
DeCarlo, P., Ulbrich, I., Crounse, J., Foy, B. d., Dunlea, E., Aiken, A., Knapp, D., Weinheimer, A., Campos, T., Wennberg, P., and Jimenez, J.: Investigation of the sources and processing of organic aerosol over the Central Mexican Plateau from aircraft measurements during MILAGRO, Atmospheric Chemistry and Physics, 10, 5257-5280, 2010.
Desservettaz, M., Paton-Walsh, C., Griffith, D., Kettlewell, G., Keywood, M., Schoot, M. V., JasonWard, Mallet, M., Ristovski, Z., Miljevic, B., Milic, A., Howard, D., Edwards, G., and Atkinson, B.: Emission factors of trace gases and particles from tropical savanna fires in Australia, submitted to Journal of Geophysical Research 2016.
Edwards, D., Pétron, G., Novelli, P., Emmons, L., Gille, J., and Drummond, J.: Southern Hemisphere carbon monoxide interannual variability observed by Terra/Measurement of Pollution in the Troposphere (MOPITT), Journal of Geophysical Research: Atmospheres, 111, 2006.
Formenti, P., Elbert, W., Maenhaut, W., Haywood, J., Osborne, S., and Andreae, M.: Inorganic and carbonaceous aerosols during the Southern African Regional Science Initiative (SAFARI 2000) experiment: Chemical characteristics, physical properties, and emission data for smoke from African biomass burning, Journal of Geophysical Research: Atmospheres (1984–2012), 108, 2003.
Grieshop, A., Logue, J., Donahue, N., and Robinson, A.: Laboratory investigation of photochemical oxidation of organic aerosol from wood fires 1: measurement and simulation of organic aerosol evolution, Atmospheric Chemistry and Physics, 9, 1263-1277, 2009.
Griffith, D., Deutscher, N., Caldow, C., Kettlewell, G., Riggenbach, M., and Hammer, S.: A Fourier transform infrared trace gas and isotope analyser for atmospheric applications, Atmospheric Measurement Techniques, 5, 2481-2498, 2012.
Griffith, D. W.: Synthetic calibration and quantitative analysis of gas-phase FT-IR spectra, Applied spectroscopy, 50, 59-70, 1996.
Guenther, A., Jiang, X., Heald, C., Sakulyanontvittaya, T., Duhl, T., Emmons, L., and Wang, X.: The Model of Emissions of Gases and Aerosols from Nature version 2.1 (MEGAN2. 1): an extended and updated framework for modeling biogenic emissions, 2012.

Guenther, C.: Estimates of global terrestrial isoprene emissions using MEGAN (Model of Emissions of Gases and Aerosols from Nature), Atmospheric Chemistry and Physics, 6, 2006.
Hallquist, M., Wenger, J., Baltensperger, U., Rudich, Y., Simpson, D., Claeys, M., Dommen, J., Donahue, N., George, C., Goldstein, A., Hamilton, J., Herrmann, H., Hoffmann, D., Iinuma, Y., Jang, M., Jenkin, M., Jimenez, J., Keindler-Scharr, A., Maenhaut, W., McFiggans, G., Mentel, T., Monod, A., Prevot, A., Seinfeld, J., Surratt, J., Szmigielski, R., and Wildt, J.: The formation, properties and impact of secondary organic aerosol: current and emerging issues, Atmos. Chem. Phys, 9, 5155-5236, 2009.
Haywood, J., and Boucher, O.: Estimates of the direct and indirect radiative forcing due to tropospheric aerosols: A review, Reviews of geophysics, 38, 513-543, 2000.
He, C., Murray, F., and Lyons, T.: Monoterpene and isoprene emissions from 15 Eucalyptus species in Australia, Atmospheric Environment, 34, 645-655, 2000.
Heringa, M., DeCarlo, P., Chirico, R., Tritscher, T., Dommen, J., Weingartner, E., Richter, R., Wehrle, G., Prévôt, A., and Baltensperger, U.: Investigations of primary and secondary particulate matter of different wood combustion appliances with a high-resolution time-of-flight aerosol mass spectrometer, Atmos. Chem. Phys, 11, 5945-5957, 2011.
Heringa, M., DeCarlo, P., Chirico, R., Lauber, A., Doberer, A., Good, J., Nussbaumer, T., Keller, A., Burtscher, H., and Richard, A.: Time-resolved characterization of primary emissions from residential wood combustion appliances, Environmental science & technology, 46, 11418-11425, 2012.
Hobbs, P. V., Sinha, P., Yokelson, R. J., Christian, T. J., Blake, D. R., Gao, S., Kirchstetter, T. W., Novakov, T., and Pilewskie, P.: Evolution of gases and particles from a savanna fire in South Africa, Journal of Geophysical Research: Atmospheres (1984–2012), 108, 2003.
Hu, W., Campuzano-Jost, P., Palm, B., Day, D., Ortega, A., Hayes, P., Krechmer, J., Chen, Q., Kuwata, M., Liu, Y., McKinney, K., Martin, S. T., Hu, M., Budisulistiorini, S. H., Riva, M., Surratt, J., Clair, J. M. S., Isaacman, G., Yee, L., Goldstein, A., Carbone, S., Brito, J., Artaxo, P., De Gouw, J., Koss, A., Wisthaler, A., Mikoviny, T., Karl, T., Kaser, L., Jud, W., Hansel, A., Docherty, K., Alexander, M., Robinson, A., Coe, H., Allan, J., Canagaratna, M., Paulot, F., and Jimenez, J.: Characterization of a real-time tracer for isoprene epoxydiols-derived secondary organic aerosol (IEPOX-SOA) from aerosol mass spectrometer measurements, Atmospheric Chemistry and Physics, 15, 11807-11833, 2015.
Hurst, D. F., Griffith, D. W., and Cook, G. D.: Trace gas emissions from biomass burning in tropical Australian savannas, Journal of Geophysical Research: Atmospheres, 99, 16441-16456, 1994.
Jaffe, D. A., and Wigder, N. L.: Ozone production from wildfires: A critical review, Atmospheric Environment, 51, 1-10, 2012.
Jimenez, J., Canagaratna, M., Donahue, N., Prevot, A., Zhang, Q., Kroll, J. H., DeCarlo, P. F., Allan, J. D., Coe, H., Ng, N., Aiken, A., Docherty, K., Ulbrich, I., Grieshop, A. P., Robinson, A., Duplissy, J., Smith, J. D., Wilson, K. R., Lanz, V., Hueglin, C., Sun, J., Tian, J., Laaksonen, A., Raatikainen, T., Rautiainen, J., Vaattovaara, P., Ehn, M., Kulmala, M., Tomlinson, J., Collins, D., Cubison, M. J., Dunlea, E., Huffman, J. A., Onasch, T., Alfarra, M. R., Williams, P., Bower, K. N., Kondo, Y., Schneider, J., Drewnick, F., Borrmann, S., Weimer, S., Demerjian, K. L., Salcedo, D., Cottrell, L., Griffin, R., Takami, A., Miyoshi, T., Hatakeyama, S., Shimono, A., Sun, J., Zhang, J., Dzepina, K., Kimmel, J. R., Sueper, D., Jayne, J. T., Herndon, S., Trimborn, A., Williams, L. R., Wood, E., Middlebrook, A., Kolb, C. E., Baltensperger, U., and Worsnop, D. R.: Evolution of organic aerosols in the atmosphere, Science, 326, 1525-1529, 2009.
Jolleys, M., Coe, H., McFiggans, G., Taylor, J., O'Shea, S., Le Breton, M., Bauguitte, S.-B., Moller, S., Di Carlo, P., and Aruffo, E.: Properties and evolution of biomass burning organic aerosol from Canadian boreal forest fires, Atmospheric Chemistry and Physics, 15, 3077-3095, 2015.
Jordan, T. B., Seen, A. J., and Jacobsen, G. E.: Levoglucosan as an atmospheric tracer for woodsmoke, Atmospheric Environment, 40, 5316-5321, 2006.
Kleinman, L. I., Springston, S. R., Daum, P. H., Lee, Y.-N., Nunnermacker, L., Senum, G., Wang, J., Weinstein-Lloyd, J., Alexander, M., Hubbe, J., Ortega, A., Canagaratna, M., and Jayne, J. T.: The time evolution of aerosol composition over the Mexico City plateau, Atmospheric Chemistry and Physics, 8, 1559-1575, 2008.
Kroll, J. H., Smith, J. D., Che, D. L., Kessler, S. H., Worsnop, D. R., and Wilson, K. R.: Measurement of fragmentation and functionalization pathways in the heterogeneous oxidation of oxidized organic aerosol, Physical Chemistry Chemical Physics, 11, 8005-8014, 2009.

Lacey, C., Walker, J., and Noble, I.: Fire in Australian tropical savannas, in: Ecology of tropical savannas, Springer, 246-272, 1982.
Lambe, A., Chhabra, P., Onasch, T., Brune, W., Hunter, J., Kroll, J., Cummings, M., Brogan, J., Parmar, Y., and Worsnop, D.: Effect of oxidant concentration, exposure time, and seed particles on secondary organic aerosol chemical composition and yield, Atmospheric Chemistry and Physics, 15, 3063-3075, 2015.
Lanz, V., Alfarra, M., Baltensperger, U., Buchmann, B., Hueglin, C., and Prévôt, A.: Source apportionment of submicron organic aerosols at an urban site by factor analytical modelling of aerosol mass spectra, Atmospheric Chemistry and Physics, 7, 1503-1522, 2007.
Li, J., Pósfai, M., Hobbs, P. V., and Buseck, P. R.: Individual aerosol particles from biomass burning in southern Africa: 2, Compositions and aging of inorganic particles, Journal of Geophysical Research: Atmospheres, 108, 2003.
Li, W., Shao, L., and Buseck, P.: Haze types in Beijing and the influence of agricultural biomass burning, Atmospheric Chemistry and Physics, 10, 8119-8130, 2010.
Lin, Y.-H., Zhang, Z., Docherty, K. S., Zhang, H., Budisulistiorini, S. H., Rubitschun, C. L., Shaw, S. L., Knipping, E. M., Edgerton, E. S., Kleindienst, T. E., Gold, A., and Surratt, J.: Isoprene epoxydiols as precursors to secondary organic aerosol formation: acid-catalyzed reactive uptake studies with authentic compounds, Environmental science & technology, 46, 250-258, 2011.
Liu, X., Van Espen, P., Adams, F., Cafmeyer, J., and Maenhaut, W.: Biomass burning in southern Africa: Individual particle characterization of atmospheric aerosols and savanna fire samples, Journal of Atmospheric Chemistry, 36, 135-155, 2000.
Mallet, M. D., Desservettaz, M. J., Miljevic, B., Milic, A., Ristovski, Z. D., Alroe, J., Cravigan, L. T., Jayaratne, E. R., Paton-Walsh, C., Griffith, D. W. T., Wilson, S. R., Kettlewell, G., Vanderschoot, M. V., Selleck, P., Reisen, F., Lawson, S. J., Ward, J., Harnwell, J., Cheng, M., Gillett, R. W., Molloy, S. B., Howard, D., Nelson, P. F., Morrison, A. L., Edwards, G. C., Williams, A. G., Chambers, S. D., Werczynski, S., Williams, L. R., Winton, V. H. L., Atkinson, B., Wang, X., and Keywood, M. D.: Biomass burning emissions in north Australia during the early dry season: an overview of the 2014 SAFIRED campaign, Phys. Discuss., doi:10.5194/acp-2016-866, in review, 2016.
Martins, J. V., Dunlap, M. R., and Liousse, C.: Physical, chemical, and optical properties of regional hazes dominated by smoke in Brazil, Journal of Geophysical Research, 103, 32,059-032,080, 1998.
Middlebrook, A. M., Bahreini, R., Jimenez, J. L., and Canagaratna, M. R.: Evaluation of composition-dependent collection efficiencies for the aerodyne aerosol mass spectrometer using field data, Aerosol Science and Technology, 46, 258-271, 2012.
Mitchell, R., Forgan, B., Campbell, S., and Qin, Y.: The climatology of Australian tropical aerosol: evidence for regional correlation, Geophysical Research Letters, 40, 2384-2389, 2013.
Ng, N., Canagaratna, M., Zhang, Q., Jimenez, J., Tian, J., Ulbrich, I., Kroll, J., Docherty, K., Chhabra, P., Bahreini, R., Murphy, S., Seinfeld, J., Hildebrandt Ruiz, L., Donahue, N. M., DeCarlo, P., Lanz, V., Prevot, A., Dinar, E., Rudich, Y., and Worsnop, D. R.: Organic aerosol components observed in Northern Hemispheric datasets from Aerosol Mass Spectrometry, Atmospheric Chemistry and Physics, 10, 4625-4641, 2010.
O'Brien, D., and Mitchell, R.: Atmospheric heating due to carbonaceous aerosol in northern Australia—confidence limits based on TOMS aerosol index and sun-photometer data, Atmospheric Research, 66, 21-41, 2003.
Ortega, A., Day, D., Cubison, M., Brune, W., Bon, D., de Gouw, J., and Jimenez, J.: Secondary organic aerosol formation and primary organic aerosol oxidation from biomass-burning smoke in a flow reactor during FLAME-3, Atmospheric Chemistry and Physics, 13, 11551-11571, 2013.
Paatero, P., and Tapper, U.: Positive matrix factorization: A non-negative factor model with optimal utilization of error estimates of data values, Environmetrics, 5, 111-126, 1994.
Paatero, P.: The multilinear engine—a table-driven, least squares program for solving multilinear problems, including the n-way parallel factor analysis model, Journal of Computational and Graphical Statistics, 8, 854-888, 1999.
Paatero, P., and Hopke, P. K.: Rotational tools for factor analytic models, Journal of Chemometrics, 23, 91-100, 2009.
Parrington, M., Palmer, P., Lewis, A., Lee, J., Rickard, A., Carlo, P. D., Taylor, J., Hopkins, J., Punjabi, S., Oram, D., Forster, G., Aruffo, E., Moller, S., Bauguitte, S.-B., Allan, J., Coe, H., and Leigh, R.: Ozone photochemistry in boreal biomass burning plumes, Atmospheric Chemistry and Physics, 13, 7321-7341, 2013.
Paulot, F., Crounse, J. D., Kjaergaard, H. G., Kürten, A., Clair, J. M. S., Seinfeld, J. H., and Wennberg, P. O.: Unexpected epoxide formation in the gas-phase photooxidation of isoprene, Science, 325, 730-733, 2009.

Penner, J., Chuang, C., and Grant, K.: Climate forcing by carbonaceous and sulfate aerosols, Clim. Dynamm., 14, 839–851, ISI, 1998.
Pye, H. O., Murphy, B. N., Xu, L., Ng, N. L., Carlton, A. G., Guo, H., Weber, R., Vasilakos, P., Appel, K. W., and Budisulistiorini, S. H.: On the implications of aerosol liquid water and phase separation for organic aerosol mass,
Real, E., Law, K., Weinzierl, B., Fiebig, M., Petzold, A., Wild, O., Methven, J., Arnold, S., Stohl, A., Huntrieser, H., Roiger, A., Schlager, H., Stewart, D., Avery, M., Sachse, G. W., Browell, E., Ferrare, R., and Blake, D. R.: Processes influencing ozone levels in Alaskan forest fire plumes during long-range transport over the North Atlantic, Journal of Geophysical Research: Atmospheres (1984–2012), 112, 2007.
Reid, J., Koppmann, R., Eck, T., and Eleuterio, D.: A review of biomass burning emissions part II: intensive physical properties of biomass burning particles, Atmospheric Chemistry and Physics, 5, 799-825, 2005.
Ristovski, Z. D., Wardoyo, A. Y., Morawska, L., Jamriska, M., Carr, S., and Johnson, G.: Biomass burning influenced particle characteristics in Northern Territory Australia based on airborne measurements, Atmospheric Research, 96, 103-109, 2010.
Roberts, G. C., Artaxo, P., Zhou, J., Swietlicki, E., and Andreae, M. O.: Sensitivity of CCN spectra on chemical and physical properties of aerosol: A case study from the Amazon Basin, Journal of Geophysical Research: Atmospheres (1984–2012), 107, LBA 37-31-LBA 37-18, 2002.
Robinson, N., Hamilton, J., Allan, J., Langford, B., Oram, D., Chen, Q., Docherty, K., Farmer, D., Jimenez, J., and Ward, M.: Evidence for a significant proportion of Secondary Organic Aerosol from isoprene above a maritime tropical forest, Atmospheric Chemistry and Physics, 11, 1039-1050, 2011.
Rotstayn, L. D., Keywood, M. D., Forgan, B. W., Gabric, A. J., Galbally, I. E., Gras, J. L., Luhar, A. K., McTainsh, G. H., Mitchell, R. M., and Young, S. A.: Possible impacts of anthropogenic and natural aerosols on Australian climate: a review, International Journal of Climatology, 29, 461-479, 2009.
Russell-Smith, J., Yates, C. P., Whitehead, P. J., Smith, R., Craig, R., Allan, G. E., Thackway, R., Frakes, I., Cridland, S., Meyer, M. C., and Gill, A.: Bushfires' down under': patterns and implications of contemporary Australian landscape burning, International Journal of Wildland Fire, 16, 361-377, 2007.
Schwantes, R. H., Teng, A. P., Nguyen, T. B., Coggon, M. M., Crounse, J. D., St. Clair, J. M., Zhang, X., Schilling, K. A., Seinfeld, J. H., and Wennberg, P. O.: Isoprene NO3 Oxidation Products from the RO2+ HO2 Pathway, The Journal of Physical Chemistry A, 119, 10158-10171, 2015.
Simoneit, B. R., Schauer, J. J., Nolte, C., Oros, D. R., Elias, V. O., Fraser, M., Rogge, W., and Cass, G. R.: Levoglucosan, a tracer for cellulose in biomass burning and atmospheric particles, Atmospheric Environment, 33, 173-182, 1999.
Simoneit, B. R.: Biomass burning—a review of organic tracers for smoke from incomplete combustion, Applied Geochemistry, 17, 129-162, 2002.
Ulbrich, I., Canagaratna, M., Zhang, Q., Worsnop, D., and Jimenez, J.: Interpretation of organic components from Positive Matrix Factorization of aerosol mass spectrometric data, Atmospheric Chemistry and Physics, 9, 2891-2918, 2009.
Wang, C., and Prinn, R. G.: Impact of emissions, chemistry and climate on atmospheric carbon monoxide: 100-yr predictions from a global chemistry–climate model, Chemosphere-Global Change Science, 1, 73-81, 1999.
Ward, D., and Radke, L.: Emissions measurements from vegetation fires: A comparative evaluation of methods and results, 1993.
Wardoyo, A. Y., Morawska, L., Ristovski, Z. D., Jamriska, M., Carr, S., and Johnson, G.: Size distribution of particles emitted from grass fires in the Northern Territory, Australia, Atmospheric Environment, 41, 8609-8619, 2007.
Warneke, C., Roberts, J., Veres, P., Gilman, J., Kuster, W., Burling, I., Yokelson, R., and de Gouw, J.: VOC identification and inter-comparison from laboratory biomass burning using PTR-MS and PIT-MS, International Journal of Mass Spectrometry, 303, 6-14, 2011.
Weimer, S., Alfarra, M., Schreiber, D., Mohr, M., Prévôt, A., and Baltensperger, U.: Organic aerosol mass spectral signatures from wood-burning emissions: Influence of burning conditions and wood type, Journal of Geophysical Research: Atmospheres (1984–2012), 113, 2008.
Williams, R., Gill, A., and Moore, P.: Seasonal changes in fire behaviour in a tropical savanna in northern Australia, International Journal of Wildland Fire, 8, 227-239, 1998.

Xu, L., Middlebrook, A. M., Liao, J., Gouw, J. A., Guo, H., Weber, R. J., Nenes, A., Lopez-Hilfiker, F. D., Lee, B. H., and Thornton, J. A.: Enhanced formation of isoprene-derived organic aerosol in sulfur-rich power plant plumes during Southeast Nexus, Journal of Geophysical Research: Atmospheres, 121, 2016.
Yokelson, R. J., Bertschi, I. T., Christian, T. J., Hobbs, P. V., Ward, D. E., and Hao, W. M.: Trace gas measurements in nascent, aged, and cloud-processed smoke from African savanna fires by airborne Fourier transform infrared spectroscopy (AFTIR), Journal of Geophysical Research: Atmospheres (1984–2012), 108, 2003.
Yokelson, R. J., Crounse, J., DeCarlo, P., Karl, T., Urbanski, S., Atlas, E., Campos, T., Shinozuka, Y., Kapustin, V., Clarke, A., Weinheimer, A., Knapp, D., Montzga, L., Holloway, J., Weibring, P., Flocke, F., Zheng, W., Toohey, D., Wennberg, P. O., Wiedinmyer, C., Mauldin, R. L., Fried, A., Richter, D., Walega, J., Jimenez, J., Adachi, K., Buseck, P. R., Hall, S., and Shetter, R.: Emissions from biomass burning in the Yucatan, Atmospheric Chemistry and Physics, 9, 5785-5812, 2009.
Zhang, Q., Jimenez, J., Canagaratna, M., Allan, J., Coe, H., Ulbrich, I., Alfarra, M., Takami, A., Middlebrook, A., Sun, Y., Dzepina, K., Dunlea, E., Docherty, K., DeCarlo, P., Salcedo, D., Onasch, T., Jayne, J. T., Miyoshi, T., Shimono, A., Hatakeyama, S., Takegawa, N., Kondo, Y., Schneider, J., Drewnick, F., Borrmann, S., Weimer, S., Demerjian, K. L., Williams, P., Bower, K. N., Bahreini, R., Cottrell, L., Griffin, R., Rautiainen, J., Sun, J., Zhang, Y., and Worsnop, D. R.: Ubiquity and dominance of oxygenated species in organic aerosols in anthropogenically-influenced Northern Hemisphere midlatitudes, Geophysical Research Letters, 34, 2007.
Zhao, R., Mungall, E. L., Lee, A. K., Aljawhary, D., and Abbatt, J. P.: Aqueous-phase photooxidation of levoglucosan–a mechanistic study using Aerosol Time of Flight Chemical Ionization Mass Spectrometry (Aerosol-ToF-CIMS), Atmospheric Chemistry and Physics Discussions, 14, 8819-8850, 2014.

5.6 Supplementary material

5.6.1 Data analysis

High organic loadings during heavy biomass burning (BB) episodes interfered with sulfate detection by the AMS in unit mass resolution (UMR), resulting in negative sulfate readings and scattered data points (Fig. 5.S1a). Adjustments in Squirrel to the fragmentation table addressed the negative data points (Fig. 5.S1b), however significant data dispersion still remained. High resolution (HR) fitting using PIKA improved correlation among different sulfate fragments (Fig. 5.S1c).

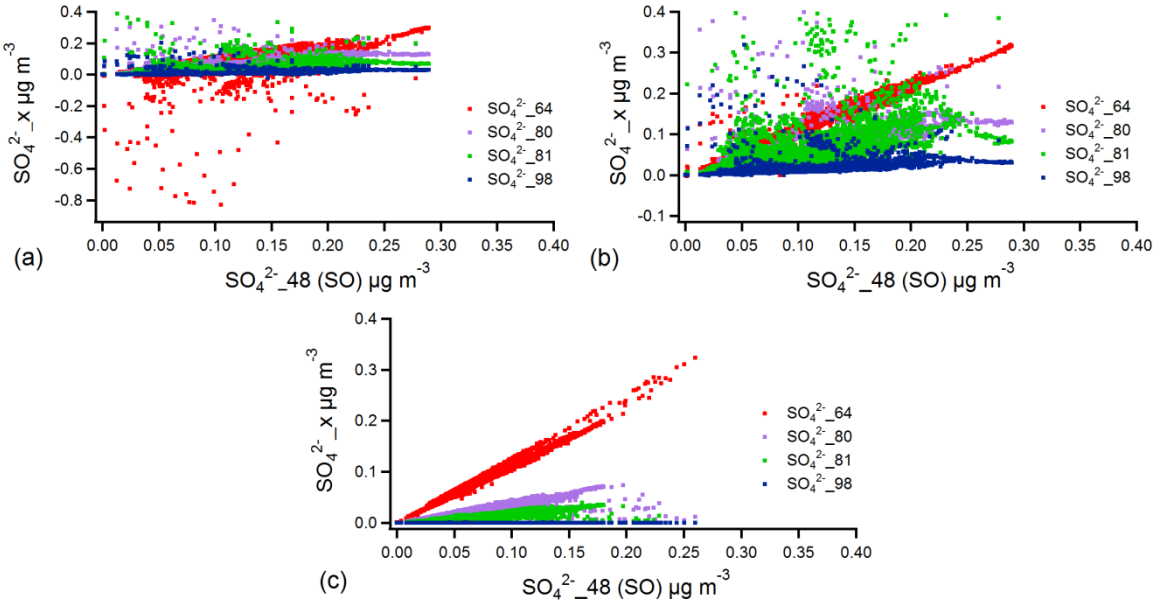

Figure 5.S21 Sulfate fragments plots (a) before and (b) after Squirrel fragmentation table adjustments, and (c) after HR fitting in PIKA; SO_4^{2-}_x indicates sulfate fragments at m/z 64, 80, 81 and 96 plotted against the sulfate fragment at m/z 48.

PM1 soluble ions measured by ion suppressed chromatography and OM (converted from OC that was determined by the Thermal-Optical Carbon Analyser) were compared to the corresponding AMS UMR and HR data. A considerable improvement was observed in the HR analysis results for sulfate (Fig. 5.S2b), with R changing from 0.4 to 0.8. HR fitting did not result in significant change for the other inorganic species or organics. However, improvement in the sulfate signals was significant and HR peak fitting data were used in further analysis.

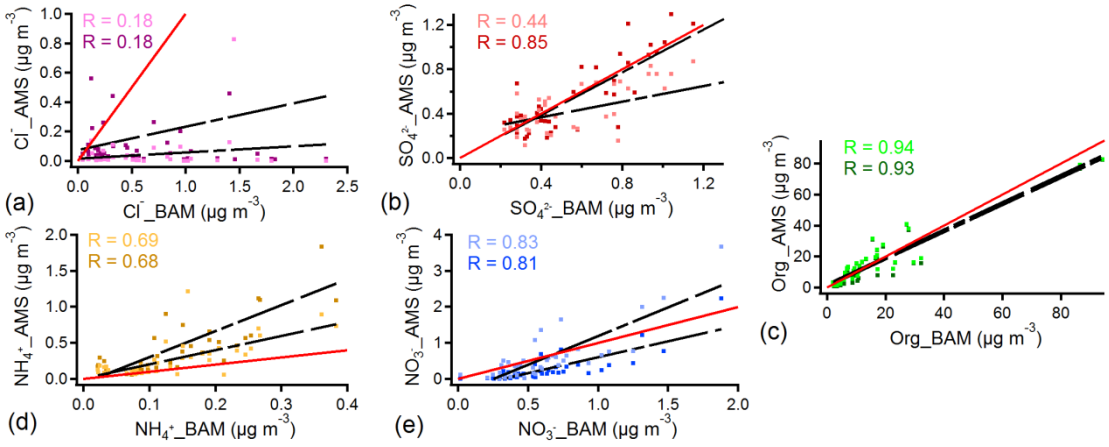

Figure 5.S22 Correlation between BAM PM1 soluble ions and corresponding AMS species including (a) chloride, (b) sulfate, (c) organics, (d) ammonia and (e) nitrate; The lighter points and first number present correlation of BAM data with UMR AMS data, while the darker points and the second number illustrates the correlation for BAM and HR AMS data. Red line represents 1:1 line (absolute concentration between AMS and BAM). BAM organic mass (OM) was converted from OC mass using the conversion coefficient of 1.4. R refers to Pearson correlation coefficient. The AMS data were averaged to BAM 12h data.

Table 5.S3 Correlation values between inorganic species and organics during the campaign, and close and distant periods separately. Inorganic species measured during the whole period (X), close BB periods (X(c)) and distant BB periods (X(d)) were compared to organics measured during the same time period (Org, Org(c), Org(d)).

	Cl^-	Cl^- (c)	Cl^- (d)	NH_4^+	NH_4^+ (c)	NH_4^+ (d)	NO_3^-	NO_3^- (c)	NO_3^- (d)	SO_4^{2-}	SO_4^{2-} (c)	SO_4^{2-} (d)
Org	0.65			0.92			0.75			0.55		
Org(c)		0.67			0.92			0.72			0.49	
Org(d)			0.47			0.73			0.77			0.48

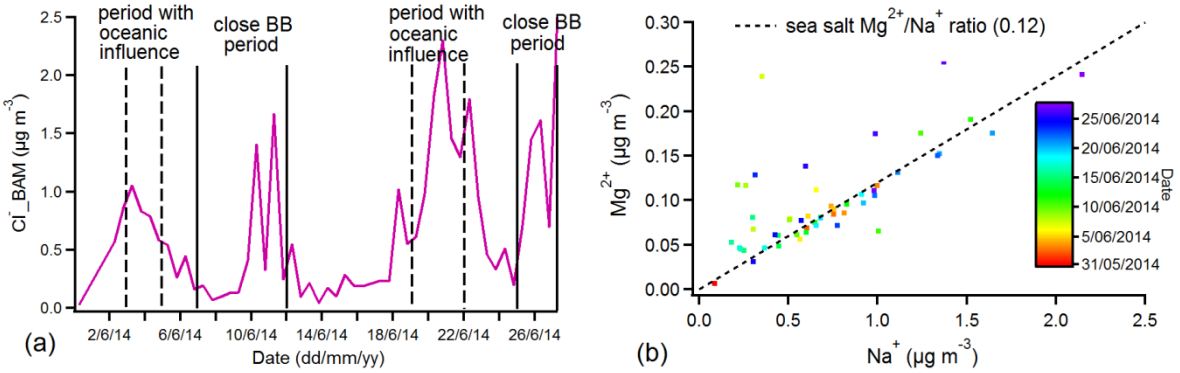

Figure 5.S23 (a) Time series of chlorides collected on the filters (BAM). Dashed lines are defining the periods with oceanic influence, while solid lines illustrate close BB periods. (b) The filter (BAM) data for magnesium (Mg^{2+}) and sodium (Na^+). Black line illustrates Mg^{2+}/Na^+ ratio for the sea salt (0.12).

5.6.2 Biomass burning aerosols and aging

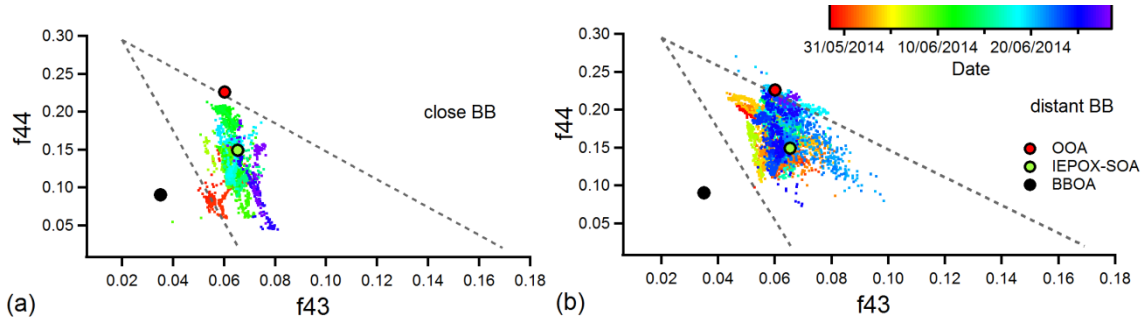

Figure 5.S24 f44 vs. f43 coloured by date for (a) close and (b) distant BB periods. PMF-resolved factors are also indicated. The **dashed lines represent boundaries for typical ambient aerosol as presented in Ng et al. (2010).**

Secondary organic aerosol (SOA) formation

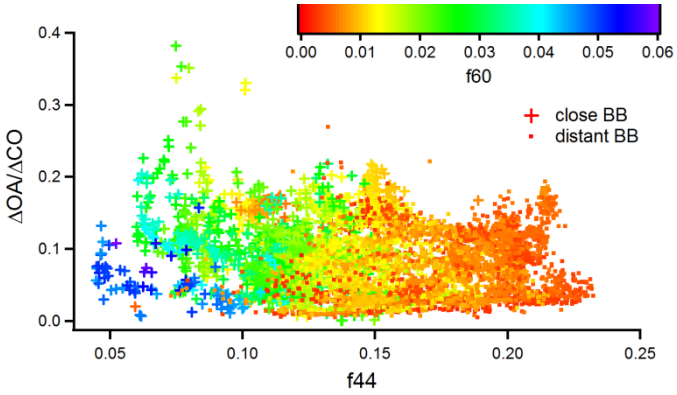

Figure 5.S25 Change in ΔOA/ΔCO ratio with aging (represented by f44 values) for close (crosses) and distant (dots) fires coloured by f60.

Biomass burning events

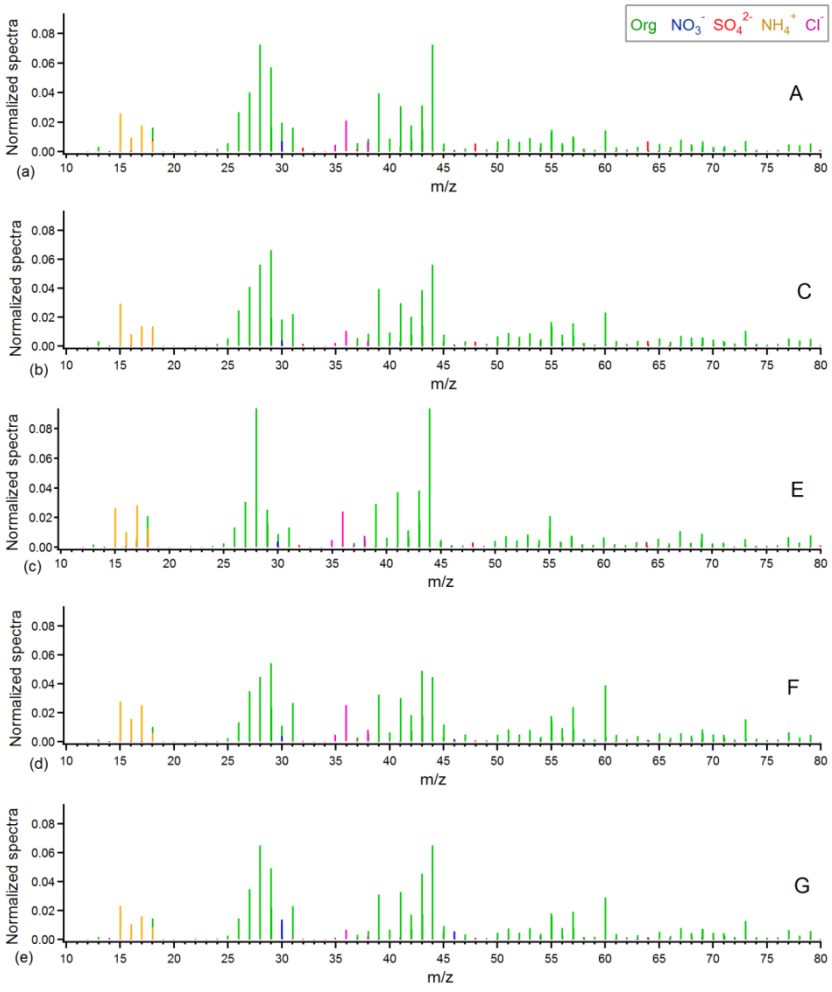

Figure 5.S26 Normalised mass spectra (sum=1) for selected BB events (A (30/05/14, 18:34-19:25), C (30/05/14, 23:41-31/05/14 00:59), E (09/06/14, 19:45-10/06/14 00:32), F (25/06/14, 12:28-16:59) and G (25/06/14, 21:40-26/06/14 03:59) are shown respectively.

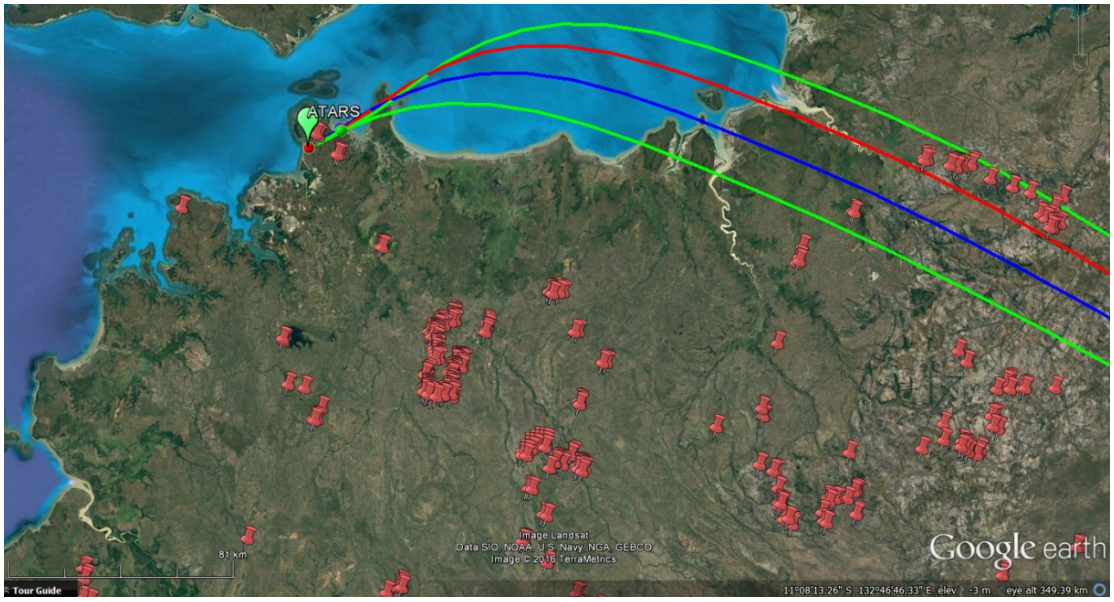
ATARS
Image Landsat
Data SIO, NOAA, U.S. Navy, NGA, GEBCO
Image © 2016 TerraMetrics
81 km
Google earth
Tour Guide
11°08'13.26" S 132°46'46.33" E elev -3 m eye alt 349.39 km

(a)


ATARS

(b)

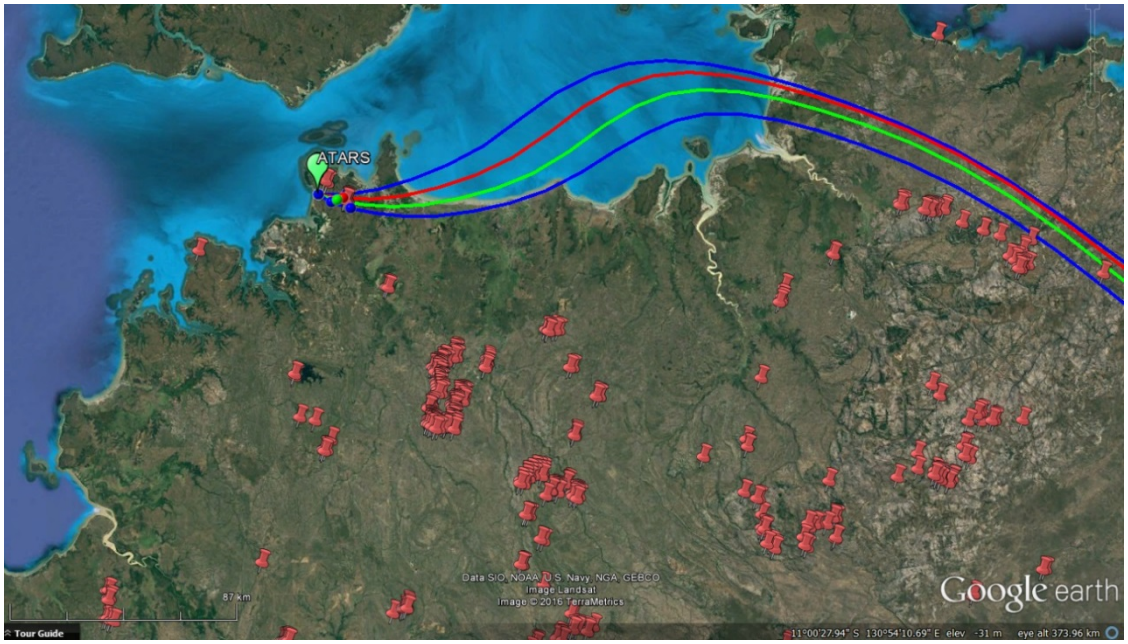
ATARS
Data SIO, NOAA, U.S. Navy, NGA, GEBCO
Image Landsat
Image © 2016 TerraMetrics
Google earth
87 km
Tour Guide
11°00'27.94" S 130°54'10.69" E elev -31 m eye alt 373.96 km

(c)

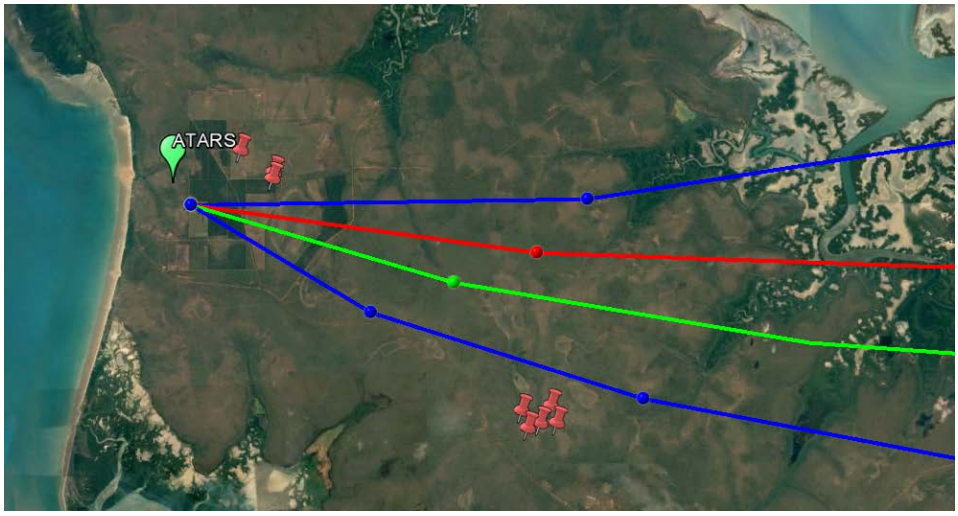
ATARS

(d)

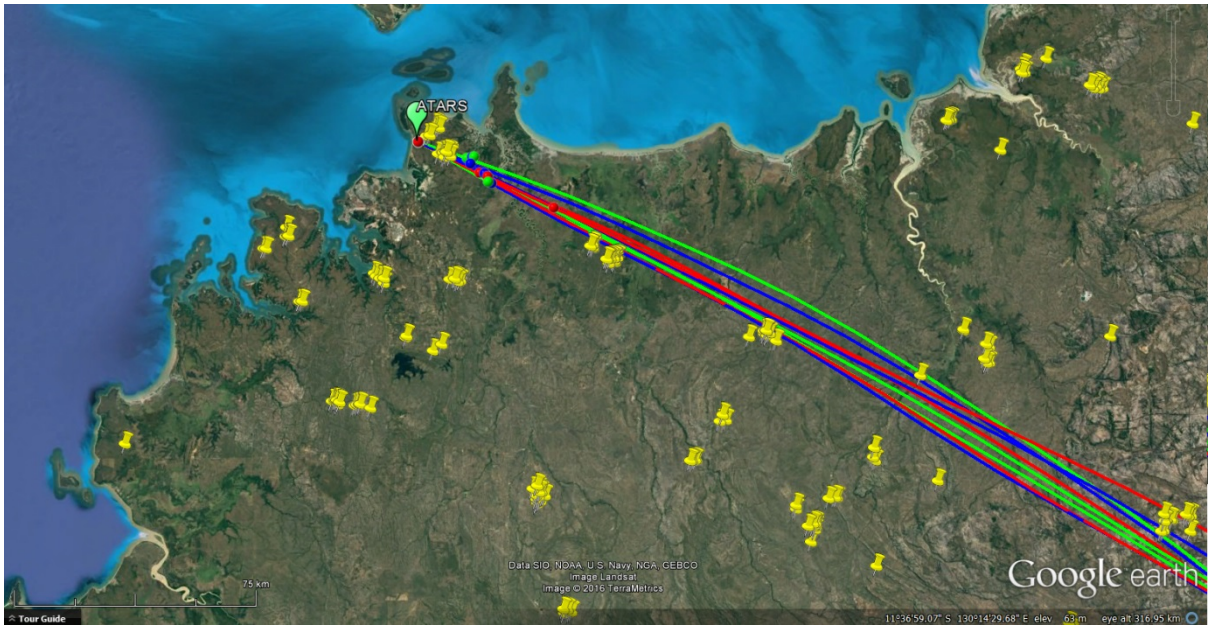
ATARS
Data SIO, NOAA, U.S. Navy, NGA, GEBCO
Image Landsat
Image © 2016 TerraMetrics
75 km
Google earth
Tour Guide

(e)

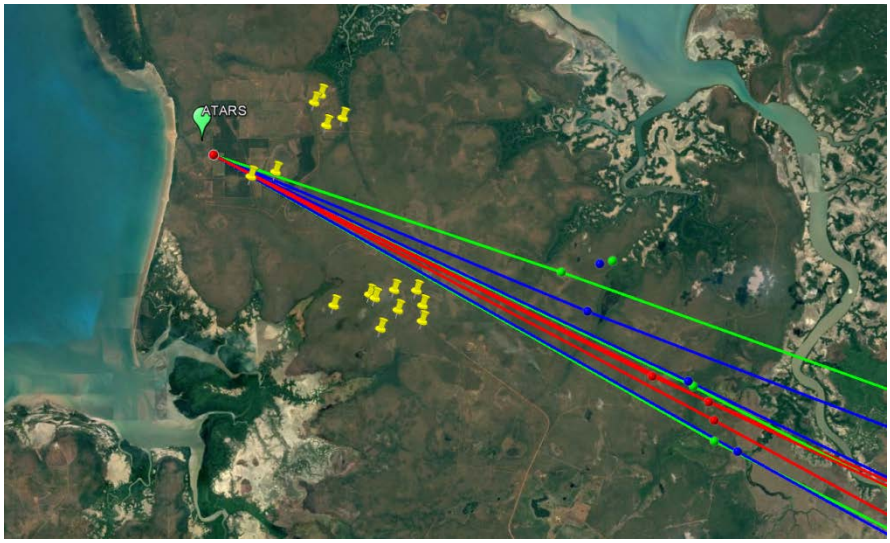
ATARS

(f)

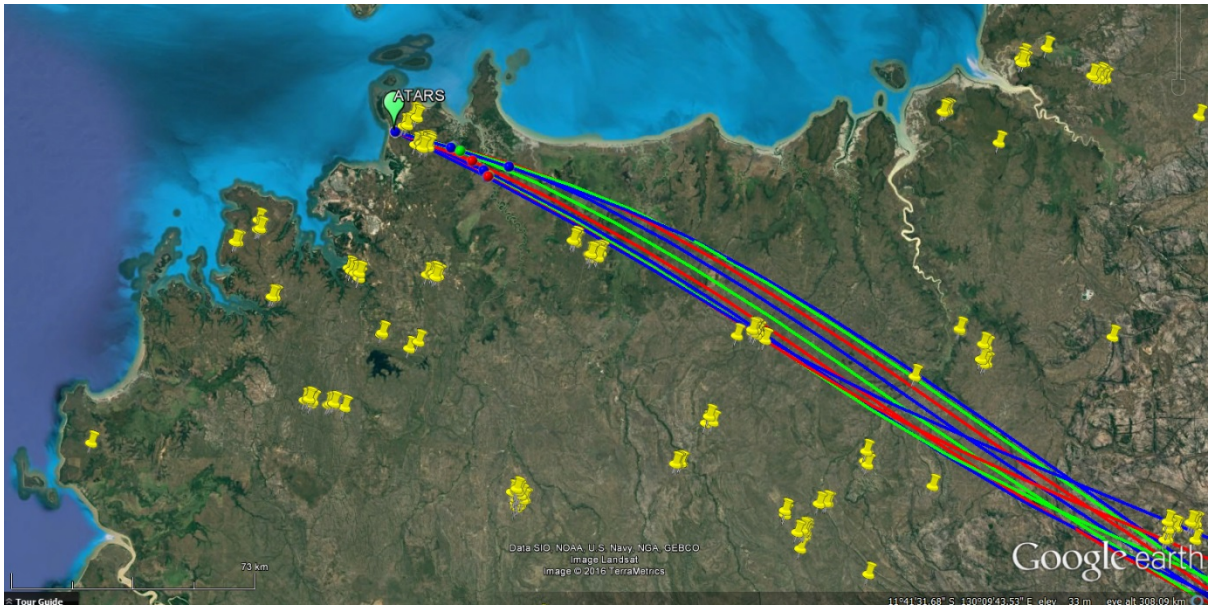
ATARS
Data SIO, NOAA, U.S. Navy, NGA, GEBCO
Image Landsat
Image © 2016 TerraMetrics
73 km
Google earth

(g)

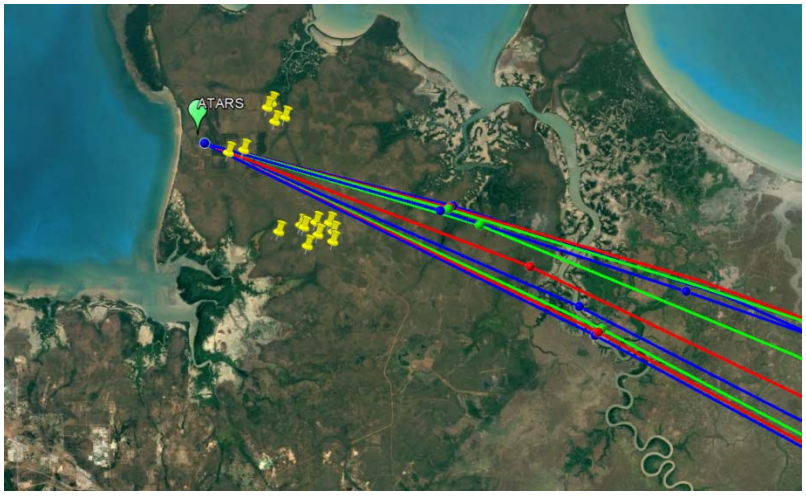
ATARS

(h)

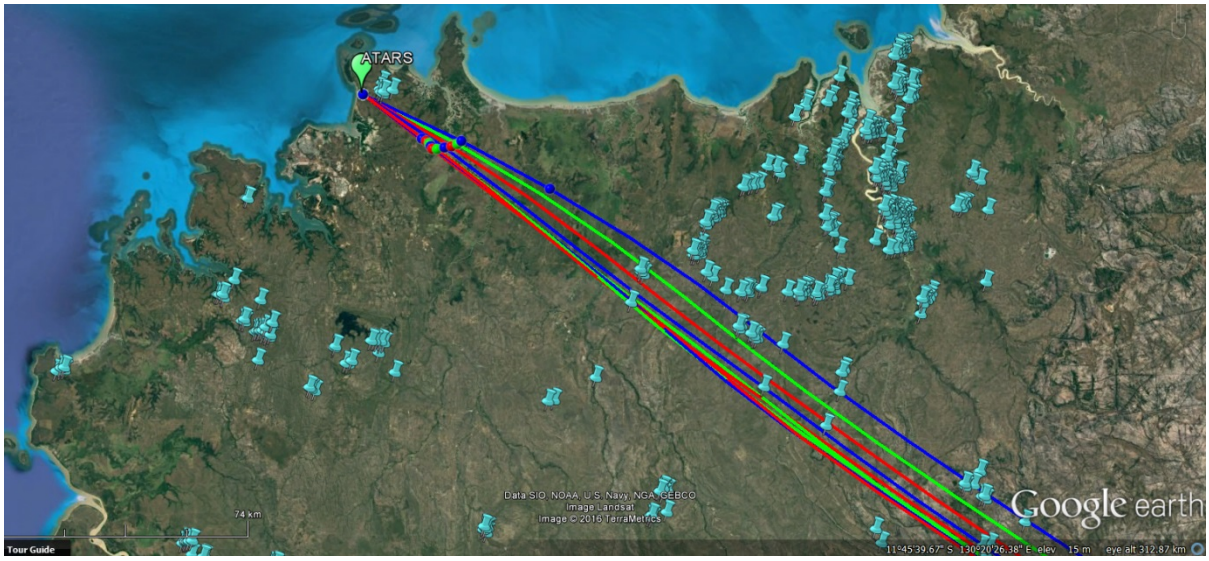

(i)

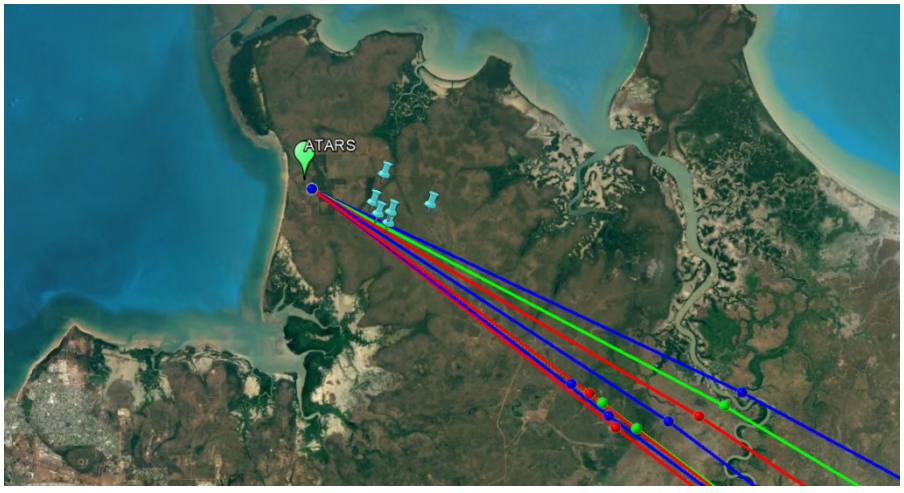

(j)

Figure 5.S27 Backtrajectories for event A, with close hot spots (a) and close and distant hot spots (b), for event C, with close hot spots (c) and close and distant hot spots (d), for event F, with close hot spots (e) and close and distant hot spots (f), for event G, with close hot spots (g) and close and distant hot spots (h) and for event E, with close hot spots (i) and close and distant hot spots (j). The backtrajectories were computed using the HYSPLIT (Hybrid Single-Particle Lagrangian Integrated Trajectory) model. All backtrajectories were run for 24h back in time. Different colours illustrate different starting time.

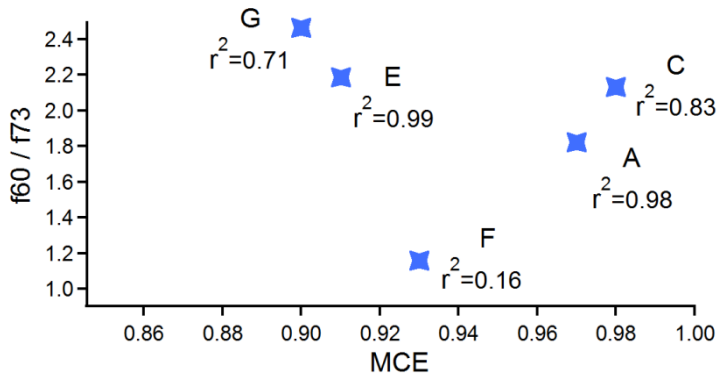

Figure 5.S28 f60/f73 ratio vs. modified combustion efficiency (MCE) for different events. Each point label indicates name of event and correlation value between f60 and f73.

5.6.3 PMF performed on the whole dataset

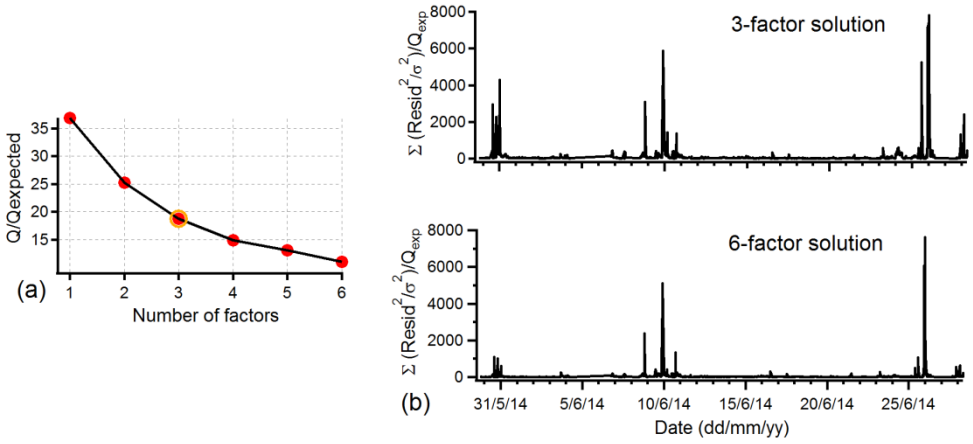

Figure 5.S29 (a) Q/Qexpected (Q refers to the sum of squared scaled residuals over the whole dataset) vs. number of factors, illustrating high error and residual values. (b) Time series of Q/Q expected contribution for 3 and 6-factor solutions where it is clear that higher number of factors does not make the residual structure during BB events significantly lower.

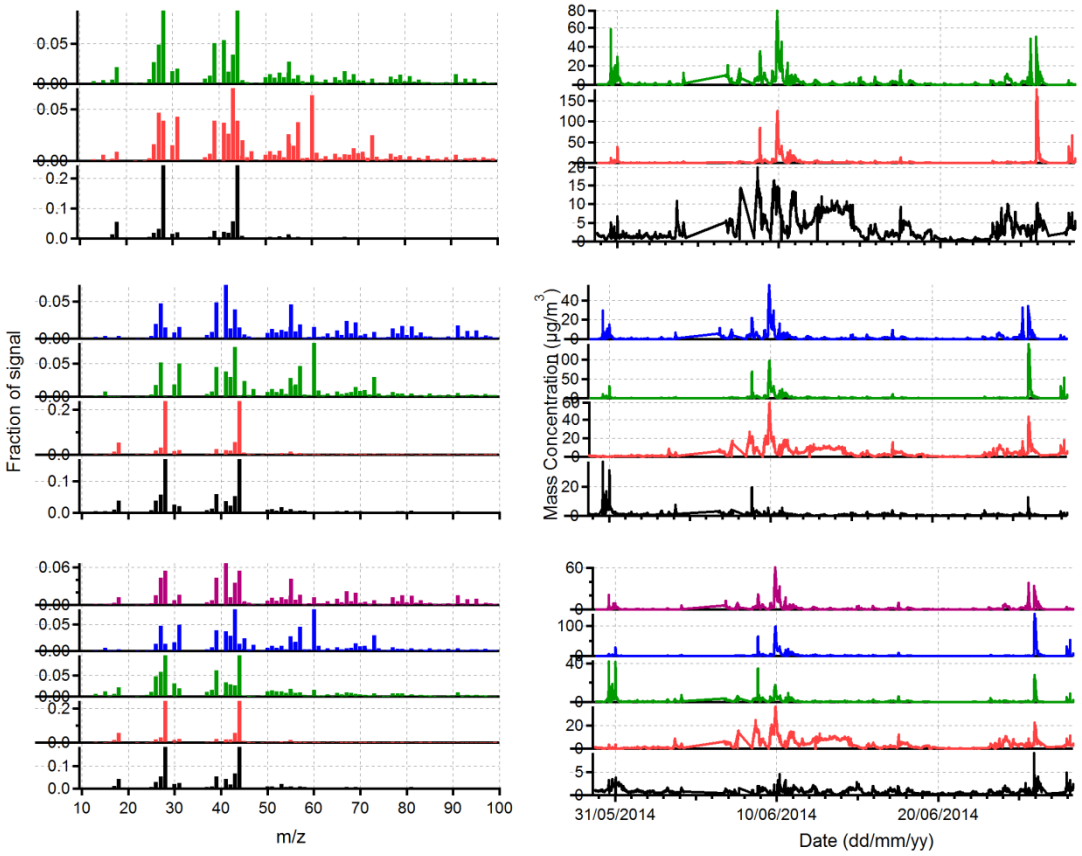

Figure 5.S30 Factor profiles and time series for 3, 4 and 5-factor solutions showing BBOA factor splitting, suggesting that plumes are apportioned to different PMF factors.

5.6.4 PMF performed on the background dataset

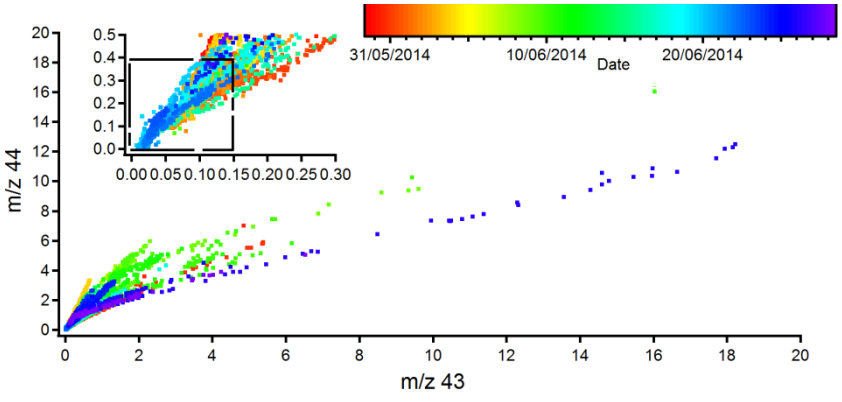

Figure 5.S31 m/z 44 vs. m/z 43 coloured by date for the whole dataset and for background periods (inset). Black dashed box in inset graph illustrates cut-offs of 0.15 for m/z 43 and 0.4 for m/z 44 chosen for background data.

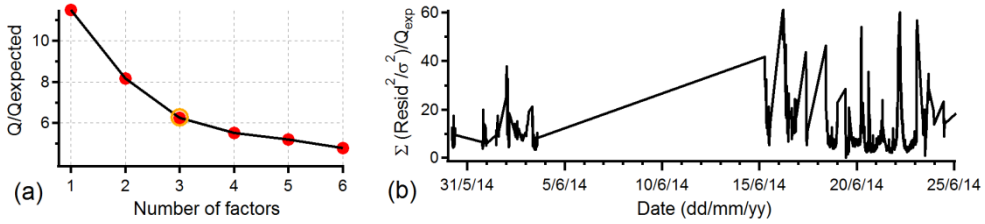

Figure 5.S32 (a) Q/Qexpected vs. number of factors and (b) time series of Q/Q expected contribution for the 3-factor solution illustrating significantly smaller residuals in the case of the background dataset, compared to the whole dataset.

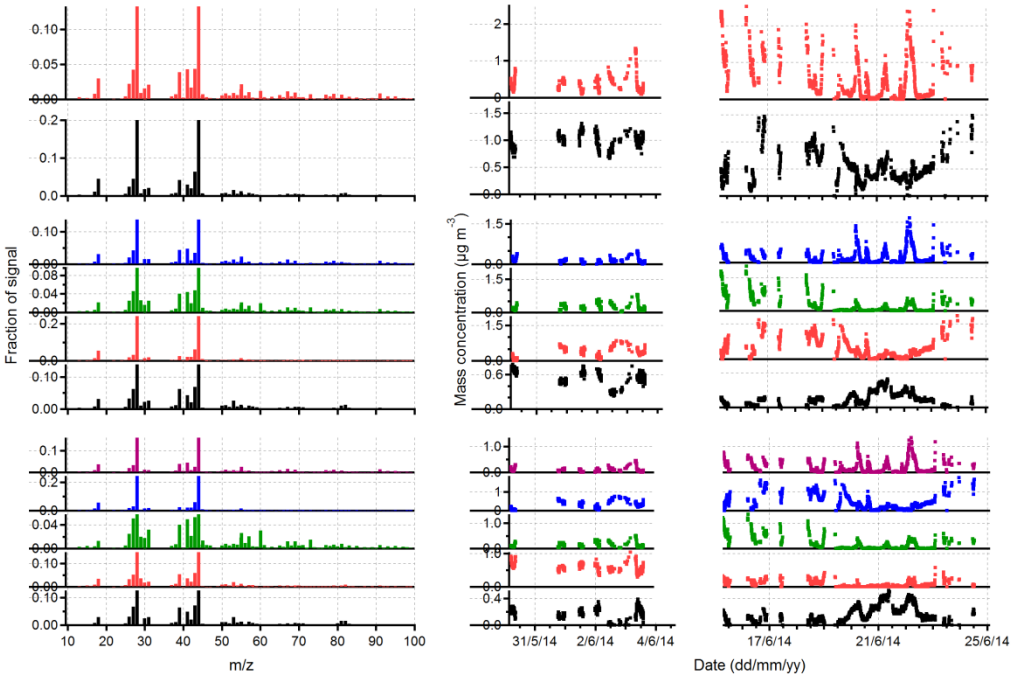

Figure 5.S33 Factor profiles and time series for 2, 4 and 5-factor solutions for the background dataset.

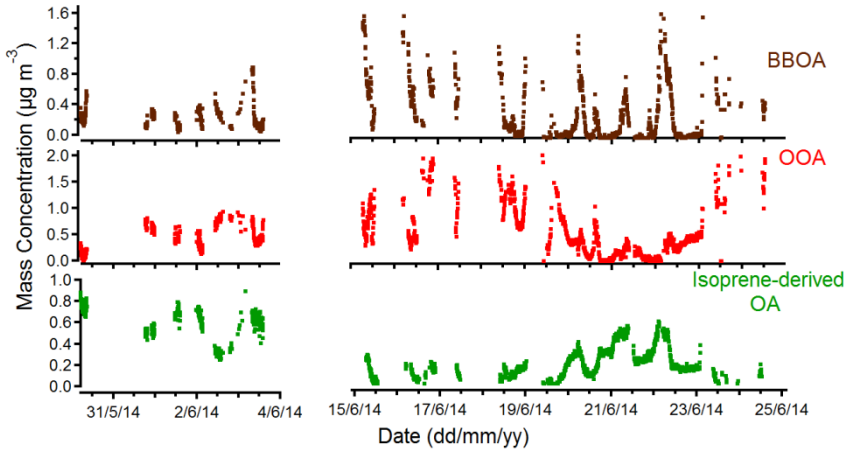

Figure 5.S34 Time series for 3-factor solution for the background dataset.

Isoprene-derived- organic aerosol

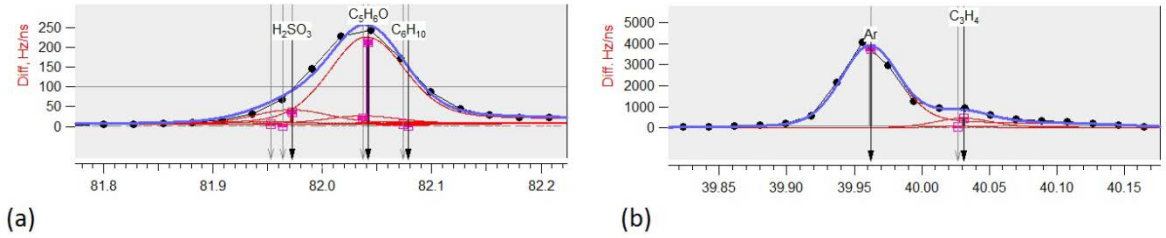

Figure 5.S35 HR peak fitting at (a) m/z 82 showing the dominance of the $C_5H_6O^+$ fragment and (b) m/z 40 demonstrating good m/z calibration.

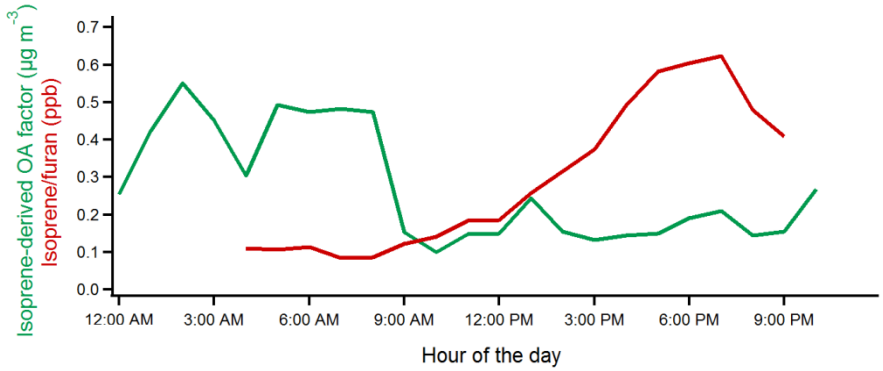

Figure 5.S36 Diurnal trend of PMF IEPOX-SOA factor and isoprene/furan concentration measured by PTR-MS.

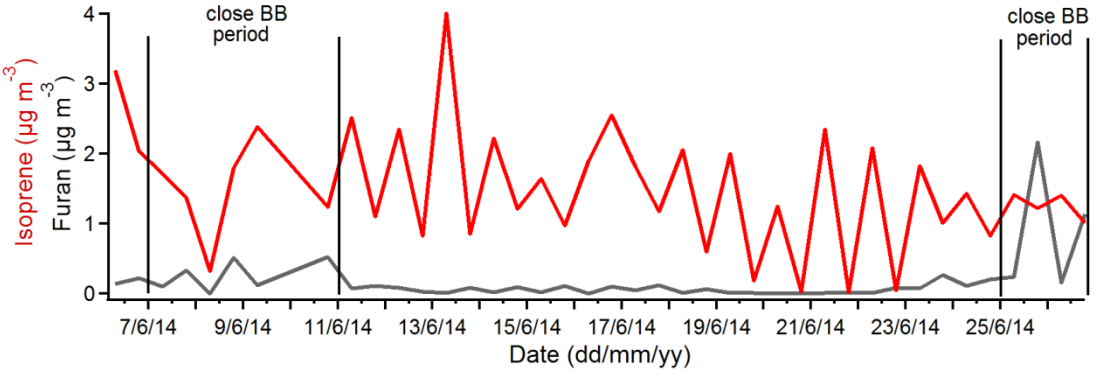

Figure 5.S37 Time series of isoprene and furan concentrations analysed by the gas chromatography-mass spectrometry. Black lines illustrate close BB periods.

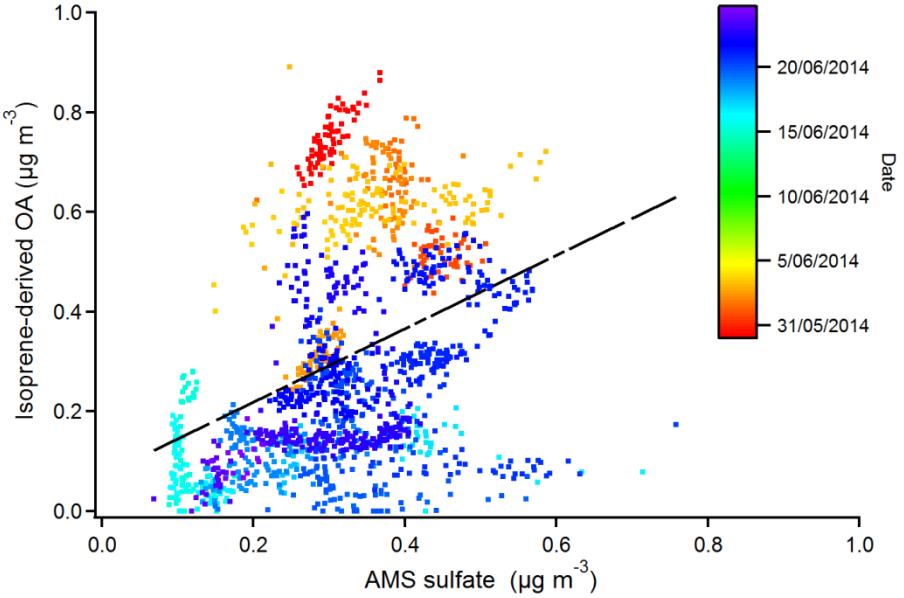

Figure 5.S38 Correlation between of AMS sulfate with the isoprene-derived OA PMF factor.

Chapter 6

CONCLUSIONS

Chapter 6 provides conclusions that are made based on the study results, and significance of the research findings. The contribution to the research knowledge is framed by the recommendations for future research that can serve as the research gaps for future studies.

6.1 Conclusions and significance of the research findings

A one month long Brisbane campaign during the prescribed burning period provided insight into the chemical composition, sources and aging degree of the ambient aerosols, and moreover the contribution of BBs in an urban, subtropical area (Milic et al., 2016b). The ambient aerosol characterization using the compact time of flight aerosol mass spectrometer (cToF-AMS) was reported for the same sampling site (Crilley et al., 2014b) and in the short term sampling during prescribed burning period (He et al., 2016).Crilley et al. (2014) observed the similar factors to our study (HOA, COA, BBOA and OOA), however the authors did not examine the BB aerosols. On another side, He et al. (2016) obtained various data related to the burning period, however, study was the short term sampling (4 days) and PMF was not applied on this dataset. Continuous sampling in the specific period of the prescribed biomass burnings (BB) was not previously performed. The dominant aerosol submicron non-refractory fraction was found to be organic mass (64 %). The source apportionment of the OA was improved using the multilinear engine solver (ME-2) and applying the constrain technique (a value) within the recently developed Source Finder (SoFi) interface. The urban aerosol was described with PMF-resolved factors including hydrocarbon-like OA (HOA), cooking-related OA (COA), biomass burning OA (BBOA), low-volatility oxygenated OA (LV-OOA), semivolatile oxygenated OA (SV-OOA), and nitrogen-enriched OA (NOA). Fire emissions had little influence on the observed aerosol, as illustrated through the low contribution of PMF-resolved BBOA factor (on average 9 %). This can be attributed to a mixing of BB emissions with the background urban aerosol and intensive aging during their transport to the sampling site. The biomass burning emissions could have contributed to oxygenated organic aerosol (OOA), typically representing aged emissions. The high OOA fraction likely includes a fraction of oxygenated species transformed from BB-related organic components on their way to the sampling site. Another possible explanation of low BB influence can be a limited number of plumes that were transported towards the measurement location. The high portion of LV-OOA and its O/C ratio (Table 6.1) agrees with previous results for the same sampling site, confirming the significant aging for Brisbane urban area and an environment for SOA production. The PMF-resolved NOA factor is not a commonly detected component and has not been previously observed in Australia. The distinctive diurnal trend of NOA that is characterised by a broad peak between midnight and approximately 8 am correlates with temperature decrease and relative humidity increase. However, the factor could not be related to any specific source. The extraction of NOA factor provides a room for further research on

identification of possible factor source(s) and chemical processes involved. This work is an important step in characterizing the ambient aerosol sources with an accent on the BB aerosol in the Brisbane urban environment, and also wider understanding of BB impact in subtropical urban environments and more wider in the Southern Hemisphere.

A field campaign, Savannah fires in the early dry season (SAFIRED), is to date the largest collaborative study looking at the Australian savanna fire emissions during the early dry intense BB period (Mallet et al., 2016). A month-long study was performed to assemble information about atmospheric processes and compositional change of BB emissions. Number of the campaign outcomes will be presented through comprehensive interpretation of study results in separate publications, which are and will be submitted in the near future. The specific subjects that have been covered are emission factors, physicochemical aerosol properties, aerosol aging and aerosol water uptake. This information will provide foundation for BB emissions in the Northern Territory, and wider for a tropical, remote regions and the Southern Hemisphere.

One of the important outcomes of the SAFIRED campaign is chemical characterisation and aging of the ambient aerosols during the early dry BB season (Milic et al., 2016a). The aim was also to contribute to the research knowledge regarding the aging of BB aerosols in the Southern Hemisphere and more specific in the tropics. The chemical characterization and aging of aerosols monitored during the SAFIRED campaign, with an emphasis on chemical signature and aging of OA was provided. The dominant aerosol submicron non-refractory fraction was found to be organic mass (90 %). The overall trend of an increase in OOA and a decrease in BB-related organics with aging was observed. There was a high contribution of fresh and processed fire emissions. The fire diversity was seen through variability in the chemical signature of selected events, more precisely according to wide range in f44. The observed ozone enrichment in distant BB emissions illustrated the increased photochemical activity of aged plume masses. The OA enhancement in aged BB emissions was shown in the afternoon hours indicating additional production of the organics (SOA production). In addition, the decrease in organic loadings for processed masses observed later in the afternoon can be associated with OA loss due to fragmentation and subsequent evaporation from the particulate phase, probably when more oxidized species are present. The OA oxidation degree also influenced particle size distribution. The shift in particle size towards larger particles in the aged emissions may be due to OA partitioning to the aerosol-phase. In addition, high OOA fraction of submicron background aerosols (47 %) indicated the importance of aerosol aging in northern Australia. The PMF-resolved isoprene organic aerosol factor illustrated the importance of biogenic sources. This is the first time the isoprene-related OA factor was identified in Australia. The need for further research related to tropical biomass burns and biogenic-related SOA in Australia introduced by Rotstayn et al. (2009) and Spracklen et al. (2011) shows the significance of this research study.

To put the BB aerosol aging issue into a more wider global context the comprehensive review manuscript (Chen et al., 2016) gathered the studies performed to date, making a large database that can be used as a foundation of performed research on BB emissions and the aging of BB emissions, around the world with a special focus on China. The significant influence of

fresh and processed BB that are mainly products of agricultural post-harvest activities is evident. After detailed literature research it can be concluded that regulations of BB activities should be revised and frequency and extend of BB sources, particularly open post-harvest burning, should be reduced. The monitoring of the aerosol aging is in the initial stage in China and should be taken more seriously due to observed SOA and ozone formation and significant air pollution, climate and health issues related to the BB sources.

Table 6.1 O/C ratios for urban cities over the world (some content of the Table adjusted from Crilley et al. (2014a)). O/C ratio is calculated based on equation introduced by Aiken et al. (2008). It is important to emphasise that O/C ratio for Gun Point is for OOA of the background aerosol fraction.

Location	O/C ratio (LV-OOA)	Reference
Mexico City	*0.83*	*(Aiken et al., 2008)*
Northern Hemisphere	*0.73*	*(Ng et al., 2010)*
New York	*0.63*	*(Sun et al., 2011)*
Beijing	*0.48*	*(Huang et al., 2010)*
PRD Region, China	*0.59*	*(He et al., 2011)*
Brisbane	*1.25*	*(Crilley et al., 2014a)*
Brisbane	***1.44***	***(Milic et al., 2016b)***
Gunn Point	***0.87***	***(Milic et al., 2016a)***

In general, the source apportionment illustrates the typical urban components for Brisbane and significance of biogenic sources in remote northern Australia. The influence of fire emissions was seen in both studies with a much stronger influence in the Northern Territory during the dry season (94% of f60 is above the background value and BBOA makes up 24 % of the background OA), than in Brisbane during the prescribed BB period (on average 45 % of f60 is above the background value and BBOA contribution makes up 9 % of the OA). Both Australian environments have high contribution of OOA (high f44 values and PMF OOA factor contributions). The results for Brisbane and Gunn Point in terms of O/C level of LV-OOA factors complies with the previous observations that aerosols in the Southern Hemisphere have a higher degree of aging compared to the aerosols in the Northern Hemisphere, including China (Table 6.1). Presence of more aged aerosols in the Southern Hemisphere is probably related to different meteorological conditions and atmospheric photochemistry (aging processes) like those suggested in Crilley et al. (2014a). However, further research is needed to provide information about this observation. The urban Brisbane area has higher portion of processed air masses (72 % of OOA, maximum f44 value ranged between 0.25 and 0.35) compared to the remote Australian area (47 % of OOA, maximum f44 value ranged between 0.20 and 0.25). It has to be emphasised that in case of the SAFIRED background OOA portion was investigated. The higher portion of aged air masses in urban atmosphere likely illustrates the importance of urban aerosol contribution in SOA generation.

The results from this research study are an important addition to the literature on the chemical characterization and aging of ambient aerosols in particular biomass burning organic aerosols. The results provide important information about the ambient aerosol of the Southern Hemisphere region where little or no data were taken previously. The NOA and isoprene-related OA PMF-resolved factors that were identified for the first time in Australia provide a base for the future research.

6.2 Direction for future research

The low influence of BB sources was observed during the prescribed burning season in Brisbane in 2013. However, monitoring of the BB emissions during the prescribed period should be continued as contributions significantly vary depending on the year, as stated in Milic et al. (2016b). This can allow the estimation of influence of prescribed BBs on the Brisbane urban aerosols. The same can be applied for the influence of dry season fires in the northern Australia. Future measurements at Gunn Point sampling site including continuous measurements throughout the whole dry season and over a long-term scale can provide more accurate inventories and modelling data for tropical savannah fires. More research should be also put into the late dry season in the savannah region (October and November), as more intense and frequent fires occur during this period (Andersen et al., 2005; Williams et al., 1998). In addition, it was suggested that the late dry season experiences more aged emissions (Ristovski et al., 2010; Wardoyo et al., 2007) and thus additional study should be performed on SOA and ozone formation during this period. In general, there is still significant room for improvement in terms of SOA yields, which are considerably underestimated, and SOA formation which is still not sufficiently understood.

The NOA component observed in the Brisbane urban area and isoprene-related OA in the Northern Territory should be further investigated. Revealing the profiles of these factors will facilitate the determination of source profiles in the Australian urban and remote areas.

AMS methods using electron ionization method have been most widely applied in the aerosol measurements. Besides the undeniable AMS capability, the electron ionization induces extensive fragmentation of the molecules and makes detection of specific molecular species hardly doable. Therefore, some other methods such as an electrospray ionization mass spectrometry and a chemical ionization mass spectrometry which apply soft ionization induced methods should be used to provide more detailed compositional information and to support the AMS data. Moreover, the new technology that combines TAG and ToF-AMS can provide detailed organic composition using the molecular source-specific markers and can identify, separate and quantify different OA species, such as HOA and OOA. This will facilitate performance of organic aerosol source apportionment.

A laboratory-based studies using the typical Australian biomass (e.g. eucalyptus wood) under controlled conditions (e.g. wood stove), and the aging of the generated BB emissions in the chamber can provide a base for chemical composition of fresh and processed emissions.

Tracking the plume using aircraft-based instrumentation would improve the knowledge on atmospheric reactions that BB emissions undergo during their transport in Australia. More observational data are in general needed for both urban and remote Australian area in order to improve inventories, and climate and air quality models.

6.3 References

Aiken AC, DeCarlo PF, Kroll JH, Worsnop DR, Huffman JA, Docherty KS, et al. O/C and OM/OC ratios of primary, secondary, and ambient organic aerosols with high-resolution time-of-flight aerosol mass spectrometry. Environmental Science & Technology 2008; 42: 4478-4485.

Andersen AN, Cook GD, Corbett LK, Douglas MM, Eager RW, Russell-Smith J, et al. Fire frequency and biodiversity conservation in Australian tropical savannas: implications from the Kapalga fire experiment. Austral Ecology 2005; 30: 155-167.

Chen J, Li C, Ristovski Z, Gu Y, Wang S, Hao J, et al. A Review of Biomass Burning: Emissions and their impacts on air quality, health and climate in China. in preparation 2016.

Crilley LR, Ayoko GA, Morawska L. First measurements of source apportionment of organic aerosols in the Southern Hemisphere. Environmental Pollution 2014a; 184: 81-88.

Crilley LR, Jayaratne ER, Ayoko GA, Miljevic B, Ristovski Z, Morawska L. Observations on the formation, growth and chemical composition of aerosols in an urban environment. Environmental science & technology 2014b; 48: 6588-6596.

He C, Miljevic B, Crilley LR, Surawski NC, Bartsch J, Salimi F, et al. Characterisation of the impact of open biomass burning on urban air quality in Brisbane, Australia. Environment international 2016; 91: 230-242.

He LY, Huang XF, Xue L, Hu M, Lin Y, Zheng J, et al. Submicron aerosol analysis and organic source apportionment in an urban atmosphere in Pearl River Delta of China using high-resolution aerosol mass spectrometry. Journal of Geophysical Research: Atmospheres (1984–2012) 2011; 116.

Huang X-F, He L-Y, Hu M, Canagaratna M, Sun Y, Zhang Q, et al. Highly time-resolved chemical characterization of atmospheric submicron particles during 2008 Beijing Olympic Games using an Aerodyne High-Resolution Aerosol Mass Spectrometer. Atmospheric Chemistry and Physics 2010; 10: 8933-8945.

Mallet MD, Desservettaz MJ, Miljevic B, Milic A, Ristovski ZD, Alroe J, et al. Biomass burning emissions in north Australia during the early dry season: an overview of the 2014 SAFIRED campaign, submitted to Atmos. Chem. Phys., 2016

Milic A, Mallet MD, Cravigan L, Alroe J, Ristovski ZD, Selleck P, et al. Aging of aerosols emitted from biomass burning in northern Australia. Atmos. Chem. Phys. Discuss., doi:10.5194/acp-2016-730, in review 2016a.

Milic A, Miljevic B, Alroe J, Mallet M, Canonaco F, Prevot A, et al. The ambient aerosol characterization during the prescribed bushfire season in Brisbane 2013. Science of The Total Environment 2016b; 560: 225-232.

Ng N, Canagaratna M, Zhang Q, Jimenez J, Tian J, Ulbrich I, et al. Organic aerosol components observed in Northern Hemispheric datasets from Aerosol Mass Spectrometry. Atmospheric Chemistry and Physics 2010; 10: 4625-4641.

Ristovski ZD, Wardoyo AY, Morawska L, Jamriska M, Carr S, Johnson G. Biomass burning influenced particle characteristics in Northern Territory Australia based on airborne measurements. Atmospheric Research 2010; 96: 103-109.

Rotstayn LD, Keywood MD, Forgan BW, Gabric AJ, Galbally IE, Gras JL, et al. Possible impacts of anthropogenic and natural aerosols on Australian climate: a review. International Journal of Climatology 2009; 29: 461-479.

Spracklen D, Jimenez J, Carslaw K, Worsnop D, Evans M, Mann G, et al. Aerosol mass spectrometer constraint on the global secondary organic aerosol budget. Atmospheric Chemistry and Physics 2011; 11: 12109-12136.

Sun Y-L, Zhang Q, Schwab J, Demerjian K, Chen W-N, Bae M-S, et al. Characterization of the sources and processes of organic and inorganic aerosols in New York city with a high-resolution time-of-flight aerosol mass apectrometer. Atmospheric Chemistry and Physics 2011; 11: 1581-1602.

Wardoyo AY, Morawska L, Ristovski ZD, Jamriska M, Carr S, Johnson G. Size distribution of particles emitted from grass fires in the Northern Territory, Australia. Atmospheric Environment 2007; 41: 8609-8619.
Williams R, Gill A, Moore P. Seasonal changes in fire behaviour in a tropical savanna in northern Australia. International Journal of Wildland Fire 1998; 8: 227-239.

Chapter 7
APPENDIX

A REVIEW OF BIOMASS BURNING: EMISSIONS AND IMPACT ON AIR QUALITY, HEALTH AND CLIMATE IN CHINA

Jianmin Chen [a,h,*], Chunlin Li [a], Zoran Ristovski [b], Andelija Milic [b], Yuantong Gu [b], Mohammad S. Islam [b], Shuxiao Wang [c], Jiming Hao [c,*], Hefeng Zhang [d], Congrong He [b], Hai Guo [e], Hongbo Fu [a], Branka Milijevic [b], Lidia Morawska [b,*], Phong Thai [b], Yun Fat Lam [f], Gavin Pereira [g], Aijun Ding [h], Xin Huang [h], Umesh C. Dumka [a, i]

[a] Shanghai Key Laboratory of Atmospheric Particle Pollution and Prevention, Department of Environmental Science and Engineering, Fudan University, Shanghai 200433, China
[b] International Laboratory for Air Quality and Health, Institute of Health and Biomedical Innovation, Queensland University of Technology, Brisbane, QLD 4001, Australia
[c] School of Environment, Tsinghua University, Beijing 100084, China
[d] State Key Laboratory of Environmental Criteria and Risk Assessment, Chinese Research Academy of Environmental Sciences, Beijing 100012, China
[e] Department of Civil and Environmental Engineering, Hong Kong Polytechnic University, Hong Kong, China
[f] School of Energy and Environment, City University of Hong Kong, HKSAR, China
[g] Center for Perinatal Pediatric and Environmental Epidemiology, School of Medicine, Yale University, New Haven, Connecticut, USA
[h] Collaborative Inovation Center of Climate Change, School of Atmospheric Sciences, Nanjing University, Nanjing 210023, China
[i] Aryabhatta Research Institute of Observational Sciences, Manora Peak, Nainital 263001, India

Published in Science of the Total Environment, 579 (2017), Pages 1000–1034.

STATEMENT OF JOINT AUTHORSHIP

The authors listed below have certified that:

1. they meet the criteria for authorship in that they have participated in the conception, execution, or interpretation, of at least that part of the publication in their field of expertise;
2. they take public responsibility for their part of the publication, except for the responsible author who accepts overall responsibility for the publication;
3. there are no other authors of the publication according to these criteria;
4. potential conflicts of interest have been disclosed to (a) granting bodies, (b) the editor or publisher of journals or other publications, and (c) the head of the responsible academic unit, and
5. they agree to the use of the publication in the student's thesis and its publication on the QUT ePrints database consistent with any limitations set by publisher requirements.

In the case of this chapter: Chapter 5

Andelija Milic (candidate) wrote the manuscript Chapter 7.4.1 (Particulate Matter) and Chapter 7.5.2 (Atmospheric aging)

All authors declare that they have no conflict of interest.

Principal Supervisor Confirmation

I have sighted email or other correspondence from all Co-authors confirming their certifying authorship.

Zoran Ristovski		26/09/2016
Name	Signature	Date

A REVIEW OF BIOMASS BURNING: EMISSIONS AND IMPACT ON AIR QUALITY, HEALTH AND CLIMATE IN CHINA

Jianmin Chen [a,h,*], Chunlin Li [a], Zoran Ristovski [b], Andelija Milic [b], Yuantong Gu [b], Mohammad S. Islam [b], Shuxiao Wang [c], Jiming Hao [c,*], Hefeng Zhang [d], Congrong He [b], Hai Guo [e], Hongbo Fu [a], Branka Milijevic [b], Lidia Morawska [b,*], Phong Thai [b], Yun Fat Lam [f], Gavin Pereira [g], Aijun Ding [h], Xin Huang [h], Umesh C. Dumka [a, i]

[a] Shanghai Key Laboratory of Atmospheric Particle Pollution and Prevention, Department of Environmental Science and Engineering, Fudan University, Shanghai 200433, China
[b] International Laboratory for Air Quality and Health, Institute of Health and Biomedical Innovation, Queensland University of Technology, Brisbane, QLD 4001, Australia
[c] School of Environment, Tsinghua University, Beijing 100084, China
[d] State Key Laboratory of Environmental Criteria and Risk Assessment, Chinese Research Academy of Environmental Sciences, Beijing 100012, China
[e] Department of Civil and Environmental Engineering, Hong Kong Polytechnic University, Hong Kong, China
[f] School of Energy and Environment, City University of Hong Kong, HKSAR, China
[g] Center for Perinatal Pediatric and Environmental Epidemiology, School of Medicine, Yale University, New Haven, Connecticut, USA
[h] Collaborative Inovation Center of Climate Change, School of Atmospheric Sciences, Nanjing University, Nanjing 210023, China
[i] Aryabhatta Research Institute of Observational Sciences, Manora Peak, Nainital 263001, India

Correspondence to: Jianmin Chen (jmchen@fudan.edu.cn), Jiming Hao (hjm-den@tsinghua.edu.cn) and Lidia Morawska (l.morawska@qut.edu.au)

Abstract. Biomass burning (BB) is a significant air pollution source, with global, regional and local impacts on air quality, public health and climate. Worldwide an extensive range of studies has been conducted on almost all the aspects of BB, including its specific types, on quantification of emissions and on assessing its various impacts. China is one of the countries where the significance of BB has been recognized, and a lot of research efforts devoted to investigate it, however, so far no systematic reviews were conducted to synthesize the information which has been emerging. Therefore the aim of this work was to comprehensively review most of the studies published on this topic in China, including literature concerning field measurements, laboratory studies and the impacts of BB indoors and outdoors in China. In addition, this review provides insights into the role of wildfire and anthropogenic BB on air quality and health globally. Further, we attempted to provide a basis for formulation of policies and regulations by policy makers in China.

Keywords. Biomass burning, savannah fires, organic aerosol, aerosol aging

7.1 Introduction

Traditionally, Chinese families used to collect and store the biomass of crop residues, weeds, branches and leaves as irreplaceable fuel for cooking or heating, and there are still some rural areas where this practice continues (Fig. 7.1a and 7.1b). Usually, this does not produce distinct air pollution events as the BB emissions are similar through the year. Recently, due to rapid economic growth and urbanization in China, crop residues have been often field burnt post harvests in a couple of days to prepare for planting the next season's crops (Fig. 7.1c and 7.1d).

Figure 7.1 Representative figures for biomass burning in China.

Rice, wheat and corn straws are the top three crop residues in China, which make up 75% of total straw productions. Usually, there are three concentrated periods of BB: i) rice/wheat straw field burning from South to North of China, which is called summer harvest season (some reports call this spring harvest) in the late of May to the end of June; ii) crop residue burning in October, mainly corn residue burning in North China, and second season rice straw burning in South China; iii) heating in winter in North China. This seasonality in BB was observed by Cheng et al. (2014a). They monitored air pollution in five cities (Shanghai, Hangzhou, Ningbo, Suzhou and Nanjing) of the Yangtze River delta (YRD), and found a ten days heavy haze episode with visibility of 2.9–9.8 km from 28 May to 6 June 2011. The average and maximum daily PM2.5

concentrations during the episode were 82 and 144 μg/m^3, respectively. Estimation based on observation data and Community Multi-scale Air Quality (CMAQ) model simulation indicated that biomass open burning contributed 37 % of ambient PM2.5 in the harvest period in YRD (Cheng et al., 2014a). An on-line study on water-soluble potassium ion (K^+) in PM10 and trace gaseous pollutants revealed that BB had a significant im- pact on Shanghai air quality from 22 May to 30 June during the summer harvest time of 2009 (Li et al., 2010a). The average K^+ concentration (3.96 μg/m^3) of severely polluted days within 2.0–8.5 μg/m^3 was more than 24 times that of clear days, in the range of 0.0–0.3 μg/m^3 (Li et al., 2010a). Three-year on-line measurements of PM2.5 chemical compositions have shown that PM2.5 mass concentration could increase because of BB to a high level with an average of 134 μg/m^3, being three times higher than that of clear days from 2011 to 2013 in Shanghai (Wang et al., 2015a).

Biomass burning has played a noticeable role in unexpected severe haze episodes that overlapped with the primary and secondary pollutants derived from engine exhausts and coal combustion. Huang et al. (2014) investigated the chemical components and sources of PM2.5 in Beijing, Shanghai, Guangzhou and Xi'an upon a severe and persistent haze pollution, which affected 1.3 million km^2 and 800 million people in January 2013. The calculated contributions of fossil origin secondary organic aerosol (SOA) to the total organic aerosol (OA) mass were 1.1–2.4 times larger for high pollution events than for clear or less polluted days, highlighting the importance of fossil-derived SOA, or fossil SOA, to particulate pollution. Fossil SOA accounts for 25–40% of OA mass or 45–65% of SOA mass in Shanghai and Beijing, consistent with the large emissions of SOA precursors from high traffic flow and/or large coal usage for domestic heating/cooking at these locations. The fossil SOA fraction decreases to 10–20% of OA mass in Guangzhou and Xi'an, with the non-fossil SOA fraction increasing to 30–60% of the OA mass or 65–85% of the SOA mass, mostly due to the enhanced BB activities (Huang et al., 2014).

Agricultural residues burning calls for close attention in China as it emits significant amounts of greenhouse gases such as CO2, CO and hydrocarbons, other gaseous pollutants such as SO_2 and NO_X, and smoke particles carrying carcinogenic substances with a wide size distribution (Li et al., 2007; Zhang et al., 2008a; Zhang et al., 2011a; Li et al., 2016a; Sun et al., 2016a). A significant amount of toluene, isoprene, and propene (active volatile organic components (VOCs) and O_3 precursors (Mellouki et al., 2015), have been detected with high total ozone formation potential (OFP) values from BB observation at a rural site in Northern China during summer 2013 (Zhu et al., 2016b). The spatial– temporal variation of BB in June from 2005 to 2012 has revealed that the wheat harvest season in the North China has a significant influence on the regional aerosol optical depth (AOD) and the chemical compositions of size-segregated aerosols (Wang et al., 2015b). Under high relative humidity and south winds, emissions from straw burning combined with high urban/industrial emissions to produce intensive regional haze pollution in the North Plain. The formation of secondary inorganic particles was intensified due to the interactions of smoke plumes of BB and urban/industrial pollutants in an urban environment (Wang et al., 2015b).

Polycyclic aromatic hydrocarbons (PAHs) are typical carcinogenic substances. As a respiratory exposure health care, laboratory studies are conducted to determine PAHs emissions from the burning of rice, wheat, and corn straws in China (Zhang et al., 2011a). PAHs in both particulate and gaseous phases were simultaneously collected and analyzed. It shows that PAHs emission factors of rice, wheat, and corn straws were 5.26, 1.37, and 1.74 mg/kg, respectively. The total PAHs emissions from the burning of three agricultural crop residues in China were estimated to be 1.09 Gg for the year 2004 (Zhang et al., 2011a). However, there are only a handful of reports on the impact of BB on health in China (Zhang et al., 2011a; Lin et al., 2015a).

Biomass burning is of global concern, particularly in recent years due to its link to climate changes. BB emits significant amounts of short-living global warming substances (Gustafsson et al., 2009; Ramana et al., 2010; Lack et al., 2012; Victor et al., 2015) such as black carbon, and also significantly contributes to ozone formation by photochemical reactions among its precursor VOCs and NOx. An excellent review has covered optical properties of smoke particles relative to radiative forcing (Reid et al., 2005a). It included available data from published sensitivity studies, field campaigns, and inversions from the Aerosol Robotic Network (AERONET) of Sun photometer sites (Reid et al., 2005a). So far, there has been less work conducted on this aspect in China.

Here, we include advances on BB emissions and their impacts on air quality, public health and climate in China. This may be helpful to assess the regional emissions of BB and its connection and role on a global scope.

7.2 Monitoring of biomass burning

7.2.1. Field observations

Field observation is a practical way to characterize properties and dynamic changes of BB pollutants (Reid et al., 2005a, b). Outdoor studies concerning BB try i) to depict the contribution of smoke plumes to re- gional or global reactive trace gases, PM2.5, and cloud condensation nuclei (CCN) concentrations lifting via transportation (Du et al., 2011; Rose et al., 2011; Wang et al., 2013; Zauscher et al., 2013; Ding et al., 2015; Bougiatioti et al., 2016), ii) to elucidate the role of smoke aerosol in triggering haze and new particle formation (NPF) (Ding et al., 2013a; Wang et al., 2013; Yang et al., 2015; Sun et al., 2016b), iii) to figure out the relationship between smoke aerosol emissions and social welfare loss (e.g., air quality deterioration in visibility decrease, public health hazard, etc.) (Lai and Sequeira, 2001; Fullerton et al., 2008; Bølling et al., 2009; Saffari et al., 2013), iv) to explain the mechanism of smoke particles aging and internal mixing with ambient aerosols (Capes et al., 2008; Jolleys et al., 2012; Zauscher et al., 2013), and v) to describe the influence of smoke particle emission and aging on the physiochemical property changes of ambient aerosols (e.g., chemical compositions, redox activity, morphology, light scattering-absorption, hygroscopicity, etc.) and also the influence on the atmospheric chemical process (e.g., diurnal O_3 formation, nocturnal chloride and NO_Y chemistry, HONO chemistry, etc.) (Cape et al., 2011; Jaffe and

Wigder, 2012; Saffari et al., 2013; Li et al., 2015; Nie et al., 2015; Bougiatioti et al., 2016; Hu et al., 2016). Field observations have a definite advantage over laboratory study, as the investigations are conducted on-site close to the actual burning (Li et al., 2007; Ding et al., 2013a, 2013b; Brito et al., 2014; Liu et al., 2014). However, some unfavorable factors such as variable environmental conditions, random burning process, inevitable chemical contaminations and ultra-low concentration of target components due to atmospheric dilution also add the challenges to the practical work, and the deviations between field research and laboratory study were also reported (Dhammapala et al., 2007; Mohr et al., 2009; Aurell et al., 2015; Carrico et al., 2016). Actually, results from field investigation incorporated with laboratory studies and numerical simulations would supply more precise and thorough results (Huang et al., 2012a; Calfapietra et al., 2016; Huo et al., 2016; Pokhrel et al., 2016).

Field fire can be classified as agricultural open burning, forest and basin fire in term of burning activity, scales, and fuel issues (e.g., straw stack burning, residue field burning, grassland fire, forest fire, biofuel waste open burning) (Li et al., 2003, 2007; Martins et al., 2009; Huang et al., 2012b; Da Rocha et al., 2005). In China, in-situ fire studies have mainly focused on the agricultural straw burning, and field observations monitor and discriminate pollutants from BB via the methods including but not limited to instrumental on-line measurements and offline analysis of PM and gas samples (Du et al., 2011; Rose et al., 2011; Ding et al.,2013a; Huang et al., 2014; Wang et al., 2015a; Yao et al., 2016a). Chemical markers or signals (e.g., potassium, levoglucose, mannosan, galactosan, and some non-methane VOCs), diagnostic ratios (e.g., K^+/ EC, OC/EC, char-EC/soot-EC, ratios of PAHs and some gaseous species), and specific target particles (e.g., soot, tar ball, crystal KCl particles) are commonly used to trace BB in the field and help make source apportionment of BB emissions (Guo et al., 2004; Bo et al., 2008; Han et al., 2009; Li and Shao, 2009; Wang et al., 2011; Fu et al., 2012; Saffari et al., 2013; Li et al., 2015; Li et al., 2016a). BB as a potential source of ambient primary and secondary carbonaceous aerosol has been widely reported, and BB events have also been found to be highly correlated with heavy pollution events like haze, fog, NPF, and photochemical smog (Kaul et al., 2011; Li et al., 2011b; Wang et al., 2013; Yang et al., 2015; Wang et al., 2016a).

By a synergy of ground-based monitoring and satellite-lidar observation, three typical haze types in Shanghai are identified as the secondary inorganic aerosol (SIA) pollution, dust, and BB (Du et al., 2011; Huang et al., 2012d). Even in the dust haze (dust storm) episode, soot and tar ball internally mixing with K-rich particles are encountered frequently, and heterogeneous reactions occur to convert Cl^- into SO_2^- and NO^- during smoke plume transportation, while BB emissions also facilitate solubility of iron in dust (Fu et al., 2012; Fu et al., 2014). Field studies in multi-cities over China suggest that severe haze episodes are driven to a large extent, by secondary organic and inorganic aerosols (SIA and SOA are of similar importance). BB primary emissions contributed 5–20% of PM2.5 mass generally during haze episodes, while VOCs and SO_2-NO_x-NH_3 from BB may present even more contribution to SOA and SIA (Streets et al., 2003; Huang et al., 2014). Apart from elevating aerosol mass concentration, BB plume suppresses nucleation mode and CCN activity of ambient particles, while increases

field AOD and absorption angstrom exponent (AAE) in mixing and transportation process (Agus et al., 2008; Nowak et al., 2010; He et al., 2015).

7.2.2. Satellite remote sensing

The ground-based instruments are very useful for continuous measurements of local and regional properties of atmospheric aerosols, which play an important role in the estimation of BB aerosol's impact on the Earth's radiation budget and, hence, local and regional climate (e.g. Badarinath et al., 2009; Mielonen et al., 2013). However, for the global monitoring of the BB aerosol properties, in general, and fire spots, emissions, concentrations, distribution, vertical profiles and long-range transport, in particular, multiple satellite sensors such as MODIS (Moderate Resolution Imaging Spectroradiometer), MISR (Multi-Angle Imaging Spectroradiometer), CALIPSO (Cloud-Aerosol Lidar Infrared Pathfinder Satellite Observation), OMI (Ozone Monitoring Instrument), MOPITT (Measurements of Pollution in the Troposphere) and AIRS (Atmospheric Infrared Sounder), among others are commonly used. These sensors help in studying the BB aerosols by retrieving various products of aerosol optical and physical properties, precursors and trace gases, vertical profiles, fire count, Fire Radiative Power (FRP), smoke-plume characteristics and long-range transport and mapping of the burned areas (e.g. Guan et al., 2010; Kaskaoutis et al., 2011; Witte et al., 2011; Giglio et al., 2013; Kumar et al., 2011, 2013; Mielonen et al., 2013; Qin et al., 2014; Kumar et al., 2015; Vadrevu et al., 2015; Zhu et al., 2016a). The satellite monitoring over the vulnerable regions of the Earth for any kind of burning (i.e. tropical wildfires, boreal forest fires, peat fires, agricultural burning, waste-material burning, bio- fuel burning, etc.) gives important information about the number of fire count (FC), location of fires, smoke-plume distribution and its injection height, which are the key factors for local/regional meteorology and cli- mate, as well as for ecosystems, socio-economic and human health-related issues (Barnaba et al., 2011; Hodnebrog et al., 2012; Kaskaoutis et al., 2012, 2014; Chakrabarty et al., 2016).

The MODIS on-board the Terra (known as EOS AM-1) and Aqua (known as EOS PM-1) satellites is a key instrument for identification of the BB activities over the globe. The MODIS (Terra + Aqua) retrievals provide daily global AOD, fine mode fraction (FMF) and Ångström exponent (AE) over land (0.47, 0.55 and 0.66 μm) and Ocean (0.47, 0.55, 0.65, 0.86, 1.20, 1.60 and 2.10 μm). Based on the relationship between AOD vs FMF and AOD vs AE, several researchers have investigated the aerosol types such as urban/industrial, BB, dust, urban mixed one, etc. (Kaskaoutis et al., 2012; Pathak et al., 2012; Levy et al., 2013; Kumar et al., 2015; Zhu et al., 2016a). Furthermore, the MODIS global monthly fire location product (MCD14ML; spatial resolution 1 × 1 km) is available from the University of Maryland website (*ftp://fuoco.geog.umd.edu*), and contains the information about the geographical location of fires and their intensity (Giglio, 2010). The fire-detection algorithm (Giglio et al., 2003) uses the variation in the brightness temperatures obtained from the MODIS measurements of 4 and 11 μm channels (Matson and Dozier, 1981; Dozier, 1981) in order to detect the fire locations over the globe. The fire detection strategy is based on the absolute detection in the cases when fire strength is sufficiently

high and on the detection relative to the background thermal emissions of the surrounding pixels (Justice et al., 2002). This algorithm examines each pixel of the MODIS swath and assigns them into the following classes: i) missing data, ii) cloud, iii) water, iv) non-fire, v) fire and vi) unknown. MODIS provides data for fire location, fire count detection confidence and FRP. Further details about the data description and validation are presented in the literature (Giglio, 2010; Giglio et al., 2013; Justice et al., 2006). In the present study, we have used the FC retrievals from Terra-MODIS during January 2001–December 2015 and analyzed their seasonal spatial distribution over south, southeast and east Asia (Fig. 7.2) with 80% confidence level. Furthermore, the seasonal mean MODIS AOD550 spatial distribu- tions from Terra (MOD08_D03.006) and Aqua (MYD03_D3.006) are examined over the same area in order to reveal the influence of BB on seasonal variability of AOD550 (Fig. 7.3).

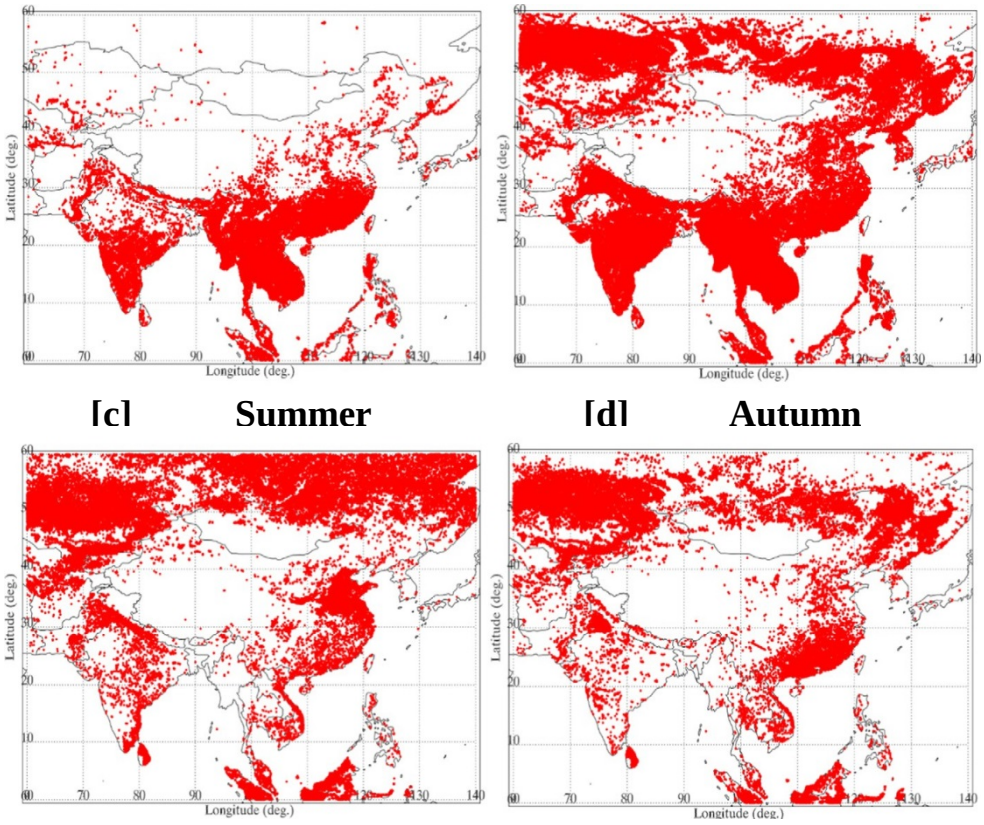

Figure 7.2 Seasonal distribution of MODIS (Terra + Aqua) forest fire counts at 80% confidence level during January 2001 to December 2015. (Source: ftp://fuoco.geog.umd.edu)

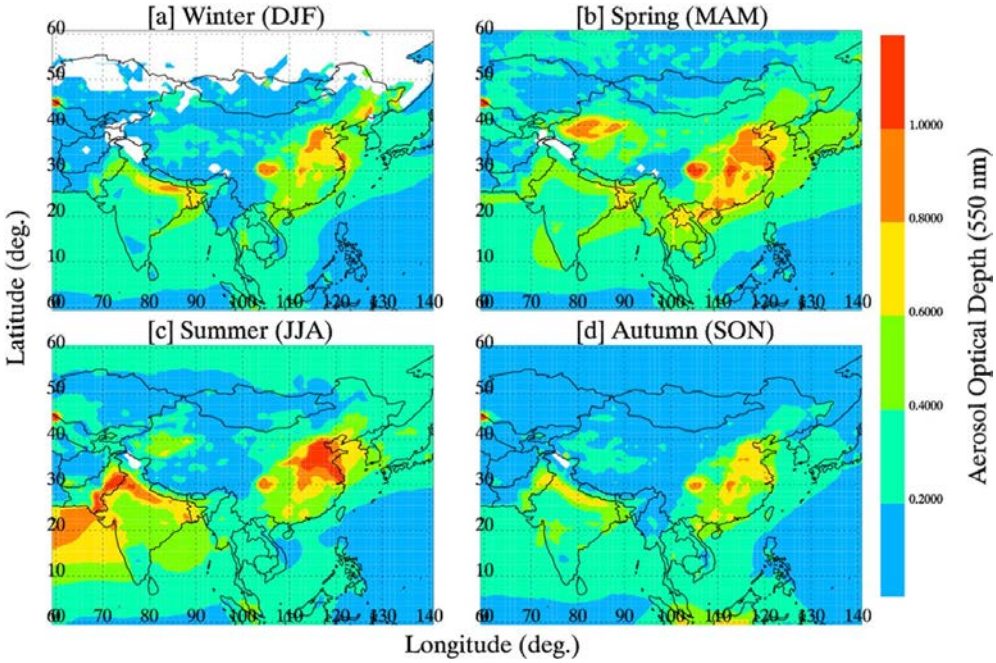

Figure 7.3 Seasonal distribution of aerosol optical depth (AOD) at 550 nm during January 2000 to December 2015 via using the Moderate Resolution Imaging Spectroradiometer (MODIS) Terra + Aqua satellite (Source: http://giovanni.gsfc.nasa.gov/giovanni/).

As shown in Fig. 7.2, the fire counts cover nearly the whole South and Southeast Asian region in winter and spring due to extensive forest fires during the dry seasons. During the summer monsoon, the fire counts are much less over India and Indochina due to extensive rainfall, while they significantly increase over Siberia due to the seasonal forest and peat fires. Over eastern part of China, the fire counts are really large, especially in winter and spring. Arid regions like Tibetan Plateau, central and western China exhibit very fewer fire counts as shown in Fig. 7.3 (Huang et al., 2012b). The seasonal mean spatial distributions of AOD550 from Terra and Aqua MODIS retrievals exhibit great similarities for each month, with the highest AODs in winter to be detected over the densely populated regions of Indo-Gangetic Plains (IGP), central and eastern parts of China. The large anthropogenic emissions from the highly urbanized and industrialized centers over this region contribute to the high AODs, which are the highest over the globe. During spring, high AODs are also shown over the Taklimakan desert in western China, while in summer the AOD increases significantly over the western IGP and the Arabian Sea due to enhanced desert-dust emissions. In general, autumn is characterized with the lowest AODs over the region, with the same hot-spot areas. The seasonal-mean spatial distribution of AOD550 shows that the fire counts do not seem to affect the aerosol loading and distribution of seasonal scales. Sparse fire and the associated plumes on certain days have been shown to strongly affect the local/regional AODs (Arola et al., 2007; Kaskaoutis et al., 2011), but without a strong influence on seasonal aerosols. Therefore, the seasonal mean AOD spatial distribution over the South and East Asia is mostly controlled by the local anthropogenic emissions and the large influence of sand and dust storms during the spring and

summer. However, at local scales, and especially over the Indochina, the increased BB during the winter and spring seems to affect the AOD distribution (note also the lower AODs associated with much lesser fire counts during the summer).

The CALIOP (Cloud-Aerosol Lidar with Orthogonal Polarization) is an instrument onboard the CALIPSO satellite, which provides new insight into observing the vertical profile of aerosols and clouds at 532 and 1064 nm, and the linear depolarization profile at 532 nm (Winker et al., 2003; Omar et al., 2009; Winker et al., 2009). The CALIPSO level 1 profiles at 532 nm (version 3.30) are commonly used to monitor the long-range transport of the BB aerosols, providing information mainly on the concentrations and shape (via attenuated backscatter coefficient and Volume Depolarization Ratio, VDR), vertical profiles and injection height of the smoke plumes (Turquety et al., 2009; Guan et al., 2010; Kaskaoutis et al., 2014). Furthermore, the CALIOP products can differentiate the aerosol types, by considering "smoke" in their retrievals for the easier monitoring of the biomass-burning aerosols.

The AIRS are on board the Aqua satellite (with MODIS) and part of the A-Train constellation, covering the entire Earth from pole to pole twice a day (*http://airs.jpl.nasa.gov/mission/description/*). It provides very high spectral resolution measurements of emitted radiation in three spectral bands (3.74–4.61, 6.20–8.22 and 8.80–15.40 μm) using 2378 channels. In addition, four channels in the visible/near infrared range (between 0.4 and 1 μm) are used for detecting the cloud cover and its spatial vari- ability. The spatial resolution of the measurements is 13.5 km at nadir. AIRS standard products include temperature, water vapor mixing ratios and trace-gas concentrations (e.g., O_3, CO, CO_2, CH_4), which are usually products or by-products from biomass-burning processes (Galanter et al., 2000; Lawrence and Lelieveld, 2010; Mielonen et al., 2013; Kumar et al., 2013). In the present study, level 3 daily carbon monoxide (CO) data from both daytime ascending orbit of AIRS with a spatial resolution of 1° × 1° in order was used to assess the spatial distribution of CO over south and East Asia on a seasonal basis during 2003–2015 (Fig. 7.4). In accordance with the FC, the highest CO levels were found in spring over the tropical regions of India and Indochina, eastern China and Siberia. However, the high CO concentrations over the same regions in winter did not coincide with the very fewer fire counts in Siberia. Also, the CO is less during the summer monsoon over the tropical regions due to extensive rainfall and less number of fires, while low level also exhibited over Siberia, despite the tremendous increase in fire counts. Thus, on the seasonal basis, the CO does not coincide so well with the fire counts, especially over Siberia, while better correspondence is shown over the tropical regions of southern India and Indochina.

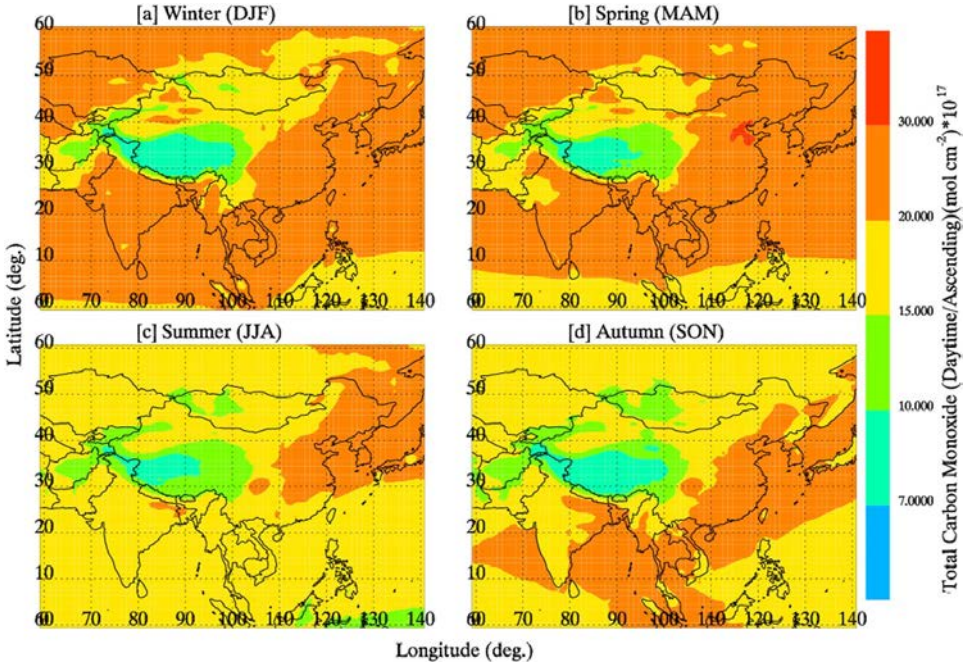

Figure 7.4 Seasonal distribution of total carbon monoxide (daytime/ascending) during January 2003 to December 2015 (Source: http://giovanni.gsfc.nasa.gov/giovanni/).

In addition to AIRS, continuous measurements of regional and global observations of CO are taken from MOPITT, a sun-synchronous polar orbit satellite. The MOPITT makes 14–15 daytime and nighttime passes per day and crosses the equator around 10:45 and 22:45 local time (*http://www.atmosp.physics.utoronto.ca/MOPITT/MOPoverview.html*). The MOPITT retrieval provides the near surface, total column, and vertical profiles of CO at 10 pressure levels between the surface and 100 hPa with a resolution of 100 Pa, which has extensively been used for monitoring of BB emissions (Liu et al., 2006; Kaskaoutis et al., 2011; Kumar et al., 2013; Ding et al., 2015).

7.2.3. Laboratory studies

Laboratory experiments to investigate BB are typically conducted to characterize the performance of domestic heaters, and in particular to quantify emission factors of the heaters operating in different conditions (in terms of burning rate), fueled by different types of wood fuels, and the condition of the wood (dry or wet). As such they are not designed to establish burning conditions similar to those of wide, open fires. Since combustion process is very sensitive to the burning conditions, and a small change in the conditions may results in large variation in the emission factors, it cannot be considered that emission factors obtained from such investigation could be utilized in the qualification of emissions from wild fires.

Several examples of the studies on various types of heaters were reported in the literature since 2000. McDonald et al. (2000) characterized emissions from wood burnings in a fireplace and found that PM2.5 emission factors ranged from 2.9 to 9 g/kg

for softwoods and 2.3 to 8.3 g/kg for hardwoods. In another study, PM2.5 emission factors of birch wood burned in a stove ranged from 0.1 to 2.6 g/kg (Hedberg et al., 2002). Burning wood logs in several combustion systems resulted in PM2.5 emission factors ranging from 0.13 to 1.68 g/kg and particle number emission factors, from 3 × 1015 to 40 × 1016 particles/cm3 (Wieser and Gaegauf, 2000). Calvo et al. (2015) comprehensively investigated combustion of three common southern and mid-European woods, burned in a fireplace and a stove and found that emission factors of some pollutants were similar for both devices for the same woods, but some differed. For example, mean PM2.5 emission factor of the fireplace operating on *P. nigra* as a fuel was 14.0 ± 5.1 g/kg, while of the stove operating on the same fuel, 4.4 ± 1.4 g/kg.

In general, the studies reported in literature showed that the majority of particles resulting from BB were less than 2.5 μm in diameter (Wieser and Gaegauf, 2000; Hays et al., 2002; Hedberg et al., 2002; Ferge et al., 2005). The PM2.5 emission factors have been measured in the range of 0.2 to 12 g/kg (McDonald et al., 2000; Fine et al., 2002; Hays et al., 2002).

Somewhat different was the study conducted by Wardoyo et al. (2006) with an aim to quantify emission factors under laboratory conditions, but to capture the maximum number of parameters which could be controlled in such conditions, and to maintain them at the levels similar to these of wide fires. To do this, Wardoyo et al. (2006) used a commercial stove, but modified for the purpose of these experiments. Therefore the focus was not on the operation of the stove, but on establishing the wide fires burning conditions. Five common tree species found in South East Queensland (Australia) forests: Spotted Gum (*Corymbia citriodora*), Blue Gum (*Eucalyptus tereticornis*), Bloodwood (*Eucalyptus intermedia*), Iron Bark (*Eucalyptus crebra*), and Stringybark (*Eucalyptus umbra*) have been studied (Wardoyo et al., 2006). The results demonstrated that PM2.5 and particle number emission factors depend on the type of tree and the burning rate. The average particle number emission factors for fast burning conditions are in the range of 3.3 to 5.7 × 1015 particles/kg for woods and 0.5 to 6.9 × 1015 particles/kg for leaves and branches (Wardoyo et al., 2006). The PM2.5 emission factors are in the range of 0.14 to 0.21 g/kg for woods and 0.45 to 4.70 g/kg for leaves and branches (Wardoyo et al., 2006). For slow burning conditions, the average particle number emission factors are in the range of 2.8 to 44.8 × 1013 particles/kg for woods and 0.5 to 9.3 × 1013 particles/kg for leaves and branches (Wardoyo et al., 2006). And the PM2.5 emissions factors are in the range of 0.12 to 0.48 g/kg for woods and 3.30 to 4.90 mg/kg for leaves and branches (Wardoyo et al., 2006).

7.2.4. Campaigns for biomass burning

Several campaigns (e.g., CARE-Beijing, PRIDE-PRD, and PEACE-YRB) have been programmed and conducted to investigate regional and large-scale air quality systematically, provided detail information about pollution conditions, physiochemical profile, sources, and atmospheric chemistry. The research supported establishment and enforcement of some environmental policy, and the sound database which accumulated from these campaigns also helped numerical model simulation and further studies.

CARE-Beijing campaigns (Campaign of Air Quality Research in Bei- jing and Surrounding Region) have been operated several times (e.g., CARE-Beijing 2006, 2008, 2013, North China Plain) to help get full view of air pollution in the North China Plain, which highlighted local and transported BB pollutants as a potential source in Beijing and surrounding areas (Ho et al., 2010; Wu et al., 2011; Liu et al., 2012; Zhang et al., 2014b; Zhang et al., 2015b; George et al., 2016).

PRIDE-PRD campaigns (Program of Regional Integrated Experiments of Air Quality over the Pearl River Delta) conducted in 2004 concentrated on in depth characterization of the pollution, and on improvement of the understanding of chemical and radiative process in the atmosphere of the Pearl River Delta region. PRIDE-PRD 2006 focused on the CCN in polluted air and BB smoke near the megacity of Guangzhou. Severe haze episodes were observed in PRIDE-PRD from October 4th to November 5th in 2004, and chemical profile of the haze aerosol indicated a great contribution from BB (Andreae et al., 2008; Zhang et al., 2008d). Efficiency spectra, size-resolved chemical composition, mixing state, optical scattering coefficient, and CCN effective activity of aerosol particles were measured online using various online measurement techniques from 1 to 30 July 2006 at a rural site of Guangzhou. The study found that strong local BB emissions and mixing decreased ambient average hygroscopicity parameter κ from 0.3 to 0.2, which is similar to the characteristic value for freshly emitted smoke from agricultural fires, of which soot particles with low hygroscopicity contribute a substantial portion. Moreover, CCN activity for aerosol was parameterized with volatility and chemical characters, bi- nary function between bulk κ and number fraction of low volatility particles or ensemble particle chemical mass fraction was extrapolated from the linear relationship of size-dependent CCN activity and volatile fraction or chemical compositions, and the functions fitted well for aerosol particles, including or excluding BB plume. The results confirmed that κ value can be more simplified in global and climate modeling (Nowak et al., 2010; Gunthe et al., 2011; Rose et al., 2011).

PEACE-YRB 2015 (Program of Extensive Air Quality Research Campaign over the Yangtze River Basin in 2015) organized by the Fudan University in collaboration with many international institutions, including Queensland University of Technology, Cambridge University, Manchester University and Nanjing University was conducted from November 20th to December 5th, 2015. The campaign was carried out both on board and land using the well-equipped ship, which sailed from Shanghai Port to Wuhan City in round trip through a total distance of 2150 km, as well as a mobile van, which followed on the ground.

Extensive smoke emissions from domestic use and field burning were distinguished by preliminary analysis, and were showed to make up a considerable contribution to the Yangtze River Basin pollution in mixing with engine exhaust from vehicle and ship (Morawska et al., 2016; Ouyang et al., 2016). Detailed emissions and pollution conditions will be elucidated in the later publications.

7.3. Types of biomass burning

7.3.1. Forest fire

Forests are the main part of the terrain ecosystem and play an important role in maintaining the balance of terrain ecosystem. The forest coverages are very limited and it accounts for only 21% of the mainland of the nation (Zhang et al., 2011b; Li et al., 2011a). The seventh National Forest Resources Inventory during 2004–2008 shows that the forest area was enhanced at ~200 million ha stocking ~14/m^3 billion and ranking fifth in the world after Russia, Brazil, Canada and USA (Li et al., 2004; Li et al., 2011a). During the last few decades, due to the deforestation, number of forest fires and burned area has drastically increased (Zhou and Lu, 2000; Shao, 2000). One of the largest forest fire, well known as black dragon fire, occurred in northeast China during May 1987, where the areas over 1.3 million ha (Cahoon et al., 1994) of forest were charred. The forest fire or wildland fires have become an important and more frequent issue in China (Kong et al., 2003), and the Indo-China peninsula is one of the most active fire hotspots in the world, which is a matter of great concern because of the high population densities (Gautam et al., 2013; Johnston et al., 2015). Prior to the onset of monsoon, the Indo-China Peninsula region is the witness of intense BB in the form of forest fires, which significantly increase the aerosol concentration (Gautam et al., 2013).

Forest fires have had impact on biosphere-atmosphere interface, atmospheric chemistry, composition of ecosystem system and its distribution, environmental degradation and air quality monitoring (Crutzen and Andreae, 1990; Penner et al., 1992; Costanza et al., 1997; Bond and Keeley, 2005; Randerson et al., 2006; Zhang et al., 2011b). They emit large amounts of trace gases (both chemically active and greenhouse gases), non-methane hydrocarbons, and aerosols (Crutzen and Andreae, 1990). These aerosols and pollutants are significantly affecting atmospheric chemistry, cloud properties, Earth radiation budget and cli- mate change, global carbon cycle, ecosystem and biodiversity, vegetation, rainfall, air quality and atmospheric circulation (Crutzen and Andreae, 1990; Ramanathan et al., 2001; Andreae et al., 2004; Liu, 2005; IPCC, 2013). A recent study by Johnston et al. (2015) showed that the forest fire BB was responsible for about 339,000 premature deaths per year. The increasing intensity and spread of forest fires in Asian countries, and their impact on ecosystems and climate change suggest that the real-time monitoring of forest fire activities is essential. Fire monitoring due to high potential hazards associated with forest fires, the ground-based and airborne fire monitoring, space-borne satellite sensors have been widely used to detect and monitor the forest fires (Prins et al., 1998; Justice et al., 2002). Fire monitoring via satellite remote sensing such as MODIS Rapid Response System Global Fire Maps, GLOBSCAR, European Forest Fire Information System, NOAA/AVHRR (the National Oceanic and Atmospheric Administration/the Advance Very High Resolution Radiometer), Landsat, Chinese Feng-Yun series have been widely used to detect the forest fire hot spots and burned areas across China (Zhang et al., 2011b). The MODIS data sets provide a vast temporal coverage along with high spectral (36 bands total) and spatial resolution (250, 500, and 1000 m). In general MODIS provides information on the burned areas and smoke, and is used to detect active fires.

7.3.2. Agricultural straw open burning

China is among the major agricultural nations in the world. Agricultural crop production generates tremendous amounts of agricultural crop residues such as rice, wheat, and corn straws etc., which account for 17.3% of the global crop residues production and rank the first in the world (Bi et al., 2010). During the summer/autumn harvest season, a large amount of agricultural straws are removed by burning in a short period in order to prepare the next crop planting. Open burning is the most convenient and less expensive way to eliminate agricultural straw. In China, studies on gaseous and particulate pollutant emissions from open burning of agricultural straw have been presented in previous publications (Li et al., 2007; Zhang and Smith, 2007; Zhang et al., 2008a; Zhang et al., 2011a; Huang et al., 2012a; Tian et al., 2015). Efforts have been also made to characterize particle number emission factors and size distributions from agricultural straw burning in the laboratory simulation experiments (Hays et al., 2005; Zhang et al., 2008a; Zhang et al., 2011a). Particle size distribution from agricultural straw open burning is mainly dominated by an accumulation mode, with a count median diameter of 0.10–0.15 μm (Zhang et al., 2011a). In addition, trace gas emission inventories (CO_2, CO, NO_x and BC etc.) from agricultural straw open burning had been estimated in China (Zhang et al., 2008a; Huang et al., 2016; Sun et al., 2016a).

In addition to emission characteristics, understanding of the impact of agricultural straw open burning on urban and regional air quality is essential. In China, especially during and shortly after the harvest seasons, open burning of agricultural straw has a significant impact on urban and regional air quality. In extreme cases, agricultural straw open burning would trigger the explosive growth of secondary PM2.5 and accelerate the heavy haze formation in the urban and regional atmosphere (Nie et al., 2015; Xie et al., 2015). However, detailed information on the effects of smoke from agricultural straw open burning on urban and regional air quality is still rare (Zhang et al., 2010a; Li et al., 2010a). It is well known that the impact of agricultural straw open burning on heavy haze formation during and shortly after the harvest seasons is complex, and not only contributes to primary PM2.5 emissions but also includes the potential contribution to secondary PM2.5 forma- tion. For instance, during the process of smoke plume transport, organic compounds (such as VOCs) in the presence of NOx can be oxidized to generate secondary organic aerosol (SOA) (Wang et al., 2009a, 2009b; Li et al., 2014a). Similarly, atmospheric gases, such as SO_2 and NO_X, can also be oxidized to form the secondary inorganic aerosol (SIA, such as sulfate and nitrate) (Cheng et al., 2013; Zha, 2013; Tao et al., 2013; Cheng et al., 2014a, 2014b; Chen and Xie, 2014; Zhang et al., 2016a, 2016b, 2016c). Heterogeneous reactions in BB plume also played important roles in the formation of HONO (Nie et al., 2015). High concentration of NO_2 together with high concentration of NH_3 in the BB plume has been found to enhance sulfate formation through aqueous-phase reactions and to produce HONO as a by-product (Nie et al., 2015). Both SOA and SIA are the most important components of secondary PM2.5. Therefore, when smoke plume is transported to the urban atmosphere, secondary PM2.5 can rapidly increase in a short time under the stagnant weather conditions, and can further aggravate haze pollution and/or result in increase of the frequency of heavy haze pollution through the interactions

between physical and chemical processes (Ding et al., 2013a; Huang et al., 2016; Ding et al., 2016a). That is why the heavy haze pollution often happened in North, Central and eastern China, especially during and shortly after the harvest season.

7.3.3. Wood and straw combution as fuel

Approximately half of China's population lives in rural areas and use biomass fuels (such as wood and straw) as the domestic fuel for cooking/ heating. Biomass fuels burnt in low-efficient stoves would produce substantial air pollutants and increase fine particulate matter (PM2.5) exposure in the indoor environment (Wei et al., 2014), which is associated with adverse health impacts such as pneumonia, tuberculosis and chronic obstructive pulmonary disease (Pope et al., 2002). In China, household combustion of wood and straw, is the dominant source of indoor air pollution in rural areas and contribute significantly to human health burden (Zhang et al., 2012, 2014a). Household combustion methods of both wood and straw in rural China are of low energy conversion efficiency and result in high pollutant emissions (Zeng et al., 2007).

Characteristics of pollutants from wood and crop straw combustion as domestic fuel have been studied in China by several research groups (He et al., 2005; Jin et al., 2005; Shen et al., 2010; Zhang et al., 2012; Zhang et al., 2014a). Jin et al. (2005) monitored indoor air pollutant (respirable particles, CO and SO2) emissions from wood and straw burning in the rural households of Inner Mongolia and Gansu provinces of China. He et al. (2005) measured multiple pollutant emissions from wood and straw burning in the rural household of Guizhou and Shaanxi provinces of China. Shen et al. (2010) calculated emission factors of particulate matter (PM) and elemental carbon (EC) from domestic crop straw burning in typical household stoves. Zhang et al. (2012) measured chemical and size characteristics of particulate matter from domestic wood burning in rural areas of southwestern China. Zhang et al. (2014a) conducted field experiments to measure indoor emissions of carbonaceous aerosols (OC and EC) and other air pollutants (CO, PM1, PM2.5 and PM10) from household wood burning in southwest China.

As noted by a number of studies (Zhang et al., 2012; Zhang et al.,2014a), low combustion efficiency leads to high emission factors for wood and straw burning. High emissions do not necessarily mean high exposures unless they reach human breathing zones. However, available evidence indicates that total exposure to combustion-derived fine particles from domestic use of wood and straw in indoor environment is larger than that from all outdoor sources (Zhang and Smith, 2007; Fullerton et al., 2008). Epidemiological studies have shown that exposure to high levels of indoor PM2.5 contributed to a consistent increase in cardiac and respiratory morbidity and mortality (Pope et al., 2002). For instance, pulmonary effects of indoor PM2.5 include the triggering of inflammation in the smaller airways, which can result in the exacerbation of asthma and chronic bronchitis, airway obstruction, and decreased gas exchange (Nel, 2005). Moreover, high concentrations of PM2.5 in the indoor environment have been regarded as a cardiovascular risk factor that is associated with heart attacks, stroke, heart rhythm disturbances, and sudden death. Inhalation of fine particles elicits proinflammatory effects, cytokine production, and enhancement of allergic responses in the upper and lower airways (Perez-Padilla et al., 2010).

7.3.4. Miscellaneous

In China, annual biomass waste productions contain ~ 2.6 × 105 GWh energy that equals to the energy storage of ~ 3.65 × 108 tons coal (Chen et al., 2009; Zhang, 2011; Koppejan et al., 2012). Apart from traditional field burning and domestic use of biomass waste, co-firing with coal or municipal solid waste (MSW) in power stations or incineration plants is indeed a practical method to deal with biomass waste, and many studies have focused on the development of combustion technologies and emission control of pyrogenic pollutants (Waldheim et al., 2000; Nussbaumer, 2003; Tian et al., 2005). Somewhat comparable heat density of biomass to fossil fuels such as coal and petrochemical products implies that biomass fuel represents a considerable amount of renewable energy (Zhang et al., 2005), and scientific utilization of biomass energy would partly relieve shortage of fossil fuels and ameliorate the serious atmospheric pollution (Baxter, 2005; Koppejan and Van Loo, 2012). Robinson et al. (2003) suggested that biomass co-firing with coal is a possible way to achieve significant near term CO_2 emission mitigation through economic analysis. Ross et al. (2002) found that co-combustion of coal and biomass can decrease emission factors of multiple gaseous and particulate pollutants. However, a mixture of pollutants from the co-firing process can be more complex. Zhang et al. (2009c) observed Pb-chlorine co-enriched particles that are formed from waste incineration, as high concentrated HCl in the gas stream from the combustion of garbage (chlorine-rich plastic, biomass, etc.) has volatile effect on Pb to form $PbCl_2$. Wang et al. (2006, 2007b) and Jiménez and Ballester (2005) found distinctly different particle size distribution and PM chemical profiles from co-firing of coal and biomass compared to that from the sole fuel combustion.

7.4. Pollutants from biomass burning

7.4.1. Particulate matter

Particulate matter refers to a mixture of solid particles and liquid droplets in the air (Hinds, 2012), with a varying physical and chemical properties. PM is a dominant contributor to the air pollution in China (Fang et al., 2009). In particular, Beijing-Tianjin-Hebei (BTH) Province, the Yangtze River Delta (YRD) and the Pearl River Delta (PRD) are subject to severe PM pollution. Daily average PM2.5 concentrations during severe haze periods in 2013 are 159, 91, 69 and 345 μg/m^3 for Beijing, Shanghai, Guangzhou and Xi'an, respectively (Huang et al., 2014). All PM2.5 values are significantly higher than mean concentration of 25 μg/m^3, recommended by the World Health Organization (WHO). In order to address serious PM pollution issue, the Chinese government announced the long-term plan to reduce the PM2.5 concentration by 25%, 20%, 15% and 10% compared to 2012 levels by 2017, in BTH, YRD, PRD and other cities, respectively (*http://www.gov.cn/zwgk/2013-09/12/content_ 2486773.htm).* For instance, annual value for PM2.5 in Beijing is targeted as 60 μg/m^3, which would be still high compared to the values recommended by WHO (annual mean of 10 μg/m3), but a big step in air pollution regulation in China. It will certainly be a challenge to achieve this level because of the heavy pollution

prevailing currently, for example, it was observed in Beijing in 2014 that PM2.5 mean annual value was 86 μg/m^3 (Zhang et al., 2016a).

Carbonaceous material

Dominant Dominant PM fraction emitted into the atmosphere is carbonaceous material (Chan and Yao, 2008), which is composed of organic carbon (OC) and EC. Carbonaceous species influences Earth's radiation balance. While BC absorbs incoming solar radiation contributing to increased atmospheric temperatures, OC cools the atmosphere by scattering the solar radiation (Penner et al., 1998; Haywood and Boucher, 2000). Carbonaceous particles can efficiently act as CCN, having an influence on cloud formation and their properties (Hallett et al., 1989; Roberts et al., 2002; Reid et al., 2005b). They can also contribute to various health issues (Pope and Dockery, 2006). Emissions of carbonaceous matter in China have increased by approximately 20% from 1996 to 2010 (Lu et al., 2011). It is estimated that a portion of this fraction can vary between 20% and 50% of PM2.5 mass (Cao et al., 2007).

In general, the dominant particle-phase fraction detected in BB emissions is found to be carbonaceous matter (Formenti et al., 2003; Bond et al., 2004; Reid et al., 2005b; Hallquist et al., 2009; Fu et al., 2012, 2014; Li et al., 2016a, b). In fact, BB combustion sources are considered as the largest contributors to the primary carbonaceous particles in the atmosphere (Hallquist et al., 2009; Bond et al., 2004; Crutzen and Andreae, 1990). Many studies investigated the dominant sources of PM2.5 and carbonaceous species in China, mostly using the offline sampling technique in urban Beijing region (Zheng et al., 2005; Song et al., 2006; Song et al., 2007; Wang et al., 2007a, 2007b; Wang et al., 2009a; Cheng et al., 2013; Yu et al., 2013a; Cheng et al., 2014a) with some of them illustrated in Table 7.1. For instance, Positive Matrix Factorization (PMF) source apportionment performed on data collected over the whole year 2000 in Beijing, shows that on average 11% of PM2.5 was influenced by BB activities (Song et al., 2006). Using the same source apportionment method, Yu et al. (2013a) observe a similar con- tribution in Beijing in 2010. According to studies summarized in Table 7.1, the contribution of BB activities can go up to 19%, 25% and 37% in autumn, winter and summer months, respectively. It is observed that BB is one of the main sources that contribute to fine particle and carbonaceous emissions (besides traffic and coal combustion sources) in China (Chan and Yao, 2008). Moreover, in recent years source apportionment has been performed on the organic aerosol (OA) data collected by Aerosol mass spectrometer (AMS) using mostly PMF.

Table 7.1 Source apportionment studies including location (and type), season (and date), average contribution of BB to PM2.5,OC (OA), EC and average values for potassium and levoglucosan are given in table; Index next to the reference refers to BB activities a) Open field post-harvest agricultural BB b) softwood and stalks burning for heating.

Location Location type	Season/date	Average BB to $PM_{2.5}$ (%)	Average BB to OC (%)	Average BB to EC (%)	Average K^+ conc. ($\mu g/m^3$)	Average levoglucosan	Reference
PRD (Guangzhou) urban/suburban	(Autumn) 6-31 Oct 2004	4.0-19.0%/3.0- urban/suburban			2.26 ± 0.50/1.70 ± urban/suburban	0.20-0.66/0.12-0.95 urban/suburban	Wang et al.
BTH (Beijing) urban	(Summer, Autumn, Winter) 25 July-5 Aug 2002 27 Oct-3 Nov. 2002 3-10 Jan 2003					0.03, 0.12 and 0.08/0.07, 0.24, 0.15 for summer, autumn and	He et al. (2006) [a]
YRD (Shanghai) urban	(Summer) 28 May-3				2.84		Huang et al. (2012a, b) [a]
BTH (Beijing)	June 2009 (Summer and winter)	8.4% and 24.9% summer	11.7%, 9.9% and 26.1% summer			0.08, 0.17 and 0.68 summer 2005,	Wang et al. (2009b) [a, b]
urban	2-31 Aug 2005 16 Aug – 10 Sep 16 Jan-2 Feb 2007	2006 and winter 2007	2005, summer 2006 and winter 2007			summer 2006 and winter 2007	
BTH (Beijing) urban	(All Seasons) Jan, Apr, July and Oct 2000	annual average of 11%					Song et al. (2006) [a]
BTH (Beijing)	(Summer and winter)	13% and 15% in summer				0.31 and 3.10 in summer and	Song et al. (2007) [a, b]
Urban (6 sites)	11-19 Aug 2004 11-19 Jan 2004	and winter				winter	
BTH (Beijing)	(Summer and winter)		~50%	~50%	1.74 ± 2.29 and 2.42 ± 5.86 in	0.23 ± 0.37/2.30 and 0.59	Cheng et al. (2013) [a, b]
urban	3 June-23 July 2011 1 Dec-30 Jan				summer and winter 5.81 ± 2.75 (for episode)	±0.42/1.94 summer and 0.75 ± 0.68 (for summer episode) and annual 0.43 ± 0.44	
YRD	(Summer)	37%	70%	61%	1.6-4.9 (measured at three sites)		Cheng et al. (2014) [a]
urban (5 sites) BTH (Beijing)	28 May-6 June 2011 (All	5.8 $\mu g/m^3$; 11.2%			annual average of 2.22		Yu et al. (2013) [a]
urban	1 Jan-31 Dec 2010	4.1, 5.8 6.1 and 7.1 spring, summer, and winter			1.88, 2.09, 2.14 and summer, autumn		
PRD (Hong Kong) urban	(Autumn) 25 Oct-2 Dec 2009		24.1% (AMS)				He et al. (2011) [a]
PRD (Kaiping) rural	(Autumn) 12 Oct-18 Nov 2008		24.5% (AMS)				Huang et al.
YRD (Jiaxing) regional	(Summer and Winter) 29 June-15 July 11-23		30.1% in winter (AMS)				Huang et al. (2013a) [a]
YRD (Nanjing) urban	December (Summer and 1-15 June 2013 15-30 Oct 2013		15% and 8% in summer and autumn (AMS)				Zhang et al. (2015b) [a]
BTH (Beijing) urban	(Autumn) 14 Oct-12 Nov 2014		12-19% (AMS)				Xu et al. (2015) [a]

The significance of BB emissions (mainly due to burning of crop residues during harvesting periods) in urban and rural areas of China is shown through the high contribution of PMF-resolved BB-related factors. Similar BB OA contribution is found for urban and rural PRD area (24%), and is smaller in urban Beijing (12–19%) and Nanjing (8%) in the autumn period (Zhang et al., 2010a; He et al., 2011a; Huang et al., 2011; Zhang et al., 2015b; Xu et al., 2015). A significant contribution of the BB-related organic aerosol is also found in the winter period (30%) and over the summer months (15%) (Huang et al., 2013a; Zhang et al., 2015a). As it can be seen, there is significant seasonality in BB activities and contribution to PM pollution in China. BB contribution seen through increased PM2.5 and its constituents is highly seasonal in magnitude, but present over the whole year. The PM2.5 increase in autumn and spring is mainly attributed to BB from crop residues burning. In late September and October harvesting takes place and then contribution of BB is found to be the highest in North China (Duan et al., 2004; Zheng et al., 2005; Yu et al., 2013a; Zhang et al., 2015c), which is different from an early summer maximum in East China (Ding et al., 2013ab). Over the summer months BB contribution from wheat straw burning is significant, while winter PM pollution is mainly driven by coal combustion sources that are predominantly used as heating systems, although BB contribution can be significant (Li et al., 2008; Yu et al., 2013a). Apart from seasonal differences, the portion of aerosol mass influenced by BB varies depending on the region of China. Huang et al. (2014) illustrate the higher BB contribution in Guangzhou and Xi'an (5–9% of PM2.5) compared to Beijing and Shanghai (4–7% of PM2.5).

The main component of smoke submicron carbonaceous mass is the organic aerosol fraction that can go up to 90% (Bond et al., 2004). Global annual emission of OC and BC emitted in open fire events is estimated to be approximately 70% and 40%, respectively (Bond et al., 2004). Studies on both urban and rural areas of Beijing show that during intense BB pollution episodes, more than a half of OC and EC could be from smoke emissions (Duan et al., 2004; Cheng et al., 2013; Cheng et al., 2014b; Yao et al., 2016a).

Other important particulate components

Study has confirmed Levoglucosan-like species (levoglucosan, mannosan, galactosan) are anhydrosaccharides formed in the pyrolysis of cellulose and common organic molecular constituents of BB emissions (Simoneit et al., 1999; Li et al., 2016c). Many studies worldwide including China have used levoglucosan (dominant anhydrosaccharide emitted) as a distinctive BB chemical signature (Simoneit et al., 1999; Simoneit, 2002; Fraser et al., 2003; Jordan et al., 2006; Song et al., 2007; Wang et al., 2007a; Zhang et al., 2008c; Wang et al., 2009a; Zhang et al., 2010a). Levoglucosan concentrations considerably vary depending on season and region (Table 7.1). For instance, He et al. (2006) investigated organic tracer compounds including particulate levoglucosan during all seasons in Beijing. Levoglucosan average mass concentrations were observed to be 0.12, 0.08 and 0.03 $\mu g/m^3$ in autumn, winter and summer, respectively. Considerable higher levoglucosan concentrations are found by Wang et al. (2007a) in autumn (0.1–0.9 μg/m3). Moreover, there is a wide range of levoglucosan in winter (0.08–3.10 μg/m3) and summer (0.03–0.31 μg/m3). Potassium rich particles are observed to be a common fraction of BB emissions

in China (Li et al., 2007; Li et al., 2010b). BB contributes to high potassium levels in smoke emissions and it has been used as a BB tracer (Duan et al., 2004; Wang et al., 2007a; Zhang et al., 2010a; He et al., 2011a; Huang et al., 2012d; Cheng et al., 2013; Yu et al., 2013a; Cheng et al., 2014b; Zhang et al., 2015b). Similar average potassium concentrations can be observed according to studies summarized in Table 7.1. Potassium average value varies from 2.42 to 2.78 in winter, 1.6 to 4.9 in summer and 1.7 to 2.26 $\mu g/m^3$ in autumn months, depending on the monitored areas. Yu et al. (2013a) suggest 2.2 $\mu g/m^3$ for the annual potassium value, based on continuous measurements for one year in Beijing. In contrast to source-specific levoglucosan, water-soluble potassium can indicate particles of more than one origin (Zhang et al., 2010b; Aiken et al., 2010). In the absence of other important sources, such as soil dust, sea salt and meat charbroiling, water soluble potassium can be a satisfactory BB marker (Andreae, 1983; Schauer et al., 1999). Wang et al. (2007a) showed that application of potassium as a reliable smoke tracer has limitations in Guangzhou area during the October BB period due to interferences with meat charbroiling and transportation-related potassium emissions. Fireworks are also found to elevate potassium concentrations (Vecchi et al., 2008; Zhang et al., 2010a). In particular, water soluble potassium has not been considered to be suitable, or at least it should not be used as the only BB tracer during winter in Beijing, which is a season with significant festival fireworks influences (Yu et al., 2013a; Cheng et al., 2013; Cheng et al., 2014a).

Although all results illustrate the significant impact of BB sources on PM pollution over China, until recently, it has been mostly ignored as a significant contributor in pollution inventories (e.g. Zhang et al., 2009a). Zhang and Cao (2015a, b) suggested that regulations on BB emissions should be revised, and it should be scaled down in both urban and rural areas and for open BB as well as in household consumption. It is estimated by Cheng et al. (2014b) that PM2.5 level could be reduced by 47% in the YRD region if open post-harvest BB activities were banned, suggesting significant benefits for the environment and human health.

7.4.2. Physical properties of smoke particles

Size distribution

Studies have confirmed BB as a major source of fine particles in the atmosphere, and size distribution of freshly emitted smoke particles resides mainly within the accumulation mode with geometric median diameter (GMD) at 50– 200 nm. Unimodal and bimodal distributions in volume concentration have both been reported, and the discrepancy of GMD and distribution pattern relates to fuel type, combustion environment, burning conditions, measurement technologies, and also aging extent of smoke plumes (Reid et al., 2005b; Capes et al., 2008; Gunthe et al., 2011; Zhang et al., 2011a; Nie et al., 2015; Li et al., 2015). Rapid growth in size occurs immediately after smoke particle emissions, and tens of nanometers per hour increment in GMD has been observed for smoke particles in ambient atmospheric investigations during transport and in aerosol chamber simulations. It has also been found that coagulation is the dominant mechanism contributing to particle growth, and that humidity facilitates the process (Reid et al., 2005b; Capes et al., 2008; Li et al., 2015). The ultrafine size enables smoke particles to be efficient CCN/IN and also to deposit deeper in the respiratory system, presenting potential

climate effect and human health hazards, respectively, while changes in size distribution alter the optical properties, increasing the single scattering albedo (SSA) as smoke particles increase towards sizes where scattering is more efficient (Li et al., 2002; Delfino et al., 2005; Dusek et al., 2006; Pierce and Adams, 2007; Araujo et al., 2008; Gunthe et al., 2011). Atmospheric aging of smoke particles has a direct impact on particle size and chemical composition changes; changes in particle composition and morphology associated with gas-to-particle transformation and internal mixing are also shown to increase the SSA and light extinction coefficient (Abel et al., 2003; Capes et al., 2008).

Hygroscopicity

Hygroscopicity of smoke particle has been characterized using ensemble (e.g., Hygroscopic-Tandem Differential Mobility Analyzers, H-TDMA; scanning mobility CCN counter) and single-particle techniques (e.g., TEM, electrodynamic balance , and optical tweezers) to denote as hygroscopic growth factor (GF) and hygroscopicity parameter κ (Semeniuk et al., 2007; Lewis et al., 2009; Li et al., 2016; Rickards et al., 2013; Rose et al., 2011). κ parameter is commonly used to link hygroscopicity and CCN activity of particles, which displays as a function of particle size and chemical compositions, while consistency between κ estimated from hygroscopic growth and critical supersaturation measurements is still in study (Petters et al., 2013; Rickards et al., 2013; Su et al., 2010). Smoke particles range from weakly hygroscopic (κ~0.02) to strongly hygroscopic (κ~0.80) (Petters et al., 2009; Dusek et al., 2011; Li et al., 2016), and the values vary with particle source of fuel type and burning condition. Smoldering of biomass produces more hydrophobic organic aerosol like tar ball particles with less κ, while particles emitted from flaming phase under higher temperature contains more inorganic salts with stronger hygroscopicity. Empirical function of $\kappa = f_{inorg} \times \kappa_{inorg} + f_{org} \times \kappa_{org}$ is widely applied in outdoor investigation and aerosol chamber simulation to extrapolate κ_{inorg} and κ_{org} from linear regression of size-resolved bulk κ value and particulate organic and inorganic mass fractions (Dusek et al., 2010; Li et al., 2016; Rose et al., 2010), constant κ_{inorg} (0.6~0.8) and κ_{org} (~0.1) corresponding to inorganic and organic components for ambient aerosol and fresh/aged smoke aerosol are derived, implicating the significant role of alkali species in CCN activity of particles, especially for smoke particles, in which carbonaceous materials dominates. κ_{org} of smoke particles is within the characteristic range for individual organic components from zero of absolute insoluble species like soot to ~0.5 of more hygroscopic oxalic acid, and study has reported humic-like substances (mainly carboxylic acids and levoglucose) are the primary hygroscopic materials in smoke particles (Giordano et al., 2013; Carrico et al., 2008; Wex et al., 2007). κ_{inorg} should deposit in the character of $(NH_4)_2SO_4$-NH_4NO_3 mixtures for ambient aerosol and KCl dominated inorganic mixtures for smoke particles (Li et al., 2016; Rose et al., 2011). Variation of κ responses to chemical composition and physical characteristic changes of aerosol, though photochemical oxidation produces more organic aerosol (OA) and increases O/C ratio in organic components, the change of hygroscopicity is still in doubt (Duplissy et al., 2011; Dusek et al., 2010; Engelhart et al., 2012; Giordano et al., 2013; Jimenez et al., 2009; Mcintire et al., 2010; Rickards et al., 2013). Engelhart et al. (2012) find photochemical processing reduces variability of smoke particle CCN activity, and initial discrete κ parameters converge to a value of 0.2

after several hours oxidation. Tritscher et al. (2011) conclude that the hygroscopicity of SOA will increase from initial formation, then roughly stays constant for the further ripening and oxidation. Heterogeneous reactions of inorganic salts can also change κ_{inorg} and inorganic mass fraction to alter bulk κ of smoke particles eventually (Li et al., 2015). Besides, mixing state, morphology, and size changes during aging (e.g., from initial amorphous non-uniformly internal mixing to more homogeneously mixing state, size growth, mixing with ambient aerosol like sea salts, dust, engine emissions etc.) influence the κ values (Chen et al., 2015; Lewis et al., 2009; Rose et al., 2011; Zhang et al., 2008).

Density

Effective density bonds the aerodynamic diameter of particle and its mobility diameter, it also plays a crucial role in the mass concentration conversion, mass closure calculation and deposition model assessment of aerosol (Beddows et al., 2010; DeCarlo et al., 2004). Smoke particle density as a function of individual compound density and mixing state influence the estimation of bulk hygroscopicity parameter and refractive index of OC and EC content (Petters et al., 2007; Schkolnik et al., 2007; Schmid et al., 2009). Based on different techniques, density can be measured as online size-resolved effective one using APM (Aerosol Particle Mass Analyzer) combined with SMPS/TDMA system (Li et al., 2016; Rissler et al., 2014; Yin et al., 2015), or estimated as bulk density from volume and corresponded mass concentrations for PM (Kostenidou et al., 2007; Pitz et al., 2003), Khlystov et al. (2004) and Schmid et al. (2007) also report an algorithm method to derive particle density via merging coincident aerodynamic and mobility size distributions. Smoke particle densities are reported to vary from 1.0 to 1.9 g/cm^3, Rose et al. (2011) apply density as 1.7 g/cm^3 in ambient biomass smoke plume research, Martins et al. (1996) derive particle density to be 1.5 g/cm^3 from temperate forest fire, Levin et al. (2010) calculate bulk densities of various BB aerosol from chemical compositions to be 1.2–1.9 g/cm^3, Hennigan et al. (2011) assume smoke aerosol density to be 1.3 g/cm^3 throughout photo-oxidation process, while Li et al. (2015, 2016) report densities for fresh particles from crop residues burning to be 1.1–1.4 g/cm^3, which are size and fuel type dependent, and particle densities scale with inorganic mass fractions, with the aging of smoke aerosol, density increase and size-dependence phase out.

Volatility

Volatility is an important property of the organic materials and it determines SOA formation and partition between gaseous and particulate phases (Seinfeld et al., 2012). Volatility of PM has been commonly applied in thermo-optical method based OC-EC measurement, organic chemical compound analysis with thermal-denuder mass spectrometer, and thermogravimetric analysis (Pratt et al., 2009; Seinfeld et al., 2012). Particles' volatility expressed as refractory fraction remaining in term of volume (VFR) and mass (MFR) at a function of temperature are measured using V-TDMA (Volatility-TDMA) system or combined with APM, MS techniques (e.g., ATOFMS, AMS, CIMS), which can help get insight into the mixing state of particle and also thermodynamics mechanisms of carbonaceous aerosol formation and aging processes (Pratt et al., 2009; Tiitta et al., 2010; Tritscher et al., 2011; Wehner et al., 2009). However, volatility of smoke particles from primary emission to atmospheric evolution remain poorly characterized (Li et al., 2016; Rose et al., 2011). Li et al. (2016) combine on-line V-

TDMA-APM and off-line OC-EC measurements for various fresh smoke particles, they conclude VFR-MFR are size and fuel types dependent, and more volatile organic materials have less density and lower OM/OC (organic matter to organic carbon) ratios in the external mixed smoke particles. In polluted urban air, particles with smaller radius and larger volatile fractions at 300^{o}C can be regarded as aged and internal mixed soot particles, and the refractory materials are considered to be mostly engine and combustion sourced soot or EC (Cheng et al., 2009; Sadezky et al., 2005; Wehner et al., 2009). Tan et al. (2016) report external and core-shell mixture of BC particles leading to high σ_{sp} and SSA in the Pearl River Delta regions. Wehner et al. (2009) monitor mixing state of nonvolatile aerosol and the corresponded light absorption during CAREBeijing-2006 campaign. Rose et al. (2011) find external mixed soot particles from biomass combustion to be less volatile and weak CCN-activated. Photochemical oxidation effect on the volatility changes of organic aerosol depends on detailed physiochemical mechanisms, formation of SOA upon oxidation of semi-volatile vapors from primary emissions to less volatile species which transfer to organic aerosol will increase the volatility of preexist particles. Heterogeneous reaction like functionalization and oligomerization decrease volatility of OA, while fragmentation forms species in various thermostabilities albeit mostly at lower volatilities (Reinhardt et al., 2007; Tritscher et al., 2011).

Optical properties

Smoke particles contain major organic materials (over 70 wt. % on average) and a considerable amount of inorganic salts, which present distinct different optical properties (Reid et al., 2005; Seinfeld et al., 2012). Carbonaceous materials like BC-soot particles are the main light absorbers over the entire visible spectrum, light absorption components (like humic species, PAHs, and lignin etc.) enrichment make the rest smoke organic matter to be brown carbon with light absorbing efficiency next to BC, and most absorption by brown carbon takes place in the UV brand and in the short visible wavelength due to the presence of resonant ring structures (Hoffer et al., 2006; Lin et al., 2010; Mustard et al., 2008), while inorganic salts like sulfate and nitrate exhibit specific light scattering character, which can cool the atmosphere by increasing the Earth's reflectivity. To smoke particles, internal mixed or coated inorganic salts can act as lens to enhance light absorption of BC. The net BB radiative forcing is small (0.0±0.2 W/m^2) (IPCC, 2013) but represent great uncertainty in climate effect assessment due to the need to resolve the balance between the positive radiative forcing by BC and BrC and the negative radiative forcing by OC and inorganics. Mass absorption efficiency (MAE) of fresh soot particle is 4-9 m^2/g at 550 nm wavelength, aggregation and encapsulation with organic or inorganic condensates though atmospheric aging might increase its MAE by 30%-50% (Bond et al., 2006; Fuller et al., 1999; Mustard et al., 2008; Yang et al., 2009; Zhang et al., 2008). MAE for the BrC in smoke particles varies from 0.03 to 0.60 m^2/g at 550 nm, depending on different measurement techniques and derived chemical fractions (Kirchstetter et al., 2004; Yang et al., 2009). Mustard et al. (2008) estimate MAE of brown carbon sphere to be 3.6-4.1 m^2/g at 550 nm, and Chakrabarty et al. (2010) measure MAE for tar ball particle to be ~2.5 m^2/g at 530-730 nm. Single scattering albedo (SSA) is the key optical parameter that describes the strength of aerosol's direct radiative forcing, and spectral defined SSA for smoke aerosol mainly depends on burning condition but also fuel types and oxidation level (Ramanathan et al., 2001; Liu et al., 2014; Ramanathan et al., 2001; Saleh et al., 2014). SSA is inversely

related to MCE, smoldering phase emits more nonopaque carbonaceous materials with higher SSA (~1.0 at MCE<0.9), smoke particles from flaming fire containing more BC have much lower SSA (Ramanathan et al., 2001; Liu et al., 2014; McMeeking et al., 2009). Sharp increment of aerosol scattering and absorption coefficients shall be observed during field burning events (Garland et al., 2008; Yu et al., 2013). Atmospheric aging processes including photochemical oxidation to produce more SOA increase the SSA (Abel et al., 2003; Liu et al., 2014; Yokelson et al., 2009), humidification to change the mixing state and morphology also decreases light absorption of smoke particles (Adler et al., 2011; Guyon et al., 2003; Haywood et al., 2003; Lewis et al., 2009).

7.4.3. Morphology and mixing state

Analytical TEM is a powerful tool for characterizing individual aerosol particles because it provides simultaneous morphological, compositional, and structural information. Individual aerosol particles in smoke plumes from biomass fires have been studied using analytical transmission electron microscopy (TEM) in southern Africa and China, which allowed detailed characterization of particle types in smoke. Based on composition, morphology, and microstructure, three distinct types of BB particles are present in the smoke: (1) soot, (2) “tar ball” particles (carbon-rich, spherical particles), and (3) organic particles with inorganic (K-salt) inclusions. It was well known that the relative number concentrations of organic particles with inorganic inclusions were largest in young smoke, whereas tar balls were dominant in a slightly aged smoke from a smoldering fire. Flaming fires emitted relatively more soot particles than smoldering fires.

Soot

Soot i.e. BC, is common in BB smokes, which is believed to be formed via a vaporization-condensation mechanism during combustion processes (Li et al., 2003; Chen et al., 2005; Chen et al., 2006). Soot is clearly distinguishable from the other particles under the TEM. Soot forms branching aggregates containing from less than ten to thousands of spheres, each of which is 20 to 60 nm in diameter. Typical soot aggregate with fractal-like chain structures can extend to a couple of micrometers or more. HRTEM image of the soot spheres shows onion-like structures of curved, disordered graphitic layers. STEM-EDX mapping shows the soot aggregate mainly contains C and minor O. Typical SAED patterns of soot aggregates exhibit three distinct rings, which are indexed to the crystalline structure of graphite (Viktória et al., 2006). The SAED pattern obtained from soot aggregates shows broad and diffuse 002 and hk rings, indicating a microstructure consisting of randomly distributed crystallites that have a fine size and do not possess long range order (Chen et al., 2005). Dark-field imaging has been used to visualize individual microcrystallites. The bright spots in the dark field image are produced by diffraction from the 002 planes of microcrystallites. These bright spots are distributed unevenly within the particles. Observation of such patterns could be due to a different density of circumferential 002 lattice planes parallel to the electron beam (Chen et al., 2005; Viktória et al., 2006).

The soot content varied greatly in different smoke samples. Besides the major component of C and O, most of the soot aggregates contained potassium, and some had minor amounts of silicon. The potassium enrichment in soot has been used as

a fingerprint of its BB origin. High spatial- resolution electron energy-loss spectroscopy (EELS) results showed chemical heterogeneity even within one aggregate, with varied potassium contents in different soot spheres. Some of the soot particles showed a modified morphology, which most likely resulted from atmospheric aging (China et al., 2013; Adachi and Buseck, 2013). Once emitted into the air, the irregular geometry and complex microstructure of soot aggregates may provide active sites for deposition of common atmospheric gases such as O_3, NO_2, and SO_2, which could readily oxidize soot surfaces (Decesari et al., 2002). The soot-O_3 reaction is particularly rapid, and prolonged exposure to ozone under laboratory conditions may lead to the collapse of the graphitic structure (Zhang et al., 2008b; Yokelson et al., 2009).

Tar ball

Tar ball particles formed an important fraction of the total particle number concentration in some of the smoke plumes. Tar balls were readily recognized in TEM images (Fig. 7.5a and 7.5b) by their spherical shape, amorphous, and are typically not aggregated with other particle types. Tar balls are produced by a gas-to-particle transformation followed by condensational growth in biomass smoke (Pósfai et al., 2003; Hand et al., 2005). Tar balls had a diameter range from 100-500 nm with a few particles larger than 1 µm. HRTEM images (Fig. 7.5c) of tar balls did not indicate any semiordered graphitic microstructure typical of soot. Their EDX spectra indicated elemental compositions consisting of C and O with trace amounts of S, K, Cl and Si. Electron energy-loss maps show that the distribution of C and O in tar ball is homogeneous, and thickness profiles indicate that most are perfectly spherical. In contrast to other widespread and spherical aerosol particle types, such as sulphate and K-rich particles, tar balls were stable under the TEM and did not change visibly under prolonged exposure to the electron beam, suggesting they were composed of refractory material. It has been reported that the chemical compositions, densities, and carbon functional groups of tar balls were distinctly different from soot and black carbon and more closely resemble high molecular weight polymeric humic-like substances, which could account for their reported optical properties (Pósfai et al., 2004; Hoffer et al., 2006; Li et al., 2003).

Of special interest was to compare tar ball with K-containing organic particles, both of which showed similar elemental compositions, with comparable amounts, amorphous microstructures, overlapping sizes, and strong resistances against electron bombardment. Since Pósfai et al. (2003) proposed that tar balls probably corresponded to an intermediate stage in the aging of organic particles from BB, it was proposed that a fraction of K-containing organic particles could originate from tar balls. When exposed to an electron beam, surface sulfates sublimated. Elemental maps proved that C, O, and Si elements homogeneously distribute within the bulk of the particle. Homogeneous internal distributions of C and O in tar balls were previously reported (Hand et al., 2005). Also such assumption was supported by a few field studies performed in southern Africa and California (Pósfai et al., 2003; Pósfai et al., 2004; Hand et al., 2005). Both tar balls and the organic particles with minor K, Cl, and S contents were characteristic products in aged biomass plumes.

Organic particles with inorganic inclusions

"Organic particles with inorganic inclusions" referring to the crystalline, visible inorganic constituents and the high C contents of particles that belong to this type. Organic particles with inorganic inclusions do not have distinct morphologies under the TEM (Fig. 7.5). They typically contain crystalline K-salts, primarily either KCl or K_2SO_4, but the presence of KNO_3 was also inferred from compositional data. The bulks of the particles containing C and minor O and are stable in the electron beam. The compositions of the inorganic inclusions varied with age of the smoke, and probably the type of burnt biomass type. Potassium-salt particles were the most abundant inorganic aerosol constituents in the smoke from BB (Hand et al., 2010). Most had amorphous organic coatings or formed small inclusions in organic particles. These potassium salts were very beam-sensitive. They ranged in diameter from 20 nm to 1.5 μm, with most from 100-600 nm. Most KCl particles had euhedral morphologies, and some were rounded. Some round particles contained potassium and chlorine, and they were more beam-sensitive than the pure KCl particles. These particles were likely mixtures of KCl and NH_4Cl, which formed through reactions of chlorine and NH_3 species emitted from the biomass fire (Duo et al., 2015). Some of the potassium sulfate and nitrate crystals were rectangular or rounded, but most were irregularly shaped. Selected-area diffraction patterns of KCl and K_2SO_4 particles were obtained to confirm their crystallinity.

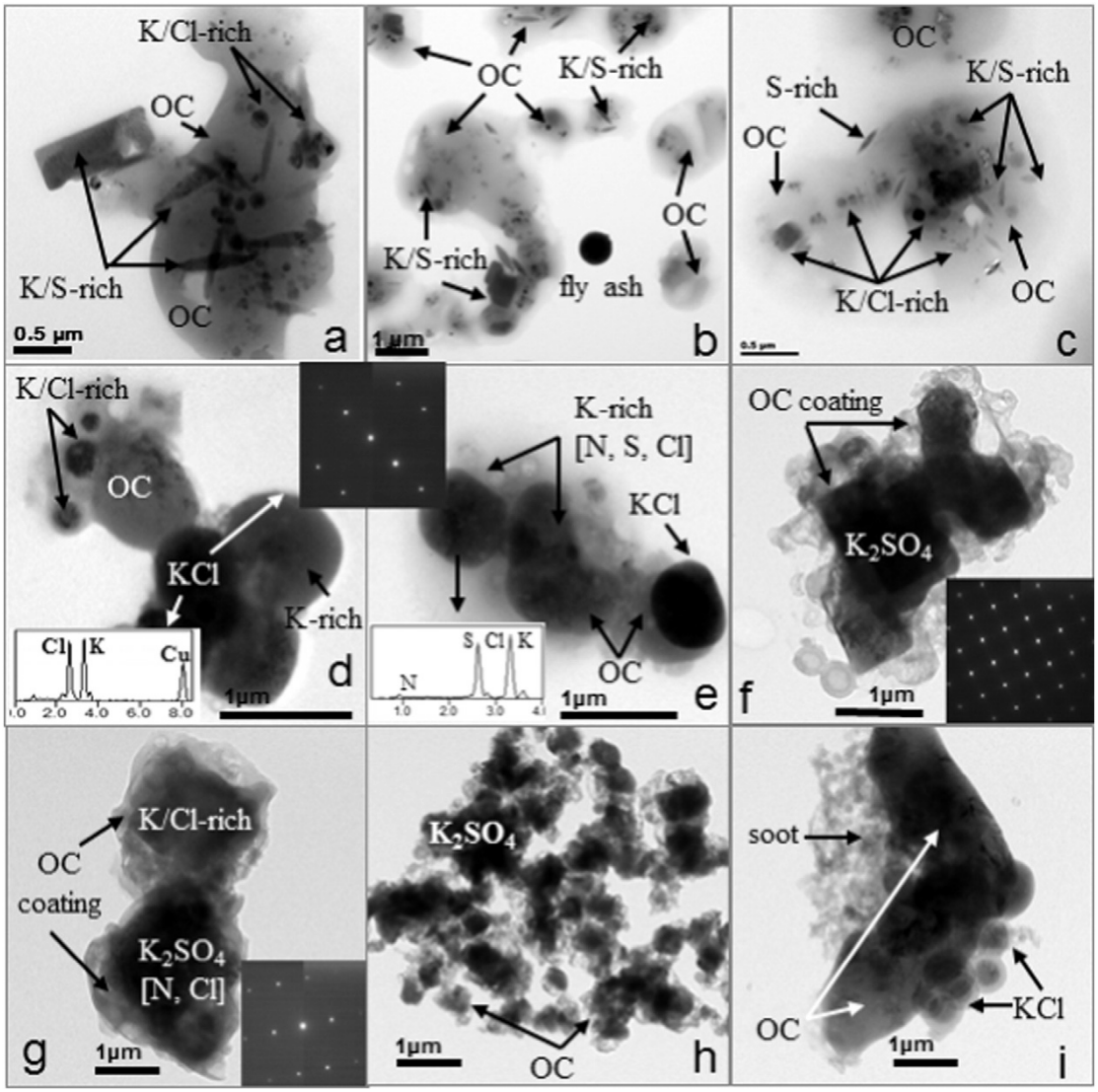

Figure 7.5 TEM images of typical organic particles with inorganic inclusions. (a), (b) and (c) organic particle internally mixed with K/Cl-rich, K/S-rich and/or S-rich particles. (d) the rounded crystal KCl mixed with OC and K-rich particle. The inset is the diffraction pattern of potassium chloride. (e) the irregular K-rich particle with OC coating containing minor N, S, and Cl elements, which were likely mixtures of KCl and NH_4Cl. (f) the rectangular potassium sulfate particle with OC coating. The diffraction pattern is indexed into K_2SO_4. (g) the euhedral K_2SO_4 particle and K/Cl-rich particle coated by the OC layer. (h) the aggregated K_2SO_4 particles attached with OC particle. (i) the OC attached with soot and rounded KCl particle.

Particles with organic coatings

Several TEM studies have shown the biomass particles with organic coating were widespread in urban atmosphere (Li et al., 2010b; Adachi et al., 2008). Most of smoke particles were coated with a carbonaceous film when they emitted into the atmosphere, and a few typical particles with organic coating are shown in Figs. 7.10a-c. Similar particles, with coatings of

various thickness of organic coating, have been widely observed in a variety of samples, including those from polluted continental environments (Niemi et al., 2006; Adachi et al., 2008; Li et al., 2010b; Russell et al., 2002), especially in the serious fog and haze episodes in China. Organic coatings were lost under strong beam bombardment although they were less sensitive to the electron beam than sulfates and nitrates, which were different from tar ball and soot. It was believed that organic coating was composed of second organic aerosol (SOA), which commonly forms through condensation of precursor gases on pre-existing particles such as soot (Fan et al., 2006). The high ozone and VOC concentrations in urban Shanghai atmosphere suggested that the formation of SOA in the vapor phase and their subsequent condensation may be a significant pathway in the formation of the organic coating. Previous studies have suggested that ozone, hydroxyl radical, nitrate radical, and other oxidants presented during atmospheric transport played a central role on the formation of SOA in Beijing atmosphere (Li et al., 2010c). In Shanghai, about half of VOCs come from motor vehicles, and 10-35% of VOCs was from industrial activities, indicating the organic coating in these aerosol particles were likely formed by VOCs from fuel combustion, and a lesser extent, from industrial activities (Geng et al., 2009). Laboratory experiments have found that SOA is slightly hygroscopic and exhibits a smooth water uptake with increasing (Varutbangkul et al., 2006; Semeniuk et al., 2007), suggesting the formation of such coating by aqueous-phase processing of the particles during transport in the atmosphere. Organic coatings could modify the particle hygroscopicity, CCN abilities and heterogeneous chemical reactivity, indicating that the ubiquitous presence of this particle type in the atmosphere had important ramifications of the regional climate (Li et al., 2003; Adachi et al., 2008; Russell et al., 2002).

Internally mixed particles

The smoke particles, such as soot or organic particles, often internally mixed with S-rich particles during aging in the atmosphere. In TEM images, S-rich particles were euhedral or rounded. The sulfates readily decomposed when exposed to an electron beam. When decomposing, they left a similar carbonaceous residue. Laboratory studies showed that sulphate nucleation was often coupled with aromatic acids (Zhang et al., 2004); thus, it was not surprised that organics were present in small sulphate particles. A smaller size of the sulphate grains seemed to be homogeneous and was commonly coated by an organic layer, while the larger ones were commonly internally mixed with soot and organic matter (or more chemical species). Within the internally mixed particles, most of the organics may be beam-sensitive SOA. Consistent with the usual findings that SOA was coupled with S-rich particles (Kanakidou et al., 2005). However, some particles also contained beam-resistant dark inclusions without clear morphological characteristics, which may be organic particles, collapsed soot or tar ball. Previous water dialysis experiments of individual particles have demonstrated that the coatings were water soluble, while organic inclusions were insoluble (Okada et al., 2001; Li et al., 2010c).

Such internally mixed particles may be preferentially formed in an aerosol mass stagnates which often occurs during episodes of serious pollution (such as urban haze), when there is insufficient wind velocity to carry pollutants away from the city. During these periods of pollutant retention, aerosols continue to collide and combine with each other, resulting in larger

average sizes and complex components (Li et al., 2011). Larger sizes are commonly associated with the polluted environment and adverse meteorological conditions (Li et al., 2010b). In high pollution areas such as Mexico City, over half of the aerosol particles consist of internally mixed soot, organic matter, and sulfates (Moffet et al., 2010; Adachi et al., 2008). Sulphate coatings can have either negative or positive effects on the radiative forcing of BC. On one hand, the internally mixed sulfates can make organic matter and soot more hydrophilic and eventually make them efficient CCN. While, on the other hand, embedding sulfates act as lenses that focus light on soot and thus amplify absorption of the internal particles (Healy et al., 2015; Adachi and Buseck, 2008; Adachi et al., 2010).

7.4.4. Gaseous pollutants

BB is an important source of volatile organic compounds (VOCs) and carbon monoxide (CO), which are precursors of ozone (O_3) and secondary organic aerosol (SOA), posing damage to air quality and human health. Guo et al. (2004) identified the contribution of BB to VOCs to be 11% ± 1% at a background site in eastern China (*i.e.*, Lin'an in Zhejiang Province). The comparable contribution to VOCs was determined at a background site in central Pearl River Delta (PRD) (*i.e.*, 11% ± 1%), southern China, and an urban site in southwestern Hong Kong (*i.e.*, 9% ± 2%) (Guo et al., 2011). With the source-tracer-ratio method, Yuan et al. (2010) identified the average BB contribution of 12.6% to VOCs including the oxygenated VOCs (OVOCs) in PRD. In central China, BB even accounted for 54.8% ± 0.5% of VOCs during the haze episodes in the autumn harvest season, and it was identified as the main cause of the haze pollution in warm seasons in that region (Lyu et al., 2016). Through the bottom-up approach, the contribution of BB to VOCs was also estimated based on the emission inventories. However, they varied in a large range. For example, the contributions increased from 1.82-3.17% not necessarily the lowest (Zhang et al., 2013), to 7.6% (Bo et al., 2008), up to 13.9% not necessarily the highest (Yan et al., 2006) in Guangdong province. The uncertainties in emission factors and activity levels were the main causes of these discrepancies. In addition to these factors, the differences between the results from the top-down (*e.g.*, source apportionment) and bottom-up methods were also due to the fact that the contributions of BB beyond the study area might be included in the results as determined by the receptor-oriented source apportionment model, due to the long lifetimes of some BB related VOCs (*i.e.*, ethane, ethyne and benzene). On the other hand, CO was also largely emitted from BB. Wang et al. (2002) found that CO increased considerably during the autumn season and correlated well with methyl chloride (CH_3Cl), a common tracer of BB, at a rural site in eastern China, indicating the contribution of BB to CO. This contribution was further quantified as 18±3% by Guo et al. (2004). Based on the emission inventory, the CO emissions from BB reached 0.5 Tg/yr in PRD (He et al., 2011b) and even summed up to 16.5 Tg/yr in whole China in the early 2000s (Yan et al., 2006).

The source profiles of VOCs for the BB were determined from the laboratory and field tests. Although the physical and chemical characteristics of the combustion materials and combustion modes (*i.e.*, fire burning and smoldering) influenced the VOCs emissions, many similarities were found. Zhang et al. (2013) collected the rice straw and sugarcane leaves in PRD and tested the emission factors of VOCs in the laboratory. The results indicated that the top 10 non-methane VOCs

(NMVOCs) in the emissions were ethene, ethane, propene, toluene, ethyne, propane, benzene, isoprene, 1-butene and *m*/*p*-xylene, among which the C_2 species accounted for >50% by volume. However, ethane, ethene, propane, ethyne, *n*-butane, propene, *i*-pentane, *n*-pentane, toluene and *i*-butane were the most abundant VOCs in the combustion of sugarcane leaves. Liu et al. (2008) collected the biofuel burning samples in a farmer's house in PRD, and analyzed the source profiles for the combustion of wheat, corn and wood, according to which CH_3Cl, ethene, ethane, ethyne, propene, 1,3-butadiene and BTEX (benzene, toluene, ethylbenzene and xylenes) were suggested as the tracers of BB. In Hong Kong, the outdoor barbecue was a typical type of BB. Two samples were collected near a barbecue stove. Table 7.2. lists the top 10 NMVOCs in the two samples. It was found that the C_2-C_4 hydrocarbons, benzene and toluene were the main VOCs emitted from barbecues.

Table 7.2 Top 10 NMVOCs in the two samples collected near a barbeque stove in Hong Kong

Sample 1		Sample 2	
Species	Mixing ratio/ppbv	Species	Mixing ratio/ppbv
Ethene	458.7	Ethane	2049.5
Ethane	275.4	Ethene	936.7
Ethyne	184.8	Propene	289.9
Propene	94.5	Propane	265.6
Benzene	50.7	Ethyne	253.4
Propane	41.5	Benzene	143.0
1,3-Butadiene	21.2	Toluene	82.0
i-Butane	19.7	*n*-Hexane	33.7
Toluene	18.7	*n*-Butane	32.3
n-Hexane	12.7	1-Butene	28.2

Based on the known source profiles of BB, the species-specific loadings of VOCs could be determined with the source apportionment techniques. $CHCl_3$ and acetonitrile (CH_3CN) were often treated as the tracers of BB. It was found that the mixing ratios of CH_3Cl increased significantly in summer and autumn at Lin'an site (p<0.05), when the field and domestic combustion of crop residues increased (Guo et al., 2004). In addition, Lyu et al. (2016) found that CH_3Cl and CH_3CN were both higher on the BB induced haze days than those on the non-haze days in Wuhan, central China. Apart from the typical tracers, BB gave off a large amount of VOCs, such as ethane, ethene and ethyne, representative of incomplete combustion,

and the aromatics including benzene, toluene and xylene isomers. It was found that C_2-C_3 alkene, ethyne and benzene were the predominant VOCs in the emissions of BB, which was responsible for 16% ± 3% and 11% ± 2% of ethyne and benzene, respectively, upon the basis of the source profiles determined in eastern China (Guo et al., 2004). Similarly, the C_2 hydrocarbons (*i.e.*, ethane, ethene and ethyne) dominated in the emissions of BB in Hong Kong and PRD (southern China), which comprised ~45% and ~80% of ethene in Hong Kong and PRD, respectively (Guo et al., 2011). During the autumn haze episodes in Wuhan (central China), BB emissions contributed 60.8% ± 0.3%, 71.3% ± 0.5%, 65.0% ± 0.4% and 85.2% ± 0.7% to ethane, ethene, ethyne and benzene, respectively (Lyu et al., 2016). OVOCs were also a significant group in BB emissions. It was reported that acetone and acetaldehyde were the most abundant two OVOCs in the emissions of straw burning (Zhang et al., 2013). With CH_3CN as the tracer, Yuan et al. (2010) found that an autumn BB contributed 17.7% and 12.3% to acetaldehyde and acetone, respectively. Apart from these two species, formaldehyde, propanal, methylglyoxal, methanol and isoprene and its oxidation products were also detected in BB emissions.

The ratios between VOCs species were often employed to help identify the sources of VOCs. For example, the ratio of ethyne/ethane (0.49-1.02) in the source of BB identified by Guo et al. (2011) was comparable to that (0.57) in the plume of a fresh BB (Blake et al., 1994). A comparable ratio of ethyne/ethane (0.67) was also observed in a sample collected near a barbecue stove in Hong Kong. However, it was much lower in another barbecue sample (0.12) and those (0.30 and 0.21 for the combustion of rice straw and sugarcane leaves, respectively) determined by laboratory experiments in PRD (Zhang et al., 2013). Similarly, the dry grass combustion samples collected in central PRD had high ratios of ethyne/propane (8.3) and benzene/propane (1.6) (Wang et al., 2005). However, the ratios were much lower in the combustion emissions of rice straw and sugarcane (Zhang et al., 2013), and barbecue samples. Noticeably, the ratios of VOCs varied in a large range in different studies, which might relate to the materials and modes of the combustions. Therefore, it was not reliable to identify BB with the only signature of VOC ratios. Evident analyses should be based on the variations of the tracer concentrations and/or the source apportionments.

7.4.5. PAHs

Polycyclic aromatic hydrocarbons (PAHs) are a class of hazardous air pollutants, which are predominantly produced during the incomplete combustion of organic materials, e.g. coal, wood and other biomasses. Because PAHs are classified as carcinogenic (IARC, 2014), the US EPA has issued a list of 16 priority PAHs to be monitored in risk assessment exercises. For example, a large scale study by Zhang et al. (2009) has estimated that the inhalation of airborne PAHs led to the overall population annual excess of lung cancer incidence rate of 0.65×10^{-5} in China. Meanwhile, BB is an important source of PAHs, especially because most BB provided favorable condition for PAH formations and consequently has high emission factors for PAHs (Ravindra et al., 2008).

In China, recent studies by Li et al. (2016) and Tao et al. (2011) have estimated the contribution of BB to the total PAH emission. The combination of firewood and straw burning accounted for the largest proportion of PAH emission in China. But the overall contribution of BB to total emission of PAHs decreased from about 55% in 2003 (Zhang et al., 2008a) to about 40% (Li et al., 2016). Zhang et al. (2008b) also estimated the PAH emission from open straw burning during the harvest season at 2.4% of the total PAH emission in China in 2003. Although there are differences in the calculation between the two studies in term of PAH emission factors from different sources, the reduction of PAH emission from BB can partly be explained by the reduction in biomass consumption (National Bureau Statistic Commission, NBSC, 2004-2013). The emissions of PAHs to the atmosphere were dominated by the light weight PAHs such as Naphthalene, Phenanthrene, Pyrene, Fluorene, Acenaphthylene, Anthracene, and Acenaphlene while the emissions of the heavier PAHs such as Benzo[a]pyrene (BaP), Benzo[b]fluoranthene, Benzo[k]flouranthene, Benzo[ghi]perylene, Dibenz(ah)anthracene, and Indeno(1,2,3-cd)pyrene were minimal (Li et al., 2016).

As the extent of BB varies across China, the level of PAH emission from BB also varies from region to region. It was estimated that the Northern China Plain and the Sichuan Basin and southern China region are heavy emitters of biofuel PAHs while the Northeast region of China is the main emitter of PAHs from wildfire burnings (Zhang et al., 2008b). It is because the Northern China Plain and the Sichuan Basin produce the bulk of wheat straw from its crop which has significantly higher emission factors of PAHs compared with other kinds of crop residues. The southern China region also burns a large quantity of rice straw but the emission of PAHs is lower thanks to the much lower emission factor of rice straw (Zhang et al., 2008a). A more recent research by Lin et al. (2015)also confirmed that the high level of PAHs in the North China region was due to biomass/coal combustion using diagnostic ratio of different PAHs although there was no method to clearly distinguish between emissions from biomass and coal burnings (Shen et al., 2013).

The seasonal variation of PAH emissions across China was first evaluated by Zhang and Tao (2008b) for two types of BBs including biofuel burning from residential sector and open burning of agricultural wastes and wildfires where the authors used regression model for energy consumption in all provinces of China. Overall, PAH emissions from BB (a combination of biofuel combustion and open fires) were higher in cold season (from November to March) for heating purpose and were lower in warm season except a small emission peak in July and August due to the occurrence of wildfires but the profiles differed greatly among the six geographical zones of China (Northeast, North, Northwest, South, Southwest and Tibetan plateau). For example, while North China had the largest variation of PAH emission between winter and summer and was also impacted by open fires in summer, South and Southwest China had smaller variation thanks to weaker heating demand in winter and were not affected by open fires as they are far away from the burning areas (Zhang et al., 2008b).

In order to better understand the profiles and inventories of PAH emissions from BB, it is important to obtain the reliable emission factors (EFs). However, EFs of PAHs are usually the main source of uncertainty in the emission inventory in

recently developed emission inventories (Shen et al., 2013). There are multiple causes for this situation. First, there are a limited number of studies reporting EFs of PAHs from BB in the literature including in China. Second, the results of emission measurement varied remarkably depending on fuel types and the design of burning facilities. For example, EFs of ∑15PAHs for wheat straw was reported at as high as 234 mg/kg by Zhang et al. (2008a) but was reported only at 1.1 mg/kg in a different study later (Zhang et al., 2011). Therefore, it is necessary to conduct more measurements and to agree on a common measurement protocol so that the experimental outcomes are compatible and utilized in different contexts. It is also noted that PAHs emitted from BB are in both gaseous and particulate phases and their emissions were reported to be closely related to the emission of particulate matters (PM) of different sizes (Shen et al., 2013). Therefore, the types of biomass fuels that have high EFs for PM would likely to have high EFs for PAHs, posing an increased risk for the exposed population.

Emissions of PAHs from BB, particularly from the residential sector, are important contributors to the total emission of PAHs in China. More importantly, indoor BB generates a range of air pollutants including PAHs that threaten the healthy living of the inhabitants. Controlling the residential emission of PAHs will not only reduce the total emissions of PAHs but also lower the health risk of the population with lower economic status. The most effective approach may be to encourage use of clean stoves or alternative fuels. While BB will continue to be an important energy source in the rural areas because of easy access and very low cost the introduction of new clean stoves will improve fuel efficiency and indoor reduce air pollution (Chen et al., 2016). At the same time, traditional biomass fuels should be replaced with biogas or pelletized biomass. Those alternative fuels can be produced locally and are not likely to add significant cost to the household energy budget. Such program can also be promoted by the government through economic incentives and technical assistance to achieve the better population health outcome.

7.4.6. Emissions, trends and control

Studies have estimated short- and long-term BB emissions of carbonaceous aerosol (e.g., BC, OC, $PM_{2.5}$) and pollutants like PAHs, CO_2, VOCs etc. in China, the tempo-spatial distributions and dynamic trends for the emissions have also been characterized based on inventory calculation, atmospheric chemical transportation simulation, and national economic-official data assessments (Li et al., 2014; Qin et al., 2012; Saikawa et al., 2009; Zhang et al., 2015; Zhao et al., 2011). Domestic fuel use of biomass has declined dramatically in rural area due to more widely supply of clean and cheap energy like electricity, LPG (liquid petroleum gases), and methane in the process of new countryside construction and urbanization (Zeng et al., 2007; Zhang, 2011). In contrast, field burnings especially agricultural fire emissions increase sharply over the past decades (He et al., 2011; Lu et al., 2011; Qin et al., 2011, 2012). Crop straw productions and percentage of straw field burnt are two key parameters to assess agricultural open burning emissions, and they are also what make BB a major source of anthropogenic pollutions (Cao et al., 2006; Reid et al., 2005; Zhao et al., 2012). Annual crop straw productions are on the magnitude of 10^2 million tons in China, a significant yearly exponential growth of straw productions by 3.4% has been observed since 1949 when crop productions are only ~0.8×10^{14} g, and then increase rapidly to over 7.4×10^{14} g in 2014.

National field burning rate of the crop residues is commonly believed to be 15.2%-27.2% (Cao et al., 2006; Wang et al., 2008; Zhang et al., 2011), that means over 100 million tons crop straws will be burnt annually in the field. Vast uncertainties in provincial or regional burning rates are reported in different literatures, e.g., the variable rate is 0 in Beijing in the work of Cao et al. (Cao et al., 2006, 2011), but to be 17% from Wang et al (2008). He et al. (2011) estimate field burning rate for Pearl River Delta to be 31.9%, however, according to government report in 2013(National Development and Reform Commission report, [2014] No. 516, data available at http://www.sdpc.gov.cn/, in Chinese), corresponded figure is 28.4%. Zhao et al. (2012) ever assume 100% of crop straws are field combusted in Huabei region, while official reported data to be 22.3%. Besides, regional field burning rates are proposed and proved to be proportional to peasants' income level, i.e., ignoring government policy-profit orientation and awaken of public environment protection awareness, more agricultural residues will be discarded to be burnt with development of rural economies (Cao et al., 2006; Chen, 2001; Qin et al., 2011). Qin et al. (2011, 2012) ever deduce year-specific regional open burning rates from 1980 to 2009 based on parameters of fixed year, over tenfold increment of the burning rates are found within recent decades. Furthermore, multi-year anthropogenic BC emission figures are characterized using the dynamic emission factors and burning activity rates, presenting rapid increase with annual fluctuation of national BC emissions from ~0.87 Tg in 1980 to ~1.88 Tg in 2009, of which residential biofuel consumption contributed ~40% with 15%-20% from crop residues burning and 15%-30% from firewood combustion, while agricultural waste open burnings make up less than 6%, temporal emission characters of BC show a diminishing trend of residential contribution since 1996 but a rapid and steady increase trend of biomass open burning production (Qin et al., 2011, 2012). Moreover, specific spatial distributions of BB emissions have also been depicted, the emissions were produced mainly in the North Plain, the Northeast and the Pan-Pearl River delta regions, echoing the distributions of fire sites and the crop planting or forestry regions, especially Shandong, Hebei, Henan, Anhui and Heilongjiang where contribute over 65% of the total emissions, leading the top five provinces of BB emissions (Cao et al., 2006; Wang et al., 2008; Yuan et al., 2010; Zha, 2013; Zhao et al., 2012). The seasonal pattern of open burning in China that favors to occur in the autumn and winter is significant, and agricultural field fires are commonly observed during post-harvest period that concentrated in June to November (Wang et al., 2008; Zha, 2013), great emissions from biomass open burnings facilitate the haze formations over the entire China, mainly the North and East areas, leading to serious health and climate effects (Cheng et al., 2014; Gao et al., 2015; Ge, 2008; He et al., 2015; Hua et al., 2015; Yang et al., 2015).

Streets et al. (2003) conclude open burning is much more serious in China that contribute 25% of the total biomass burnt in Asia, producing 0.11 Tg BC and 0.73 Tg OC annually. Ohara et al. (2007) believe domestic combustion is primary source for BC (~1.08 Tg/yr) and OC (~2.56 Tg/yr) emissions in China, and residential biofuel burning contribute 43% BC and 82% OC emissions, which are comparable to that of coal use. Study from Lu et al. (2011) and Streets et al. (2008) also confirm the historical trends of carbonaceous aerosol emissions in China over 1980-2010, a slight decrease of OC and BC emissions during 1995-2000 over the entire increasing trends is observed and attributed to the less use of biofuel and coal, contribution of biofuel burning presented the inverted figure towards the trends of OC and BC emissions. Forecasting of BB emissions

for the nearest future in China has been conducted by many studies, Zhou et al. (2003) develop three emission scenarios for 2010 and 2030 based on long-range energy-economic structures and energy-emission control technology development, on the basis of emission scenarios and emissions for 2000, biofuel burning emissions and contributions all decreased under the three scenarios for 2010 and 2030. Ohara et al. (2007) apply the projection from Zhou et al. (2003) to assess emissions in China for 2010-2020, they find that BC emissions in 2020 decrease by ~28.7% on average compared with that in 1995, mainly results from reduction in emissions from biofuel and coal. Driven by IPCC scenarios, Streets et al. (2001) predict the same BC emission changes by 8% decrement for 2020 in China (open burning emissions were excluded) because of less use of biofuel and coal. Later, Streets et al. (2004) forecast the future worldwide emissions of primary carbonaceous aerosol for 2030 and 2050 on the basis of 1996 emission figures, considering the only sources of energy generation and open BB, they project the decline of both OC and EC emissions for 2030 and 2050 in the East Asia, as China moves away from residential use of coal and also biomass open burning. Based on emission inventories for BC, OC, sulfate and SO_2 in China for 2000 (BB emissions dominated), Saikawa et al. (2009) analyze future emissions for 2030 upon the hypothesis of governmental policy implementation and enforcement, they find aggressive emission control will lead to 50% reduction in premature deaths, while high emission scenario presents the inverse effect, and the radiative forcing effect changes also depend on the emission scenarios.

However, the predications of BB emissions in China driven by environmental and economic prospects or historical trends are all moderate and conservative, the government policy enforcement can be more severe and effective, may be not economic efficient, but harsh enough to achieve the emission control goal, like the forbidden-fire policy implementations during Beijing Olympic Games 2008, Shanghai World EXPO 2010, Beijing APEC 2015, and the nearest Hangzhou G20 Forum 2016, etc., primary emissions over wide-scale regions are surely decreased to realize the short-term control policy and meet the “blue sky” standard (e.g., APEC blue) (Chen et al., 2015; Guo et al., 2013; Huang et al., 2013; Huang et al., 2012; Wang et al., 2010; Xin et al., 2010; Yang et al., 2016). Normalization of BB or agricultural field burning forbidden will be forecastable, the reduction of primary anthropogenic pollutants emissions will also be divinable, and we will surely meet more complicated environmental problems, such as the transformation from atmospheric pollutions leading by fine particles to ozone pollution, and marginal effect in pollutants control to meet the WHO (World Health Organization) standard (Doherty, 2015; Hope, 2008; Huang et al., 2014; Shindell et al., 2012; Wang et al., 2016).

7.5. Biomass burning plume

7.5.1. Transport

Smoke plumes from BB and desert dust are one of the main atmospheric constituents that affect the air quality and climate due to their massive plumes that can travel thousands of kilometers downwind. The monitoring of these plumes is only possible through the satellite measurements (Kahn et al., 2007). The OMI is a nadir viewing imaging spectrometer onboard

NASA's Aura satellite, which was especially designed to replace Total Ozone Mapping Spectrometer (TOMS) in measurements of ozone and UV-absorbing aerosols, such as smoke and desert dust (Torres et al., 2007; Torres et al., 2013) via the UV aerosol index (AI)/absorbing aerosol index (AAI). Therefore, smoke plumes have a clear signal in AI values (Kaskaoutis et al., 2011, 2014) allowing us to monitor the transport pathway of the smoke plumes. However, a similar sensitivity of AI is for the desert dust and there is no way to discriminate between these aerosol types using only OMI-AI retrievals. Thus, the discrimination between smoke plumes and desert dust is able with the combined use of other satellite retrievals, like AIRS or MOPITT CO measurements, since CO is a product of BB. Furthermore, another disadvantage in considering AI as a measure of the biomass-burning aerosols is its great sensitivity to the height of the aerosol plume. Therefore, smoke plumes at elevated heights result in larger AI values, even if they are not as thick as the plumes near the ground. This fact limits the utilization of AI for monitoring of the biomass-burning aerosols. Furthermore, the OMI measures several air pollutants, including NO_2, SO_2 with global daily coverage (*http://aura.gsfc.nasa.gov/instruments/omi.html*), which are products of any kind of burning, including biofuel and fossil-fuel combustion. Thus, in combination with FC from MODIS, NO_2 and SO_2 concentrations may be examined over areas far away from urban and industrialized centers in order to assess the contribution of BB (Kaskaoutis et al., 2014; Chubarova et al., 2012).

7.5.2. Atmospheric aging

Emissions released directly from sources are referred to as primary, or fresh emissions including gaseous organic and particle-phase organic (primary organic aerosol, POA) species. In contrast, processed emissions are the result of atmospheric photochemical processing (aging) of primary species. The aging can be referred to a variety of gas-to-particle conversions and particle changes within the atmosphere. Probably the most important aging pathway is chemical oxidation of primary gaseous compounds (volatile organic species, VOCs), emitted directly from an emission source, to form saturated low-vapor-pressure organic species that often condense onto the pre-existing particles and form secondary organic aerosol (SOA) (Seinfeld et al., 2003; Kroll et al., 2008). Gaseous species in smoke emissions can partition into the particle phase by gas-phase oxidation and form SOA. Therefore, BB aerosols are found to be strongly related to SOA formation (DeCarlo et al., 2010; Cheng et al., 2013). Secondary organic aerosol has been recognized as an important contributor to PM pollution, having considerable effects on climate (changing radiation balance by scattering insolation and acting as a cloud condensation nuclei) and adverse impacts on human health (Pope III et al., 2006; Hallquist et al., 2009). It has been assessed that 40 to 70% of the total VOC in the atmosphere are transformed through photochemical oxidation process to form SOA (Goldstein et al., 2007). The most common oxidizers in the atmosphere are hydroxyl radicals (OH) (during daytime), nitrate radical (NO_3) (during nighttime) and ozone (O_3) (during night and daytime hours) (Rollins et al., 2012; Jacobson et al., 2000; Lambe et al., 2015). In most of the environments, including China, photochemical reactions with OH are the dominant anthropogenic VOC scavengers (Yuan et al., 2013; Warneke et al., 2004). Some studies suggested the fast formation of SOA species even within a half of a day (Kleinman et al., 2008; DeCarlo et al., 2008; Dzepina et al., 2009). BB aerosol lifespan is estimated to be 3.8 ± 0.8 days, which likely provides enough time for significant atmospheric transformations (Edwards et

al., 2006). Secondary organic aerosol generation potential from VOC (using emissions inventory) was estimated throughout China. Cities characterized with the highest values were found to be Hong Kong, Beijing and Shanghai respectively (Yuan et al., 2013). According to this study aromatic VOC species can contribute most to SOA yields in China. However, large uncertainties related to this data emphasize the need of characterizing the SOA portions that cannot be estimated by known VOC emission inventories. Under ambient conditions, most of the POA are sufficiently volatile to release their content into the gaseous phase and will not remain for a long period of time in the aerosol phase (Donahue et al., 2009). Therefore another important part of aging process is oxidation of gaseous species that are transferred from primary particle-phase organics. Moreover it is observed that large portion of ambient organic fraction can be present in both, particle and gas phase due to its semivolatile nature and can shift from one phase to another (Shrivastava et al., 2006; Robinson et al., 2007). The semivolatile nature of BB aerosol has been suggested (Robinson et al., 2007; Grieshop et al., 2009). Therefore, atmospheric aging of BB plumes can be considered a complex and a very dynamic process.

So far the main approaches used in China to investigate aging of BB emissions are transmission electron microscopy coupled with energy-dispersive X-ray spectroscopy and Aerosol mass spectrometry. More details about studies performed and results obtained related to these approaches are given in the following paragraphs.

TEM coupled with energy-dispersive X-ray spectroscopy(EDX) approach

Changes in morphology, composition and mixing state of individual BB-related particles during the aging were extensively investigated in China using the TEM coupled with EDX spectroscopy. A similar approach has been used in other parts of the world (Semeniuk et al., 2007; Pósfai et al., 2003). Some important features of BB-related particles transformed during the aging are presented here. Soot (EC), organic fraction, potassium nitrate (KNO_3) and potassium sulfate (K_2SO_4) are the dominant species found in BB plumes emitted during the agricultural burning activities (Li et al., 2010), the major sources of BB aerosol in China. Potassium species are predominantly composed of KNO_3 and K_2SO_4 that are formed in heterogeneous reactions of nitric and sulfuric acids with potassium chloride (KCl), an important fraction of fresh plume emissions (Li et al., 2015; Engling et al., 2009; Li et al., 2003). It is observed that during the aging of BB smoke potassium rich particles form inclusions/aggregations with organic matter and that organic species found in these forms are mostly of hydrophobic nature. Potassium rich species in aging studies, observed in China, are also often covered by a layer of organics, which are found to be predominantly water soluble species (Li and Shao, 2010). Organic coatings are associated with SOA formation, more precisely they are formed in the partitioning of low volatility species that are products of VOC oxidation (Yao et al., 2016; Fu et al., 2012; Li et al., 2010b). Li and Shao (2009) (2009) suggested that organic coatings can be an explanation for the increased cooling effect observed in China during periods of high brown haze and relative humidity. Soot particles in BB emissions can be found in a form of aggregates or inclusions mostly with potassium and sulfur rich compounds and/or organic species (Li et al., 2010b, 2010c; Johnson et al., 2005). Therefore processing of soot aerosol with plume age often alters its inert and hydrophobic structure. Spherical species similar to tar balls, which are suggested to be a fraction of aged

plumes (Pósfai et al., 2003), were also found in BB emissions in China (Fu et al., 2012). According to these studies, organics can significantly change the morphology, composition, mixing state, size and hygroscopicity of inorganic and soot particles and can further drive the atmospheric fate of these species (e.g. CCN potential and physicochemical reactivity).

Aerosol mass spectrometry approach. In general, the main aim of monitoring aging of smoke plumes was directed to organic species as they are mostly non-inert atmospheric fractions with comprehensive structure and therefore complex atmospheric fate. The chemical aging of OA portion in BB plumes has been extensively investigated using the AMS technique (DeCarlo et al., 2010; Capes et al., 2008; Cubison et al., 2011; Yokelson et al., 2009). The AMS method provides a real time size-resolved chemical characterization of submicron ($PM_{1.0}$) non-refractory species (Jimenez et al., 2003; Drewnick et al., 2009).

Using the AMS approach fresh and aged BB emissions can be distinguished by different organic mass signatures in the AMS mass spectra (Cubison et al., 2011; Alfarra et al., 2007). The evolution of BB emissions in the ambient and simulated atmosphere often results in enhanced portion of oxygenated organic fraction (OOA) and degradation of species that are indicators of BB origin (DeCarlo et al., 2008; Capes et al., 2008; Cubison et al., 2011). The parameter f44, the ratio of the integrated signal at m/z 44 (fragment CO_2^+) to the total signal intensity originated from organic component of mass spectrum, measured by AMS technic, has been found to be the main marker for OOA fraction (Volkamer et al., 2006; Jimenez et al., 2009; Ortega et al., 2013). In addition, the AMS parameter f60 is widely used as BB emission signature. Signal intensity for m/z 60 (fragment $C_2H_4O_2^+$) is directly correlated to the concentration of levoglucosan-like species, previously identified as a substantial fraction and tracer of BB emissions (Simoneit et al., 1999; Aiken et al., 2009; Alfarra et al., 2007). It has been estimated that aerosols characterized by an f60 value higher than $0.3 \pm 0.06\%$ are influenced by plume emissions (Cubison et al., 2011).

A graphical approach introduced by Cubison et al. (2011) (Cubison et al., 2011) has been widely applied in characterization and evolution estimation of BB plumes. Fresh BB aerosols can be easily distinguished from aged, highly oxidized species by estimating f_{44} and f_{60} from the plot (f_{44} vs f_{60}). Most of the studies have demonstrated the same trend of f44 increase and f60 decrease with aging (May et al., 2015; Alfarra et al., 2007). This approach has limited use in studies performed in China due to difficulties to separate the BB plume emissions from a number of other pollutants abundant in China (Zhang et al., 2015a; Xu et al., 2015). In the Xu et al. (2015) study, that employed the AMS during intense BB periods in China, decreasing trend of f60 and increasing trend of f44 with aging was observed.

Aging of smoke plumes as they move from the source can also be illustrated by the change in the mass spectrum of different factors extracted by a Positive Matrix Factorization (PMF). The PMF evaluation tool (Paatero et al., 1994) has been extensively used in the source apportionment of the AMS OA data (Ulbrich et al., 2009; Crippa et al., 2014; Lanz et al.,

2007). PMF apportions the OA spectrum into factors that can be related to specific sources. Some studies have reported different PMF factors that correspond to smoke plumes of different degree of processing, fresh-like and aged-like BB organic aerosol (BBOA) factors (Capes et al., 2008; Bougiatioti et al., 2014; Brito et al., 2014). BBOA factors have distinctive m/z 60. However, fragments related to fresh hydrocarbon-like organic fraction m/z 27, 29, 41, 43, 55, and 57 are prominent in "fresh" BBOA spectra while enhanced OOA-related m/z 28 and 44 are signatures of "aged" BBOA MS. The oxygen-to-carbon (OC) ratio indicates the oxidation state of organic species and it strongly correlated with f44 intensity (Aiken et al., 2008). The OC ratio of BBOA factor thus reflects processing level of BB emission.

Fresh BBOA factor was extracted during the autumn season in urban and rural areas of Pearl River Delta (PRD) with OC ratio of 0.32 and 0.27, respectively (Huang et al., 2011; He et al., 2011a). Detected BB aerosol was associated with crop burning emissions. BBOA profile with the same OC ratio (0.26) was seen in winter for Yangtze River Delta (YRD) region, possibly due to open burning in the farmlands (Huang et al., 2013). Low OC ratio in these studies indicates presence of primary emissions. BBOA profiles with similar OC contribution were extracted in many laboratory and ambient studies (He et al., 2010; Aiken et al., 2009; Chirico et al., 2010; Crippa et al., 2014; DeCarlo et al., 2008; Grieshop et al., 2009). PMF-resolved aged BBOA profile was also extracted in China. During an autumn period in Beijing (Xu et al., 2015) BBOA factor with OC ratio of 0.5 was extracted, similarly to the profile observed in YRD during the same season period (Zhang et al., 2015a). These oxygenated BB profiles are comparable to studies outside of China (DeCarlo et al., 2010; Brito et al., 2014) and can be related to aged plumes probably transported from the surrounding regions. Aged BB aerosol can lose its BB signature during the atmospheric transformations and transit to a highly oxygenated aerosol fraction, which corresponds to the PMF-resolved low volatility OOA (LVOOA) factor (Jimenez et al., 2009). Zhang et al. (2015) (2015a) observed a decreasing trend of BBOA factors with aging suggesting the fast evolution of smoke organic fraction into OOA-like species.

Aerosol processing has been investigated in Beijing during winter (Sun et al., 2013) and summer (Sun et al., 2012) periods, using an aerosol chemical speciation monitor for chemical composition measurements. The portion of organic fraction was found to be higher in winter time (52%) compared to summer time (40%). This trend was attributed to increased POA fraction (mainly coal emissions but also includes BB and traffic plumes) that contributes to 70% of OC, while SOA contribution was shown to be similar in both seasons. In addition, it is suggested that contrary to the summer period, when photochemical processing is dominant due to increased temperature and solar radiation, winter time is instead characterized by aqueous reactions of primary emissions that are emitted and accumulated over the night, when partitioning of gaseous species due to low temperature and high relative humidity is taking place.

Ozone formation in biomass burning emissions

It has been observed that aging of BB plumes can induce production of tropospheric ozone (Real et al., 2007). Excess of main ozone precursors, VOCs, nitrogen oxides and carbon monoxide (CO), generated by fire emissions promote additional

atmospheric pathways for ozone production (Real et al., 2007; Jaffe et al., 2012; Parrington et al., 2013). Ozone enrichments that have been associated with BB have been observed mainly in Eastern China. The highest ozone concentration over the PRD region was showed to be in the spring season with concentrations up to 138 ppbv (Liu et al., 1999). Increased ozone pollution in this region has frequently been observed by number of studies and attributed to transport of photochemically produced ozone initiated by the BB plumes from fires in the South-East Asia (Indo Burma region) (Deng et al., 2008; Chan et al., 2003; Chan et al., 2000). Increased ozone concentrations related to BB activities (dominantly from post-harvest crop burning) during the summer period has also been observed in YRD (Cheung et al., 2001) and in urban and rural parts of Northern China (Meng et al., 2009; Ding et al., 2007). These authors also suggested a significant impact of transported aged smoke masses that carry photochemically formed ozone.

As ozone is a secondary pollutant that reflects the photochemical potential of the atmosphere, ozone enhancement in BB emissions has been used as a proxy for air mass photochemical activity (Yokelson et al., 2009; Hobbs et al., 2003; Jaffe et al., 2012; Real et al., 2007). According to studies in China, high photochemical activity illustrated by ozone enrichments can indicate an environment conducive to secondary aerosol formation. The ratio of ozone relative to CO ($\Delta O_3/\Delta CO$) increases with the aging of BB aerosols (Yokelson et al., 2009; Jaffe et al., 2013; Wigder et al., 2013). According to Mauzerall et al. (1998) (1998) and Honrath et al. (2004) (2004), $\Delta O_3/\Delta CO$ values for aged BB aerosols range between 0.1 and 0.7 (Jaffe et al., 2012). To the best of our knowledge studies like this have not been published so far in China. This again emphasizes the need to perform smoke tracking experiments in China especially in the highly polluted Eastern part, in order to estimate the potential for SOA formation and the role of ozone in this process in highly polluted areas.

Overall, numerous AMS measurements in regards to BB aging have been performed worldwide. Field studies included ground-based measurements and aircraft measurements, where more details can be obtained by tracking the plume (Yokelson et al., 2009; Capes et al., 2008; DeCarlo et al., 2010). Tracking smoke plumes provides insights into the real time atmospheric transformation processes (dilution, nucleation, condensation, repartitioning, oxidation, fragmentation etc.). There are also many laboratory-based measurements on this subject (Ortega et al., 2013; Hennigan et al., 2011; Heringa et al., 2011). Many studies have investigated the evolution of smoke plume emissions and there is no demonstrated consistency in the OA production in BB emission with aging. While some studies have shown increase in OA mass with plume age (Yokelson et al., 2009; DeCarlo et al., 2010; Heringa et al., 2011; Lee et al., 2008), others have found no-significant change in OA fraction (May et al., 2015; Akagi et al., 2012; Brito et al., 2014; Capes et al., 2008; Cubison et al., 2011).

The evolution and processing of smoke emissions and their influence on air quality in China is still poorly understood (Zhang et al., 2015a). It is a challenge to isolate the plume emissions and monitor them in highly polluted environments with a number of different sources. It has been observed that BB emissions which are in the process of aging can be promptly transformed into the OOA fraction. Therefore BB emissions can influence the SOA budget in China. Ozone enrichments in

BB plumes also suggest intensive photochemistry in the atmosphere across China. It is also important to characterize the mixing of plumes with other regional pollutants in the atmosphere during the aging process (Cubison et al., 2011), as China has many other important pollution sources. According to the reviewed studies, better regulation of BB activities is still needed in order to provide a less polluted environment. Huang et al. (2014) (2014) suggested regulating BB activities in China, especially in Guangzhou and Xi'an where higher non-fossil carbon fractions of SOA (up to 85% of SOA mass) than in Shanghai and Beijing was attributed to enhanced BB contribution.

7.6. Impacts derived by Biomass Burning

7.6.1. Severe haze events

According to Du et al.'s classification, haze episode is defined as the visibility is below 10 km and accompanied by relative humidity less than 90% (RH < 90%) for a period lasting longer than 4 h (Du et al., 2011). As the low visibility is mainly because of high $PM_{2.5}$ mass concentration during haze episodes, here, we simply define severe haze episodes as $PM_{2.5}$ mass concentration is higher than 200 μg/m^3 and accompanied by RH<90% and longer than 4 h. Many severe haze episodes accompanying with BB were promptly reported by news, TV and media in China. Literatures could be one or more years later than severe haze episodes with BB. During 9-11 June 2012, a thick yellow haze blanketed Nanjing and adjacent cities in the west Yangtze River delta region (Ding et al., 2013). In late afternoon of 9 June, 2012, the $PM_{2.5}$ concentration experienced a sharp increase with a 5 min maximum up to 468 μg/m^3 at 20:00 LT, followed by the high concentration of $PM_{2.5}$ mass with an average value in excess of 200 μg/m^3 that lasted for about 36 h. Higher KCl /$PM_{2.5}$ ratios and lower SO_4^{2-}/$PM_{2.5}$ and CO/$PM_{2.5}$ ratios were evident during the episode days, suggesting emission and chemical characteristics by BB and fossil fuel combustion plumes (Ding et al., 2013).

Sun et al. reported aerosol chemical species from a summer campaign at Xianghe, a suburban site located between the megacities of Beijing and Tianjin during 1–30 June 2013 (Sun et al., 2015). The mass concentration of organics in PM_1 rapidly increased from <20 μg/m^3 to 247 μg/m^3 on 23 June due to the impact of agricultural burning. They found that the contribution of BBOA (BB organic aerosol) was increased to 21% during the BB period in late June, indicating a large impact of agricultural burning on air pollution in summer 2013. BB also exerted a significant impact on aerosol optical properties, and it was estimated that ~60% enhancement of absorption at the ultraviolet spectral region was caused by the organic compounds from BB (Sun et al., 2015).

Wang et al. investigated the mixing state of individual carbonaceous particles during the severe haze episode by a single-particle aerosol mass spectrometer (SPAMS) in Nanjing in January 2013 (Wang et al., 2016). On clear days, the top ranked carbonaceous particle types were biomass (48.2%), EC-biomass (15.7%), OC/EC (11.1%), and sodium (9.6%), while on hazy days they were biomass (37.3%), EC-biomass (17.6%), EC-secondary (16.6%), and sodium (12.7%) (Wang et al., 2016). In the average mass spectra for EC-biomass particles, large peaks for dual polarity EC cluster ions (12[C]$^{+/-}$,

24$[C2]^{+/-}$, 36$[C3]^{+/-}$, . . . $[Cn]^{+/-}$) suggested that biomass particles may be mixed with EC or aggregated with EC particles during aging process of EC. The fractions of EC-biomass particles were 15.7% and 17.6% on clear and hazy days, respectively (Wang et al., 2016).

There have been reported many cases of haze episodes by BB with seized-resolved source apportionment and water-soluble potassium (K^+) increased properties (Tian et al., 2016; Liu et al., 2016; Wang et al., 2014). It is obvious that BB is one of the most reasons to drive rapidly server haze episodes (Wang et al., 2005).

7.6.2. Air quality impact

BB is a global phenomenon that releases large quantities of gaseous and particulate pollutants into the ambient atmosphere, including CO_2, CO, volatile organic compounds (VOCs), PM_{10}, $PM_{2.5}$, black carbon (BC), organic carbon (OC), elemental carbon (EC) and others (Ding et al., 2016; Li et al., 2007; Shi et al., 2014; Streets et al., 2003; Yamaji et al., 2009; Zhang et al., 2015e). In China, it has been estimated that the total annual emissions due to crop residue burning were 120 Tg CO_2, 4.6 Tg CO, 0.88 Tg $PM_{2.5}$, 0.39 Tg OC and 0.02 Tg EC in the year 2008 (Ni et al., 2015). The tremendous annual amounts of combustion products from BB into the atmosphere pose a threat to China's air quality. Literature indicated that BB has adverse environmental effects both locally and at large distances downwind via emitting various air pollutants. It is necessary to prohibit the open burning of crop residues in order to protect public health and the environment (Zhang et al., 2015d; Gustafsson et al., 2009).

Annual and seasonal characteristics

The annual and seasonal contributions of the biomass-burning source to ambient $PM_{2.5}$ have been reported in Beijing, Dongying and Chengdu (Yao et al., 2016; Tao et al., 2014; Zhang et al., 2013), three cities located in North, Central East, and Southwest China, respectively. Combining positive matrix factorization (PMF) receptor model and BB markers (levoglucosan and K^+), the results of these studies indicated that BB had higher contributions in busy farming (spring and autumn) and cold (winter) seasons than in the hot season (summer) (Fig. 7.6), consistent with the timings of open burning of crop residues for elimination of agricultural waste and domestic combustion of biomass fuels for heating and cooking. On annual average, BB contributed 12%, 15.8%, and 11% of $PM_{2.5}$ mass in Beijing, Dongying, and Chengdu, respectively.

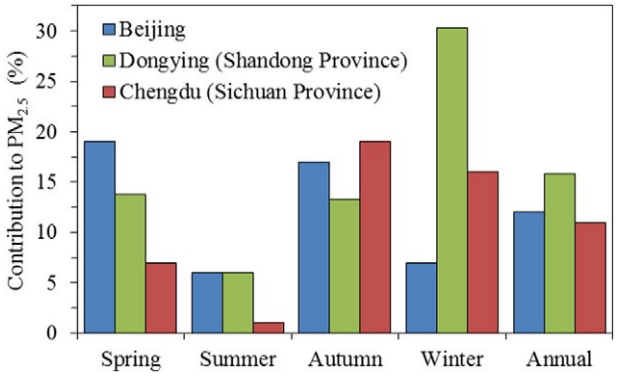

Figure 7.6 Annual and seasonal contributions of biomass burning to PM2.5 mass using PMF model in Beijing (Zhang et al., 2013), Dongying (Yao et al., 2016) and Chengdu (Tao et al., 2014).

Besides using receptor statistical models for source apportionment, satellite remote sensing sensor such as MODIS (Moderate Resolution Imaging Spectroradiometer) is also frequently used to detect agricultural fires on the ground (Wang et al., 2015; Chen et al., 2014; Sang et al., 2011; Hua et al., 2015; Huang et al., 2012b; Zhang et al., 2010c). According to Zha et al. (2013), the number of total agricultural fire sites in China was separately 5514 in 2009 and 4225 in 2010, among which more than 80% scattered in the heartland of agricultural regions such as Anhui, Jiangsu, Shandong, Henan and Hebei provinces. Moreover, the agricultural fire had a seasonal pattern, with two distinct peaks in summer (late spring/early summer) and autumn harvest periods, especially in June (61–86%) and October (5–14%) (Zha et al., 2013). This seasonal pattern was also supported by Zhang et al. (2016b) since their results revealed that the monthly $PM_{2.5}$ emission ratios of straw burning to other anthropogenic sources during June, the harvest period for many regions, were several times larger than the annual ratios at national, regional, and province levels.

Impact assessment during biomass burning episodes

Field burning of crop residues is common both in rural agricultural regions and peri-urban areas in China which are used to control weeds and clear agricultural combustible waste inexpensively. Although the emissions are not spread evenly throughout the year, open burning of biomass (e.g. rice straw, wheat straw, corn stalk, etc.) intensively emits abundant air pollutants into the environment in a short period, which rapidly degrades the local air quality and eventually causes the regional air pollution. Assessments of air quality impact due to BB events with respect to particulate matter and gaseous pollutants are studied over many regions of China, focusing on North, East, South, and Southwest China. The locations of some mentioned provinces and cities can be referred to the map in Fig. 7.7.

Figure 7.7 Locations of some mentioned provinces and cities in China.

North China. Based on MODIS images, large-scale flow field charts and environmental monitoring data, Li et al. (2008) found that winter wheat area of the North China Plain was the main source of straw burning pollution in Beijing in June and the transport paths for this type of pollution were mainly southerly.

Due to BB activities, the AOD (aerosol optical depth) from Giovanni map showed that the monthly average value of 550 nm in northern China had its maximum of 0.7 in June 2007 (Li et al., 2010b). Yu et al. (2013) characterized the aerosol optical properties during different pollution episodes in Beijing and found both total AOD and single scattering albedo (SSA) increased during BB days, from 0.24 and 0.865 for AOD and SSA on clean days to corresponding 0.64 and 0.922 on BB days.

Impacts on specific species of air pollutants from BB have been reported in North China. Based on radiocarbon (^{14}C) measurements at a regional background site in Bohai Rim in June 2013, Zong et al. (2015) found 74% of water-insoluble OC and 59% of EC in $PM_{2.5}$ derived from BB and biogenic sources when the air masses were from south region, and 63% and 48% for the air masses from north, respectively. In Beijing, high $PM_{2.5}$ levoglucosan concentrations (0.23 ± 0.37 μg/m^3 in summer and 0.59 ± 0.42 μg/m^3 in winter) were reported by Cheng et al. (2013) and their PMF model analysis showed that about 50% of the OC and EC in $PM_{2.5}$ in Beijing were associated with BB processes. They also suggested combustion of crop residuals was the major source of BB aerosol in Beijing (Cheng et al., 2013). Recently, the VOCs measurement was carried out at a rural site in North China during summer of 2013 indicated that extensive transport of BB emissions from

Shandong and Hebei provinces had an important effect on the local VOCs pollution levels and during the BB period VOCs had higher ozone formation potential values, especially the aromatics and alkynes (Zhu et al., 2016).

Transported BB emissions not only increased the atmospheric loading but also changed the chemical and physical properties of aerosol particles in downwind areas. During June 2013 at a suburban site in the North China, Sun et al. (2016b) found that the contribution of BB OA (organic aerosol) to PM_1 OA was significantly elevated from 11% to 21% during the period with agricultural burning influence and about 60% enhancement of absorption coefficient at ultraviolet spectral region for submicron aerosols was caused by BB emissions. Using transmission electron microscopy for individual-particle analysis, Li et al. (2010b) found that the copious organic matter, soot particles, and gases emitted by agricultural BB enhanced the formation of secondary particles and the coagulation of pre-existing inorganic particles during a haze period in urban Beijing in June 2007.

East China. East China is a major agricultural zone with a dense population and suffers from severe air pollution during June, the agricultural harvest season. MODIS remote sensing fire map revealed about 80% agricultural fires occurred in the agriculture areas of Anhui, Jiangsu, Shandong, and Henan provinces (Huang et al., 2012b; Li et al., 2010a) and these fires had significant contributions to worsen the regional air quality of East China during the harvest season. Integrating field investigations, satellite observations and model calculations, Cheng et al. (2014b) and Li et al. (2014a) analysed the courses of pollution episodes that took place in harvest season (May-June) and quantified the contributions of BB to particulate pollution. In both of the studies, the pollution episodes were divided into three phases: pre-pollution, pollution, and post-pollution periods. The sharp increases in PM, fine particulate OC, EC and K^+ observed during pollution periods, which confirmed the notable contribution of BB to elevated PM concentrations. The contributions of BB to $PM_{2.5}$, OC, and EC during pollution periods were estimated to be 23-51%, 48-86%, and 38-78%, respectively (Cheng et al., 2014b; Li et al., 2014a). Cheng et al. (2014b) suggested that, if open BB is completely eliminated, the average $PM_{2.5}$ concentration could be reduced by 51% for the Yangtze River Delta region, and the exposure level would decrease 47% during the post-harvest season.

Changes in the optical and physical properties of aerosols in Shanghai due to the transport of biomass-burning plumes in May 2009 were reported by He et al. (2015). They found that the biomass-burning plume led to a 37% increase in the average AOD at 500 nm (from 0.73 to 1.00) and a remarkable decrease in SSA at 670 nm and the volume concentration of fine-mode aerosols increased significantly under the effects of the BB (He et al., 2015). Wang et al. (2009b) investigated a haze event in June 2007 in urban Nanjing and found concentrations of levoglucosan, high molecular weight (HMW) n-alkanes, and HMW fatty acids in aerosols elevated by 3-40 times on hazy days mainly due to the emissions from field burning of wheat straw. In particular, the work of Liu and Li (2013) indicated BB was one of the major contributors to

water-insoluble OC in $PM_{2.5}$ in Ningbo whereas the work of Fu et al. (2014) highlighted BB could be an important source of soluble iron in $PM_{2.5}$ to Shanghai in summer.

South China. Combining the back trajectory analysis, fire count maps and field observations, Zhang et al. (2010c) found that regional open BB in the Indo-Myanmar region of Asia was probably one of the major potential sources of carbonaceous aerosols in South China region. In summer 2006, the intensive measurements conducted by Zhang et al. (2010a) in Guangzhou revealed that the relative contributions of smoke particles to OC in PM_{10} were on average 7.0 and 14% at daytime and nighttime, respectively, with maxima of 9.7 and 32% during the episodic transport events, indicating the significant impact from the biomass and biofuel burning activities in the rural parts of the Pearl River Delta and neighboring regions. Moreover, Zhang et al. (2014b) also found that during the periods with enhanced open biomass-burning activities in Southeast Asia or Southeast China, the EC and OC in $PM_{2.5}$ contributed by nonfossil combustion would have an increase by 5-10% in Hainan Island, the southernmost province of China.

The impact of BB on $PM_{2.5}$ in Guangzhou has been estimated during BB seasons by using acetonitrile and levoglucosan as tracers (Wang et al., 2007). According to Wang et al. (2007), the frequencies of $PM_{2.5}$ pollution episodes significantly influenced by BB were 100% for Xinken (a suburban site in Guangzhou) and 58% for downtown Guangzhou in October 2004; and during that period BB contributed 3.0–16.8% and 4.0–19.0% of $PM_{2.5}$ concentrations in Xinken and Guangzhou downtown, respectively. The results showed that the impact of BB on $PM_{2.5}$ was ubiquitous in both suburban and urban Guangzhou.

An investigation of CO characteristic during BB period was carried out by Yu et al. (2010) at the summit of Mountain Lulin in central Taiwan. The results showed that the average difference of CO levels between the two air parcel categories (one passed over the fire regions and the other did not) was approximately 79 ppb, suggesting that Asian BB played an important role in CO levels at this remote site during the springtime (Yu et al., 2010). In another study at Mei-Feng mountain site in central Taiwan, they also reported a net influence of Southeast Asian BB on both tropospheric O_3 and CO was approximately 23% in March (Lin et al., 2013). Yuan et al. (2010) measured ambient VOCs at a rural site (Jiangmen) in the Pearl River Delta during autumn 2008 and found BB contributed 9.5–17.7% to mixing ratios of the nine measured VOCs using two different tracer methods. Particularly, Shih et al. (2008) selected two areas in southern Taiwan to measure polychlorinated dibenzo-p-dioxins and dibenzofurans (PCDD/Fs) concentrations in the ambient air and their results revealed that during the BB season, the total PCDD/F I-TEQ (international-toxic equivalent quantity) concentrations in the ambient air were approximately 4 and 17 times higher than those without biomass open burning, respectively.

Southwest China. Compared with the three regions mentioned above, the studies focusing on BB impacts were relatively limited in the Southwest China. However, a recent study showed that BB activities in late spring and early summer seemed

to be a very important factor affecting $PM_{2.5}$ mass concentration and its chemical composition in megacity of Chengdu (Tao et al., 2013). During BB episodes, $PM_{2.5}$-bound levoglucosan, OC and K^+ concentrations in Chengdu increased by a factor of 2-7 (Tao et al., 2013). Using a synergy of on-line measurement, manual sampling, and remote sensing, Chen and Xie (2014) studied the heaviest and most long-lasting pollution event in the historical record of Chengdu during 18-21 May 2012. Their results showed that this pollution event in Chengdu was mainly caused by a combination of increased PM emission from BB and poor meteorological conditions (Chen and Xie, 2014).

BB had a significant influence on ambient VOCs in Chengdu–Chongqing Region as concluded by Li et al. (2014b). They intensively measured VOCs at Ziyang (a suburban site of Chengdu-Chongqing Region) and found BB contributed 9.4-36.8% to the mixing ratios of selected VOC species, and contributed most (above 30% each) to aromatics, formaldehyde, and acetaldehyde (Li et al., 2014b). Yang et al. (2012) examined the variability of fungal abundance in $PM_{2.5}$ during a BB season (spring 2009) in Chengdu. They found in the case of influence by pollution plumes from BB regions, the concentrations of fungal tracers (arabitol and mannitol) reached very high values and statistically significant correlations were found between fungal and BB tracers, suggesting elevated fungal material in $PM_{2.5}$ was mainly associated with BB activities (Yang et al., 2012).

7.6.3. Health impacts

As a renewable energy source, biomass materials include wood, animal waste, crops, and seaweed. From the very early stage of the civilization, people have been using biomass energy for surviving. Biomass based energy was the most popular energy before the industrial revolution (Fernandes et al., 2007). The use of biomass energy is getting popular in the current century (Field et al., 2008). According to the annual global energy consumption Gtoe, 2010, the total biomass energy usage all over the world is approximately 8-14% (Fossil fuels 10.45, Oil 4.03, Coal 3.56, Natural gas 2.86, Renewables 0.94, Hydro 0.78, Wind, commercial biomass 0.16, Estimated biomass 1-2) (Wit et al., 2009; Agarwal, 2007; Berndes et al., 2003; Bioenergy, 2007; Demirbas, 2007; Hoogwijk et al., 2005; Parikka, 2004; Williams et al., 2012). Ethanol and biodiesel fuel, wood and agricultural products, gas and biogas, and solid waste are the most popular biomass in the current century. Thermal, chemical, electrochemical, and biochemical conversion process are commonly used to convert the biomass into the other forms of energy. During the conversion process, biomass emits carbon dioxide, carbon monoxide, voltage organic compounds, nitrogen oxides, and other pollutant particles (Andreae et al., 2001; Baxter, 2005; Zhang et al., 2007). The open burning of biomass emits polycyclic aromatic hydrocarbons (PAH), and PAH is a group of more than 100 different chemicals (Jenkins et al., 1996). PAHs are usually formed during the incomplete burning of the biomass and produce pollutant particulates matter. The common source of PAHs is cigarette smoke, asphalt road, coal exhaust, vehicle engine exhaust, wood burning for cooking, agricultural burning, hazardous waste management, and bushfire (Finlayson-Pitts et al., 1997; Mumtaz et al., 1995). The atmospheric air contains a significant amount of suspended particles, liquid as well as solid, organic and inorganic substances, viruses, and bacteria (Seinfeld et al., 2008; Seaton et al., 1995;Tena et al., 2012). PAHs

can be in the form of volatile, semi-volatile and particulates pollutants (Allen et al., 1996; Finlayson-Pitts et al., 1997; Thrane et al., 1981). The PAHs sometimes attached to the dust particle in the air and the particle-bound PAHs are treated as threats to the human health (Organization., 2010). The PAHs has a significant impact on respiratory health, and an experiment in 1942 produced cancer in an experimental animal (Leiter et al., 1942). The PAHs in the atmosphere usually stuck to the dust and pollutant particle. During the inhalation process, the pollutant particulates and the compound mixture of the dust particle-PAHs enter into the human respiratory system.

Fig. 7.8 shows the schematic of the human lung upper and lower respiratory system. Throughout the inhalation and exhalation process, depending on the particle size, shape, and flow rate, particles deposit at the different portion of the respiratory airways (Islam et al., 2015).

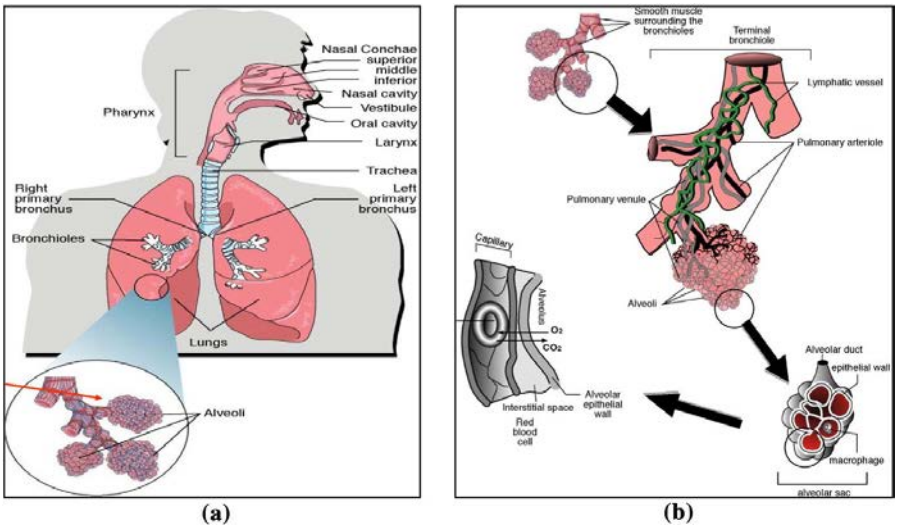

Figure 7.8 (a) Schematic representation of human lung upper airway, and alveoli, and (b) alveolar sacs, and alveolar capillary for blood transport (http://www.who.int/indoorair/ interventions/antiguamod21.pdf).

Depending on the inhaled particle size distribution, the smaller particle can reach the alveolar region of the respiratory system. The fine particulates are penetrated into the alveolar region and might be absorbed into the bloodstream of the human body. The fine particulates matter enters inside the alveolar sacs and cross the alveolar epithelial wall (Fig. 7.8b). After that particulates matter enter into the interstitial space and finally get access to the blood stream of the lung capillary. Generally, after deposition, particle gets clear from the lung wall by mucociliary clearance. Depending on the residence time of the pollutant particle in the lung airways, different respiratory diseases like asthma and respiratory allergies, chronic obstructive pulmonary diseases (COPD) chronic bronchitis, cystic fibrosis, lung cancer occurs. According to World Health Organization (WHO), 235 million people affected by asthma and more than 3 million people die each year from COPD, which is 6% of all deaths all over the world (*http://www.who.int/respiratory/en/*). WHO accounting 8.2 million people died

of cancer in 2012 and among them 1.59 million died of lung cancer which is the most common cause of cancer death (http://www.who.int/mediacentre/factsheets/fs297/en/). The rates of asthma, COPD, and lung cancer are increasing all over the world in the past few decades, and air pollution is the only reason for these respiratory diseases. The exposure of the biomass fuel smoke and the burning biomass for different purpose emits a significant amount of suspended particles into the atmosphere (Laumbach et al., 2012). Biomass is the only cooking or heating fuel for more than 2.4 billion household people around the world, and more than 90% of the rural people (low- and middle-income countries) use solid biomass (wood, crop waste, charcoal, and coal) energy in their daily life (Smith et al., 2004). The insufficient burning of the cooking materials produce highly toxic, and health-damaging pollutant particle. The emitted PAHs and ultra-fine particle penetrates at the alveolar region and enter the bloodstream of the human body. Eventually, the penetrated pollutants occur severe respiratory health hazards. Women and children are the main exposure of the household biomass pollutant emission. According to WHO, 4.3 million people died prematurely from household air pollution illness in 2012, and 22% of them are due to COPD, and 6% from lung cancer (*http://www.who.int/mediacentre/factsheets/fs292/en/*). Women are highly affected by COPD compare to men as they intake high level of household smoke from different sources. For men, whose are cigarette-addicted, have a strong possibility of COPD and lung cancer due to a serious lung infection. Pneumonia is the life threating diseases for the child less than 5 year old. The exposure of the indoor air pollution highly affects the children and acute lower respiratory infection occurs. In 2012, 12% of the children died due to pneumonia around the world among 4.3 million air pollution death. A meta-analysis of 24 studies found that the exposure of the biomass suspended PAHs increase the threat of pneumonia by 2-fold (Ciencewicki et al., 2008). The household biomass exposure also occurs stroke (34% death in 2012) and ischemic heart diseases (26% death in 2012) (*http://www.who.int/mediacentre/factsheets/fs292/en/*). Also, the biomass suspended ultrafine particle attack the respiratory airway, damaging the immune system and plummeting the oxygen transportability of the blood. There is a link between indoor air pollution and low birth weight, tuberculosis, and laryngeal cancer (*http://www.who.int/mediacentre/factsheets/fs292/en/*)(Bruce et al., 2000). Indoor and active outdoor smoking and second-hand tobacco smoke are the primary reason for the lung cancer. There is evidence that the respiratory growth of the children in the significantly polluted area is lower than those who live in the less polluted place (Eisner et al., 2010). The findings also suggest that the movement from the pollutant place to clean air place improve the lung growth of the children. The highly toxic particle bounded PAHs produce respiratory epithelium inflammation categorized by inflammable cell employment and vascular endothelial adhesion molecules (Laumbach et al., 2012). The respiratory epithelium damage eventually decreases the mucociliary clearance in the respiratory system, and the pollutant matter occurs severe lung diseases (Diat-Sanchez, 1997).

The BB also produces black carbon (BC). BC is the dark, light-absorbing components of atmospheric aerosols which contain elemental carbon. BC is usually produced during combustion reaction of burning biomass. The size of the BC particle ranging from 20 to 150 nanometer. BC is a subcategory of $PM_{2.5}$ with a diameter less than 2.5 micrometers. Indoor sources, such as cooking and environmental tobacco smoke also produce the significant amount of BC, which may guide to peaks in

exposure (Raaschou-Nielsen et al., 2011; Lanki et al., 2007). In general, BC can reach at the very deeper portion of the respiratory system due to its small size distribution. Smallest diameter BC can penetrate at the alveoli sacs and finally enter into the blood stream. It is well established that there is no threshold below which exposure has no effects. There is a conceptual disagreement about the straight toxicity of BC, this material acts beyond doubt as a transporter for different toxic substances, like PAH and heavy metals. Brussels Environmental report 2007-2008 shows the lung function may be reduced due to the BC penetration in the respiratory system. Epidemiological studies present adequate data of the association of cardiopulmonary morbidity and mortality with contact to BC. The long term and short term exposure to the $PM_{2.5}$ in the respiratory system is likely to be casual. The multiple linear and logistic regressions illustrate that BC had an important effect on lung function and on most respiratory symptoms, respectively (Gardiner et al., 2001).

7.6.4. Climate and weather impact

BB has long been considered as an important source influencing global and regional climate change. Fires of plants and agricultural straw influence vegetation at the surface and chemical composition in the atmosphere hence play important role in climate change and water cycle by influencing surface energy fluxes and radiative forcing (Randerson et al., 2006; Andreae et al., 2001; Bond et al., 2005; Penner et al., 1992; Robock, 1991).

From a global perspective, BB play an important role to the global warming because 1/5 of the emission of carbon dioxide (CO_2) and other greenhouse gases (GHGs) can be traced back to BB including wildfires, slash-and-burn agriculture and the burning of wood waste (Jacobson, 2014; Langenfelds et al., 2002). Unlike the long-lived and well-mixed GHGs, carbonaceous aerosols (black carbon and brown carbon) emitted directly or secondly formed during BB are distributed much less uniformly, posing impacts on climate mostly on a regional scale and in a much more complex way. IPCC (2013) gave an estimation of the radiative forcing due to BB particles as 0.0 (-0.2 to +0.2) W m^{-2} in the Fifth Assessment Report (AR5) at the top of the atmosphere (TOA). Though a near-zero global forcing at TOA, BB-induced climate forcing differ vertically. Smoke plumes consisting light-absorbing components generally absorb the solar radiation and thus heat the middle and lower atmosphere but decrease net radiation at the surface (Ramanathan et al., 2008; Hobbs et al., 1997; Randerson et al., 2006). In addition to this, through perturbations on solar radiation and acting as the cloud condensation nuclei (CCN), smoke particles cool the surface, stabilize the atmosphere, reduce the evaporation, and change the dynamic and microphysical evolution of cloud, plausibly induce feedbacks on cloudiness, precipitation, the hydrological cycle and even large scale circulations (Lee et al., 2014; Ackerman et al., 2000; Andreae et al., 2004; Hansen et al., 1997; Koren et al., 2004; Ramanathan et al., 2001; Sakaeda et al., 2011; Tosca et al., 2013).

In China and other Asian monsoon region, the impact of BB on regional climate and weather has been mainly studied with a focus on springtime forest burning in the South Asia and agricultural burning in East China in early summer. With an important contribution from BB, the carbonaceous aerosol layer in Southeast Asia, also known as Atmospheric Brown

Clouds (ABC), has been found to partly responsible for surface cooling, reduced evaporation, a latitudinal asymmetry in sea surface temperature, a delaying of the start of the Asian monsoon and regional drought (Ramanathan et al., 2005). Based on GEOS-5/AGCM model, Lee et al. (2014) investigated the impact of BB emission in Southeast Asia to precipitation in South China in pre-monsoon period (February-May). They found that BB aerosols could stabilize the atmosphere by reducing surface latent heat fluxes and cooling land surface temperature, but at the same time could increase cloud droplet number concentrations and decrease droplet effective radii. However, the indirect effect of absorption aerosols is less important when the plumes experienced a short transport time. Based on ground based measurement in Guangzhou, South China, Rose et al. (2010) also found that aerosol particles from open burning of agricultural waste were generally less CCN active, especially for the freshly emitted smoke with more organic aerosols.

The impact of BB to regional or weather in the Central east China is more complicated because of an overlap of straw burning area with fossil fuel combustion sources (Ding et al., 2013; Huang et al., 2012b). Based on MODIS data and WRF-Chem simulations, Guo et al. (2014) reported a case of mixed BB and anthropogenic pollution on the convective precipitation on 4 July 2008, and found that precipitation amount was increased up to 17% and the maximum rainfall rate was enhanced during the whole cloud lifetime under the influence of air pollution. However, based on measurement at a "flagship" type station SORPES in the Yangtze River Delta region and modeling simulation, Ding et al. (2013) reported a unique episode with two-fold influence from mixed BB and anthropogenic sources. During the daytime, a local convective precipitation was "burned off" by BB aerosols due to its direct effect in reducing the surface flux and change the boundary layer dynamics (see conceptual model given in Fig. 7.9); while at nighttime the downwind rainfall was enhanced because of its indirect effect in change microphysics of cloud and change of circulation due to dynamic forcing (Ding et al., 2013). These results are also consistent with that reported in a study for Amazon by Vendrasco et al. (2009).

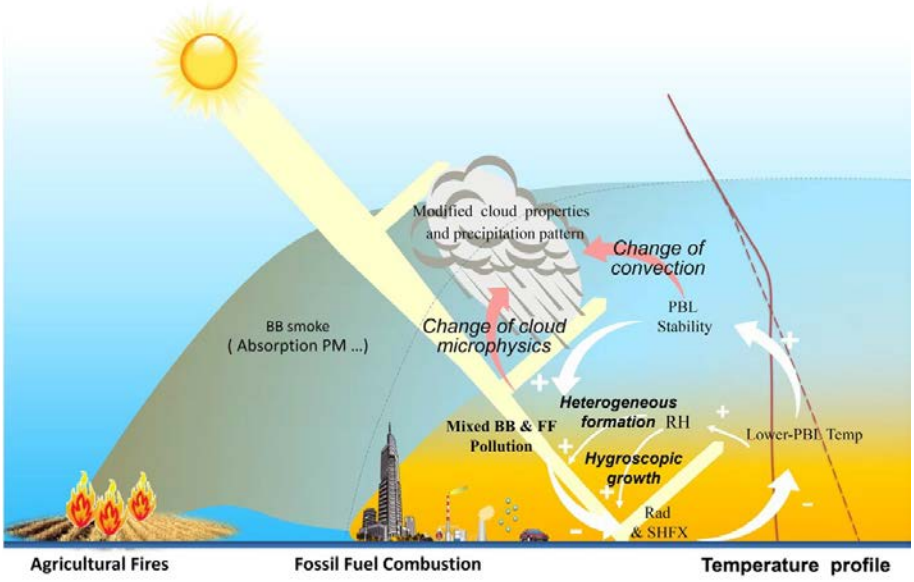

Figure 7.9 A schematic figure for interactions of air pollution-boundary layer-weather under a condition of mixed agricultural burning and fossil fuel combustion plumes (Modified from Ding et al., 2013a).

The impact of BB to climate and weather will further cause feedback to air pollution dispersion and atmospheric chemistry. As an important source of absorption aerosols, like BC and BrC, BB plume could cause significant impact to the boundary layer dynamics through the "Dome effect" (Ding et al., 2016), and further enhance the air pollution in megacities and in the downwind region of the BB emissions. The mixture of BB pollutants with anthropogenic sources could also enhance heterogeneous reactions and contributes to the formation of reactive trace gases, like HONO, and secondary aerosols, such as sulfate, especially after an enhancement of relative humidity trough aerosol-PBL-weather interactions (Xie et al., 2015; Nie et al., 2015). The complex physical and chemical interactions/feedbacks bring great challenges to understanding the climate system (Menon et al., 2002) and also to weather forecast in East Asia (Fan et al., 2015; Ding et al., 2013).

7.7. Research priorities and insights

This review focuses on literature findings concerning BB on the emissions, the impacts on air quality, health and climate in China, including the relationship to atmospheric dynamics and chemical processes. We address the following conclusions and recommendations as fellow:

Field Campaigns. BB is the main focused point which has been conducted in many campaigns like CAREBeijing in 2013 and 2014. The research region covers 65,000 km^2 (Yao et al., 2016). The new findings conducted with Atmospheric PAHs in

North China: Spatial distribution, OH reactivity, Air pollutants distribution in the North China Plain (Zhu et al., 2016; Fuchs et al., 2016; Yao et al., 2016).

The crop residue is so far the most bulk biomass open-burned in China. As BB plume is flowable with the meteorological factors, weather condition, it is strongly suggested that BB campaigns should be systematically developed in harvest seasons and in winter in larger regions with available technologies to recognize the emission factors, aging, transport, and chemical processes. It is necessary to carry out BB campaigns in different regions since the type of crop residue emits OC/EC, PAHs and pollutants quite different from South China to North China with size distribution and components (Zhang et al., 2011; Li et al., 2015; Zhang et al., 2016).

Aging. Primary pollutants from BB lead to an appearance of the changing fraction with inorganic inclusions such as KCl, sulfate and nitrite (Li et al., 2016b; Li et al., 2015; Popovicheva et al., 2016) in dark chamber simulations. The organic coatings observed on sulphur-rich and potassium-rich particles indicated the formation of SOA from the oxidation of precursor VOCs during the aging of smoke released from BB (Yao et al., 2016). Water-soluble organics in atmospheric aerosols are particularly important as they are main parts of aqSOA (Kawamura et al., 2016).

We recommend that smoke particles and their components during aging are needed to be investigated on the optical properties (Peng et al., 2016; Chen et al., 2015), morphology, mixing state with urban pollutants and toxicological organics. These data are assignable to modelers for the health and climate assessments.

Health and Climate. The BB smoke particles serve as a major source of BC and BrC, which adverse health and climate effects. Indoor smoke particles for cooking and heating are of importance in China. Therefore, it would be interesting to compare the biological effect of indoor smoke particle and its outlet aged smoke particles carrying carcinogenic substances' heterogeneous reactions as ambient fine particles are found an amount of PAHs and their nitrated, hydroxylated, and oxygenated derivatives (Lin et al., 2015). Given that a significant fraction of the Earth's BB-bearing in China, studies probing the climate effects of BC and BrC should be given high priority by the international research community.

Acknowledgments. This work is supported by National Natural Science Foundation of China (21190053, 21177025, 41275122, 41422504), Cyrus Tang Foundation (No. CTF-FD2014001), Ministry of Science and Technology of the People's Republic of China (2016YFC0202700, 2014BAC22B01), Research Grants Council of the Hong Kong Special Administrative Region (PolyU152052/14E), Australian Research Council Discovery grant (DP120100126, DP150100828, LP150100737), Environment and Conservation Fund (ECF 16/2015), City University of Hong Kong (7004470), Ministry of Environmental Protection of China (201509002), State Key Joint Laboratory of Environment Simulation and Pollution Control (15K08ESPCT), State Key Laboratory of Environmental Criteria and Risk Assessment (SKLECRA201641), and

Australia-China Centre for Air Quality Science and Management for organizing this special issue on air pollution in China. Phong Thai is funded by a QUT VC Research Fellowship. We are grateful to the GIOVANNI (*http://giovanni.gsfc.nasa.gov/giovanni*) NASA teams for providing data through their websites. MODIS fire product MCD14ML used in this study is downloaded from an ftp server at University of Maryland (*http//:fuoco.geog.umd.edu*).

7.8 References

Abel, S.J., Haywood, J.M., Highwood, E.J., Li, J., Buseck, P.R., 2003. Evolution of biomass burning aerosol properties from an agricultural fire in southern Africa. Geophys. Res. Lett. 30 (15). http://dx.doi.org/10.1029/2003GL017342.

Ackerman, A.S., Toon, O.B., Stevens, D.E., Heymsfield, A.J., Ramanathan, V., Welton, E.J., 2000. Reduction of tropical cloudiness by soot. Science 288 (5468), 1042–1047.

Adachi, K., Buseck, P.R., 2008. Internally mixed soot, sulfates, and organic matter in aero- sol particles from Mexico City. Atmos. Chem. Phys. 8 (21), 6469–6481.

Adachi, K., Buseck, P.R., 2013. Changes of ns-soot mixing states and shapes in an urban area during CalNex. J. Geophys. Res. Atmos. 9:3723–3730. http://dx.doi.org/10. 1002/jgrd.50321.

Adachi, K., Chung, S.H., Buseck, P.R., 2010. Shapes of soot aerosol particles and implica- tions for their effects on climate. J. Geophys. Res. Atmos. 115 (D15). http://dx.doi. org/10.1029/2009JD012868.

Adler, G., Flores, J.M., Abo Riziq, A., Borrmann, S., Rudich, Y., 2011. Chemical, physical, and optical evolution of biomass burning aerosols: a case study. Atmos. Chem. Phys. 11 (4), 1491–1503.

Agarwal, A.K., 2007. Biofuels (alcohols and biodiesel) applications as fuels for internal combustion engines. Prog. Energy Combust. Sci. 33 (3), 233–271.

Agus, E.L., Lingard, J.J.N., Tomlin, A.S., 2008. Suppression of nucleation mode particles by biomass burning in an urban environment: a case study. J. Environ. Monit. 10 (8), 979.

Aiken, A.C., Decarlo, P.F., Kroll, J.H., Worsnop, D.R., Huffman, J.A., Docherty, K.S., Ulbrich, I.M., et al., 2008. O/C and OM/OC ratios of primary, secondary, and ambient organic aerosols with high-resolution time-of-flight aerosol mass spectrometry. Environ. Sci. Technol. 42 (12), 4478–4485.

Aiken, A.C., Salcedo, D., Cubison, M.J., Huffman, J.A., DeCarlo, P.F., Ulbrich, I.M., Docherty, K.S., et al., 2009. Mexico City aerosol analysis during MILAGRO using high resolution aerosol mass spectrometry at the urban supersite (T0)– part 1: fine particle composi- tion and organic source apportionment. Atmos. Chem. Phys. 9 (17), 6633–6653.

Aiken, A.C., Foy, B.D., Wiedinmyer, C., DeCarlo, P.F., Ulbrich, I.M., Wehrli, M.N., Szidat, S., et al., 2010. Mexico city aerosol analysis during MILAGRO using high resolution aerosol mass spectrometry at the urban supersite (T0)–part 2: analysis of the biomass burn- ing contribution and the non-fossil carbon fraction. Atmos. Chem. Phys. 10 (12), 5315–5341.

Akagi, S.K., Craven, J.S., Taylor, J.W., McMeeking, G.R., Yokelson, R.J., Burling, I.R., Urbanski, S.P., et al., 2012. Evolution of trace gases and particles emitted by a chaparral fire in California. Atmos. Chem. Phys. 12 (3), 1397–1421.

Alfarra, M.R., Prevot, A.S., Szidat, S., Sandradewi, J., Weimer, S., Lanz, V.A., Schreiber, D., et al., 2007. Identification of the mass spectral signature of organic aerosols from wood burning emissions. Environ. Sci. Technol. 41 (16), 5770–5777.

Allen, J.O., Dookeran, N.M., And, K.A.S., Sarofim, A.F., And, K.T., Lafleur, A.L., 1996. Measure- ment of polycyclic aromatic hydrocarbons associated with size-segregated atmo- spheric aerosols in Massachusetts. Environ. Sci. Technol. 30 (3), 1023–1031.

Andreae, M.O., 1983. Soot carbon and excess fine potassium: long-range transport of combustion-derived aerosols. Science 220 (4602), 1148–1151.

Andreae, M.O., Merlet, P., 2001. Emission of trace gases and aerosols from biomass burn- ing. Glob. Biogeochem. Cycles 15 (4), 955–966.

Andreae, M.O., Rosenfeld, D., Artaxo, P., Costa, A.A., Frank, G.P., Longo, K.M., Silva-Dias, M., 2004. Smoking rain clouds over the Amazon. Science 303 (5662), 1337–1342.

Andreae, M.O., Schmid, O., Yang, H., Chand, D., Yu, J.Z., Zeng, L., Zhang, Y., 2008. Optical properties and chemical composition of the atmospheric aerosol in urban Guang- zhou, China. Atmos. Environ. 42 (25), 6335–6350.

Araujo, J.A., Barajas, B., Kleinman, M., Wang, X., Bennett, B.J., Gong, K.W., Navab, M., et al., 2008. Ambient particulate pollutants in the ultrafine range promote early atheroscle- rosis and systemic oxidative stress. Circ. Res. 102 (5), 589–596.

Arola, A., Lindfors, A., Natunen, A., Lehtinen, K., 2007. A case study on biomass burning aerosols: effects on aerosol optical properties and surface radiation levels. Atmos. Chem. Phys. 7 (16), 4257–4266.

Aurell, J., Gullett, B.K., Tabor, D., 2015. Emissions from southeastern U.S. Grasslands and pine savannas: comparison of aerial and ground field measurements with laboratory burns. Atmos. Environ. 111, 170–178.

Badarinath, K., Kharol, S.K., Sharma, A.R., 2009. Long-range transport of aerosols from ag- riculture crop residue burning in Indo-Gangetic Plains-a study using LIDAR, ground measurements and satellite data. J. Atmos. Sol. Terr. Phys. 71 (1), 112–120.

Barnaba, F., Angelini, F., Curci, G., Gobbi, G.P., 2011. An important fingerprint of wildfires on the European aerosol load. Atmos. Chem. Phys. 11 (20), 10487–10501.

Baxter, L., 2005. Biomass-coal co-combustion: opportunity for affordable renewable ener- gy. Fuel 84 (10), 1295–1302.

Beddows, D.C.S., Dall'Osto, M., Harrison, R.M., 2010. An enhanced procedure for the merg- ing of atmospheric particle size distribution data measured using electrical mobility and time-of-flight analysers. Aerosol Sci. Technol. 44 (11), 930–938.

Berndes, G., Hoogwijk, M., Broek, R.V.D., 2003. The contribution of biomass in the future global energy supply: a review of 17 studies. Biomass Bioenergy 25 (1), 1–28.

Bi, Y.Y., Wang, Y.J., Gao, C.Y., 2010. Straw resource quantity and its regional distribution in China. J. Agric. Mechanizat. Res. 3, 1–7.

Bioenergy, I., 2007. Potential Contribution of Bioenergy to the World's Future Energy Demand.

Blake, D.R., Smith, T.W., Chen, T.Y., Whipple, W.J., Rowland, F.S., 1994. Effects of biomass burn- ing on summertime nonmethane hydrocarbon concentrations in the Canadian wetlands. J. Geophys. Res. Atmos. 99 (D1):1699–1719. http://dx.doi.org/10.1029/93JD02598.

Bo, Y., Cai, H., Xie, S.D., 2008. Spatial and temporal variation of historical anthropogenic NMVOCs emission inventories in China. Atmos. Chem. Phys. 8 (23), 7297–7316.

Bølling, A.K., Pagels, J., Yttri, K.E., Barregard, L., Sallsten, G., Schwarze, P.E., Boman, C., 2009. Health effects of residential wood smoke particles: the importance of combustion conditions and physicochemical particle properties. Part. Fibre Toxicol. 6 (29), 20.

Bond, T.C., Bergstrom, R.W., 2006. Light absorption by carbonaceous particles: an investi- gative review. Aerosol Sci. Technol. 40 (1), 27–67.

Bond, W.J., Keeley, J.E., 2005. Fire as a global “herbivore”: the ecology and evolution of flammable ecosystems. Trends Ecol. Evol. 20 (7), 387–394.

Bond, T.C., Streets, D.G., Yarber, K.F., Nelson, S.M., Woo, J.H., Klimont, Z., 2004. A technol- ogy-based global inventory of black and organic carbon emissions from combustion. J. Geophys. Res. Atmos. 109 (D14). http://dx.doi.org/10.1029/2003JD003697.

Bougiatioti, A., Stavroulas, I., Kostenidou, E., Zarmpas, P., Theodosi, C., Kouvarakis, G., Canonaco, F., et al., 2014. Processing of biomass-burning aerosol in the eastern Med- iterranean during summertime. Atmos. Chem. Phys. 14 (9), 4793–4807.

Bougiatioti, A., Bezantakos, S., Stavroulas, I., Kalivitis, N., Kokkalis, P., Biskos, G., Mihalopoulos, N., et al., 2016. Biomass-burning impact on CCN number, hygroscopic- ity and cloud formation during summertime in the eastern Mediterranean. Atmos. Chem. Phys. 16 (11), 7389–7409.

Brito, J., Rizzo, L.V., Morgan, W.T., Coe, H., Johnson, B., Haywood, J., Longo, K., et al., 2014. Ground-based aerosol characterization during the South American Biomass Burning Analysis (SAMBBA) field experiment. Atmos. Chem. Phys. 14 (22), 12069–12083.

Bruce, N., Perez-Padilla, R., Albalak, R., 2000. Indoor air pollution in developing countries: a major environmental and public health challenge. World Health Organ. 78 (9), 1078–1092.

Cahoon Jr., D.R., Stocks, B.J., Levine, J.S., Cofer III, W.R., Pierson, J.M., 1994. Satellite analysis of the severe 1987 forest fires in northern China and southeastern Siberia. J. Geophys. Res. 99 (D9):18627–18638. http://dx.doi.org/10.1029/94JD01024.

Calfapietra, C., Morani, A., Sgrigna, G., Di Giovanni, S., Muzzini, V., Pallozzi, E., Guidolotti, G., et al., 2016. Removal of ozone by urban and peri-urban forests: evidence from lab- oratory, field, and modeling approaches. J. Environ. Qual. 45 (1), 224–233.

Calvo, A.I., Martins, V., Nunes, T., Duarte, M., Hillamo, R., Teinilä, K., Pont, V., et al., 2015. Residential wood combustion in two domestic devices: relationship of different pa- rameters throughout the combustion cycle. Atmos. Environ. 116, 72–82.

Cao, G., Zhang, X., Zheng, F., 2006. Inventory of black carbon and organic carbon emissions from China. Atmos. Environ. 40 (34), 6516–6527.

Cao, J.J., Lee, S.C., Chow, J.C., Watson, J.G., Ho, K.F., Zhang, R.J., Jin, Z.D., et al., 2007. Spatial and seasonal distributions of carbonaceous aerosols over China. J. Geophys. Res. Atmos. 112 (D22). http://dx.doi.org/10.1029/2006JD008205.

Cao, G., Zhang, X., Gong, S., An, X., Wang, Y., 2011. Emission inventories of primary parti- cles and pollutant gases for China. Chin. Sci. Bull. 56 (8), 781–788.

Cape, J.N., Cornell, S.E., Jickells, T.D., Nemitz, E., 2011. Organic nitrogen in the atmosphere- where does it come from? A review of sources and methods. Atmos. Res. 102 (1–2), 30–48.

Capes, G., Johnson, B., McFiggans, G., Williams, P.I., Haywood, J., Coe, H., 2008. Aging of biomass burning aerosols over West Africa: Aircraft measurements of chemical com- position, microphysical properties, and emission ratios. J. Geophys. Res. Atmos. 113 (D23). http://dx.doi.org/10.1029/2008JD009845.

Carrico, C.M., Petters, M.D., Kreidenweis, S.M., Collett, J.L., Engling, G., Malm, W.C., 2008. Aerosol hygroscopicity and cloud droplet activation of extracts of filters from biomass burning experiments. J. Geophys. Res. Atmos. 113 (D8). http://dx.doi.org/10.1029/ 2007JD009274.

Carrico, C.M., Prenni, A.J., Kreidenweis, S.M., Levin, E.J., McCluskey, C.S., DeMott, P.J., McMeeking, G.R., et al., 2016. Rapidly evolving ultrafine and fine mode biomass smoke physical properties: comparing laboratory and field results. J. Geophys. Res. Atmos. 121 (10). http://dx.doi.org/10.1002/2015JD024389.

Chakrabarty, R.K., Moosmüller, H., Chen, L.W.A., Lewis, K., Arnott, W.P., Mazzoleni, C., Dubey, M.K., et al., 2010. Brown carbon in tar balls from smoldering biomass combus- tion. Atmos. Chem. Phys. 10 (13), 6363–6370.

Chakrabarty, R.K., Gyawali, M., Yatavelli, R.L., Pandey, A., Watts, A.C., Knue, J., Chen, L.A., et al., 2016. Brown carbon aerosols from burning of boreal peatlands: microphysical properties, emission factors, and implications for direct radiative forcing. Atmos. Chem. Phys. 16 (5), 3033–3040.

Chan, C.K., Yao, X., 2008. Air pollution in mega cities in China. Atmos. Environ. 42 (1), 1–42. Chan, L.Y., Liu, H.Y., Lam, K.S., Wang, T., 1998. Analysis of the seasonal behavior of tropo-spheric ozone at Hong Kong. Atmos. Environ. 32 (2), 159–168.

Chan, L.Y., Chan, C.Y., Liu, H.Y., Christopher, S., Oltmans, S.J., Harris, J.M., 2000. A case study on the biomass burning in Southeast Asia and enhancement of tropospheric ozone over Hong Kong. Geophys. Res. Lett. 27 (10):1479–1482. http://dx.doi.org/10.1029/ 1999GL010855.

Chan, C.Y., Chan, L.Y., Harris, J.M., Oltmans, S.J., Blake, D.R., Qin, Y., Zheng, Y.G., et al., 2003. Characteristics of biomass burning emission sources, transport, and chemical specia- tion in enhanced springtime tropospheric ozone profile over Hong Kong. J. Geophys. Res. Atmos. 108 (D1). http://dx.doi.org/10.1029/2001JD001555.

Chen, X.F., 2001. Economics analysis on pollution from straw burning and managing in rural China. China Rural Economy, pp. 47–52 (in Chinese).

Chen, Y., Xie, S.D., 2014. Characteristics and formation mechanism of a heavy air pollution episode caused by biomass burning in Chengdu, Southwest China. Sci. Total Environ. 473–474 (3), 507–517.

Chen, Y., Shah, N., Braun, A., Huggins, F.E., Huffman, G.P., 2005. Electron microscopy inves- tigation of carbonaceous particulate matter generated by combustion of fossil fuels. Energy Fuel 19 (4), 1644–1651.

Chen, Y., Shah, N., Huggins, F.E., Huffman, G.P., 2006. Microanalysis of ambient particles from Lexington, KY, by electron microscopy. Atmos. Environ. 40 (4), 651–663.

Chen, L., Xing, L., Han, L., 2009. Renewable energy from agro-residues in China: solid biofuels and biomass briquetting technology. Renew. Sust. Energ. Rev. 13 (9), 2689–2695.

Chen, H., Hu, D., Wang, L., Mellouki, A., Chen, J., 2015a. Modification in light absorption cross section of laboratory-generated black carbon-brown carbon particles upon sur- face reaction and hydration. Atmos. Environ. 116, 253–261.

Chen, C., Sun, Y.L., Xu, W.Q., Du, W., Zhou, L.B., Han, T.T., Wang, Q.Q., et al., 2015b. Charac- teristics and sources of submicron aerosols above the urban canopy (260 m) in Bei- jing, China, during the 2014 APEC summit. Atmos. Chem. Phys. 15 (22), 812–879
(895).

Chen, Y., Shen, G., Huang, Y., Zhang, Y., Han, Y., Wang, R., Shen, H., et al., 2016. Household air pollution and personal exposure risk of polycyclic aromatic hydrocarbons among rural residents in Shanxi, China. Indoor Air 26 (2), 246–258.

Cheng, Y.F., Berghof, M., Garland, R.M., Wiedensohler, A., Wehner, B., Müller, T., Su, H., et al., 2009. Influence of soot mixing state on aerosol light absorption and single scatter- ing albedo during air mass aging at a polluted regional site in northeastern China. J. Geophys. Res. Atmos. 114 (D2). http://dx.doi.org/10.1029/2008JD010883.

Cheng, Y., Engling, G., He, K., Duan, F., Ma, Y., Du, Z., Liu, J., et al., 2013. Biomass burning contribution to Beijing aerosol. Atmos. Chem. Phys. 13 (15), 7765–7781.

Cheng, Z., Wang, S., Fu, X., Watson, J.G., Jiang, J., Fu, Q., Chen, C., et al., 2014a. Impact of bio- mass burning on haze pollution in the Yangtze River delta, China: a case study in summer 2011. Atmos. Chem. Phys. 14 (9), 4573–4585.

Cheng, Y., Engling, G., He, K., Duan, F., Du, Z., Ma, Y., Liang, L., et al., 2014b. The character- istics of Beijing aerosol during two distinct episodes: impacts of biomass burning and fireworks. Environ. Pollut. 185, 149–157.

Cheung, V.T., Wang, T., 2001. Observational study of ozone pollution at a rural site in the Yangtze Delta of China. Atmos. Environ. 35 (29), 4947–4958.

China, S., Mazzoleni, C., Gorkowski, K., Aiken, A.C., Dubey, M.K., 2013. Morphology and mixing state of individual freshly emitted wildfire carbonaceous particles. Nat. Commun.:2122 http://dx.doi.org/10.1038/ncomms3122.

Chirico, R., DeCarlo, P.F., Heringa, M.F., Tritscher, T., Richter, R., Prévôt, A., Dommen, J., et al., 2010. Impact of aftertreatment devices on primary emissions and secondary or- ganic aerosol formation potential from in-use diesel vehicles: results from smog chamber experiments. Atmos. Chem. Phys. 10 (23), 11545–11563.

Chubarova, N., Nezval, Y., Sviridenkov, I., Smirnov, A., Slutsker, I., 2012. Smoke aerosol and its radiative effects during extreme fire event over Central Russia in summer 2010. Atmos. Meas. Tech. 5 (3), 557–568.

Ciencewicki, J., Jaspers, I., 2008. Air pollution and respiratory viral infection. Inhal. Toxicol.

19 (19), 1135–1146.

Costanza, R., D'Arge, R., De Groot, R., Faber, S., Grasso, M., Hannon, B., Limburg, K., et al., 1997. The Value of the World's Ecosystem Services and Natural Capital.

Crippa, M., Canonaco, F., Lanz, V.A., Äijälä, M., Allan, J.D., Carbone, S., Capes, G., et al., 2014. Organic aerosol components derived from 25 AMS data sets across Europe using a consistent ME-2 based source apportionment approach. Atmos. Chem. Phys. 14 (12), 6159–6176.

Crutzen, P.J., Andreae, M.O., 1990. Biomass burning in the tropics: impact on atmospheric chemistry and biogeochemical cycles. Science 250, 1669–1678.

Cubison, M.J., Ortega, A.M., Hayes, P.L., Farmer, D.K., Day, D., Lechner, M.J., Brune, W.H., et al., 2011. Effects of aging on organic aerosol from open biomass burning smoke in air- craft and laboratory studies. Atmos. Chem. Phys. 11 (23), 12049–12064.

Da Rocha, G.O., Allen, A.G., Cardoso, A.A., 2005. Influence of agricultural biomass burning on aerosol size distribution and dry deposition in Southeastern Brazil. Environ. Sci. Technol. 39 (14), 5293–5301.

DeCarlo, P.F., Slowik, J.G., Worsnop, D.R., Davidovits, P., Jimenez, J.L., 2004. Particle mor- phology and density characterization by combined mobility and aerodynamic diam- eter measurements. Part 1: theory. Aerosol Sci. Technol. 38 (12), 1185–1205.

DeCarlo, P.F., Dunlea, E.J., Kimmel, J.R., Aiken, A.C., Sueper, D., Crounse, J., Wennberg, P.O., et al., 2008. Fast airborne aerosol size and chemistry measurements above Mexico City and Central Mexico during the MILAGRO campaign. Atmos. Chem. Phys. 8 (14), 4027–4048.

DeCarlo, P.F., Ulbrich, I.M., Crounse, J., Foy, B.D., Dunlea, E.J., Aiken, A.C., Knapp, D., et al., 2010. Investigation of the sources and processing of organic aerosol over the Central Mexican Plateau from aircraft measurements during MILAGRO. Atmos. Chem. Phys. 10 (12), 5257–5280.

Decesari, S., Facchini, M.C., Matta, E., Mircea, M., Fuzzi, S., Chughtai, A.R., Smith, D.M., 2002. Water soluble organic compounds formed by oxidation of soot. Atmos. Environ. 36 (11), 1827–1832.

Delfino, R.J., Sioutas, C., Malik, S., 2005. Potential role of ultrafine particles in associations between airborne particle mass and cardiovascular health. Environ. Health Perspect. 113 (8), 934–946.

Demirbas, A., 2007. Progress and recent trends in biofuels. Prog. Energy Combust. Sci. 33 (1), 1–18.

Deng, X., Tie, X., Zhou, X., Wu, D., Zhong, L., Tan, H., Li, F., et al., 2008. Effects of Southeast Asia biomass burning on aerosols and ozone concentrations over the Pearl River Delta (PRD) region. Atmos. Environ. 42 (36), 8493–8501.

Dhammapala, R., Claiborn, C., Simpson, C., Jimenez, J., 2007. Emission factors from wheat and Kentucky bluegrass stubble burning: comparison of field and simulated burn ex- periments. Atmos. Environ. 41 (7), 1512–1520.

Diat-Sanchez, D., 1997. The role of diesel exhaust particles and their associated polyaromatic hydrocarbons in the induction of allergic airway disease. Allergy 52 (38), 57–58.

Ding, A.J., Wang, T., Thouret, V., Cammas, J., Nédélec, P., 2008. Tropospheric ozone clima- tology over Beijing: analysis of aircraft data from the MOZAIC program. Atmos. Chem. Phys. 4 (7), 9795–9827.

Ding, A.J., Fu, C.B., Yang, X.Q., Sun, J.N., Petäjä, T., Kerminen, V., Wang, T., et al., 2013a. In- tense atmospheric pollution modifies weather: a case of mixed biomass burning with fossil fuel combustion pollution in eastern China. Atmos. Chem. Phys. 13 (20), 10545–10554.

Ding, A.J., Fu, C.B., Yang, X.Q., Sun, J.N., Zheng, L.F., Xie, Y.N., Herrmann, E., Nie, W., Petaja, T., Kerminen, V.-M., Kulmala, M., 2013b. Ozone and fine particle in the western Yang- tze River Delta: an overview of 1 yr data at the SORPES station. Atmos. Chem. Phys. 13 (11), 5813–5830.

Ding, K., Liu, J., Ding, A., Liu, Q., Zhao, T.L., Shi, J., Han, Y., Wang, H., Jiang, F., 2015. Uplifting of carbon monoxide from biomass burning and anthropogenic sources to the free tro- posphere in East Asia. Atmos. Chem. Phys. 15 (5), 2843–2866.

Ding, A.J., Huang, X., Nie, W., Sun, J.N., Kerminen, V.-M., Petaja, T., Su, H., Cheng, Y.F., Yang, X.Q., Wang, M.H., Chi, X.G., Wang, J.P., Virkkula, A., Guo, W.D., Yuan, J., Wang, S.Y., Zhang, R.J., Wu, Y.F., Song, Y., Zhu, T., Zilitinkevich, S., Kulmala, M., Fu, C.B., 2016a. En- hanced haze pollution by black carbon in megacities in China. Geophys. Res. Lett. 43: 2873–2879. http://dx.doi.org/10.1002/2016GL067745.

Ding, X., He, Q.F., Shen, R.Q., Yu, Q.Q., Zhang, Y.Q., Xin, J.Y., Wen, T.X., et al., 2016b. Spatial and seasonal variations of isoprene secondary organic aerosol in China: Significant impact of biomass burning during winter. Sci. Rep.-Uk http://dx.doi.org/10.1038/ srep20411.

Doherty, R.M., 2015. Atmospheric chemistry: ozone pollution from near and far. Nat. Geosci. 8 (9), 664–665.

Donahue, N.M., Robinson, A.L., Pandis, S.N., 2009. Atmospheric organic particulate matter: from smoke to secondary organic aerosol. Atmos. Environ. 43 (1), 94–106.

Dozier, J., 1981. A method for satellite identification of surface temperature fields of subpixel resolution. Remote Sens. Environ. 11, 221–229.

Drewnick, F., Hings, S.S., Alfarra, M.R., Prevot, A., Borrmann, S., 2009. Aerosol quantifica- tion with the aerodyne aerosol mass spectrometer: detection limits and ionizer back- ground effects. Atmos. Meas. Tech. 2 (1), 33–46.

Du, H., Kong, L., Cheng, T., Chen, J., Du, J., Li, L., Xia, X., et al., 2011. Insights into summer- time haze pollution events over shanghai based on online water-soluble ionic com- position of aerosols. Atmos. Environ. 45 (29), 5131–5137.

Duan, F., Liu, X., Yu, T., Cachier, H., 2004. Identification and estimate of biomass burning contribution to the urban aerosol organic carbon concentrations in Beijing. Atmos. Environ. 38 (9), 1275–1282.

Duo, B., Zhang, Y., Kong, L., Fu, H., Hu, Y., Chen, J., Li, L., et al., 2015. Individual particle analysis of aerosols collected at Lhasa City in the Tibetan plateau. J. Environ. Sci. 29, 165–177.

Duplissy, J., DeCarlo, P.F., Dommen, J., Alfarra, M.R., Metzger, A., Barmpadimos, I., Prevot, A.S., et al., 2011. Relating hygroscopicity and composition of organic aerosol particu- late matter. Atmos. Chem. Phys. 11 (3), 1155–1165.

Dusek, U., Frank, G.P., Hildebrandt, L., Curtius, J., Schneider, J., Walter, S., Chand, D., et al., 2006. Size matters more than chemistry for cloud-nucleating ability of aerosol parti- cles. Science 312 (5778), 1375–1378.

Dusek, U., Frank, G.P., Curtius, J., Drewnick, F., Schneider, J., Kürten, A., Rose, D., et al., 2010. Enhanced organic mass fraction and decreased hygroscopicity of cloud condensation nuclei (CCN) during new particle formation events. Geophys. Res. Lett. 37 (3). http:// dx.doi.org/10.1029/2009GL040930.

Dusek, U., Frank, G.P., Massling, A., Zeromskiene, K., Iinuma, Y., Schmid, O., Helas, G., et al., 2011. Water uptake by biomass burning aerosol at sub- and supersaturated condi- tions: closure studies and implications for the role of organics. Atmos. Chem. Phys. 11 (18), 9519–9532.

Dzepina, K., Volkamer, R.M., Madronich, S., Tulet, P., Ulbrich, I.M., Zhang, Q., Cappa, C.D., et al., 2009. Evaluation of recently-proposed secondary organic aerosol models for a case study in Mexico City. Atmos. Chem. Phys. 9 (15), 5681–5709.

Edwards, D.P., Emmons, L.K., Gille, J.C., Chu, A., Attié, J.L., Giglio, L., Wood, S.W., et al., 2006. Satellite-observed pollution from Southern Hemisphere biomass burning. J. Geophys. Res. Atmos. 111 (D14). http://dx.doi.org/10.1029/2005JD006655.

Eisner, M.D., Anthonisen, N., Coultas, D., Kuenzli, N., Perez-Padilla, R., Postma, D., Romieu, I., et al., 2010. An official American Thoracic Society public policy statement: novel risk factors and the global burden of chronic obstructive pulmonary disease. Am.
J. Respir. Crit. Care Med. 5 (182), 52–56.

Engelhart, G.J., Hennigan, C.J., Miracolo, M.A., Robinson, A.L., Pandis, S.N., 2012. Cloud con- densation nuclei activity of fresh primary and aged biomass burning aerosol. Atmos. Chem. Phys. 12 (15), 7285–7293.

Engling, G., Lee, J.J., Tsai, Y., Lung, S.C., Chou, C.C., Chan, C., 2009. Size-resolved anhydrosugar composition in smoke aerosol from controlled field burning of rice straw. Aerosol Sci. Technol. 7, 662–672.

Fan, J., Zhang, R., Collins, D., Li, G., 2006. Contribution of secondary condensable organics to new particle formation: a case study in Houston, Texas. Geophys. Res. Lett. 33 (15). http://dx.doi.org/10.1029/2006GL026295.

Fan, J., Rosenfeld, D., Yang, Y., Zhao, C., Leung, L.R., Li, Z., 2015. Substantial contribution of anthropogenic air pollution to catastrophic floods in Southwest China. Geophys. Res. Lett. 42 (14):6066–6075. http://dx.doi.org/10.1002/2015GL06447.

Fang, M., Chan, C.K., Yao, X., 2009. Managing air quality in a rapidly developing nation: China. Atmos. Environ. 43 (1), 79–86.

Ferge, T., Maguhn, J., Hafner, K., Mühlberger, F., Davidovic, M., Warnecke, R., Zimmermann, R., 2005. On-line analysis of gas-phase composition in the combustion chamber and particle emission characteristics during combustion of wood and waste in a small batch reactor. Environ. Sci. Technol. 39 (6), 1393–1402.

Fernandes, S. D., Trautmann, N. M., Streets, D. G., Roden, C. A. and Bond, T. C. Global biofuel use, 1850–2000, Glob. Biogeochem. Cycles 2007; 2:241–253.

Field, C.B., Campbell, J.E., Lobell, D.B., 2008. Biomass energy: the scale of the potential re- source. Trends Ecol. Evol. 2 (23), 65–72.

Fine, P.M., Cass, G.R., Simoneit, B.R., 2002. Chemical characterization of fine particle emis- sions from the fireplace combustion of woods grown in the southern United States. Environ. Sci. Technol. 36 (7), 1442–1451.

Finlayson-Pitts, B.J., Pitts, J.N., 1997. Tropospheric air pollution: ozone, airborne toxics, polycyclic aromatic hydrocarbons, and particles. Science 276 (5315), 1045–1052.

Formenti, P., Elbert, W., Maenhaut, W., Haywood, J., Osborne, S., Andreae, M.O., 2003. In- organic and carbonaceous aerosols during the Southern African Regional Science Ini- tiative (SAFARI 2000) experiment: chemical characteristics, physical properties, and emission data for smoke from African biomass burning. J. Geophys. Res. Atmos. 108 (D13). http://dx.doi.org/10.1029/2002JD002408.

Fraser, M.P., Yue, Z.W., Buzcu, B., 2003. Source apportionment of fine particulate matter in Houston, TX, using organic molecular markers. Atmos. Environ. 37 (15), 2117–2123.

Fu, H., Zhang, M., Li, W., Chen, J., Wang, L., Quan, X., Wang, W., 2012. Morphology, compo- sition and mixing state of individual carbonaceous aerosol in urban Shanghai. Atmos. Chem. Phys. 481 (2), 693–707.

Fu, H.B., Shang, G.F., Lin, J., Hu, Y.J., Hu, Q.Q., Guo, L., Zhang, Y.C., et al., 2014. Fractional iron solubility of aerosol particles enhanced by biomass burning and ship emission in Shanghai, East China. Sci. Total Environ. 2, 377–391.

Fuchs, H., Tan, Z., Lu, K., Bohn, B., Broch, S., Brown, S.S., Dong, H., et al., 2016. OH reactivity at a rural site (Wangdu) in the North China Plain: Contributions from OH reactants and experimental OH budget. Atmos. Chem. Phys. Discuss. http://dx.doi.org/10. 5194/acp-2016-716.

Fuller, K.A., Malm, W.C., Kreidenweis, S.M., 1999. Effects of mixing on extinction by carbona- ceous particles. J. Geophys. Res. 15:941–954. http://dx.doi.org/10.1029/1998JD100069.

Fullerton, D.G., Bruce, N., Gordon, S.B., 2008. Indoor air pollution from biomass fuel smoke is a major health concern in the developing world. T. Roy Soc. Trop. Med.e H 102 (9), 843–851.

Galanter, M., Levy, H., Carmichael, G.R., 2000. Impacts of biomass burning on tropospheric CO, NOx, and O3. J. Geophys. Res. Atmos. 105 (D5), 6633–6653.

Gao, M., Guttikunda, S.K., Carmichael, G.R., Wang, Y., Liu, Z., Stanier, C.O., Saide, P.E., et al., 2015. Health impacts and economic losses assessment of the 2013 severe haze event in Beijing area. Sci. Total Environ. 511, 553–561.

Garland, R.M., Yang, H., Schmid, O., Rose, D., Nowak, A., Achtert, P., Wiedensohler, A., et al., 2008. Aerosol optical properties in a rural environment near the mega-city Guang- zhou, China: implications for regional air pollution, radiative forcing and remote sensing. Atmos. Chem. Phys. 8 (17), 5161–5186.

Gautam, R., Hsu, N.C., Eck, T.F., Holben, B.N., Janjai, S., Jantarach, T., Tsay, S., et al., 2013. Characterization of aerosols over the Indochina peninsula from satellite-surface ob- servations during biomass burning pre-monsoon season. Atmos. Environ. 78, 51–59.

Ge, G., 2008. The climatic characteristics and change of haze days over China during 1961–2005. Acta Geograph. Sin. 7(13) (in Chinese).

Geng, F., Zhang, Q., Tie, X., Huang, M., Ma, X., Deng, Z., Yu, Q., et al., 2009. Aircraft measure- ments of O3, NOx, CO, VOCs, and SO2 in the Yangtze River Delta region. Atmos. Envi- ron. 43 (3), 584–593.

George, M., Suhail, S., Chandran, S., Chen, J., Lu, K., Ruth, A., Venables, D., et al., 2016. Open- path in situ measurement of the nitrate radical concentrations during the CAREBeijing-NCP 2014 summer campaign. EGU General Assembly Conference Ab- stracts. 12189.

Giglio, L., 2010. MODIS Collection 5 Active Fire Product User's Guide Version 2.4. Science Systems and Applications, Inc.

Giglio, L., Descloitres, J., Justice, C.O., Kaufman, Y.J., 2003. An enhanced contextual fire de- tection algorithm for MODIS. Remote Sens. Environ. 87 (2), 273–282.

Giglio, L., Randerson, J.T., Werf, G.R., 2013. Analysis of daily, monthly, and annual burned area using the fourth-generation global fire emissions database (GFED4). J. Geophys. Res. Biogeosci. 118 (1):317–328. http://dx.doi.org/10.1002/jgrg.20042.

Giordano, M.R., Short, D.Z., Hosseini, S., Lichtenberg, W., Asa-Awuku, A.A., 2013. Changes in droplet surface tension affect the observed hygroscopicity of photochemically aged biomass burning aerosol. Environ. Sci. Technol. 47 (19), 10980–10986.

Goldstein, A.H., Galbally, I.E., 2007. Known and unexplored organic constituents in the earth's atmosphere. Environ. Sci. Technol. 41 (5), 1514–1521.

Grahame, T.J., Klemm, R., Schlesinger, R.B., 2014. Public health and components of partic- ulate matter: the changing assessment of black carbon. J. Air Waste Manage. Assoc. 64 (6), 620–660.

Grieshop, A.P., Donahue, N.M., Robinson, A.L., 2009. Laboratory investigation of photo- chemical oxidation of organic aerosol from wood fires 2: analysis of aerosol mass spectrometer data. Atmos. Chem. Phys. 9 (4), 2227–2240.

Guan, H., Esswein, R., Lopez, J., Bergstrom, R., Warnock, A., Follette-Cook, M., Fromm, M., et al., 2010. A multi-decadal history of biomass burning plume heights identified using aerosol index measurements. Atmos. Chem. Phys. 10 (14), 6461–6469.

Gunthe, S.S., Rose, D., Su, H., Garland, R.M., Achtert, P., Nowak, A., Wiedensohler, A., et al., 2011. Cloud condensation nuclei (CCN) from fresh and aged air pollution in the megacity region of Beijing. Atmos. Chem. Phys. 11 (21), 11023–11039.

Guo, H., Wang, T., Simpson, I.J., Blake, D.R., Yu, X.M., Kwok, Y.H., Li, Y.S., 2004. Source con- tributions to ambient VOCs and CO at a rural site in eastern China. Atmos. Environ. 38 (27), 4551–4560.

Guo, H., Cheng, H.R., Ling, Z.H., Louie, P., Ayoko, G.A., 2011. Which emission sources are responsible for the volatile organic compounds in the atmosphere of Pearl River Delta? J. Hazard. Mater. 188 (1), 116–124.

Guo, S., Hu, M., Guo, Q., Zhang, X., Schauer, J.J., Zhang, R., 2013. Quantitative evaluation of emission controls on primary and secondary organic aerosol sources during Beijing 2008 Olympics. Atmos. Chem. Phys. 13 (16), 8303–8314.

Guo, X., Fu, D., Guo, X., Zhang, C., 2014. A case study of aerosol impacts on summer con- vective clouds and precipitation over northern China. Atmos. Res. 142, 142–157.

Gustafsson, Ö., Kruså, M., Zencak, Z., Sheesley, R.J., Granat, L., Engström, E., Praveen, P.S., et al., 2009. Brown clouds over South Asia: biomass or fossil fuel combustion? Science 323 (5913), 495–498.

Guyon, P., Boucher, O., Graham, B., Beck, J., Mayol-Bracero, O.L., Roberts, G.C., Maenhaut, W., et al., 2003. Refractive index of aerosol particles over the Amazon tropical forest during LBA-EUSTACH 1999. J. Aerosol Sci. 34 (7), 883–907.

Hallett, J., Hudson, J.G., Rogers, C.F., 1989. Characterization of combustion aerosols for haze and cloud formation. Aerosol Sci. Technol. 10 (1), 70–83.

Hallquist, M., Wenger, J.C., Baltensperger, U., Rudich, Y., Simpson, D., Claeys, M., Dommen, J., et al., 2009. The formation, properties and impact of secondary organic aerosol: current and emerging issues. Atmos. Chem. Phys. 9 (14), 5155–5236.

Han, Y.M., Lee, S.C., Cao, J.J., Ho, K.F., An, Z.S., 2009. Spatial distribution and seasonal var- iation of char-EC and soot-EC in the atmosphere over China. Atmos. Environ. 43 (38), 6066–6073.

Hand, J.L., Malm, W.C., Laskin, A., Day, D., Lee, T., Wang, C., Carrico, C., et al., 2005. Optical, physical, and chemical properties of tar balls observed during the Yosemite Aerosol Characterization Study. J. Geophys. Res. Atmos. 110 (D21). http://dx.doi.org/10. 1029/2004JD005728.

Hand, J.L., Day, D.E., McMeeking, G.M., Levin, E., Carrico, C.M., Kreidenweis, S.M., Malm, W.C., et al., 2010. Measured and modeled humidification factors of fresh smoke par- ticles from biomass burning: role of inorganic constituents. Atmos. Chem. Phys. 10 (13), 6179–6194.

Hansen, J., Sato, M., Ruedy, R., 1997. Radiative forcing and climate response. J. Geophys. Res. Atmos. 102 (D6):6831–6864. http://dx.doi.org/10.1029/96JD03436.

Hays, M.D., Geron, C.D., Linna, K.J., Smith, N.D., Schauer, J.J., 2002. Speciation of gas-phase and fine particle emissions from burning of foliar fuels. Environ. Sci. Technol. 36 (11), 2281–2295.

Hays, M.D., Fine, P.M., Geron, C.D., Kleeman, M.J., Gullett, B.K., 2005. Open burning of ag- ricultural biomass: physical and chemical properties of particle-phase emissions. Atmos. Environ. 39 (36), 6747–6764.

Haywood, J., Boucher, O., 2000. Estimates of the direct and indirect radiative forcing due to tropospheric aerosols: a review. Rev. Geophys. 38 (4), 513–543.

Haywood, J.M., Osborne, S.R., Francis, P.N., Keil, A., Formenti, P., Andreae, M.O., Kaye, P.H., 2003. The mean physical and optical properties of regional haze dominated by bio- mass burning aerosol measured from the C-130 aircraft during SAFARI 2000. J. Geophys. Res. Atmos. 108 (D13). http://dx.doi.org/10.1029/2002JD002226.

He, G., Ying, B., Liu, J., Gao, S., Shen, S., Balakrishnan, K., Jin, Y., et al., 2005. Patterns of household concentrations of multiple indoor air pollutants in China. Environ. Sci. Technol. 39 (4), 991–998.

He, L., Hu, M., Huang, X., Zhang, Y., Tang, X., 2006. Seasonal pollution characteristics of or- ganic compounds in atmospheric fine particles in Beijing. Sci. Total Environ. 359 (1), 167–176.

He, L., Lin, Y., Huang, X., Guo, S., Xue, L., Su, Q., Hu, M., et al., 2010. Characterization of high-resolution aerosol mass spectra of primary organic aerosol emissions from Chi- nese cooking and biomass burning. Atmos. Chem. Phys. 10 (23), 11535–11543.

He, L.Y., Huang, X.F., Xue, L., Hu, M., Lin, Y., Zheng, J., Zhang, R., et al., 2011a. Submicron aerosol analysis and organic source apportionment in an urban atmosphere in Pearl River Delta of China using high-resolution aerosol mass spectrometry. J. Geophys. Res. Atmos. 116 (D12). http://dx.doi.org/10.1029/2010JD014566.

He, M., Zheng, J., Yin, S., Zhang, Y., 2011b. Trends, temporal and spatial characteristics, and uncertainties in biomass burning emissions in the Pearl River Delta, China. Atmos. En- viron. 45 (24), 4051–4059.

He, Q., Zhao, X., Lu, J., Zhou, G., Yang, H., Gao, W., Yu, W., et al., 2015. Impacts of biomass- burning on aerosol properties of a severe haze event over Shanghai. Particuology 20 (3), 52–60.

Healy, R.M., Wang, J.M., Jeong, C.H., Lee, A., Willis, M.D., Jaroudi, E., Zimmerman, N., et al., 2015. Light-absorbing properties of ambient black carbon and brown carbon from fossil fuel and biomass burning sources. J. Geophys. Res. Atmos. 120 (13): 6619–6633. http://dx.doi.org/10.1002/2015JD023382.

Hedberg, E., Kristensson, A., Ohlsson, M., Johansson, C., Johansson, P., Swietlicki, E., Vesely, V., et al., 2002. Chemical and physical characterization of emissions from birch wood combustion in a wood stove. Atmos. Environ. 36 (30), 4823–4837.

Hennigan, C.J., Miracolo, M.A., Engelhart, G.J., May, A.A., Presto, A.A., Lee, T., Sullivan, A.P., et al., 2011. Chemical and physical transformations of organic aerosol from the photo- oxidation of open biomass burning emissions in an environmental chamber. Atmos. Chem. Phys. 11 (15), 7669–7686.

Heringa, M.F., DeCarlo, P.F., Chirico, R., Tritscher, T., Dommen, J., Weingartner, E., Richter, R., et al., 2011. Investigations of primary and secondary particulate matter of different wood combustion appliances with a high-resolution time-of-flight aerosol mass spectrometer. Atmos. Chem. Phys. 11 (12), 5945–5957.

Hinds, W.C., 2012. Aerosol Technology: Properties, Behavior, and Measurement of Air- borne Particles. John Wiley & Sons.

Ho, K.F., Lee, S.C., Ho, S.S.H., Kawamura, K., Tachibana, E., Cheng, Y., Zhu, T., 2010. Dicar- boxylic acids, ketocarboxylic acids, α-dicarbonyls, fatty acids, and benzoic acid in urban aerosols collected during the 2006 Campaign of Air Quality Research in Beijing (CAREBeijing-2006). J. Geophys. Res. Atmos. 115 (D19). http://dx.doi.org/10.1029/ 2009JD013304.

Hobbs, P.V., Reid, J.S., Kotchenruther, R.A., Ferek, R.J., Weiss, R., 1997. Direct radiative forc- ing by smoke from biomass burning. Science 275 (5307), 1777–1778.

Hobbs, P.V., Sinha, P., Yokelson, R.J., Christian, T.J., Blake, D.R., Gao, S., Kirchstetter, T.W., et al., 2003. Evolution of gases and particles from a savanna fire in South Africa. J. Geophys. Res. Atmos. 108 (D13). http://dx.doi.org/10.1029/2002JD002352.

Hodnebrog, Ø., Solberg, S., Stordal, F., Svendby, T.M., Simpson, D., Gauss, M., Hilboll, A., et al., 2012. Impact of forest fires, biogenic emissions and high temperatures on the el- evated Eastern Mediterranean ozone levels during the hot summer of 2007. Atmos. Chem. Phys. 12 (18), 8727–8750.

Hoffer, A., Gelencsér, A., Guyon, P., Kiss, G., Schmid, O., Frank, G.P.A., 2006. Optical proper- ties of humic-like substances (HULIS) in biomass-burning aerosols. Atmos. Chem. Phys. 6 (11), 3563–3570.

Honrath, R.E., Owen, R.C., Val Martin, M., Reid, J.S., Lapina, K., Fialho, P., Dziobak, M.P., et al., 2004. Regional and hemispheric impacts of anthropogenic and biomass burning emissions on summertime CO and O_3 in the North Atlantic lower free troposphere. J. Geophys. Res. Atmos. 109 (D24). http://dx.doi.org/10.1029/2004JD005147.

Hoogwijk, M., Faaij, A., Eickhout, B., Vries, B.D., Turkenburg, W., 2005. Potential of biomass energy out to 2100, for four IPCC SRES land-use scenarios. Biomass Bioenergy 29 (4), 225–257.

Hope, C., 2008. Discount rates, equity weights and the social cost of carbon. Energy Econ.

30 (3), 1011–1019.

Hu, W., Hu, M., Hu, W., Niu, H., Zheng, J., Wu, Y., Chen, W., et al., 2016. Characterization of submicron aerosols influenced by biomass burning at a site in the Sichuan Basin, southwestern China. Atmos. Chem. Phys.:1–39 http://dx.doi.org/10.5194/acp-2016- 114.

Hua, Y., Cheng, Z., Wang, S., Jiang, J., Chen, D., Cai, S., Fu, X., et al., 2015. Characteristics and source apportionment of $PM_{2.5}$ during a fall heavy haze episode in the Yangtze River Delta of China. Atmos. Environ. 123, 380–391.

Huang, X., He, L., Hu, M., Canagaratna, M.R., Kroll, J.H., Ng, N.L., Zhang, Y., et al., 2011. Char- acterization of submicron aerosols at a rural site in Pearl River Delta of China using an aerodyne high-resolution aerosol mass spectrometer. Atmos. Chem. Phys. 11 (5), 1865–1877.

Huang, K., Zhuang, G., Lin, Y., Fu, J.S., Wang, Q., Liu, T., Zhang, R., et al., 2012a. Typical types and formation mechanisms of haze in an Eastern Asia megacity, Shanghai. Atmos. Chem. Phys. 12 (1), 105–124.

Huang, X., He, L., Xue, L., Sun, T., Zeng, L., Gong, Z., Hu, M., et al., 2012b. Highly time-re- solved chemical characterization of atmospheric fine particles during 2010 Shanghai World Expo. Atmos. Chem. Phys. 12 (11), 4897–4907.

Huang, X., Song, Y., Li, M., Zhu, T., 2012c. Harvest season, high polluted season in East China. Environ. Res. Lett. 7 (4), 044033.

Huang, X., Li, M., Li, J., Song, Y., 2012d. A high-resolution emission inventory of crop burning in fields in China based on MODIS Thermal Anomalies/Fire products. Atmos. Environ. 50, 9–15.

Huang, K., Zhuang, G., Lin, Y., Wang, Q., Fu, J.S., Fu, Q., Liu, T., et al., 2013a. How to improve the air quality over megacities in China: pollution characterization and source analy- sis in Shanghai before, during, and after the 2010 World Expo. Atmos. Chem. Phys. 13 (12), 5927–5942.

Huang, X., Xue, L., Tian, X., Shao, W., Sun, T., Gong, Z., Ju, W., et al., 2013b. Highly time-re- solved carbonaceous aerosol characterization in Yangtze River Delta of China: com- position, mixing state and secondary formation. Atmos. Environ. 64, 200–207.

Huang, R., Zhang, Y., Bozzetti, C., Ho, K., Cao, J., Han, Y., Daellenbach, K.R., et al., 2014. High secondary aerosol contribution to particulate pollution during haze events in China. Nature 7521, 218–222.

Huang, X., Ding, A., Liu, L., Liu, Q., Ding, K., Niu, X., Nie, W., Xu, Z., Chi, X., Wang, M., Sun, J., Guo, W., Fu, C., 2016. Effects of aerosol–radiation interaction on precipitation during biomass-burning season in East China. Atmos. Chem. Phys. 16, 10063–10082.

Huo, J., Lu, X., Wang, X., Chen, H., Ye, X., Gao, S., Gross, D.S., et al., 2016. Online single par- ticle analysis of chemical composition and mixing state of crop straw burning parti- cles: from laboratory study to field measurement. Front. Environ. Sci. Eng. 10 (2), 244–252.

IARC, 2010. IARC monographs on the evaluation of carcinogenic risks to humans. Volume 92. Some non-heterocyclic polycyclic aromatic hydrocarbons and some related expo- sures. Lyon: International Agency for Research on Cancer.

IPCC, 2013. Anthropogenic and Natural Radiative Forcing, in Climate Change 2013: The Physical Science Basis. Cambridge Univ. Press, New York, USA.

Islam, S., Saha, S.C., Sauret, E., Gu, Y.T., Ristovski, Z.D., 2015. Numerical investigation of aerosol particle transport and deposition in realistic lung airway. 6th International Conference on Computational Methods, pp. 56–68.

Jacob, D.J., Crawford, J.H., Kleb, M.M., Connors, V.S., Bendura, R.J., Raper, J.L., Sachse, G.W., Gille, J.C., Emmons, L., Heald, C.L., 2003. Transport and chemical evolution over the Pacific(TRACE-P) aircraft mission: design, execution and first results. J. Geophys. Res. 108:D20. http://dx.doi.org/10.1029/2002JD003276.

Jacobson, M.Z., 2014. Effects of biomass burning on climate, accounting for heat and mois- ture fluxes, black and brown carbon, and cloud absorption effects. J. Geophys. Res. Atmos. 119 (14):8980–9002. http://dx.doi.org/10.1002/2014JD021861.

Jacobson, M.C., Hansson, H.C., Noone, K.J., Charlson, R.J., 2000. Organic atmospheric aero- sols: review and state of the science. Rev. Geophys. 38 (2), 267–294.

Jaffe, D.A., Wigder, N.L., 2012. Ozone production from wildfires: a critical review. Atmos. Environ. 51, 1–10.

Jaffe, D.A., Wigder, N., Downey, N., Pfister, G., Boynard, A., Reid, S.B., 2013. Impact of wild- fires on ozone exceptional events in the western US. Environ. Sci. Technol. 47 (19), 11065–11072.

Janssen, N.A.H., Hoek, G., Simic-Lawson, M., Fischer, P., van Bree, L., Ten Brink, H., Keuken, M., Atkinson, R.W., Anderson, H.R., Brunekreef, B., Cassee, F.R., 2011. Black carbon as an additional indicator of the adverse health effects of airborne particles compared with PM10 and PM2.5. Environ. Health Perspect. 119 (12), 1691–1699.

Jenkins, B.M., Jones, A.D., Turn, S.Q., Williams, R.B., 1996. Particle concentrations, gas-particle partitioning, and species intercorrelations for polycyclic aromatic hydro- carbons (PAH) emitted during biomass burning. Atmos. Environ. 30 (22), 3825–3835.

Jiménez, S., Ballester, J., 2005. Effect of co-firing on the properties of submicron aerosols from biomass combustion. P. Combust. Inst. 30 (2), 2965–2972.

Jimenez, J.L., Jayne, J.T., Shi, Q., Kolb, C.E., Worsnop, D.R., Yourshaw, I., Seinfeld, J.H., et al., 2003. Ambient aerosol sampling using the aerodyne aerosol mass spectrometer. J. Geophys. Res. Atmos. (D7) http://dx.doi.org/10.1029/2001JD001213.

Jimenez, J.L., Canagaratna, M.R., Donahue, N.M., Prevot, A., Zhang, Q., Kroll, J.H., DeCarlo, P.F., et al., 2009. Evolution of organic aerosols in the atmosphere. Science 326 (5959), 1525–1529.

Jin, Y., Zhou, Z., He, G., Wei, H., Liu, J., Liu, F., Tang, N., et al., 2005. Geographical, spatial, and temporal distributions of multiple indoor air pollutants in four Chinese provinces. En- viron. Sci. Technol. 39 (24), 9431–9439.

Johnson, K.S., Zuberi, B., Molina, L.T., Molina, M.J., Iedema, M.J., Cowin, J.P., Gaspar, D.J., et al., 2005. Processing of soot in an urban environment: case study from the Mexico City metropolitan area. Atmos. Chem. Phys. 5 (11), 3033–3043.

Johnston, F.H., Henderson, S.B., Chen, Y., Randerson, J.T., Marlier, M., DeFries, R.S., Kinney, P., et al., 2015. Estimated Global Mortality Attributable to Smoke from Landscape Fires. University of British Columbia.

Jolleys, M.D., Coe, H., McFiggans, G., Capes, G., Allan, J.D., Crosier, J., Williams, P.I., et al., 2012. Characterizing the aging of biomass burning organic aerosol by use of mixing ratios: a meta-analysis of four regions. Environ. Sci.Technol. 46 (24), 13093–13102.

Jordan, T.B., Seen, A.J., Jacobsen, G.E., 2006. Levoglucosan as an atmospheric tracer for woodsmoke. Atmos. Environ. 40 (27), 5316–5321.

Justice, C.O., Giglio, L., Korontzi, S., Owens, J., Morisette, J.T., Roy, D., Descloitres, J., et al., 2002. The MODIS fire products. Remote Sens. Environ. 83 (1), 244–262.

Justice, C., Giglio, L., Boschetti, L., Roy, D., Csiszar, I., Morisette, J., Kaufman, Y., 2006. MODIS Fire Products Algorithm Technical Background Document. MODIS Science Team.

Kahn, R.A., Li, W.H., Moroney, C., Diner, D.J., Martonchik, J.V., Fishbein, E., 2007. Aerosol source plume physical characteristics from space-based multiangle imaging. J. Geophys. Res. Atmos. (D11) http://dx.doi.org/10.1029/2006JD007647.

Kanakidou, M., Seinfeld, J.H., Pandis, S.N., Barnes, I., Dentener, F.J., Facchini, M.C., Dingenen, R.V., et al., 2005. Organic aerosol and global climate modelling: a review. Atmos. Chem. Phys. 5 (4), 1053–1123.

Kaskaoutis, D.G., Kharol, S.K., Sifakis, N., Nastos, P.T., Sharma, A.R., Badarinath, K., Kambezidis, H.D., 2011. Satellite monitoring of the biomass-burning aerosols during the wildfires of August 2007 in Greece: climate implications. Atmos. Environ. 45 (3), 716–726.

Kaskaoutis, D.G., Gautam, R., Singh, R.P., Houssos, E.E., Goto, D., Singh, S., Bartzokas, A., et al., 2012. Influence of anomalous dry conditions on aerosols over India: transport, dis- tribution and properties. J. Geophys. Res. Atmos. (D9) http://dx.doi.org/10.1029/ 2011JD017314.

Kaskaoutis, D.G., Kumar, S., Sharma, D., Singh, R.P., Kharol, S.K., Sharma, M., Singh, A.K., et al., 2014. Effects of crop residue burning on aerosol properties, plume characteristics, and long-range transport over northern India. J. Geophys. Res. Atmos. 9:5424–5444. http://dx.doi.org/10.1034/j.1600-0560.2003.00064.x.

Kaul, D.S., Gupta, T., Tripathi, S.N., Tare, V., Collett Jr., J.L., 2011. Secondary organic aerosol: a comparison between foggy and nonfoggy days. Environ. Sci. Technol. 45 (17), 7307–7313.

Kawamura, K., Bikkina, S., 2016. A review of dicarboxylic acids and related compounds in atmospheric aerosols: molecular distributions, sources and transformation. Atmos. Res. 170, 140–160.

Khlystov, A., Stanier, C., Pandis, S.N., 2004. An algorithm for combining electrical mobility and aerodynamic size distributions data when measuring ambient aerosol special issue of aerosol science and technology on findings from the fine particulate matter supersites program. Aerosol Sci. Technol. 38 (1), 229–238.

Kim, K., Jahan, S.A., Kabir, E., Brown, R.J., 2013. A review of airborne polycyclic aromatic hydrocarbons (PAHs) and their human health effects. Environ. Int. 60, 71–80.

Kirchstetter, T.W., Novakov, T., Hobbs, P.V., 2004. Evidence that the spectral dependence of light absorption by aerosols is affected by organic carbon. J. Geophys. Res. Atmos. (D21) http://dx.doi.org/10.1029/2004JD004999.

Kleinman, L.I., Springston, S.R., Daum, P.H., Lee, Y., Nunnermacker, L.J., Senum, G.I., Wang, J., et al., 2008. The time evolution of aerosol composition over the Mexico City pla- teau. Atmos. Chem. Phys. 8 (6), 1559–1575.

Kong, F.H., Li, X.Z., Zhao, S.L., Yin, H.W., 2003. Research advance in forest restoration on the burned blanks. J. Forest Res. 180–184 (in Chinese).

Koppejan, J., Van Loo, S., 2012. The Handbook of Biomass Combustion and Co-firing. Routledge.

Koren, I., Kaufman, Y.J., Remer, L.A., Martins, J.V., 2004. Measurement of the effect of Am- azon smoke on inhibition of cloud formation. Science 303 (5662), 1342–1345.

Kostenidou, E., Pathak, R.K., Pandis, S.N., 2007. An algorithm for the calculation of second- ary organic aerosol density combining AMS and SMPS data. Aerosol Sci. Technol. 41 (11), 1002–1010.

Kroll, J.H., Seinfeld, J.H., 2008. Chemistry of secondary organic aerosol: formation and evo- lution of low-volatility organics in the atmosphere. Atmos. Environ. 42 (16), 3593–3624.

Kumar, R., Naja, M., Satheesh, S.K., Ojha, N., Joshi, H., Sarangi, T., Pant, P., et al., 2011. Influ- ences of the springtime northern Indian biomass burning over the central Himalayas.
J. Geophys. Res. Atmos. (D19) http://dx.doi.org/10.1029/2010JD015509.

Kumar, R., Naja, M., Pfister, G.G., Barth, M.C., Brasseur, G.P., 2013. Source attribution of car- bon monoxide in India and surrounding regions during wintertime. J. Geophys. Res. Atmos. 118 (4):1981–1995. http://dx.doi.org/10.1002/jgrd.50134.

Kumar, K.R., Yin, Y., Sivakumar, V., Kang, N., Yu, X., Diao, Y., Adesina, A.J., et al., 2015. Aero- sol climatology and discrimination of aerosol types retrieved from MODIS, MISR and OMI over Durban (29.88°S, 31.02°E), South Africa. Atmos. Environ. 117 (117), 9–18. Lack, D.A., Langridge, J.M., Bahreini, R., Cappa, C.D., Middlebrook, A.M., Schwarz, J.P., 2012. Brown carbon and internal mixing in biomass burning particles. Proc. Natl. Acad. Sci.109 (37), 14802–14807.

Lai, L.Y., Sequeira, 2001. Visibility degradation across Hong Kong: its components and their relative contributions. Atmos. Environ. 35 (34), 5861–5872.

Lambe, A.T., Chhabra, P.S., Onasch, T.B., Brune, W.H., Hunter, J.F., Kroll, J.H., Cummings, M.J., et al., 2015. Effect of oxidant concentration, exposure time, and seed particles on secondary organic aerosol chemical composition and yield. Atmos. Chem. Phys. 15 (6), 3063–3075.

Langenfelds, R.L., Francey, R.J., Pak, B.C., Steele, L.P., Lloyd, J., Trudinger, C.M., Allison, C.E., 2002. Interannual growth rate variations of atmospheric CO_2 and its $\delta^{13}C$, H_2, CH_4,and CO between 1992 and 1999 linked to biomass burning. Glob. Biogeochem. Cycles 16(3).

Lanki, T., Ahokas, A., Alm, S., Janssen, N.A.H., Hoek, G., Hartog, J.J.D., Brunekreef, B., et al., 2007. Determinants of personal and indoor $PM_{2.5}$ and absorbance among elderly sub- jects with coronary heart disease. J. Expo. Sci. Environ. Epidemiol. 17(2).

Lanz, V.A., Alfarra, M.R., Baltensperger, U., Buchmann, B., Hueglin, C., Prévôt, A., 2007. Source apportionment of submicron organic aerosols at an urban site by factor ana- lytical modelling of aerosol mass spectra. Atmos. Chem. Phys. 7 (6), 1503–1522.

Laumbach, R.J., Kipen, H.M., 2012. Respiratory health effects of air pollution: update on biomass smoke and traffic pollution. J. Allergy Clin. Immunol. 129 (1), 3–11.

Lawrence, M.G., Lelieveld, J., 2010. Atmospheric pollutant outflow from southern Asia: a review. Atmos. Chem. Phys. 10 (22), 11017–11096.

Lee, S., Kim, H.K., Yan, B., Cobb, C.E., Hennigan, C., Nichols, S., Chamber, M., et al., 2008. Di- agnosis of aged prescribed burning plumes impacting an urban area. Environ. Sci. Technol. 42 (5), 1438–1444.

Lee, S.S., Feingold, G., McComiskey, A., Yamaguchi, T., Koren, I., Vanderlei Martins, J., Yu, H., 2014a. Effect of gradients in biomass burning aerosol on shallow cumulus convective circulations. J. Geophys. Res. Atmos. 16:9948–9964. http://dx.doi.org/10.1002/ 2014JD021819.

Lee, D., Sud, Y.C., Oreopoulos, L., Kim, K., Lau, W.K., Kang, I., 2014b. Modeling the influ- ences of aerosols on pre-monsoon circulation and rainfall over Southeast Asia. Atmos. Chem. Phys. 14 (13), 6853–6866.

Leiter, J., Shimkin, M., Shear, M., 1942. Production of subcutaneous sarcomas in mice with tars extracted from atmospheric dusts. J. Natl. Cancer Inst. 3 (2), 155–165.

Levin, E.J.T., McMeeking, G.R., Carrico, C.M., Mack, L.E., Kreidenweis, S.M., Wold, C.E., Moosmüller, H., et al., 2010. Biomass burning smoke aerosol properties measured during Fire Laboratory at Missoula Experiments (FLAME). J. Geophys. Res. 115 (D18). http://dx.doi.org/10.1029/2009JD013601.

Levy, J.I., Diez, D., Dou, Y., Barr, C.D., Dominici, F., 2012. A meta-analysis and multisite time-series analysis of the differential toxicity of major fine particulate matter con- stituents. Am. J. Epidemiol. 175 (11), 1091–1099.

Levy, R.C., Mattoo, S., Munchak, L.A., Remer, L.A., Sayer, A.M., Patadia, F., Hsu, N.C., 2013. The collection 6 MODIS aerosol products over land and ocean. Atmos. Meas. Tech. 6 (11), 2989–3034.

Lewis, K.A., Arnott, W.P., Moosmuller, H., Chakrabarty, R.K., Carrico, C.M., Kreidenweis, S.M., Day, D.E., et al., 2009. Reduction in biomass burning aerosol light absorption upon humidification: roles of inorganically-induced hygroscop- icity, particle collapse, and photoacoustic heat and mass transfer. Atmos. Chem. Phys. 9, 8949–8966.

Li, W., Shao, L., 2009. Transmission electron microscopy study of aerosol particles from the brown hazes in northern China. J. Geophys. Res. Atmos. 114 (D9). http://dx.doi. org/10.1029/2008JD011285.

Li, W., Shao, L., 2010. Mixing and water-soluble characteristics of particulate organic com- pounds in individual urban aerosol particles. J. Geophys. Res. Atmos. 115 (D2). http:// dx.doi.org/10.1029/2009JD012575.

Li, N., Sioutas, C., Cho, A., Schmitz, D., Misra, C., Sempf, J., Wang, M., et al., 2002. Ultrafine particulate pollutants induce oxidative stress and mitochondrial damage. Environ. Health Perspect. 111 (4), 455–460.

Li, J., Pósfai, M., Hobbs, P.V., Buseck, P.R., 2003. Individual aerosol particles from biomass burning in southern Africa: Compositions and aging of inorganic particles. J. Geophys. Res. Atmos. 108 (D13). http://dx.doi.org/10.1029/2002JD002310.

Li, D., Fan, S., He, A., Yin, F., 2004. Forest resources and environment in China. J. For. Res.- Jpn 9 (4), 307–312.

Li, X., Wang, S., Duan, L., Hao, J., Li, C., Chen, Y., Yang, L., 2007. Particulate and trace gas emissions from open burning of wheat straw and corn stover in China. Environ. Sci. Technol. 41 (17), 6052–6058.

Li, L., Wang, Y., Zhang, Q., Li, J., Yang, X., Jin, J., 2008. Wheat straw burning and its associ- ated impacts on Beijing air quality. Sci. China Ser. D Earth Sci. 51 (3), 403–414.

Li, H., Han, Z., Cheng, T., Du, H., Kong, L., Chen, J., Zhang, R., et al., 2010a. Agricultural fire impacts on the air quality of shanghai during summer harvesttime. Aerosol Air Qual. Res. 10 (2), 95–101.

Li, W.J., Shao, L.Y., Buseck, P.R., 2010b. Haze types in Beijing and the influence of agricul- tural biomass burning. Atmos. Chem. Phys. 10 (17), 8119–8130.

Li, W.J., Zhang, D.Z., Shao, L.Y., Zhou, S.Z., Wang, W.X., 2011a. Individual particle analysis of aerosols collected under haze and non-haze conditions at a high-elevation mountain site in the North China plain. Atmos. Chem. Phys. 11 (22), 11733–11744.

Li, X., Li, P., Yan, L., Chen, J., Cheng, T., Xu, S., 2011b. Characterization of polycyclic aromatic hydrocarbons in fog-rain events. J. Environ. Monit. 13 (11), 2988–2993.

Li, J., Song, Y., Mao, Y., Mao, Z., Wu, Y., Li, M., Huang, X., et al., 2014a. Chemical character- istics and source apportionment of PM2.5 during the harvest season in eastern China's agricultural regions. Atmos. Environ. 92, 442–448.

Li, L., Chen, Y., Zeng, L., Shao, M., Xie, S., Chen, W., Lu, S., et al., 2014b. Biomass burning contribution to ambient volatile organic compounds (VOCs) in the Chengdu-Chong- qing Region (CCR). Atmos. Environ. 99, 403–410.

Li, C., Ma, Z., Chen, J., Wang, X., Ye, X., Wang, L., Yang, X., et al., 2015. Evolution of biomass burning smoke particles in the dark. Atmos. Environ. 244-252.

Li, C., Hu, Y., Zhang, F., Chen, J., Ma, Z., Ye, X., Yang, X., et al., 2016a. Multi-pollutants emis- sions from the burning of major agricultural residues in China and the related health- economic effect assessment. Atmos. Chem. Phys. Discuss. http://dx.doi.org/10.5194/ acp-2016-651.

Li, C., Hu, Y., Chen, J., Ma, Z., Ye, X., Yang, X., Wang, L., et al., 2016b. Physiochemical prop- erties of carbonaceous aerosol from agricultural residue burning: density, volatility, and hygroscopicity. Atmos. Environ. 140, 94–105.

Li, X., Chen, M., Le, H.P., Wang, F., Guo, Z., Iinuma, Y., Chen, J., et al., 2016c. Atmospheric outflow of PM2.5 saccharides from megacity Shanghai to East China Sea: impact of bi- ological and biomass burning sources. Atmos. Environ. 143, 1–14.

Li, X., Yang, Y., Xu, X., Xu, C., Hong, J., 2016d. Air pollution from polycyclic aromatic hydro- carbons generated by human activities and their health effects in China. J. Clean. Prod. 116, 1360–1367.

Lin, P., Engling, G., Yu, J.Z., 2010. Humic-like substances in fresh emissions of rice straw burning and in ambient aerosols in the Pearl River Delta Region, China. Atmos. Chem. Phys. 10 (14), 6487–6500.

Lin, Y.C., Lin, C.Y., Lin, P.H., Engling, G., Lin, Y.C., Lan, Y.Y., Chang, C.W.J., et al., 2013. Influ- ence of Southeast Asian biomass burning on ozone and carbon monoxide over sub- tropical Taiwan. Atmos. Environ. 64 (1), 358–365.

Lin, Y., Ma, Y., Qiu, X., Li, R., Fang, Y., Wang, J., Zhu, Y., et al., 2015a. Sources, transformation, and health implications of PAHs and their nitrated, hydroxylated, and oxygenated de- rivatives in PM2.5 in Beijing. J. Geophys. Res. Atmos. 120 (14):7219–7228. http://dx. doi.org/10.1002/2015JD023628.

Lin, Y., Qiu, X., Ma, Y., Ma, J., Zheng, M., Shao, M., 2015b. Concentrations and spatial distri- bution of polycyclic aromatic hydrocarbons (PAHs) and nitrated PAHs (NPAHs) in the atmosphere of North China, and the transformation from PAHs to NPAHs. Environ. Pollut. 196, 164–170.

Liu, Y., 2005. Atmospheric response and feedback to radiative forcing from biomass burn- ing in tropical South America. Agric. For. Meteorol. 133 (1), 40–53.

Liu, H., Chang, W.L., Oltmans, S.J., Chan, L.Y., Harris, J.M., 1999. On springtime high ozone events in the lower troposphere from Southeast Asian biomass burning. Atmos. Envi- ron. 33 (15), 2403–2410.

Liu, J., Drummond, J.R., Jones, D., Cao, Z., Bremer, H., Kar, J., Zou, J., et al., 2006. Large hor- izontal gradients in atmospheric CO at the synoptic scale as seen by spaceborne Mea- surements of Pollution in the Troposphere. J. Geophys. Res. Atmos. 111 (D2). http:// dx.doi.org/10.1029/2005JD006076.

Liu, Y., Shao, M., Fu, L., Lu, S., Zeng, L., Tang, D., 2008. Source profiles of volatile organic compounds (VOCs) measured in China: part I. Atmos. Environ. 42 (25), 6247–6260.

Liu, Z., Wang, Y., Gu, D., Zhao, C., Huey, L.G., Stickel, R., Liao, J., et al., 2012. Summertime photochemistry during CAREBeijing-2007: ROx budgets and O3 formation. Atmos. Chem. Phys. 12 (16), 7737–7752.

Liu, D., Li, J., Zhang, Y., Xu, Y., Liu, X., Ding, P., Shen, C., et al., 2013. The use of levoglucosan and radiocarbon for source apportionment of PM2.5 carbonaceous aerosols at a back- ground site in East China. Environ. Sci. Technol. 47 (18), 10454–10461.

Liu, S., Aiken, A.C., Arata, C., Dubey, M.K., Stockwell, C.E., Yokelson, R.J., Stone, E.A., et al., 2014. Aerosol single scattering albedo dependence on biomass combustion efficien- cy: laboratory and field studies. Geophys. Res. Lett. 41 (2):742–748. http://dx.doi. org/10.1002/2013GL058392.

Liu, Z., Wang, Y., Hu, B., Ji, D., Zhang, J., Wu, F., Wan, X., et al., 2016. Source appointment of fine particle number and volume concentration during severe haze pollution in Bei- jing in January 2013. Environ. Sci. Pollut. R. 23 (7), 6845–6860.

Lu, Z., Zhang, Q., Streets, D.G., 2011. Sulfur dioxide and primary carbonaceous aerosol emissions in China and India, 1996-2010. Atmos. Chem. Phys. 11 (18), 9839–9864.

Lyu, X.P., Chen, N., Guo, H., Zeng, L.W., Zhang, W.H., Shen, F., Quan, J.H., et al., 2016. Chem- ical characteristics and causes of airborne particulate pollution in warm seasons in Wuhan, central China. Atmos. Chem. Phys. 16, 10671–10687.

Martins, J.V., Artaxo, P., Hobbs, P.V., Liousse, C., Cachier, H., Kaufman, Y., Plana-Fattori, A., 1996. Particle Size Distributions, Elemental Compositions, Carbon Measurements, and Optical Properties of Smoke from Biomass Burning in the Pacific Northwest of the United States, Biomass Burning and Global Change. pp. 716–732.

Martins, J.A., Gonçalves, F.L.T., Morales, C.A., Fisch, G.F., Pinheiro, F.G.M., Leal Júnior, J.B.V., Oliveira, C.J., et al., 2009. Cloud condensation nuclei from biomass burning during the Amazonian dry-to-wet transition season. Meteorog. Atmos. Phys. 104 (1–2), 83–93.

Matson, M., Dozier, J., 1981. Identification of subresolution high temperature sources using a thermal IR sensor. Photogramm. Eng. Remote. Sens. 47 (9), 1311–1318.

Mauzerall, D.L., Logan, J.A., Jacob, D.J., Anderson, B.E., Blake, D.R., Bradshaw, J.D., Heikes, B., et al., 1998. Photochemistry in biomass burning plumes and implications for tropo- spheric ozone over the tropical South Atlantic. J. Geophys. Res. Atmos. 103 (D7), 8401–8423.

May, A.A., Lee, T., McMeeking, G.R., Akagi, S., Sullivan, A.P., Urbanski, S., Yokelson, R.J., et al., 2015. Observations and analysis of organic aerosol evolution in some prescribed fire smoke plumes. Atmos. Chem. Phys. 15 (11), 6323–6335.

McDonald, J.D., Zielinska, B., Fujita, E.M., Sagebiel, J.C., Chow, J.C., Watson, J.G., 2000. Fine particle and gaseous emission rates from residential wood combustion. Environ. Sci. Technol. 34 (11), 2080–2091.

Mcintire, T.M., Ryder, O.S., Gassman, P.L., Zhu, Z., Ghosal, S., Finlayson-Pitts, B.J., 2010. Why ozonolysis may not increase the hydrophilicity of particles. Atmos. Environ. 44 (7), 939–944.

McMeeking, G.R., Kreidenweis, S.M., Baker, S., Carrico, C.M., Chow, J.C., Collett, J.L., Hao, W.M., et al., 2009. Emissions of trace gases and aerosols during the open combustion of biomass in the laboratory. J. Geophys. Res. Atmos. 114 (D19). http://dx.doi.org/10. 1029/2009JD011836.

Mellouki, A., Wallington, T.J., Chen, J., 2015. Atmospheric chemistry of oxygenated volatile organic compounds: impacts on air quality and climate. Chem. Rev. 115 (10), 3984–4014.

Meng, Z.Y., Xu, X.B., Yan, P., Ding, G.A., Tang, J., Lin, W.L., Xu, X.D., et al., 2009. Character- istics of trace gaseous pollutants at a regional background station in northern China. Atmos. Chem. Phys. 9 (3), 927–936.

Menon, S., Hansen, J., Nazarenko, L., Luo, Y., 2002. Climate effects of black carbon aerosols in China and India. Science 297 (5590), 2250–2253.

Mielonen, T., Aaltonen, V., Lihavainen, H., Hyvärinen, A., Arola, A., Komppula, M., Kivi, R., 2013. Biomass burning aerosols observed in northern Finland during the 2010 wild- fires in Russia. Atmosphere-Basel 4 (1), 17–34.

Moffet, R.C., Henn, T.R., Tivanski, A.V., Hopkins, R.J., Desyaterik, Y., Kilcoyne, A., Tyliszczak, T., et al., 2010. Microscopic characterization of carbonaceous aerosol particle aging in the outflow from Mexico City. Atmos. Chem. Phys. 10 (3), 961–976.

Mohr, C., Huffman, J.A., Cubison, M.J., Aiken, A.C., Docherty, K.S., Kimmel, J.R., Ulbrich, I.M., et al., 2009. Characterization of primary organic aerosol emissions from meat cooking, trash burning, and motor vehicles with high-resolution aerosol mass spec- trometry and comparison with ambient and chamber observations. Environ. Sci. Technol. 43 (7), 2443–2449.

Morawska, L., Chen, J., Jayaratne, R., Ye, X., Li, C., 2016. Spatial and Temporal Variation of Airborne Particle Concentration in the Yangtze River Basin.

Mumtaz, M.M., George, J.D., 1995. Toxicological profile for polycyclic aromatic hydrocar- bons. Polycyclic Compounds.

Mustard, J.F., Murchie, S.L., Pelkey, S.M., Ehlmann, B.L., Milliken, R.E., Grant, J.A., Bibring, J.P., et al., 2008. Hydrated silicate minerals on Mars observed by the Mars reconnais- sance orbiter CRISM instrument. Nature 454 (7202), 305–309.

NBSC (National Bureau of Statistic of China), 2004–2014. China Statistical Yearbook, 480 2003–2013. China Statistics Press, Beijing (in Chinese).

Nel, A., 2005. Air pollution-related illness: effects of particles. Science 308, 804–806.

Ni, H., Han, Y., Cao, J., Chen, L.W.A., Tian, J., Wang, X., Chow, J.C., et al., 2015. Emission char- acteristics of carbonaceous particles and trace gases from open burning of crop resi- dues in China. Atmos. Environ. 123, 399–406.

Nie, W., Ding, A.J., Xie, Y.N., Xu, Z., Mao, H., Kerminen, V., Zheng, L.F., et al., 2015. Influence of biomass burning plumes on HONO chemistry in eastern China. Atmos. Chem. Phys. 15 (3), 1147–1159.

Niemi, J.V., Saarikoski, S., Tervahattu, H., Mäkelä, T., Hillamo, R., Vehkamäki, H., Sogacheva, L., et al., 2006. Changes in background aerosol composition in Finland during polluted and clean periods studied by TEM/EDX individual particle analysis. Atmos. Chem. Phys. 6 (12), 5049–5066.

Nussbaumer, T., 2003. Combustion and Co-combustion of biomass: fundamentals, tech- nologies, and primary measures for emission reduction. Energy Fuel 17 (6), 1510–1521.

Ohara, T., Akimoto, H., Kurokawa, J., Horii, N., Yamaji, K., Yan, X., Hayasaka, T., 2007. An Asian emission inventory of anthropogenic emission sources for the period 1980– 2020. Atmos. Chem. Phys. 7 (16), 4419–4444.

Okada, K., Ikegami, M., Zaizen, Y., Makino, Y., Jensen, J.B., Gras, J.L., 2001. The mixture state of individual aerosol particles in the 1997 Indonesian haze episode. J. Aerosol Sci. 32 (11), 1269–1279.

Omar, A.H., Winker, D.M., Vaughan, M.A., Hu, Y., Trepte, C.R., Ferrare, R.A., Lee, K., et al., 2009. The CALIPSO automated aerosol classification and lidar ratio selection algo- rithm. J. Atmos. Ocean. Technol. 26 (10), 1994–2014.

Ortega, A.M., Day, D.A., Cubison, M.J., Brune, W.H., Bon, D., de Gouw, J.A., Jimenez, J.L., 2013. Secondary organic aerosol formation and primary organic aerosol oxidation from biomass-burning smoke in a flow reactor during FLAME-3. Atmos. Chem. Phys. 13 (22), 11551–11571.

Ostro, B., Lipsett, M., Reynolds, P., Goldberg, D., Hertz, A., Garcia, C., Henderson, K.D., Bernstein, L., 2010. Long-term exposure to constituents of fine particulate air pollu- tion and mortality: results from the California Teachers Study. Environ. Health Perspect. 118 (3), 363–369.

Ouyang, B., Popoola, L., Jones, R., Li, C., Chen, J., 2016. Portable and low-cost sensors in monitoring air qualities in China. EGU General Assembly Conference Abstracts. 16213.

Paatero, P., Tapper, U., 1994. Positive matrix factorization: a non-negative factor model with optimal utilization of error estimates of data values. Environmetrics 5 (2): 111–126. http://dx.doi.org/10.1002/env.3170050203.

Parikka, M., 2004. Global biomass fuel resources. Biomass Bioenergy 27 (6), 613–620. Parrington, M., Palmer, P.I., Lewis, A.C., Lee, J.D., Rickard, A.R., Carlo, P.D., Taylor, J.W., et al.,

2013. Ozone photochemistry in boreal biomass burning plumes. Atmos. Chem. Phys. 13 (15), 7321–7341.

Pathak, B., Bhuyan, P.K., Gogoi, M., Bhuyan, K., 2012. Seasonal heterogeneity in aerosol types over Dibrugarh-North-Eastern India. Atmos. Environ. 47, 307–315.

Peng, J., Hu, M., Guo, S., Du, Z., Zheng, J., Shang, D., Zamora, M.L., et al., 2016. Markedly en- hanced absorption and direct radiative forcing of black carbon under polluted urban environments. Proc. Natl. Acad. Sci. U. S. A. 113 (16), 4266–4271.

Penner, J.E., Dickinson, R.E., O'Neill, C.A., 1992. Effects of aerosol from biomass burning on the global radiation budget. Science 256 (5062), 1432–1434.

Penner, J.E., Chuang, C.C., Grant, K., 1998. Climate forcing by carbonaceous and sulfate aerosols. Clim. Dyn. 14 (12), 839–851.

Perez-Padilla, R., Schilmann, A., Riojas-Rodriguez, H., 2010. Respiratory health effects of indoor air pollution. Int. J. Tuberc. Lung Dis. 14 (9), 1079–1086.

Petters, M.D., Kreidenweis, S.M., 2007. A single parameter representation of hygroscopic growth and cloud condensation nucleus activity. Atmos. Chem. Phys. 7 (8), 1961–1971.

Petters, M.D., Kreidenweis, S.M., 2013. A single parameter representation of hygroscopic growth and cloud condensation nucleus activity-part 3: including surfactant partitioning. Atmos. Chem. Phys. 13 (2), 1081–1091.

Petters, M.D., Carrico, C.M., Kreidenweis, S.M., Prenni, A.J., DeMott, P.J., Collett, J.L., Moosmueller, H., 2009. Cloud condensation nucleation activity of biomass burning aerosol. J. Geophys. Res. Atmos. 114 (D22) (1984–2012). 10.1029/2009JD012353.

Pierce, J.R., Adams, 2007. Efficiency of cloud condensation nuclei formation from ultrafine particles. Atmos. Chem. Phys. 7 (5), 1367–1379.

Pitz, M., Cyrys, J., Karg, E., Wiedensohler, A., Wichmann, H., Heinrich, J., 2003. Variability of apparent particle density of an urban aerosol. Environ. Sci. Technol. 37 (19), 4336–4342.

Pokhrel, R.P., Wagner, N.L., Langridge, J.M., Lack, D.A., Jayarathne, T., Stone, E.A., Stockwell, C.E., et al., 2016. Parameterization of single scattering albedo (SSA) and absorption angstrom exponent (AAE) with EC/OC for aerosol emissions from biomass burning. Atmos. Chem. Phys. 16, 9549–9561.

Pope III, C.A., Dockery, D.W., 2006. Health effects of fine particulate air pollution: lines that connect. J. Air Waste Manage. Assoc. 56 (6), 709–742.

Pope III, C.A., Burnett, R.T., Thun, M.J., Calle, E.E., Krewski, D., Ito, K., Thurston, G.D., 2002. Lung cancer, cardiopulmonary mortality, and long-term exposure to fine particulate air pollution. JAMA 287 (9), 1132–1141.

Popovicheva, O.B., Kozlov, V.S., Rakhimov, R.F., Shmargunov, V.P., Kireeva, E.D., Persiantseva, N.M., Timofeev, M.A., et al., 2016. Optical-microphysical and physical- chemical characteristics of Siberian biomass burning: small-scale fires in an aerosol chamber. Atmos. Oceanic Opt. 29 (4), 323–331.

Pósfai, M., Simonics, R., Li, J., Hobbs, P.V., Buseck, P.R., 2003. Individual aerosol particles from biomass burning in southern Africa: 1. Compositions and size distributions of carbonaceous particles. J. Geophys. Res. Atmos. 108 (D13). http://dx.doi.org/10. 1029/2002JD002291.

Pósfai, M., Gelencsér, A., Simonics, R., Arató, K., Li, J., Hobbs, P.V., Buseck, P.R., 2004. Atmo- spheric tar balls: particles from biomass and biofuel burning. J. Geophys. Res. Atmos. 109 (D6). http://dx.doi.org/10.1029/2003JD004169.

Pratt, K.A., Prather, K.A., 2009. Real-time, single-particle volatility, size, and chemical com- position measurements of aged urban aerosols. Environ. Sci. Technol. 43 (21), 8276–8282.

Prins, E.M., Feltz, J.M., Menzel, W.P., Ward, D.E., 1998. An overview of GOES-8 diurnal fire and smoke results for SCAR-B and 1995 fire season in South America. J. Geophys. Res. Atmos. 103 (D24):31821–31835. http://dx.doi.org/10.1029/98JD01720.

Qin, Y., Xie, S.D., 2011. Historical estimation of carbonaceous aerosol emissions from bio- mass open burning in China for the period 1990–2005. Environ. Pollut. 159 (12), 3316–3323.

Qin, Y., Xie, S.D., 2012. Spatial and temporal variation of anthropogenic black carbon emis- sions in China for the period 1980–2009. Atmos. Chem. Phys. 12 (11), 4825–4841.

Qin, X., Yan, H., Zhan, Z., Li, Z., 2014. Characterising vegetative biomass burning in China using MODIS data. Int. J. Wildland Fire 23 (1), 69–77.

Raaschou-Nielsen, O., Sørensen, M., Hertel, O., Bo, L.K.C., Vissing, N., Bønnelykke, K., Bisgaard, H., 2011. Predictors of indoor fine particulate matter in infants' bedrooms in Denmark. Environ. Res. 111, 87–93.

Ramana, M.V., Ramanathan, V., Feng, Y., Yoon, S.C., Kim, S.W., Carmichael, G.R., Schauer, J.J., 2010. Warming influenced by the ratio of black carbon to sulphate and the black-carbon source. Nat. Geosci. 3 (8), 542–545.

Ramanathan, V., Carmichael, G., 2008. Global and regional climate changes due to black carbon. Nat. Geosci. 1 (4), 221–227.

Ramanathan, V., Crutzen, P.J., Kiehl, J.T., Rosenfeld, D., 2001. Aerosols, climate, and the hy- drological cycle. Science 294 (5549), 2119–2124.

Ramanathan, V., Chung, C., Kim, D., Bettge, T., Buja, L., Kiehl, J.T., Washington, W.M., et al., 2005. Atmospheric brown clouds: impacts on South Asian climate and hydrological cycle. Proc. Natl. Acad. Sci. U. S. A. 102 (15), 5326–5333.

Randerson, J.T., Liu, H., Flanner, M.G., Chambers, S.D., Jin, Y., Hess, P.G., Pfister, G., et al., 2006. The impact of boreal forest fire on climate warming. Science 314 (5802), 1130–1132.

Ravindra, K., Sokhi, R., Van Grieken, R., 2008. Atmospheric polycyclic aromatic hydrocar- bons: source attribution, emission factors and regulation. Atmos. Environ. 42 (13), 2895–2921.

Real, E., Law, K.S., Weinzierl, B., Fiebig, M., Petzold, A., Wild, O., Methven, J., et al., 2007. Processes influencing ozone levels in Alaskan forest fire plumes during long-range transport over the North Atlantic. J. Geophys. Res. Atmos. 112 (D10). http://dx.doi. org/10.1029/2006JD007576.

Reid, J.S., Eck, T.F., Christopher, S.A., Koppmann, R., Dubovik, O., Eleuterio, D.P., Holben, B.N., et al., 2005a. A review of biomass burning emissions part III: intensive optical properties of biomass burning particles. Atmos. Chem. Phys. 5, 827–849.

Reid, J.S., Koppmann, R., Eck, T.F., Eleuterio, D.P., 2005b. A review of biomass burning emissions part II: intensive physical properties of biomass burning particles. Atmos. Chem. Phys. 3, 799–825.

Reinhardt, A., Emmenegger, C., Gerrits, B., Panse, C., Dommen, J., Baltensperger, U., Zenobi, R., et al., 2007. Ultrahigh mass resolution and accurate mass measurements as a tool to characterize oligomers in secondary organic aerosols. Anal. Chem. 79 (11), 4074–4082.

Rickards, A.M.J., Miles, R.E.H., Davies, J.F., Marshall, F.H., Reid, J.P., 2013. Measurements of the sensitivity of aerosol hygroscopicity and the κ parameter to the O/C ratio. J. Phys. Chem.: Atmos. 117 (51), 14120–14131.

Rissler, J., Nordin, E.Z., Eriksson, A.C., Nilsson, P.T., Frosch, M., Sporre, M.K., Wierzbicka, A., et al., 2014. Effective density and mixing state of aerosol particles in a near-traffic urban environment. Environ. Sci. Technol. 48 (11), 6300–6308.

Roberts, G.C., Artaxo, P., Zhou, J., Swietlicki, E., Andreae, M.O., 2002. Sensitivity of CCN spectra on chemical and physical properties of aerosol: A case study from the Amazon Basin. J. Geophys. Res. Atmos. 107 (D20). http://dx.doi.org/10. 1029/2001JD000583.

Robinson, A.L., Rhodes, J.S., Keith, D.W., 2003. Assessment of potential carbon dioxide re- ductions due to biomass-coal cofiring in the United States. Environ. Sci. Technol. 37 (22), 5081–5089.

Robinson, A.L., Donahue, N.M., Shrivastava, M.K., Weitkamp, E.A., Sage, A.M., Grieshop, A.P., Lane, T.E., et al., 2007. Rethinking organic aerosols: semivolatile emissions and photochemical aging. Science 315 (5816), 1259–1262.

Robock, A., 1991. Surface cooling due to forest fire smoke. J. Geophys. Res. 96 (D11): 20869–20878, ID020435. http://dx.doi.org/10.1029/91JD02043.

Rollins, A.W., Browne, E.C., Min, K., Pusede, S.E., Wooldridge, P.J., Gentner, D.R., Goldstein, A.H., et al., 2012. Evidence for NOx control over nighttime SOA formation. Science 337 (6099), 1210–1212.

Rose, D., Nowak, A., Achtert, P., Wiedensohler, A., Hu, M., Shao, M., Zhang, Y., et al., 2010. Cloud condensation nuclei in polluted air and biomass burning smoke near the mega-city Guangzhou, China–part 1: size-resolved measurements and implications for the modeling of aerosol particle hygroscopicity and CCN activity. Atmos. Chem. Phys. 10 (7), 3365–3383.

Rose, D., Gunthe, S.S., Su, H., Garland, R.M., Yang, H., Berghof, M., Cheng, Y.F., et al., 2011. Cloud condensation nuclei in polluted air and biomass burning smoke near the mega-city Guangzhou, China-part 2: size-resolved aerosol chemical composition, di- urnal cycles, and externally mixed weakly CCN-active soot particles. Atmos. Chem. Phys. 11 (6), 2817–2836.

Ross, A.B., Jones, J.M., Chaiklangmuang, S., Pourkashanian, M., Williams, A., Kubica, K., Andersson, J.T., et al., 2002. Measurement and prediction of the emission of pollutants from the combustion of coal and biomass in a fixed bed furnace. Fuel 81 (5), 571–582.

Russell, L.M., Maria, S.F., Myneni, S.C., 2002. Mapping organic coatings on atmospheric particles. Geophys. Res. Lett. 29 (16). http://dx.doi.org/10.1029/2002GL014874.

Sadezky, A., Muckenhuber, H., Grothe, H., Niessner, R., Pöschl, U., 2005. Raman microspectroscopy of soot and related carbonaceous materials: spectral analysis and structural information. Carbon 43 (8), 1731–1742.

Saffari, A., Daher, N., Samara, C., Voutsa, D., Kouras, A., Manoli, E., Karagkiozidou, O., et al., 2013. Increased biomass burning due to the economic crisis in Greece and its adverse impact on wintertime air quality in Thessaloniki. Environ. Sci. Technol. 47 (23), 13313–13320.

Saikawa, E., Naik, V., Horowitz, L.W., Liu, J., Mauzerall, D.L., 2009. Present and potential fu- ture contributions of sulfate, black and organic carbon aerosols from China to global air quality, premature mortality and radiative forcing. Atmos. Environ. 43 (17), 2814–2822.

Sakaeda, N., Wood, R., Rasch, P.J., 2011. Direct and semidirect aerosol effects of southern African biomass burning aerosol. J. Geophys. Res. Atmos. 116 (D12). http://dx.doi. org/10.1029/2010JD015540.

Saleh, R., Robinson, E.S., Tkacik, D.S., Ahern, A.T., Liu, S., Aiken, A.C., Sullivan, R.C., et al., 2014. Brownness of organics in aerosols from biomass burning linked to their black carbon content. Nat. Geosci. 7 (9), 647–650.

Sang, X.F., Chan, C.Y., Engling, G., Chan, L.Y., Wang, X.M., Zhang, Y.N., Shi, S., et al., 2011. Levoglucosan enhancement in ambient aerosol during springtime transport events of biomass burning smoke to Southeast China. Tellus B 63 (1), 129–139.

Schauer, J.J., Kleeman, M.J., Cass, G.R., Simoneit, B.R., 1999. Measurement of emissions from air pollution sources. 1. C1 through C29 organic compounds from meat charbroiling. Environ. Sci. Technol. 33 (10), 1566–1577.

Schkolnik, G., Chand, D., Hoffer, A., Andreae, M.O., Erlick, C., Swietlicki, E., Rudich, Y., 2007. Constraining the density and complex refractive index of elemental and organic car- bon in biomass burning aerosol using optical and chemical measurements. Atmos. Environ. 41 (5), 1107–1118.

Schmid, O., Karg, E., Hagen, D.E., Whitefield, P.D., Ferron, G.A., 2007. On the effective den- sity of non-spherical particles as derived from combined measurements of aerody- namic and mobility equivalent size. J. Aerosol Sci. 38 (4), 431–443.

Schmid, O., Chand, D., Karg, E., Guyon, P., Frank, G.P., Swietlicki, E., Andreae, M.O., 2009. Derivation of the density and refractive index of organic matter and elemental carbon from closure between physical and chemical aerosol properties. Environ. Sci. Technol. 43 (4), 1166–1172.

Seaton, A., Godden, D., Macnee, W., Donaldson, K., 1995. Particulate air pollution and acute health effects. Lancet 345 (8943), 176–178.

Seinfeld, J.H., Pandis, S.N., 2012. Atmospheric Chemistry and Physics: From Air Pollution to Climate Change. John Wiley & Sons.

Seinfeld, J.H., Pankow, J.F., 2003. Organic atmospheric particulate material. Annu. Rev. Phys. Chem. 54 (1), 121–140.

Seinfeld, J.H., Pandis, S.N., Seinfeld, J.H., Pandis, S.N., 2008. Atmospheric chemistry and physics: from air pollution to climate change. Phys. Today 51 (2), 212–214.

Semeniuk, T.A., Wise, M.E., Martin, S.T., Russell, L.M., Buseck, P.R., 2007. Hygroscopic be- havior of aerosol particles from biomass fires using environmental transmission elec- tron microscopy. J. Atmos. Chem. 56 (3), 259–273.

Shao, J.Z., 2000. The destruction of the forest fire to ecosystem and ecological fireproofing countermeasures. Fire Prev Prod Inform 21–22 in Chinese.

Shen, G., Yang, Y., Wang, W., Tao, S., Zhu, C., Min, Y., Xue, M., et al., 2010. Emission factors of particulate matter and elemental carbon for crop residues and coals burned in typ- ical household stoves in China. Environ. Sci. Technol. 44 (18), 7157–7162.

Shen, G., Tao, S., Chen, Y., Zhang, Y., Wei, S., Xue, M., Wang, B., et al., 2013. Emission char- acteristics for polycyclic aromatic hydrocarbons from solid fuels burned in domestic stoves in rural China. Environ. Sci. Technol. 47 (24), 14485–14494.

Shi, Y., Yamaguchi, Y., 2014. A high-resolution and multi-year emissions inventory for biomass burning in Southeast Asia during 2001–2010. Atmos. Environ. 98 (98), 8–16. Shih, S.I., Lee, W.J., Lin, L.F., Huang, J.Y., Su, J.W., Chang-Chien, G.P., 2008. Significance of biomass open burning on the levels of polychlorinated dibenzo-p-dioxins and dibenzofurans in the ambient air. J. Hazard. Mater. 153 (1–2), 276–284.

Shindell, D., Kuylenstierna, J.C., Vignati, E., van Dingenen, R., Amann, M., Klimont, Z., Anenberg, S.C., et al., 2012. Simultaneously mitigating near-term climate change and improving human health and food security. Science 335 (6065), 183–189.

Shrivastava, M.K., Lipsky, E.M., Stanier, C.O., Robinson, A.L., 2006. Modeling semivolatile organic aerosol mass emissions from combustion systems. Environ. Sci. Technol. 40 (8), 2671–2677.

Simoneit, B.R., 2002. Biomass burning-a review of organic tracers for smoke from incom- plete combustion. Appl. Geochem. 17 (3), 129–162.

Simoneit, B.R., Schauer, J.J., Nolte, C.G., Oros, D.R., Elias, V.O., Fraser, M.P., Rogge, W.F., et al., 1999. Levoglucosan, a tracer for cellulose in biomass burning and atmospheric parti- cles. Atmos. Environ. 33 (2), 173–182.

Smith, K.R., Mehta, S., Maeusezahl-Feuz, M., 2004. Indoor air pollution from household use of solid fuels. Comparative Quantification of Health Risks, pp. 1435–1493.

Song, Y., Zhang, Y., Xie, S., Zeng, L., Zheng, M., Salmon, L.G., Shao, M., et al., 2006. Source apportionment of $PM_{2.5}$ in Beijing by positive matrix factorization. Atmos. Environ. 40 (8), 1526–1537.

Song, Y., Tang, X., Xie, S., Zhang, Y., Wei, Y., Zhang, M., Zeng, L., et al., 2007. Source appor- tionment of PM2.5 in Beijing in 2004. J. Hazard. Mater. 146 (1), 124–130.

Streets, D.G., Gupta, S., Waldhoff, S.T., Wang, M.Q., Bond, T.C., Yiyun, B., 2001. Black carbon emissions in China. Atmos. Environ. 35 (25), 4281–4296.

Streets, D.G., Yarber, K.F., Woo, J.H., Carmichael, G.R., 2003. Biomass burning in Asia: an- nual and seasonal estimates and atmospheric emissions. Glob. Biogeochem. Cycles J. 17 (4), 1759–1768.

Streets, D.G., Bond, T.C., Lee, T., Jang, C., 2004. On the future of carbonaceous aerosol emis- sions. J. Geophys. Res. Atmos. 109 (D24). http://dx.doi.org/10.1029/2004JD004902.

Streets, D.G., Yu, C., Wu, Y., Chin, M., Zhao, Z., Hayasaka, T., Shi, G., 2008. Aerosol trends over China, 1980–2000. Atmos. Res. 88 (2), 174–182.

Su, H., Rose, D., Cheng, Y.F., Gunthe, S.S., Massling, A., Stock, M., Wiedensohler, A., et al., 2010. Hygroscopicity distribution concept for measurement data analysis and model- ing of aerosol particle mixing state with regard to hygroscopic growth and CCN acti- vation. Atmos. Chem. Phys. 10 (15), 7489–7503.

Sun, Y., Wang, Z., Dong, H., Yang, T., Li, J., Pan, X., Chen, P., et al., 2012. Characterization of summer organic and inorganic aerosols in Beijing, China with an Aerosol Chemical Speciation Monitor. Atmos. Environ. 51, 250–259.

Sun, Y.L., Wang, Z.F., Fu, P.Q., Yang, T., Jiang, Q., Dong, H.B., Li, J., et al., 2013. Aerosol com- position, sources and processes during wintertime in Beijing, China. Atmos. Chem. Phys. 13 (9), 4577–4592.

Sun, L., Xia, X., Wang, P., Zhang, R., Che, H., Deng, Z., Fei, Y., et al., 2015. Surface and col- umn-integrated aerosol properties of heavy haze events in January 2013 over the North China Plain. Aerosol Air Qual. Res. 1514–1524.

Sun, J., Peng, H., Chen, J., Wang, X., Wei, M., Li, W., Yang, L., et al., 2016a. An estimation of CO2 emission via agricultural crop residue open field burning in China from 1996 to 2013. J. Clean. Prod. 112, 2625–2631.

Sun, Y., Jiang, Q., Xu, Y., Ma, Y., Zhang, Y., Liu, X., Li, W., et al., 2016b. Aerosol characteriza- tion over the North China Plain: Haze life cycle and biomass burning impacts in sum- mer. J. Geophys. Res. Atmos. 121 (5). http://dx.doi.org/10.1002/2015JD024261.

Tan, H., Liu, L., Fan, S., Li, F., Yin, Y., Cai, M., Chan, P.W., 2016. Aerosol optical properties and mixing state of black carbon in the Pearl River Delta, China. Atmos. Environ. 131, 196–208.

Tao, S., Li, B., Zhang, Y.X., Yuan, H., 2011. Emission of Polycyclic Aromatic Hydrocarbons in China. Biophysico-chemical Processes of Anthropogenic Organic Compounds in Envi- ronmental Systems. :pp. 267–281 http://dx.doi.org/10.1002/9780470944479.ch11.

Tao, J., Zhang, L., Engling, G., Zhang, R., Yang, Y., Cao, J., Zhu, C., et al., 2013. Chemical com- position of PM2.5 in an urban environment in Chengdu, China: importance of spring- time dust storms and biomass burning. Atmos. Res. 122 (3), 270–283.

Tao, J., Gao, J., Zhang, L., Zhang, R., Che, H., Zhang, Z., Lin, Z., et al., 2014. PM2.5 pollution in a megacity of southwest China: source apportionment and implication. Atmos. Chem. Phys. 14 (4), 8679–8699.

Tena, A.F., Clarà, P.C., 2012. Deposition of inhaled particles in the lungs. Arch.

Bronconeumol. 48 (7), 240–246.

Thrane, K.E., Mikalsen, A., 1981. High-volume sampling of airborne polycyclic aromatic hydrocarbons using glass fibre filters and polyurethane foam. Atmos. Environ. 15 (6), 909–918.

Tian, F., Yu, J., Mckenzie, L., Hayashi, J., Chiba, T., Li, C., 2005. Formation of NO precursors during the pyrolysis of coal and biomass. Part VII. Pyrolysis and gasification of cane trash with steam. Fuel 84 (4), 371–376.

Tian, J., Chow, J.C., Cao, J., Han, Y., Ni, H., Chen, L.A., Wang, X., et al., 2015. A biomass com- bustion chamber: design, evaluation, and a case study of wheat straw combustion emission tests. Aerosol Air Qual. Res. 15 (5), 2104–2114.

Tian, S.L., Pan, Y.P., Wang, Y.S., 2016. Size-resolved source apportionment of particulate matter in urban Beijing during haze and non-haze episodes. Atmos. Chem. Phys. 16 (1), 1–19.

Tiitta, P., Miettinen, P., Vaattovaara, P., Joutsensaari, J., Petäjä, T., Virtanen, A., Raatikainen, T., et al., 2010. Roadside aerosol study using hygroscopic, organic and volatility TDMAs: characterization and mixing state. Atmos. Environ. 44 (7), 976–986.

Torres, O., Tanskanen, A., Veihelmann, B., Ahn, C., Braak, R., Bhartia, P.K., Veefkind, P., et al., 2007. Aerosols and surface UV products from Ozone Monitoring Instrument observa- tions: an overview. J. Geophys. Res. Atmos. 112 (D24). http://dx.doi.org/10.1029/ 2007JD008809.

Torres, O., Ahn, C., Chen, Z., 2013. Improvements to the OMI near-UV aerosol algorithm using A-train CALIOP and AIRS observations. Atmos. Meas. Tech. 6 (11), 3257–3270. Tosca, M.G., Randerson, J.T., Zender, C.S., 2013. Global impact of smoke aerosols from landscape fires on climate and the Hadley circulation. Atmos. Chem. Phys. 13 (10), 5227–5241.

Tritscher, T., Dommen, J., DeCarlo, P.F., Gysel, M., Barmet, P.B., Praplan, A.P., Weingartner, E., et al., 2011. Volatility and hygroscopicity of aging secondary organic aerosol in a smog chamber. Atmos. Chem. Phys. 11 (22), 11477–11496.

Turquety, S., Hurtmans, D., Hadji-Lazaro, J., Coheur, P., Clerbaux, C., Josset, D., Tsamalis, C., 2009. Tracking the emission and transport of pollution from wildfires using the IASI CO retrievals: analysis of the summer 2007 Greek fires. Atmos. Chem. Phys. 9 (14), 4897–4913.

Ulbrich, I.M., Canagaratna, M.R., Zhang, Q., Worsnop, D.R., Jimenez, J.L., 2009. Interpreta- tion of organic components from positive matrix factorization of aerosol mass spec- trometric data. Atmos. Chem. Phys. 9 (9), 2891–2918.

Vadrevu, K.P., Lasko, K., Giglio, L., Justice, C., 2015. Vegetation fires, absorbing aerosols and smoke plume characteristics in diverse biomass burning regions of Asia. Environ. Res. Lett. 10:105003. http://dx.doi.org/10.1088/1748-9326/10/10/105003.

Varutbangkul, V., Brechtel, F.J., Bahreini, R., Ng, N.L., Keywood, M.D., Kroll, J.H., Flagan, R.C., et al., 2006. Hygroscopicity of secondary organic aerosols formed by oxidation of cycloalkenes, monoterpenes, sesquiterpenes, and related compounds. Atmos. Chem. Phys. 6 (9), 2367–2388.

Vecchi, R., Bernardoni, V., Cricchio, D., D'Alessandro, A., Fermo, P., Lucarelli, F., Nava, S., et al., 2008. The impact of fireworks on airborne particles. Atmos. Environ. 42 (6), 1121–1132.

Vendrasco, E.P., Dias, P.S., Freitas, E.D., 2009. A case study of the direct radiative effect of biomass burning aerosols on precipitation in the Eastern Amazon. Atmos. Res. 94 (3), 409–421.

Victor, D.G., Zaelke, D., Ramanathan, V., 2015. Soot and short-lived pollutants provide po- litical opportunity. Nat. Clim. Chang. 5, 796–798.

Viktória, K.K., Mihály, P., János, L., 2006. Nanostructure of atmospheric soot particles. Atmos. Environ. 40, 5533–5542.

Volkamer, R., Jimenez, J.L., San Martini, F., Dzepina, K., Zhang, Q., Salcedo, D., Molina, L.T., et al., 2006. Secondary organic aerosol formation from anthropogenic air pollution: rapid and higher than expected. Geophys. Res. Lett. 33 (17). http://dx.doi.org/10. 1029/2006GL026899.

Waldheim, L., Monis, M., Verde Leal, M.R., 2000. Biomass power generation: sugar cane bagasse and trash. Progress in Thermochemical Biomass Conversion:pp. 509–523 http://dx.doi.org/10.1002/9780470694954.ch41.

Wang, S.X., Zhang, C.Y., 2008. Spatial and temporal distribution of air pollutant emissions from open burning of crop residues in China. Science Online. 5, pp. 329–333 (in Chinese).

Wang, T., Cheung, T.F., Li, Y.S., Yu, X.M., Blake, D.R., 2002. Emission characteristics of CO, NOx, SO2 and indications of biomass burning observed at a rural site in eastern China. J. Geophys. Res. Atmos. 107 (D12). http://dx.doi.org/10.1029/2001JD000724.

Wang, T., Guo, H., Blake, D.R., Kwok, Y.H., Simpson, I.J., Li, Y.S., 2005a. Measurements of trace gases in the inflow of South China Sea background air and outflow of regional pollution at Tai O, Southern China. J. Atmos. Chem. 52 (3), 295–317.

Wang, Y., Zhuang, G., Tang, A., Yuan, H., Sun, Y., Chen, S., Zheng, A., 2005b. The ion chem- istry and the source of PM2.5 aerosol in Beijing. Atmos. Environ. 39 (21), 3771–3784. Wang, Q., Xu, M., Xia, Y., 2006. Experimental study on transformation of mineral elements of inhaled particulate matters during co-combustion of coal with biomass. Proceed-ings-Chinese Society of Electricals Engineering. 26(16), p. 103.

Wang, Q., Shao, M., Liu, Y., William, K., Paul, G., Li, X., Liu, Y., et al., 2007a. Impact of bio- mass burning on urban air quality estimated by organic tracers: Guangzhou and Bei- jing as cases. Atmos. Environ. 41 (37), 8380–8390.

Wang, Q., Xu, M., Yao, H., Dai, L., 2007b. Co-combustion characteristics of biomass with coal and its effect on inhaled particulate matters emission. Proceedings of the CSEE. 1 (in Chinese).

Wang, G., Kawamura, K., Xie, M., Hu, S., Cao, J., An, Z., Waston, J.G., et al., 2009a. Organic molecular compositions and size distributions of Chinese summer and autumn aero- sols from Nanjing: characteristic haze event caused by wheat straw burning. Environ. Sci. Technol. 43 (17), 6493–6499.

Wang, Q., Shao, M., Zhang, Y., Wei, Y., Hu, M., Guo, S., 2009b. Source apportionment of fine organic aerosols in Beijing. Atmos. Chem. Phys. 9 (21), 8573–8585.

Wang, S., Zhao, M., Xing, J., Wu, Y., Zhou, Y., Lei, Y., He, K., et al., 2010. Quantifying the air pollutants emission reduction during the 2008 Olympic Games in Beijing. Environ. Sci. Technol. 44 (7), 2490–2496.

Wang, W., Jariyasopit, N., Schrlau, J., Jia, Y., Tao, S., Yu, T., Dashwood, R.H., et al., 2011. Con- centration and photochemistry of PAHs, NPAHs, and OPAHs and toxicity of PM2.5 dur- ing the Beijing Olympic Games. Environ. Sci. Technol. 45 (16), 6887–6895.

Wang, Z., Hu, M., Yue, D., He, L., Huang, X., Yang, Q., Zheng, J., et al., 2013. New particle for- mation in the presence of a strong biomass burning episode at a downwind rural site in PRD, China. Tellus B:65 http://dx.doi.org/10.3402/tellusb.v65i0.19965.

Wang, H., An, J., Shen, L., Zhu, B., Pan, C., Liu, Z., Liu, X., et al., 2014. Mechanism for the for- mation and microphysical characteristics of submicron aerosol during heavy haze pollution episode in the Yangtze River Delta, China. Sci. Total Environ. 490, 501–508. Wang, H., Qiao, L., Lou, S., Zhou, M., Chen, J., Wang, Q., Tao, S., et al., 2015a. PM2.5 pollution episode and its contributors from 2011 to 2013 in urban Shanghai, China. Atmos. En-viron. 132, 298–305.

Wang, L., Xin, J., Li, X., Wang, Y., 2015b. The variability of biomass burning and its influ- ence on regional aerosol properties during the wheat harvest season in North China. Atmos. Res. 157, 153–163.

Wang, D., Zhou, B., Fu, Q., Zhao, Q., Zhang, Q., Chen, J., Yang, X., et al., 2016a. Intense sec- ondary aerosol formation due to strong atmospheric photochemical reactions in summer: observations at a rural site in eastern Yangtze River Delta of China. Sci. Total Environ. http://dx.doi.org/10.1016/j.scitotenv.2016.06.212.

Wang, H., An, J., Shen, L., Zhu, B., Xia, L., Duan, Q., Zou, J., 2016b. Mixing state of ambient aerosols in Nanjing city by single particle mass spectrometry. Atmos. Environ. 132, 123–132.

Wardoyo, A.Y., Morawska, L., Ristovski, Z.D., Marsh, J., 2006. Quantification of particle number and mass emission factors from combustion of Queensland trees. Environ. Sci. Technol. 40 (18), 5696–5703.

Warneke, C., De Gouw, J.A., Goldan, P.D., Kuster, W.C., Williams, E.J., Lerner, B.M., Jakoubek, R., et al., 2004. Comparison of daytime and nighttime oxidation of biogenic and anthropogenic VOCs along the New England coast in summer during New En- gland Air Quality Study 2002. J. Geophys. Res. Atmos. 109 (D10). http://dx.doi.org/10.1029/2003JD004424.

Wehner, B., Berghof, M., Cheng, Y.F., Achtert, P., Birmili, W., Nowak, A., Wiedensohler, A., et al., 2009. Mixing state of nonvolatile aerosol particle fractions and comparison with light absorption in the polluted Beijing region. J. Geophys. Res. Atmos. 114 (D2). http://dx.doi.org/10.1029/2008JD010923.

Wei, S., Shen, G., Zhang, Y., Xue, M., Xie, H., Lin, P., Chen, Y., et al., 2014. Field measurement on the emissions of PM, OC, EC and PAHs from indoor crop straw burning in rural China. Environ. Pollut. 184, 18–24.

Wex, H., Hennig, T., Salma, I., Ocskay, R., Kiselev, A., Henning, S., Massling, A., et al., 2007. Hygroscopic growth and measured and modeled critical super-saturations of an at- mospheric HULIS sample. Geophys. Res. Lett. 34 (2). http://dx.doi.org/10.1029/ 2006GL028260.

Wieser, U., Gaegauf, C.K., 2000. Nanoparticle Emissions of Wood Combustion Processes.Centre of Appropriate Technology and Social Ecology.

Wigder, N.L., Jaffe, D.A., Saketa, F.A., 2013. Ozone and particulate matter enhancements from regional wildfires observed at Mount Bachelor during 2004–2011. Atmos. Envi- ron. 75, 24–31.

Williams, A., Jones, J.M., Ma, L., Pourkashanian, M., 2012. Pollutants from the combustion of solid biomass fuels. Energy Fuels 38 (2), 113–137.

Winker, D.M., Pelon, J.R., McCormick, M.P., 2003. The CALIPSO mission: Spaceborne lidar for observation of aerosols and clouds. Third International Asia-Pacific Environmental Remote Sensing Remote Sensing of the Atmosphere, Ocean, Environment, and Space. International Society for Optics and Photonics, pp. 1–11.

Winker, D.M., Vaughan, M.A., Omar, A., Hu, Y., Powell, K.A., Liu, Z., Hunt, W.H., et al., 2009. Overview of the CALIPSO mission and CALIOP data processing algorithms. J. Atmos. Ocean. Technol. 26 (11), 2310–2323.

Wit, M.D., Faaij, A., 2009. European biomass resource potential and costs. Biomass Bioenergy 34 (2), 188–202.

Witte, J.C., Douglass, A.R., Silva, A.D., Torres, O., Levy, R., Duncan, B.N., 2011. NASA A-Train and Terra observations of the 2010 Russian wildfires. Atmos. Chem. Phys. 11 (17), 9287–9301.

World Health Organization, 2010. WHO Guidelines for Indoor Air Quality: Selected Pollut- ants. World Health Organization.

Wu, Q.Z., Wang, Z.F., Gbaguidi, A., Gao, C., Li, L.N., Wang, W., 2011. A numerical study of contributions to air pollution in Beijing during CAREBeijing-2006. Atmos. Chem. Phys. 11 (12), 5997–6011.

Xie, Y., Ding, A., Nie, W., Mao, H., Qi, X., Huang, X., Xu, Z., et al., 2015. Enhanced sulfate forma- tion by nitrogen dioxide: implications from in situ observations at the SORPES station. J. Geophys. Res. Atmos. 24:12679–12694. http://dx.doi.org/10.1002/2015JD023607.

Xin, J., Wang, Y., Tang, G., Wang, L., Sun, Y., Wang, Y., Hu, B., et al., 2010. Variability and reduction of atmospheric pollutants in Beijing and its surrounding area during the Beijing 2008 Olympic Games. Chin. Sci. Bull. 55 (18), 1937–1944.

Xu, W.Q., Sun, Y.L., Chen, C., Du, W., Han, T.T., Wang, Q.Q., Fu, P.Q., et al., 2015. Aerosol composition, oxidation properties, and sources in Beijing: results from the 2014 Asia-Pacific Economic Cooperation summit study. Atmos. Chem. Phys. 15 (23), 13681–13698.

Yamaji, K., Li, J., Uno, I., Kanaya, Y., Irie, H., Takigawa, M., Komazaki, Y., et al., 2009. Impact of open crop residual burning on air quality over Central Eastern China during the Mount Tai Experiment 2006 (MTX2006). Atmos. Chem. Phys. 696 (1), 69–80.

Yan, X., Ohara, T., Akimoto, H., 2006. Bottom-up estimate of biomass burning in mainland China. Atmos. Environ. 40 (27), 5262–5273.

Yang, M., Howell, S.G., Zhuang, J., Huebert, B.J., 2009. Attribution of aerosol light absorp- tion to black carbon, brown carbon, and dust in China-interpretations of atmospheric measurements during EAST-AIRE. Atmos. Chem. Phys. 9 (6), 2035–2050.

Yang, Y., Chan, C.Y., Tao, J., Lin, M., Engling, G., Zhang, Z., Zhang, T., et al., 2012. Observation of elevated fungal tracers due to biomass burning in the Sichuan Basin at Chengdu City, China. Sci. Total Environ. 431 (5), 68–77.

Yang, Y.R., Liu, X.G., Qu, Y., An, J.L., Jiang, R., Zhang, Y.H., Sun, Y.L., et al., 2015. Characteris- tics and formation mechanism of continuous hazes in China: a case study during the autumn of 2014 in the North China plain. Atmos. Chem. Phys. 15 (14), 8165–8178.

Yang, H., Chen, J., Wen, J., Tian, H., Liu, X., 2016. Composition and sources of $PM_{2.5}$ around the heating periods of 2013 and 2014 in Beijing: implications for efficient mitigation measures. Atmos. Environ. 124, 378–386.

Yao, H., Song, Y., Liu, M., Xu, T., Li, J., Wu, Y., Hu, M., et al., 2016a. Direct radiative effect of carbonaceous aerosols from crop residue burning during the summer harvest season in East China. Atmos. Chem. Phys. Discuss.

Yao, L., Yang, L., Chen, J., Wang, X., Xue, L., Li, W., Sui, X., et al., 2016b. Characteristics of carbonaceous aerosols: impact of biomass burning and secondary formation in sum- mertime in a rural area of the North China Plain. Sci. Total Environ. 520-530.

Yin, Z., Ye, X., Jiang, S., Tao, Y., Shi, Y., Yang, X., Chen, J., 2015. Size-resolved effective den- sity of urban aerosols in Shanghai. Atmos. Environ. 133-140.

Yokelson, R.J., Crounse, J.D., DeCarlo, P.F., Karl, T., Urbanski, S.P., Atlas, E., Campos, T., et al., 2009. Emissions from biomass burning in the Yucatan. Atmos. Chem. Phys. http://dx. doi.org/10.5194/acp-9-5785-2009.

Yu, C., Lin, C., Wei, T., 2010. Observations of carbon monoxide mixing ratios at a mountain site in central Taiwan during the Asian biomass burning season. Atmos. Res. 95 (95), 270–278.

Yu, L., Wang, G., Zhang, R., Zhang, L., Song, Y., Wu, B., Li, X., et al., 2013a. Characterization and source apportionment of PM2.5 in an urban environment in Beijing. Aerosol Air Qual. Res. 13 (2), 574–583.

Yu, X., Shi, C., Ma, J., Zhu, B., Li, M., Wang, J., Yang, S., et al., 2013b. Aerosol optical proper- ties during firework, biomass burning and dust episodes in Beijing. Atmos. Environ. 475-484.

Yuan, B., Liu, Y., Shao, M., Lu, S., Streets, D.G., 2010. Biomass burning contributions to am- bient VOCs species at a receptor site in the Pearl River Delta (PRD), China. Environ. Sci. Technol. 44 (12), 4577–4582.

Yuan, B., Hu, W., Shao, M., Wang, M., Chen, W., Lu, S., Zeng, L., et al., 2013. VOC emissions, evolutions and contributions to SOA formation at a receptor site in eastern China. Atmos. Chem. Phys. 13 (17), 8815–8832.

Zauscher, M.D., Wang, Y., Moore, M.J.K., Gaston, C.J., Prather, K.A., 2013. Air quality impact and physicochemical aging of biomass burning aerosols during the 2007 San Diego wildfires. Environ. Sci. Technol. 47 (14), 7633–7643.

Zeng, X., Ma, Y., Ma, L., 2007. Utilization of straw in biomass energy in China. Renew. Sust. Energ. Rev. 11 (5), 976–987.

Zha, S., 2013. Agricultural fires and their potential impacts on regional air quality over China. Aerosol Air Qual. Res. 3, 992–1001.

Zhang, T., 2011. Prospect of biomass energy and its potential usage in electrical power generation in China. New Energy. 56-58 (in Chinese).

Zhang, Y., Cao, F., 2015a. Fine particulate matter (PM2.5) in China at a city level. Sci. Rep.-Uk 5:14884. http://dx.doi.org/10.1038/srep14884.

Zhang, Y., Cao, F., 2015b. Is it time to tackle PM2.5 air pollutions in China from biomass- burning emissions? Environ. Pollut. 202, 217–219.

Zhang, J., Smith, K.R., 2007. Household air pollution from coal and biomass fuels in China: measurements, health impacts, and interventions. Environ. Health Perspect. 848–855.

Zhang, Y., Tao, S., 2008. Seasonal variation of polycyclic aromatic hydrocarbons (PAHs) emissions in China. Environ. Pollut. 156 (3), 657–663.

Zhang, R., Suh, I., Zhao, J., Zhang, D., Fortner, E.C., Tie, X., Molina, L.T., et al., 2004. Atmo- spheric new particle formation enhanced by organic acids. Science 304 (5676), 1487–1490.

Zhang, M., Yuan, Y., Liu, Y., 2005. Research on biomass waste combustion technologies. Energy Research and Information. 2 (in Chinese).

Zhang, Y., Min, S., Zhang, Y., Zeng, L., He, L., Bin, Z., Wei, Y., et al., 2007. Source profiles of particulate organic matters emitted from cereal straw burnings. J. Environ. Sci. 19 (2), 167–175.

Zhang, H., Ye, X., Cheng, T., Chen, J., Yang, X., Wang, L., Zhang, R., 2008a. A laboratory study of agricultural crop residue combustion in China: emission factors and emission in- ventory. Atmos. Environ. 42 (36), 8432–8441.

Zhang, R., Khalizov, A.F., Pagels, J., Zhang, D., Xue, H., McMurry, P.H., 2008b. Variability in morphology, hygroscopicity, and optical properties of soot aerosols during atmo- spheric processing. Proc. Natl. Acad. Sci. 105 (30), 10291–10296.

Zhang, T., Claeys, M., Cachier, H., Dong, S., Wang, W., Maenhaut, W., Liu, X., 2008c. Identi- fication and estimation of the biomass burning contribution to Beijing aerosol using levoglucosan as a molecular marker. Atmos. Environ. 42 (29), 7013–7021.

Zhang, Y.H., Hu, M., Zhong, L.J., Wiedensohler, A., Liu, S.C., Andreae, M.O., Wang, W., et al., 2008d. Regional integrated experiments on air quality over Pearl River Delta 2004 (PRIDE-PRD2004): overview. Atmos. Environ. 42 (25), 6157–6173.

Zhang, Y., Dou, H., Chang, B., Wei, Z., Qiu, W., Liu, S., Liu, W., et al., 2008e. Emission of poly- cyclic aromatic hydrocarbons from indoor straw burning and emission inventory updating in China. Ann. N. Y. Acad. Sci. 1140 (1), 218–227.

Zhang, Q., Streets, D.G., Carmichael, G.R., He, K.B., Huo, H., Kannari, A., Klimont, Z., et al., 2009a. Asian emissions in 2006 for the NASA INTEX-B mission. Atmos. Chem. Phys. 9 (14), 5131–5153.

Zhang, Y., Tao, S., Shen, H., Ma, J., 2009b. Inhalation exposure to ambient polycyclic aro- matic hydrocarbons and lung cancer risk of Chinese population. Proc. Natl. Acad. Sci. U. S. A. 106 (50), 21063–21067.

Zhang, Y., Wang, X., Chen, H., Yang, X., Chen, J., Allen, J.O., 2009c. Source apportionment of lead-containing aerosol particles in Shanghai using single particle mass spectrometry. Chemosphere 74 (4), 501–507.

Zhang, G., Li, J., Li, X., Xu, Y., Guo, L., Tang, J., Lee, C., et al., 2010a. Impact of anthropogenic emissions and open biomass burning on regional carbonaceous aerosols in South China. Environ. Pollut. 158 (11), 3392–3400.

Zhang, M., Wang, X., Chen, J., Cheng, T., Wang, T., Yang, X., Gong, Y., et al., 2010b. Physical characterization of aerosol particles during the Chinese New Year's firework events. Atmos. Environ. 44 (39), 5191–5198.

Zhang, Z., Engling, G., Lin, C., Chou, C.C., Lung, S.C., Chang, S., Fan, S., et al., 2010c. Chemical speciation, transport and contribution of biomass burning smoke to ambient aerosol in Guangzhou, a mega city of China. Atmos. Environ. 44 (26), 3187–3195.

Zhang, H., Hu, D., Chen, J., Ye, X., Wang, S.X., Hao, J.M., Wang, L., et al., 2011a. Particle size distribution and polycyclic aromatic hydrocarbons emissions from agricultural crop residue burning. Environ. Sci. Technol. 45 (13), 5477–5482.

Zhang, J., Yao, F., Liu, C., Yang, L., Boken, V.K., 2011b. Detection, emission estimation and risk prediction of Forest fires in China using satellite sensors and simulation models in the past three decades-an overview. Int. J. Environ. Res. Public Health 8 (8), 3156–3178.

Zhang, H., Wang, S., Hao, J., Wan, L., Jiang, J., Zhang, M., Mestl, H.E., et al., 2012. Chemical and size characterization of particles emitted from the burning of coal and wood in rural households in Guizhou, China. Atmos. Environ. 51, 94–99.

Zhang, Y., Shao, M., Lin, Y., Luan, S., Mao, N., Chen, W., Wang, M., 2013. Emission inventory of carbonaceous pollutants from biomass burning in the Pearl River Delta Region, China. Atmos. Environ. 76, 189–199.

Zhang, H., Zhu, T., Wang, S., Hao, J., Mestl, H.E., Alnes, L.W., Aunan, K., et al., 2014a. Indoor emissions of carbonaceous aerosol and other air pollutants from household fuel burn- ing in Southwest China. Aerosol Air Qual. Res. 14 (6), 1779–1788.

Zhang, W., Zhu, T., Yang, W., Bai, Z., Sun, Y.L., Xu, Y., Yin, B., et al., 2014b. Airborne mea- surements of gas and particle pollutants during CAREBeijing-2008. Atmos. Chem. Phys. 14 (1), 301–316.

Zhang, Y.L., Li, J., Zhang, G., Zotter, P., Huang, R.J., Tang, J.H., Wacker, L., et al., 2014c. Radio- carbon-based source apportionment of carbonaceous aerosols at a regional back- ground site on Hainan Island, South China. Environ. Sci. Technol. 48 (5), 2651–2659. Zhang, T., Wooster, M.J., Green, D.C., Main, B., 2015a. New field-based agricultural biomass burning trace gas, PM2.5, and black carbon emission ratios and factors measured in situ at crop residue fires in Eastern China. Atmos. Environ. 121, 22–34.

Zhang, Y.J., Tang, L.L., Wang, Z., Yu, H.X., Sun, Y.L., Liu, D., Qin, W., et al., 2015b. Insights into characteristics, sources, and evolution of submicron aerosols during harvest sea- sons in the Yangtze River delta region, China. Atmos. Chem. Phys. 15 (3), 1331–1349. Zhang, Y.X., Zhang, Q., Cheng, Y.F., Su, H., Kecorius, S., Wang, Z.B., Wu, Z.J., et al., 2015c. Measuring morphology and density of internally mixed black carbon with SP2 and VTDMA: new insight to absorption enhancement of black carbon in the atmosphere.Atmos. Meas. Tech. Discuss. 8 (11), 12025–12060.

Zhang, J.K., Cheng, M.T., Ji, D.S., Liu, Z.R., Hu, B., Sun, Y., Wang, Y.S., 2016a. Characterization of submicron particles during biomass burning and coal combustion periods in Bei- jing, China. Sci. Total Environ. 812-821.

Zhang, L., Liu, Y., Hao, L., Zhang, L., Liu, Y., Hao, L., 2016b. Contributions of open crop straw burning emissions to PM2.5 concentrations in China. Environ. Res. Lett. 11 (1). http:// dx.doi.org/10.1088/1748-9326/11/1/014014.

Zhang, Y., Lin, Y., Cai, J., Liu, Y., Hong, L., Qin, M., Zhao, Y., et al., 2016c. Atmospheric PAHs in North China: spatial distribution and sources. Sci. Total Environ. 565, 994–1000.

Zhao, Y., Nielsen, C.P., Lei, Y., McElroy, M.B., Hao, J., 2011. Quantifying the uncertainties of a bottom-up emission inventory of anthropogenic atmospheric pollutants in China. Atmos. Chem. Phys. 5 (11), 2295–2308.

Zhao, B., Wang, P., Ma, J.Z., Zhu, S., Pozzer, A., Li, W., 2012. A high-resolution emission in- ventory of primary pollutants for the Huabei region, China. Atmos. Chem. Phys. 12 (1), 481–501.

Zheng, M., Salmon, L.G., Schauer, J.J., Zeng, L., Kiang, C.S., Zhang, Y., Cass, G.R., 2005. Sea- sonal trends in PM2.5 source contributions in Beijing, China. Atmos. Environ. 39 (22), 3967–3976.

Zhou, D., Dai, Y., Yu, C., Guo, Y., Zhu, Y., 2003. China's Sustainable Energy Scenarios in 2020. China Environmental Science Publishing Company.

Zhou, D., Ding, A., Mao, H., Fu, C., Wang, T., Chan, L.Y., Ding, K., Zhang, Y., Liu, J., Lu, A., Hao, N., 2013. Impacts of the East Asian monsoon on lower tropopsheric ozone over coast- al South China. Environ. Res. Lett. 8 (4). http://dx.doi.org/10.1088/1748-9326/8/4/ 044011.

Zhou, D., Ding, A., Mao, H., Fu, C., Wang, T., Chen, L.Y., Ding, K., Zhang, Y., Liu, J., An, L., Hao, N., 2015. Impact of the East Asian monsoon on lower tropospheric ozone over coastal South China. Environ. Res. Lett. 8 (4), 575–591.

Zhu, J., Xia, X., Che, H., Wang, J., Zhang, J., Duan, Y., 2016a. Study of aerosol optical prop- erties at Kunming in southwest China and long-range transport of biomass burning aerosols from North Burma. Atmos. Res. 169, 237–247.

Zhu, Y., Yang, L., Chen, J., Wang, X., Xue, L., Sui, X., Wen, L., et al., 2016b. Characteristics of ambient volatile organic compounds and the influence of biomass burning at a rural site in Northern China during summer 2013. Atmos. Environ. 124, 156–165.

Zhu, Y., Zhang, J., Wang, J., Chen, W., Han, Y., Ye, C., Li, Y., et al., 2016c. Distribution and Sources of Air pollutants in the North China Plain Based on On-Road Mobile Measure- ments. Atmos. Chem. Phys. Discuss. http://dx.doi.org/10.5194/acp-2016-410.

Zong, Z., Chen, Y., Tian, C., Fang, Y., Wang, X., Huang, G., Zhang, F., et al., 2015. Radiocar- bon-based impact assessment of open biomass burning on regional carbonaceous aerosols in North China. Sci. Total Environ. 518-519, 1–7.